DEPARTMENT OF PHYSICS

Electron Transfer Processes in Biologically Relevant Molecules

An Experimental Study of Neutral Alkali Atom-Molecule Collisions

SARVESH KUMAR

Master of Science in Physics

DOCTORATE IN RADIATION BIOLOGY AND BIOPHYSICS

NOVA University Lisbon

June 2022

NOVA SCHOOL OF SCIENCE & TECHNOLOGY

DEPARTMENT OF PHYSICS

Electron Transfer Processes in Biologically Relevant Molecules

An Experimental Study of Neutral Alkali Atom-Molecule Collisions

SARVESH KUMAR

Master of Science in Physics

Adviser: Paulo Manuel Assis Loureiro Limão-Vieira
Full Professor, NOVA University Lisbon

Examination Committee:

Chair: José Paulo Barbosa Mota,
Full Professor, *NOVA University Lisbon*

Rapporteurs: Alexander Dorn,
Lecturer, Department of Quantum Dynamics, and Control, Ultra-cold dynamics and collisions, Max Planck Institute for Nuclear Physics, Germany

Juraj Fedor,
Researcher and Director at Dynamics of Molecules and Clusters Department, J. Heyrovsky Institute of Physical Chemistry, Prague, Czech Republic.

Adviser: Paulo Manuel Assis Loureiro Limão-Vieira
Full Professor*, NOVA University Lisbon*

Members: Gustavo García Gomez-Tejedor,
Full Professor, Institute of Fundamental Physics (IFF), CSIC, Spain.

Pedro Jorge da Silva Pereira,
Assistant Professor, Instituto Superior de Engenharia de Lisboa

Maria Alice Santos Pereira,
Associate Professor, *NOVA University Lisbon*

DOCTORATE IN RADIATION BIOLOGY AND BIOPHYSICS

NOVA University Lisbon
June 2022

Electron Transfer Processes in Biologically Relevant Molecules

Dedicated in the loving memory of my Grandfather and Grandmother.

ACKNOWLEDGMENTS

I would like to thank my esteemed supervisor – Professor Paulo Limão-Vieira for his invaluable supervision, support, and tutelage during my PhD degree. His immense knowledge and plentiful experience have encouraged me in all the time of my academic research and daily life.

My gratitude extends to the Foundation for Science and Technology (Lisbon, Portugal) for the funding opportunity as a grant no. PD/BD/142831/2018 and COVID/BD/152673/2022 to undertake my studies at the Centre of Physics and technological Research (CEFITEC), Department of Physics, NOVA School of Science and Technology, New University of Lisbon. I am thankful to COST Action CA18212: Molecular Dynamics in Gas Phase for supporting my short-term scientific missions. I am also thankful to European Union for supporting me through ERASMUS+ internship grant 29191(533)107/2019/SMT/KA-1 for my scientific visit to Madrid.

Additionally, I would like to express gratitude to Professor Gustavo García for his treasured support during my visit to CSIC, Madrid which was influential in shaping my experimental methods and critiquing my understandings. I would like to thank Mr. Carlos Guerra for his support during my scientific mission to Madrid and wonderful friendship. I would also thank Dr. Nykola Jones and Dr. Sørren Vrønning Hoffmann, for their mentorship and support during my visits to ISA, Denmark. A Sincere thanks to Prof. Stephan Denifl for hosting me during the pandemic and support provided by Mr. Farhad Izadi for DEA experiments at University of Innsbruck.

My sincere gratitude towards Prof. Pedro Tavares and Prof. Alice S. Pereira RaBBiT directors and members of the directive board. You have always supported me to think differently and encouraged me get involved in various activities. Thank you very much for always being available for fruitful scientific discussions during lunch times, and during all our scientific missions together in Denmark. I have learnt a lot from both of you. It's a blessing to have people like you around.

I would like to thank Professor Augusto Moutinho for the occasional discussions and his continued interest in my research work. My thanks to Prof. Pedro Pereira for his support.

I would like to thank Dr. Juraj Fedor for hosting me and all the hospitality during my visit to J. Heyrovsky Institute, Progue and Dr. Pamir Nag for all the wonderful discussions.

I would also like to thank Mr. Afonso Moutinho, Mr. João Faustino, Mr. Fábio Evanglista for their technical support on my study.

I would like to thank my lab mates, and colleagues –Dr. Filipe Ferreira da Silva, Dr. Ana Lozano, Dr. Mónica Mendes, Dr. João Ameixa, Mr. Alexandru Botnari, and Mr. Miguel Pacheco.

Mr. João Silva, Mr. Rodrigo Rodrigues, Mr. José Romero and recently Mr. Daniel for a cherished time spent together in the lab, and in social settings you guys have been amazing, it's great to have friends like you.

Mr. João Guerra and Ms. Ana Almeida thank you very much for always being available for help and discussions, on and off the science.

My sincere thanks to NOVA desporto (Sports office of NOVA) for supporting and believing in me and for all the amazing time I spent with Athletics team. Prof. Paulo Barrigana, you have been amazing in helping me realize my potential in long distance running, I hope someday I can make you proud. My athletics teammates Mr. Ahmad Hasan, Eszter Banhidi, and Diogo Parreira thanks for the support.

My association with various cricket clubs has kept me engaged and my spirit alive whenever I felt low. My teammates from various teams Mr. Rahul Bhardwaj, Mr. Arslan Naseem, Mr. Madhukar Thapa, Mr. Imran Khan, Mr. Manjeet Singh, Mr. Azhar Andani, Mr. Anoop, and Prof. Dr. Shiv Kumar Singh, it has been great playing alongside you guys.

Dr. Sirajul Haque Zakir and recently Dr. Navendu Deb Paul for the long late-night walks to keep the motivation alive during the hardest of times. There are so many others which I find difficult to name all, but you all know that you have siginificant contributions.

I am grateful to my father Mr. Girish Kumar Sharma, my mother Mrs. Ramayani Devi for having patience during my stay away from home and providing me with best examples of moral values. I have missed you a lot. I am thankful to my brother Mr. Giriraj Kishor Sharma and Mrs. Kanchan Sharma for taking care of everything back home in my absence. May gods bless everyone with such a family to everyone. My sisters Mrs. Rohini Sharma and Mr. Anil Sharma, Mrs. Neetu Sharma and Mr. Sanjay Sharma, and Mrs. Renu Sharma and Mr. Laxman Sharma thank you very much for showering the love upon me.

My nieces and nephew to whom I have dearly missed during my stay in Portugal, Anmol Sharma, Ajay Sharma, Madhavi Sharma, Stuti Sharma (Chhoti Guddan), Lakshya Sharma (Kanha), Yashasvi Sharma (Guddan). I am also thankful to people, who knowingly or

unknowingly gave me a lesson to become better version of myself. And many more others which are not mentioned here, but had siginificant contributions in direct and indirect way.

"Arise! Awake! and stop not until the goal is reached." - Swami Vivekanand.

ABSTRACT

The work developed within the context of this thesis includes negative ion formation in charge transfer processes from collisions of neutral potassium atoms with key selected neutral molecules. The crossed molecular beam set up used to obtain the anion yields as a function of the collision energy as well as relevant information about the lowest-lying anionic states that are accessed in the temporary negative ion formation, is fully equipped with a time−of−flight mass spectrometer and an energy loss analyser. The spectrometric technique includes a linear and a reflectron type time-of-flight mass spectrometers to provide information about the negative ions formed in such collisions. We have made use of a home−built Wiley McLaren type Linear Time-of-flight mass spectrometer (L−TOF−MS), to extract relevant information about the kinetic energy release distribution of selected fragment anions, as a function of the collision energy, while the reflectron time−of−flight mass-spectrometer (r−TOF−MS) was used due to its higher mass resolution serving as a proper tool to resolve close lying fragment anions differing by just 1 amu in the fragmentation of nimorazole. In order to obtain relevant information about the most accessed negative ion states in the collision process, a post−collision potassium cation (K^+) energy loss spectra in the forward scattering direction ($\theta \approx 0°$) with the beam's optical path have been recorded in a hemispherical energy loss analyser. The combination of TOF−MS and these two techniques helped us to gain deep insight into electron transfer processes of molecules under investigation.

The set of chlorinated molecules investigated include a group ($C_6H_5Cl, C_6D_5Cl,$ $C_6H_{11}Cl,$ and C_6Cl_6) that has been properly chosen to explore the role of direct dissociation through electron transfer into a σ^*_{Cl} antibonding orbital and more importantly to determine the role of intramolecular electron transfer through π^*/σ^*_{Cl} coupling yielding anion formation. From the comprehensive investigation of these molecules in a wide energy range of collision energies, $10 - 10^3$ eV in lab frame, we have obtained for the first time the relative cross−section for Cl^- formation.

The other group of molecules include biological relevant targets as the radiosensitizer nimorazole (NIMO) and water. Regarding the former, although the major signal is assigned to the non-dissociated parent anion (80% of the total anion yield), NO_2^- accounts for just 10−15% of the total anion yield a detailed trace fragmentation pattern indicates decomposition of NIMO's 4−nitroimidazole and morpholine rings. As far as the latter is concerned, H_2O and its deuterated counterpart D_2O were investigated and are presented in the third part of this thesis. The fragmentation pattern from H_2O includes H^-, O^-, and OH^- whereas from D_2O includes D^-, O^-, and OD^-. From the different TOF mass spectra the fragment anions' thresholds of formation have been obtained. K^+ energy loss spectra from NIMO, H_2O and D_2O were also recorded, revealing the experimental vertical electron affinities of the most accessed negative ion states.

Keywords: electron-transfer, charge transfer, atom−molecule collisions, electronic state spectroscopy, alkali energy loss spectroscopy, TOF−MS.

RESUMO

O trabalho desenvolvido no contexto desta tese inclui a formação de iões negativos em processos de transferência de carga a partir de colisões de átomos neutros de potássio com moléculas neutras. A configuração do aparelho de feixes moleculares cruzados utilizado para obter os rendimentos iónicos em função da energia de colisão, bem como informações relevantes sobre os estados aniónicos de mais baixa energia acessíveis durante a formação temporária de iões negativos, conta com um espectrómetro de massa de tempo de voo e um analisador de perda de energia. Para os estudos de espectrometria de massa, dispomos de dois espectrómetros de tempo de voo do tipo linear e reflectrão, que fornecem informação dos iões negativos produzidos em tais colisões. O espectrómetro de massa linear de tempo de voo (L−TOF−MS) é do tipo Wiley McLaren, e permitiu obter informações relevantes sobre a distribuição da energia cinética libertada na formação de fragmentos aniónicos em função da energia de colisão, enquanto que o espectrómetro de massa do tipo reflectrão (r−TOF−MS) foi utilizado devido à sua maior resolução em massa servindo como uma ferramenta adequada para identificar fragmentos aniónicos diferindo por apenas 1 u.m.a. na fragmentação do nimorazol. Para obter informação relevante dos estados aniónicos acessíveis no processo de colisão, espectros de perda de energia do ião potássio (K^+) pós−colisão na direção principal ($\theta \approx 0°$) foram obtidos num analisador hemisférico de perda de energia. A combinação da espectrometria de massa TOF−MS e analisador da perda de energia, permitiu assim obter uma descrição detalhada dos processos de transferência de electrão nas moléculas sob investigação.

O conjunto de moléculas estudadas inclui o C_6H_5Cl, C_6D_5Cl, $C_6H_{11}Cl$, e C_6Cl_6, que foi adequadamente escolhido para explorar o mecanismo de dissociação directa através da transferência de electrão para uma orbital antiligante σ^*_{Cl} e, mais importante, para determinar a relevância da transferência intramolecular através do acoplamento π^*/σ^*_{Cl} no processo de formação de um ião negativo. A partir da investigação abrangente dessas moléculas numa

ampla faixa de energias de colisão, $10 - 10^3$ eV no referencial de laboratório, obtivemos pela primeira vez a secção eficaz relativa para a formação do ião de Cl^-.

O outro grupo de moléculas inclui alvos biológicos relevantes como o radiossensibilizador nimorazol (NIMO) e água. Em relação ao primeiro, embora o sinal principal seja atribuído ao anião pai (80% do rendimento total aniónico), a formação do ião de NO_2^- representa apenas 10-15% do rendimento total. O padrão de fragmentação do nimorazol indica decomposição das suas unidades elementares de 4−nitroimidazol e morfolina. No que diz respeito a este último, H_2O e seu homólogo deuterado D_2O, o padrão de fragmentação inclui H^-, O^-, e OH^- enquanto que em D_2O obtemos a formação de D^-, O^-, e OD^-. A partir dos diferentes espectros de massa de TOF foram obtidos os limiares de formação dos respectivos fragmentos aniónicos. Espectros de perda de energia de K^+ para o NIMO, H_2O e D_2O também foram obtidos, revelando assim informação importante dos valores das afinidades eletrónicas verticais experimentais dos estados de iões negativos mais acessíveis no processo de colisão.

Palavras-chave: transferência de electrão, transferência de carga, colisões átomo−molécula, espectroscopia de estados eletrónicos, espectroscopia de perda de energia, espectrometria de massa de tempo de voo.

CONTENTS

Table of Contents

LIST OF FIGURES

LIST OF TABLES

GLOSSARY

Carcinogenicity	Cancer causing property of a substance when an animal or human is exposed to it.
Pseudo Halogens	Pseudo halogens mimic halogens, and form molecular compounds with nonmetals and Ionic compounds with alkali metals.
Elastic Scattering	Such a scattering (collision of two particles) where kinetic energy of the particle is conserved in center of mass frame, but its direction of propagation is modified by interaction with other particles and/or potentials in the vicinity.
Molecular Vibration	A molecular vibration is a periodic motion of the constituent atoms of a molecule with respect to each other, while keeping center of mass unchanged.

.

ACRONYMS

CEFITEC	Centre of Physics and Technological Research
LCAM	Atomic And Molecular Collisions Laboratory
CSIC	Consejo Superior de Investigaciones Científicas
DEA	Dissociative Electron Attachment
TOF	Time-of-Flight
MS	Mass Spectrometry
BRs	Branching Ratios
AD	Auto-detachment
DD	Direct detachment
DNA	Deoxyribose Nucleic Acid
RNA	Ribose Nucleic Acid
DSB	Double Strand Break
SSB	Single Strand Break
DFT	Density Functional Theory
IE	Ionization Energy
EA	Electron Affinity
VEA	Vertical Electron Affinity
VAE	Vertical Attachment Energy
LUMO	Lowest Unoccupied Molecular Orbital
HOMO	Highest Occupied Molecular Orbital

MO	Molecular Orbital
LZ	Landau−Zener
FC	Franck−Condon
MCP	Micro Channel Plate
HEA	Hemispherical Energy Analyzer
QMS	Quadrupole Mass Spectrometer
TNI	Transient Negative Ion
KER	Kinetic Energy Release
UV	Ultra-Violet
VUV	Vacuum Ultra-Violet
FWHM	Full Width at Half−Maximum

SYMBOLS

K^+	Cationic Potassium
K^0	Neutral Potassium
K^+_{hyp}	Hyperthermal Cationic Potassium
K^0_{hyp}	Hyperthermal Neutral Potassium
EA_{ad}	Adiabatic Electron Affinity
EA_v	Vertical Electron Affinity
E_{lab}	Energy in Lab Frame
E_{cm}	Energy in Center of Mass Frame
E_{loss}	Energy Loss
T_{Oven}	Oven Temperature
T_{CEC}	Charge Exchange Chamber Temperature
V_{acc}	Acceleration Voltage
e^-	Electron
b	Impact Parameter
R_c	Crossing Radius
t_{Coll}	Collision Time
t_{vib}	Vibrational Time
t_{rot}	Rotational Time
V_{rel}	Relative Velocity

$\mathbf{V_{rad}}$	Radial Velocity
Z	Charge of the particle
ΔE	Energy loss
m	Mass
amu	Atomic Mass Unit
$\mathbf{m_m}$	Mass of molecular target
$\mathbf{m_k}$	Mass of potassium
μ	Reduced Mass of the system
$\boldsymbol{\pi^*}$	π antibonding orbital
$\boldsymbol{\sigma^*}$	σ antibonding orbital
$\mathbf{E_{th}}$	Threshold Energy
$\mathbf{H_{11}; H_{22}}$	Diabatic Potential Curves
$\mathbf{H_{12}}$	Coupling Factor
LT	Langmuir-Taylor
$\mathbf{M^{\#-}}$	Vibrationally Excited Molecular Anion
PES	Potential Energy Surface
$\mathbf{V_{ion}}$	Ionic Potential Curve
$\mathbf{V_{cov}}$	Covalent Potential Curve

1.

INTRODUCTION

Scattering experiments between atoms and molecules have been at the forefront of research for almost a century since the pioneering work of Polanyi [1], Li [2], Herschbach [3] and Marcus [4], owing to the significance of charge (electron) transfer (CT) [5] a prevalent mechanism in various chemical reactions and physical phenomena in different environments [6]. Some examples of these environments are the reactions taking place in intersteller medium (ISM), Earth´s upper atmosphere, astrochemistry, biological environments and plasma processing, among many others. In such diverse environments, specific consequences of binary collisions e.g., a chemical reaction, ionization, excitation, and de−excitation are of great importance to probe particular spectroscopic features of atoms and molecules. The above−mentioned reactions occur at various time scales and depending on the combination of collision partners and energy available, these interaction times which are usually of the orders of few fs (femtosecond) can vary. The outcome from such experiments can be relevant giving information regarding collision dynamics, probabilities for transitions between various states of the system, branching ratios, interaction potentials and adiabatic coupling measured experimentally[7].

Molecular collisions of atoms with weakly bound electrons in their outermost orbital, mimic an analogy for electron transfer from electronically excited secondary neutrals in various environments. Some of the projectiles with such bound electrons that have been used in the past across the world are Li, Na, K, and Cs. In the present work we limit our studies with K as a projectile, owing to its availability and low I.E. (Ionization energy) = 4.3407 eV[8]. The use of energy tuneable alkali atoms to probe different molecular targets can be achieved by producing a beam of neutral species that is made to cross with a target beam yielding ion-pair formation. Such neutral alkali hyperthermal beam (K^0_{hyp}) is obtained through a charge-exchange reaction as[9].

$$\mathrm{K}^0 + \mathrm{K}^+_{\mathrm{hyp}} \rightarrow \mathrm{K}^0_{\mathrm{hyp}} + \mathrm{K}^+ \qquad (1)$$

with K^0 is a thermal potassium atom and K^+_{hyp} is potassium cation a given kinetic energy.

Ion−pair formation in neutral alkali atom−molecule collisions has attracted the attention of the international scientific community due to the unique nature of the projectile, i.e., the possibility to ionize in a chemi−ionization collision, which offers complementary information about the role of vibrational excitation of the target parent anion with positive electron affinity (EA) and enhanced fragmentation pattern which cannot be explored in free electron attachment experiments. On the other hand, alkali metal−molecule collisions represent a model process to study the mechanisms of radiation induced damage to living tissues in cancer radiotherapy, which is a more realistic model than much studied electron−molecule collisions.

The scope of this thesis is to study the collision induced fragmentation pathways of different anions formed in the collision of neutral potassium atoms with neutral polyatomic molecules with relevance in biological, environmental, and even in combustion environments.

1.1 Motivation

Negative ion formation upon electron transfer in neutral alkali atom molecule collisions provides a significant insight about the underlying molecular mechanisms governing to the various processes in chemical reactions [10], [11].

The collisions of an alkali atom (potassium) with a molecule (represented as AB) can be understood in the following reaction:

$$K^0_{hyp} + (AB) \rightarrow K^+_{hyp} + (AB^-)^{\#} \quad (2)$$

$$(AB^-)^{\#} \rightarrow A + B^- \quad (3)$$

First, a Transient Negative Ion (TNI) $(AB^-)^{\#}$ is formed, eq. (2), meaning that is formed with an excess of internal energy that may then yield a neutral and an anionic fragment as decay products. Electron transfer-induced processes in such collisions are less explored than its counterpart electron−molecule collisions. Many collisional processes are not directly electron impact but rather electron transfer processes. Potassium atom−molecule collisions provide an excellent opportunity to assessing DNA damage under biological conditions, i.e., redox reactions at sensitive sites of the DNA double helix. Such anionic formation upon collisions of a ground state atom and a ground state molecule, several fundamental processes can occur due to the increased degree of freedom in comparison to atom-atom collisions where only two processes, elastic scattering and electronically inelastic scattering can occur at collision energies from thermal values up to 1 keV. The different possible processes now in the case of atom-molecule collisions are [12]:

1. Elastic Scattering.

2. Rotational Excitation.
3. Vibrational Excitation or Collision Induced dissociation.
4. Electronic Excitation.
5. Chemical Reaction.
6. Vibronic Excitation or Simultaneous Vibrational and Electronic Excitation.
7. A Combination of these processes.

Earlier electron transfer studies in potassium atom-biomolecule collisions have led to unprecedented achievements, in terms of better understanding the underlying molecular mechanisms yielding fragmentation of selected molecules. Such achievements include electron transfer induced dissociation of thymine and uracil [13], with the most striking difference from previous DEA results being the enhanced anionic yields stemming from bond excision from the ring. It has also been shown at room temperature with random molecular orientation, that site- (N1−H vs N3−H) and bond− (C−H vs C−N) selective dissociation in DNA/RNA pyrimidine bases can be achieved by tuning the proper collision energy. Subsequent experiments have shown that the NCO^- branching ratios as a function of the collision energy are reminiscent of extraordinary site and bond selectivity in the reactions yielding its formation [14]. These studies have shown that electron transfer processes are much more effective than DEA in producing loss of integrity within DNA/RNA units. In DEA studies to several (bio)molecular targets[10], [11], [13]–[17], the dominant fragmentation channels result from very low−energy resonances (often as low as ~0 eV) consisting of Vibrational Feshbach Resonances (VFR). This can be rationalized by the fact that in DEA accessing high energy resonances (such as NCO^- in uracil/thymine) will mostly result in auto−detachment rather than in fragmentation. However, in potassium atom−molecule collisions, there is evidence that autodetachment is significantly suppressed, due to the coulombic interaction in the collision complex formed after electron transfer, i.e., $(K^+_{hyp}\ (AB^-)^{\#})$, thus enhancing fragment formation[14], [15].

These findings allowed to establish a collisional model at basic molecular level in collision induced dissociation for DNA damage [16]. This model also provides coherent explanation of the observed correlation between electron transfer to biomolecules and their carcinogenicity and may be used to suggest new compounds to be adopted in radiation therapy as treatment enhancing sensitizers.

Radiosensitisation properties of halouracils (e.g., 5−XU, X= F, Cl, Br, and I; U= Uracil) have been known for several decades. Increased frequency of single and double strand breaks has been observed for DNA thymine's replaced by a halogenated uracil in the cells upon irradiation. The electron transfer model provides an explanation for such effects with the

introduction of a strongly electrophilic atom into DNA (e.g., F, Cl), leading to an enhancement of collision induced dissociation probability and increased probability for DNA destruction in cells containing such compounds[18].
Molecular dissociation proceeding through electronic excitation can be probed efficiently in such crossed beam experiments. Importance cannot be ignored since such species formed can efficiently drive the local chemistry yielding considerable structural and functional changes in the biological environments [16].

In the last fifteen years, a very strong impetus in the field of astrochemistry came after the discovery of anionic species in comets, interstellar clouds and in Titan´s atmosphere[19]–[24]. We live in a molecular universe; hundreds of neutral molecules have been detected in space. These are amended by tens of cations, but only a handful of molecular anions are known to exist outside the Earth: these are e.g., CN^-, C_3N^-, and C_nN^-, with n = 2,4,6 [25]. Theses CN containing anions (cyanogen) are also considered pseudo halogens as to their ability to capture an electron given their relative high values of electron affinities. Their detection sparked a lot of interest about the possible production pathways within their environments. It has been quickly established that they cannot be formed via DEA to neutral molecules since this process is endothermic and free electrons in the interstellar regions are cold (typical environments at 10 K). Various alternative pathways for their formation have been put forward such as anion molecule reactions or radiative electron attachment to radicals. Nonetheless, the pseudohalides are interesting from the point of view of astrochemical synthesis, thus giving significant importance to the halogenated unsaturated hydrocarbons as model compounds to be investigated.

1.2 Biological effects and radiation

The first biological effects related to exposure to ionizing radiation had been noticed by Becquerel[26]. When he developed skin erythema and ulcers after inadvertently carrying a radioactive radium sample in his pocket. A similar exposure was later reported by Pierre Currie, in his forearm. These early observations set the framework for biological effects of ionizing radiation on living organisms. Humans are exposed in a daily life to natural radiation sources such as radioactivity, cosmic rays, however they can be exposed to artificial sources of radiation in medical imaging during PET (Positron Emission Tomography) and CT (Computed Tomography) scans, gamma γ −rays and X−rays. Depending on the dose and the type of radiation, its effects in the biological environment and the biochemical consequences of such exposure vary significantly.

Most Biological effects of radiation arise from DNA damage. Ionizing radiation may promptly cause modifications in the DNA sequences, causing direct and indirect damages varying in observation over time from fs to days, months, years and even decades.

The direct DNA damage occurs through direct interaction of radiation with molecules in the biological environment, these processes take place within femtoseconds (fs) in the form of electronic excitation and ionization events and various of other physical and physio-chemical processes that may yield chemical modification and even loss of integrity of key fundamental biological molecular compounds, e.g., DNA and RNA.

In this thesis, our interaction time between an atom and a molecule is of the order of femtoseconds, thus we will be mainly discussing interactions in the framework of early stages of radiation induced processes (physical stage) resulting in electronic excitation and/or ionization events under these interactions.

One of the greatest biological mediums in human body is water (approx. 80 %), which undergoes radiolysis due to radiation interaction in the human body and forming highly reactive radical species namely OH and H along with secondary electrons known to be precursors for DNA damage. In this stage of time frame all products undergo thermalization in the vicinity of the DNA, due to inelastic collisions within the environment, forming various radical species of salts, proteins and oxygen molecules which can cause further damage to DNA in the form of single and/or double−strand breaks. The sort of damage caused or triggered by highly reactive species is also known as free radical damage.

1.2.1 Cancer and its diagnosis methodologies

A large group of diseases characterized by the rapid creation of abnormal cells, also known as tumour cells, are coined as Cancer. Such cells suffer genetic mutations, and uncontrolled spread of such tumour cells throughout the body causes for the cancer, death [27]. Cancer can be inherited, known as hereditary cancer, it has been observed that inherited cancer only accounts for 3−10 % of total annual cancer cases[28].

The non−hereditary cancer can be caused by external factors (carcinogens) such as tobacco, food, and water contaminants (chemical carcinogens), ionizing radiation such as UV, X−rays, and γ −rays (physical carcinogens) exposure and viruses and bacteria's (biological carcinogens) [29].

The main goal of the cancer treatment is to stop the spread of the tumour cells by destroying or removing them using radiation or chemotherapy, or even by surgery[30].Surgery is the most used treatment to remove cancerous cell from patient's body. In radiation therapy, electromagnetic radiation or charged particles or fast neutrons are employed to selectively damage and kill the cancer cells. It is estimated that half of all patients receive radiotherapy during the treatment of a certain type of cancer [31]. Chemotherapy is the least used of the above mentioned two therapies, in which chemical compounds are used to target DNA, RNA and proteins to trigger the cell death [27]. These chemical compounds used in this treatment are also known as anti-cancer drugs or radiosensitizers. The last two techniques have significant side effects to patients, while used individually. However, a combination of the latter two methodologies, known as chemoradiation therapy (CRT), simultaneous use of anti-cancer drug (radiosensitizers) along with radiation, enhances the sensitivity of the tumour cells towards the radiation [32], [33].

1.3 Outline of the thesis

Earlier electron transfer experiments on potassium atom-biomolecule collisions have contributed to a deeper scientific knowledge on the following topics:

a) Site−and bond−selective excision processes in pyrimidines and derivatives[10], [11], [14], [16].
b) DNA/RNA integrity loss enhancement with high yields of fragment anions in contrast to the dehydrogenated parent anion formation (a prevalent mechanism in DEA experiments) [15].
c) The possible stabilizing effect in the collision complex by the presence of a potassium cation in the vicinity of TNI, dictating different fragmentation patterns than in DEA [14].
d) The role of increasing sidechains in amino acids enhancing small fragment anion yields.
e) Observation of other fragment anions in such noted molecules, not reported before [13].

These accomplishments, although extremely relevant within the general context of the collision dynamics, led to knowledge gained on the underlying mechanisms in negative ion formation, and the role of electron transfer to key selected biomolecular targets. Nonetheless there remain several questions unanswered, and processes that have been proposed to explain various observations still need to be probed and properly addressed for a set of molecules

with relevance to astrochemistry, biological systems, and biological environments. Potassium has loosely bound valence electron and low ionization energy, which makes it an excellent electron donor. We will exploit this property of potassium in electron transfer reactions. Such reactions will be performed considering astrochemical and biological relevance of the molecules. Astrochemical relevant molecules will serve as testbed to get hands on experience with experimental setup and fundamental understanding of negative ion chemistry to the scientific community with the concrete information about charge transfer processes. Hence, considering the relevance, molecules investigated within the scope of this thesis can be categorized into three sections, which include:

A. Molecules of Astrochemical relevance [21]

B. Molecules of Biological relevance [34].

C. Molecules of biological environment relevance[35], [36].

Due to huge significance of electron transfer processes in various environments, such experiments find significant importance in, e.g., astrochemical environments, interstellar mediums and biological mediums and their significance is highlighted and explained as follows.

A. Molecules of Astrochemical relevance: In this class of molecules, electron transfer processes in unsaturated chlorinated hydrocarbons, leading to C−Cl bond excision and intramolecular processes will be investigated. The set of chosen molecules in this class that will be investigated are C_6H_5Cl, C_6D_5Cl, $C_6H_{11}Cl$ and C_6Cl_6 followed by possible contribution in addressing the following open problems:

a) Identify and separate the contributions from processes initiated by electron transfer in the form of π^*system or σ^*(C−Cl) orbitals.

b) Explore the role of π^*/σ^* coupling and its strength and identify dynamical imprints of this coupling.

c) Explore the role of proximity in dissociation of multiply chlorinated unsaturated hydrocarbons.

To help answering the above−mentioned open problems, a selection of 4 different classes of chlorinated unsaturated hydrocarbons is justified. All four molecules have almost similar geometry (planar in the neutral ground state) except $C_6H_{11}Cl$, where its geometry is a boat like structure and the absence of double bonds makes it the perfect candidate to separate the dynamical effects of coupling to the rest of the other:

(i) The low-lying unoccupied π^*orbitals related to the presence of double bonds in such molecules are those where an incident electron can be temporarily trapped.

(ii) In C_6H_5Cl, the presence of single and double bonds, makes it one of the complicated processes, as it involves low−lying unoccupied π^* orbitals where an extra

electron is primarily trapped in a delocalized system. On the contrary the high electron affinity of chlorine atom (3.16 eV) causes the excess electron to be transferred into σ^*(C−Cl) repulsive state. Thus, this competition for an extra electron leads to coupling between the two, followed by required symmetry lowering of the system, sometimes also known as geometry distortion.

(iii) In $C_6H_{11}Cl$, the lack of double bonds ensures that an extra electron will be trapped in a low lying unoccupied π^* will be absent, leading to excess electron transfer directly into the σ^*(C−Cl) repulsive state. Hence, in this system, we expect that there will be no such coupling effects, and the formation of Cl^- anion will be purely from the σ^*(C−Cl) contribution and can be used to compare the effects with other molecules.

(iv) The selection of C_6D_5Cl, an isotope of C_6H_5Cl, may provide significant insight into the isotopic contribution in the repulsive state, thus probably responsible for delayed formation of the Cl^- anion.

(v) The final and most relevant molecule of this class is C_6Cl_6. This molecule has double bonds as C_6H_5Cl, but also symmetric distribution of Cl atoms across the ring, thus making the effectiveness of σ^*(C−Cl) state more efficient in comparison to C_6H_5Cl.

Such chlorinated unsaturated hydrocarbons will be probed using state of the art linear Time of Flight Mass Spectrometry in a wide collision energy range. The complementary results from potassium energy loss will serve to characterize various vibrationally excited states post collisions in the forward direction. The section of linear Time of flight is suitable for these set of molecules as the fragmentation is not expected to be significant and we would also like to get the information regarding the kinetic energy imparted in the collision induced dissociation to the ionic fragment.

B. Molecules of Biological relevance: Charge transfer processes in atom-molecules collisions can be used to benchmark electron transfer in biological environments due to a loosely bound electron transfer from potassium. Potassium initiated chemistry can be significant to understand some of the fundamental challenges that have been difficult to investigate from the traditional techniques. Cancer has been a key focus area of research among the international scientific community for significant time, and since the pioneering investigation by Léon Sanche and co−workers about secondary electrons and subsequent DNA damage at the cellular level [32], [37]–[40], forced somehow the scientific community to revisit such charge transfer studies.

Nimorazole (NIMO ≡ $C_9H_{14}N_4O_3$), is a chemical compound that has been widely used as an efficient hypoxic (deficient in oxygen) cell radiosensitizer in head and neck squamous carcinoma due to its low toxicity [41]. In its composition, NIMO contains a nitroimidazole and a morpholine rings bonded by their nitrogen atoms through a $-H_2C-CH_2-$ side group. NIMO's ability to scavenge low-energy electrons has been recently shown to be very efficient in producing a non-dissociate parent anion with a considerable large cross-section of $\sim 3 \times 10^{-18}$ m^2 (at ~ 0 eV) [42], [43] while dissociative electron attachment has been shown to be a minor reaction channel which is suppressed upon hydration [42]. Although the detailed mechanisms by which radiosensitisation operates are still unknown, it is believed that radiosensitizers are chemical compounds subject to redox reactions inside the hypoxic cells [44], and in case of nitroimidazoles, the ring facilitates reduction through reactive anion radicals' formation [45]–[47]. Nitroimidazole radiosensitizers have been thoroughly investigated by experimental methods on low-energy electron interactions [48]–[52] and together with nimorazole probed by electrospray ionization mass spectrometry [53]–[55]. While associative electron attachment may contribute to NIMO's radiosensitising effect, within the biological environment, electron transfer processes (redox reactions) may prevail and so these may seem more appropriate to describe the underlying molecular mechanisms of such chemical compounds and their role as radiosensitizers. Thus, we have initiated more than a decade ago an investigation methodology to explore key selected radiosensitizers by charge transfer in atom-molecule collision experiments, *viz*. halogenated uracil [56]and more recently nitroimidazoles [57], [58]. In case of the former, the decomposition yields significant ring breaking with appreciable NCO^- intensities (in 5−FU) and halogen anion formation (in 6−ClU), thus compromising the integrity of viral RNA where the neutral molecules bind. For the latter, the collision induced dissociation results in formation of several radicals, with particular attention to NO° and OH°. These radicals act as an indirect DNA damage agent triggered by ionizing radiation, while nitric oxide has been noted for sensitizing hypoxic solid tumours in radiotherapy and chemotherapy treatments [59]. Another relevant aspect pertains to the role of site and bond−selectivity in electron transfer processes to DNA/RNA nucleotides yielding bond cleavage [11], [16], which have been shown to be pivotal in controlling chemical reactions. As recently shown [57], [58], such control of a given bond breaking may have relevance to tailor chemical control for different applications such as tumour radiation therapy through nitroimidazole-based radiosensitisation.

C. Molecules of Biological Environment relevance: Our human body consists of approx. 80 % water, and most of the chemistry happens in water due to radiation and associated secondary electron and radicals' formation[60], [61]. Thus, water acts as biological environment and the role in charge transfer processes needs to be investigated properly. Research

with a water molecule is a very attractive topic in a variety of scientific areas, including but not limited to atmospheric chemistry [62], [63], chemistry [64], radiation physics [65], [66], and radiation biology [60], [67]–[69]. There has been significant amount of research on this triatomic and one of the fundamental molecules. But the chemistry in different environments is not yet fully understood[70]–[73]. We will try to shed some light on charge transfer processes on water and its deuterated analogue, D_2O. Due to the isotopic significance of D_2O, this will also be investigated to compare with bare H_2O some of the collision dynamics governing electron transfer (see Chapter 7).

In this segment of molecules (H_2O and D_2O), we will try to understand some of the charge transfer dynamics in the following form:

i. Branching ratios for different anions of water (H^-, O^-, and OH^-) will be obtained in a wide collision energy range.
ii. Similarly branching ratios for different anions of D_2O (D^-, O^-, and OD^-) will be obtained in a wide collision energy range.
iii. A threshold of formation for various anions will be obtained.
iv. Alkali energy loss spectroscopy of K^+ in forward direction upon electron transfer will be employed to investigate the role of various electronic states accessed in such collisions.

2.

GENERAL THEORETICAL APPROACH

In this chapter, the reader will find some of the established terminology and their significant role in interpreting the dynamics of charge transfer experiments in alkali atom-molecule collisions.

2.1 Introduction

Considering, a case for possible electron transfer which happens by weakly bound electrons (the outer shell electrons) of the projectile atom to a target molecule. In the case of potassium atom, it has an ionization energy of 4.34 eV [74] and therefore the practical energy range for collision experiments can vary from thermal energies up to 1 keV. If the size of the target molecule is also small, the general nuclear motion can be described classically due to the associated small de Broglie wavelength in high energy collisions. In addition, the Born−Oppenheimer approximation will be valid.

However, the Born-Oppenheimer approximation breaks down when two potential energy curves, describing different electronic states of the system with the same symmetry becomes degenerate in a certain region of the configuration space. In these degenerate regions, curve crossing or electronic transitions can occur [75].

For simplicity, consider the atom-atom (both in ground state) case in the concerned energy region (thermal energies up to 1 keV) where the two possible processes are elastic scattering and electronically inelastic scattering. When we replace one atom with a molecule (also in the ground state), the degrees of freedom involved increases significantly thus increasing the probability for various processes. Now the dynamics can no longer be described using one dimensional potential curve but rather a potential energy surface [76].

These various processes are now as following as described in section 1.1

1. Elastic Scattering.
2. Rotational Excitation.

3. Vibrational Excitation or Collision Induced dissociation.
4. Electronic Excitation.
5. Chemical Reaction.
6. Vibronic Excitation or Simultaneous Vibrational and Electronic Excitation.
7. A combination of these processes.

Negative ion formation in alkali-atom-molecule collisions is a powerful method to probe the dynamic properties (including vibrational dynamics) of negative ions on a fs timescale [75], [77]. In such collisions, one has access to the electron affinity of the molecule as it is manifested in the collision. The EAs obtained depend on the conditions of the collisions and do not have to be identical to EAs obtained by other means, thus discerning between adiabatic, vertical, and reactive EAs. The electron transfer from an alkali atom to molecule in ion-pair formation can provide significant information regarding molecular electron affinities.

Many fundamental collisional processes depend on the electron transfer in atom-atom or atom-molecule collisions where negative ions can be formed as an intermediate step or as a final product.

In atom-molecule collisions, stretching of the molecular bond in the negative ion is one of the most important consequences of the internal degrees of freedom but it is not the only one responsible when such internal degrees of freedom in molecules are increased significantly. Process such as molecular rotation, in case of polyatomic molecules, even geometry and symmetry can play a major role in transitions and interplay of various processes. These processes have been attempted to be studied in the past for the simpler diatomic electronegative molecules and very few asymmetric molecules [75], [77]–[81].

The capture of a bound electron from potassium (electron donor) into the molecule forming an ion-pair is in general endoergic (ΔE) i.e., it requires a minimum collisional energy that is given by the ionization energy of the potassium atom (IE) minus the electron affinity of the target molecule (EA) and is usually of the order of few eV.

2.1.1 Electron affinity

A quantitative measurement of the energy change that occurs when an electron is added to a neutral gas atom can be classified as electron affinity. In other words, the ability of an atom to accept an electron and become a negative ion. Hence, we can say that the energy difference between an atom in the ground state and its negative ion, is the electron affinity. Alkali metals (Li, Na K, Rb, and Cs) are considered one of the best electron donor atoms owing to their low

ionization energies (I.E.), thus have been extensively used in the past to explore electron transfer processes [82]–[86].

An electron is added to a metal element via an endothermic reaction where energy is needed to gain that electron. In metals, valence electrons are loosely bound to their nucleus, and it is easier to form cations by donating valence electrons, that's why metals have lower electron affinities and are known as electron donors. Non−metals have higher electron affinities than metals, the valence electron shell is closer to the nucleus, thus it is harder to loose an electron and easier to gain na electron than in atoms with low electron affinities. The halogen group (F, Cl, Br, and I) has one of the highest electron affinities [87], [88] due to the high ability of such atoms to attach an extra electron.

Therefore, the possibility of electron transfer between an alkali atom and a halogen containing molecule is significantly high. In the past, such collision experiments have attracted diverse areas of the international scientific community to explore various fundamental processes, e.g., reaction rates in a chemical reaction, quantifying the variety of electron affinities pointing to properties of negative ions in various environments [75], including but not limited to biological and astrophysical environments.

2.1.1.1 Adiabatic Electron affinity

The adiabatic electron affinity is the largest electron affinity possible for the molecule and is the energy separation of the potential well of the molecule and the molecular ion. It should be noted that adiabatic electron affinity does not correspond to the Franck−Condon or vertical transition [87], [88].

2.1.1.2 Vertical Electron affinity

The vertical electron affinity corresponds to the Franck−Condon or vertical transition between the molecular ground state and the negative ion state if we assume that the potentials correspond to the free molecule and molecular ion in the gas phase [87], [88].

2.1.1.3 Reactive Electron affinity

In an atom-molecule collision usually the vibrational motion of the molecule is not considered frozen during the collision, as the collision time is of the order of molecular vibrations. This is mostly the case when collisions are performed at relative low energies. Therefore, molecular potentials may be deformed with respect to those found in isolated conditions. In many cases, the effective electron affinities are encountered in ion-pair formation which are usually between the vertical and adiabatic values [87], [88].

In the theoretical framework of ion−pair formation in electron transfer processes at least three particles need to be included in the description. The well−known semi−classical Landau−Zener (LZ) method [89], [90] has been extended for atom−molecule collisions in the past [91] where all nuclear motions are treated using classical mechanics and transitions (electron transfer) between different vibronic states are computed by the LZ formula.
In a typical electron transfer reaction, the following analogy can be assumed with some possible exit channels:

$$M + X \rightarrow M^+ + X^- \quad (4)$$

$$M + XY \rightarrow M^+ + (XY)^- \quad (5)$$

$$M + XY \rightarrow M^+ + X + Y^- \quad (6)$$

$$M + XY \rightarrow M^+ + X^- + Y \quad (7)$$

2.2 Theoretical Considerations

The general theoretical approach from atom−molecule collisions stem from atom−atom collisions as explained in section 2.1.1 and later extended for diatomic and many particle collisions. The details of theoretical collisions are not the topic of this thesis and will not be explained. However, a general overview and explanation of the terminology used will be given to help interpret some of the experimental results.
Another general consideration made when moving from atom-atom to atom−molecule collisions is the collision time. In atom−atom collisions, the collision time should be comparable to the time of the electron in the Bohr orbit.

In atom−molecule collision two characteristic times must be considered in addition, the rotational time (t_{rot}), and the vibrational time (t_{vib}).

Several theories exist to describe electronically inelastic collisions or non−adiabatic processes in molecular collisions, several reviews are available for various systems [82], [83], [85], [86], [92]–[94]. In some of the classical methods, the nuclear motion of the nuclei, or of the projectile is described using classical methods thus losing the phase information i.e., interference effects, which are negligible in the higher collision energy range due to short collision time but are significant in the lower collision energy range where the collision time is of order of the vibrational time and even sometimes of the rotational time as well.
If we assume that R describes the distance between the alkali atom and the centre−of−mass of the molecule, r is the internuclear distance of the molecule, and φ is the orientation of the molecular axis with respect to the approaching alkali atom [95]. The covalent potential surface can be constructed by the following formula [77], [91]:

$$V_{cov}(R, r) = V_C(R) + V_C(r) \quad (8)$$

where, $V_C(R)$ is an isotropic Lennard-Jones 12−6 potential for K−XY interaction in the covalent surface and $V_C(r)$ is the Morse potential for the free XY molecule. Here we summarize some of the methods employed in the past with their most significant characteristics.

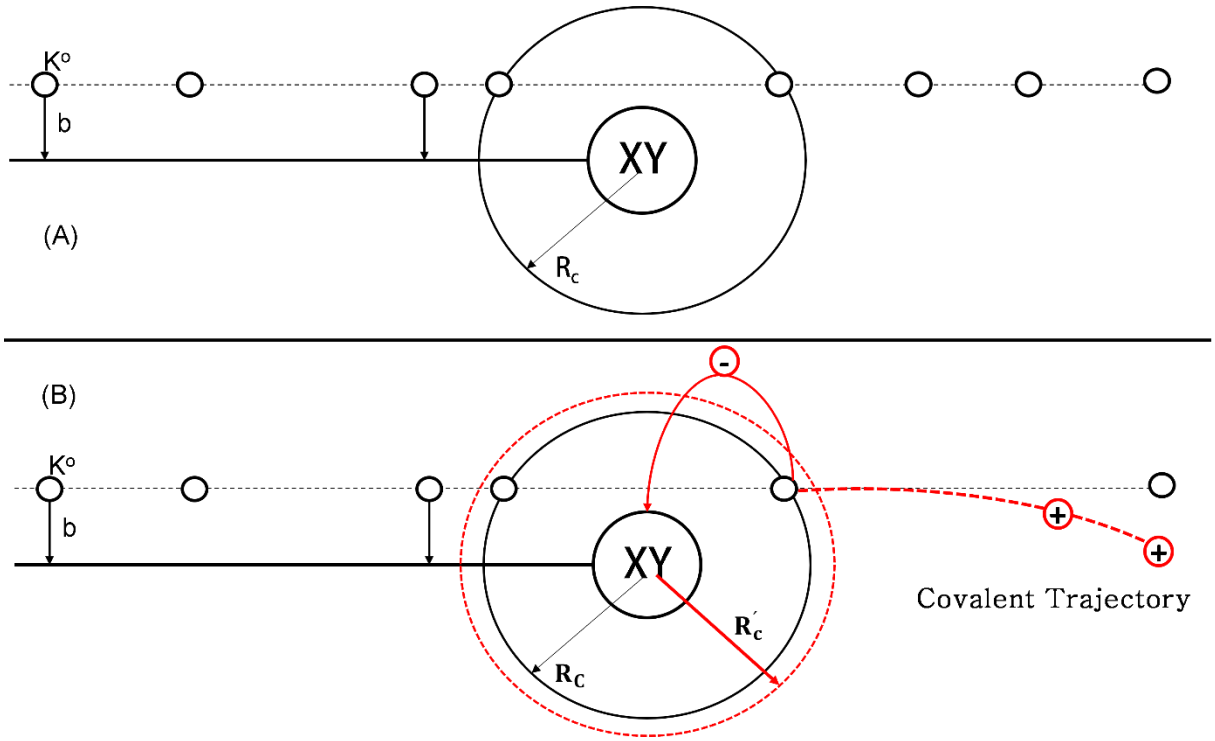

Figure 1 Schematic of covalent trajectory in atom-molecule collisions, b is the impact parameter, O represent neutral potassium, XY the molecule in consideration, R_c crossing radius at which electron transfer takes place, R_c' effective radius after transfer of an electron. (A) Neutral potassium goes without transferring the electron. (B) Neutral potassium transfers an electron to the molecule (XY) at the second crossing.

Here in the above Figure 1, when a potassium approaches the XY molecule with an impact parameter b, and transfers the electron at the exit channel i.e., the second crossing, it deviates from its original path due to coulombic interaction between the K^+ and XY^-, thus the trajectory followed by the K^+ is termed covalent trajectory.

In the ionic trajectory of the electron transfer, the potassium cation spends more time in the vicinity of the XY anion thus creating more perturbation in the electron cloud of the molecule and being deflected more from its original path in comparison to the covalent trajectory. There is also the possibility of neutralization in ionic trajectories, at the second crossing. In that case, the potassium cation can take back the donated electron from the molecule while leaving the molecular vicinity.

The potential surface for the ionic trajectory can be constructed using the following equation:

$$V_{ion}(R, r, \Phi) = V_i(R, \Phi) + V_i(r) + \Delta E \quad (9)$$

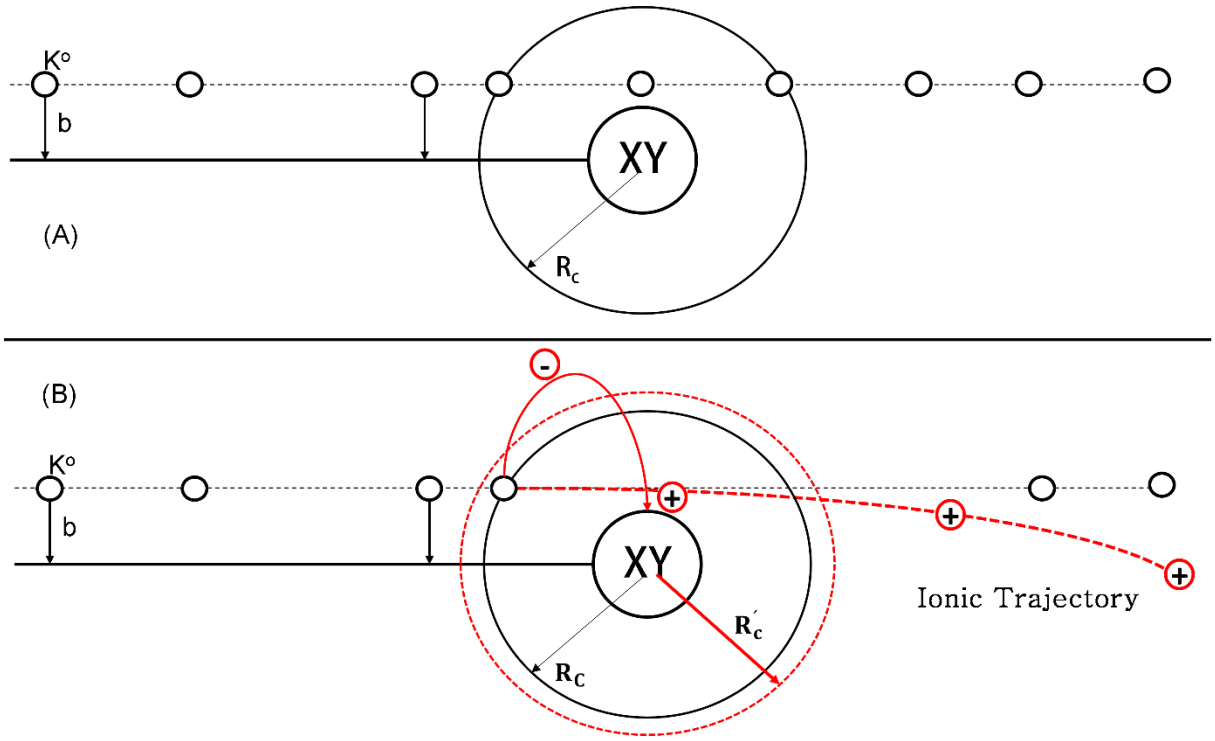

Figure 2 Schematic of ionic trajectory in atom-molecule collisions, b is the impact parameter, O represent neutral potassium, XY molecule in consideration, R_c crossing radius at which electron transfer takes place, R_c' effective radius after transfer of electron. (A) Neutral potassium goes without transferring an electron. (B) Neutral potassium transfers an electron to the molecule (XY) at the first crossing.

Here, $V_i(R, \Phi)$ is an anisotropic R dependent potential describing the $K^+ - XY^-$ interaction, and anisotropy is introduced by dividing the total charge equally on X and Y [77] , $V_i(r)$ is the non-distorted Morse Potential for the free XY^- ion, and ΔE is the asymptotic difference between covalent and ionic states also known as endoergicity of the interaction. In other words, ΔE is the energy difference at infinite separation between the ionic state and the neutral state:

$$\Delta E = I(K^0) - EA(XY) \quad (10)$$

here, $I(K^0)$ is the ionization energy of the neutral potassium, and EA(X) is the electron affinity of the XY molecule. The collision time is defined as the flight time between two crossings.

The expressions for the ionic and covalent potentials assumed that R and r dependence of the surfaces has been decoupled, meaning that the motion of the neutral molecule and molecular ion is not influenced by the projectile. Such can only be true at higher collision energies where collision times are short in comparison to vibrational and rotational motions of the molecule. Hence such considerations can no longer be valid where the collision time is of the order

of rotational or vibrational motion of the molecule. In such characteristic collisions, one can expect fingerprints of the molecular degree of freedom in total or relative cross sections.
The crossing seam or crossing radius R_c is the line of intersection of the two (diabatic) potential surfaces. Immediately after the electron transfer, a negative molecular ion (temporary negative ion) is formed on the repulsive part of the potential. Therefore, the internuclear distance (r) of the molecular ion $X - Y^-$ will gradually widen, leading to a rapid increase of the electron affinity (EA). Here, ΔE is in eVs.
Since,

$$R_C = \left(\frac{14.41}{\Delta E}\right) Å \tag{11}$$

$$R_C = \left(\frac{14.41}{I(K^0) - EA(X)}\right) Å \tag{12}$$

Here the EA of atom X is internuclear distance dependent, thus we can write,

$$R_C(r) = \left(\frac{14.41}{I(K^0) - EA(r)}\right) Å \tag{13}$$

Now, we have a crossing radius which is r dependent and can vary at approach and moving away from the target molecule. This will significantly affect the collision time.
Such approximations in R_c and EA are only valid for the large internuclear distances, where crossing occurs between 6 Å to 30Å for various atom-molecule combinations. At small internuclear distances less than 6 Å, the collision times become comparable to rotational and or vibrational motion of the molecule, hence such approximations become too crude to be included and they do not reproduce the experimental results and even symmetry, and molecular orientation needs to be considered.

2.2.1 Landau− Zenner Method

We will use this method to establish basic terminology to deal with the analysis of the experimental findings.

At the crossing point R_c, the non-adiabatic transitions can occur if the relative kinetic energy is greater than ΔE, subsequently leading to ion−pair formation on ionic and covalent trajectories. If the crossing radius R_c is bigger than the impact parameter b, ($R_c > b$) the crossing point can be passed multiple times in a collision, and the electron transfer can take place, leading to various trajectories. The effective impact parameter can be given by $b = R_c/\sqrt{2}$ [86].

When we assume that the electronic transitions occur at localized crossings, and transitions involve radial coupling, and the nuclear motion is classical, we can use the Landau−Zener Model to describe such transitions.

The LZ model assumes that the external coordinate Q and velocity of the system $\dot{Q}$ is constant in the crossing region, in diabatic representation $Q = Q_0$ (The surfaces cross at this point). Hence the interaction matrix H (Hamiltonian) can be written as,

$$H = \begin{bmatrix} H_0 + \frac{1}{2}\Delta F(Q - Q_0) & H_{12} \\ H_{21} & H_0 - \frac{1}{2}\Delta F(Q - Q_0) \end{bmatrix} \quad (14)$$

and $H_{12} = H_{21} = H_{12}(Q_0)$; $H_0 = H_{11}(Q_0) = H_{22}(Q_0)$;
and $\Delta F = (\partial/\partial Q)(H_{11} - H_{22})_{Q=Q_0}$
The probability for switching from one diabatic surface to another can be given by the following expression according to E. E. Nikitin [96] and [97]:

$$P_{12} = 1 - \exp\left[-2\pi H_{12}^2/\left(\hbar \Delta F \dot{Q}\right)\right] \quad (15)$$

In the above expression, P_{12} varies monotonically from 1 to 0 for a set of parameters, as the velocity $\dot{Q}$ increases. Here ΔF and $\dot{Q}$ are vectors and not scalers in the multidimensions. The approximations in LZ formula to obtain classical paths can also be generalized to more than one dimension [12], the one drawback is that these crossings need to be sufficiently apart.

The transition probability in this model for an adiabatic transition from the covalent to the ionic state or vice versa can be described by the following expression[75].

$$p = 1 - e^{(-\delta)} \quad (16)$$

where,

$$\delta = \left(\frac{2\pi H_{12}^2}{v_{rad} \left| \frac{d}{dR} |(V_{cov} - V_{ion})|_{R=R_c} \right|} \right) \quad (17)$$

In this expression, H_{12} represents the coupling matrix element, v_{rad} the radial component of the initial relative velocity, both evaluated at $R = R_c$, these expressions are in atomic units, and:

$$v_{rad} = V_{rel} \sqrt{1 - \frac{b^2}{R_c^2}} \quad (18)$$

If we assume V_{ion} is coulombic and V_{cov} is constant, the above expression (17) can be simplified to the following:

$$\delta = \left(\frac{2\pi H_{12}^2 R_C^2}{v_{rel}}\right)\left(1 - \frac{b^2}{R_c^2}\right)^{(-1/2)} \tag{19}$$

$$\delta = \left(\frac{\delta_0}{v_{rel}}\right)\left(1 - \frac{b^2}{R_c^2}\right)^{(-1/2)} \tag{20}$$

In the above expression, $\delta_0 = 2\pi H_{12}^2 R_c^2$, v_{rel} is the initial relative velocity of the two colliding particles.

From the above expressions, it is clearly visible that the coupling matrix element, H_{12} exponentially depends on the crossing radius R_c, which is also dependent on the internuclear separation r in the collision process. Therefore, the Landau−Zener transition probabilities are strongly dependent of r via R_c and H_{12}, leading to significant effects on the collision process [89], [90].

Olsen [98] established a semiempirical relation between r and R, by considering exponentially decaying hydrogenic wave functions in the calculation of H_{12}:

$$H_{12}^* = R_c^* \times e^{(-0.86 \times R_c^*)} \tag{21}$$

However,

$$H_{12}^* = H_{12} / \left(\sqrt{I(K^0)} \times \sqrt{EA(X)}\right) \tag{22}$$

$$R_c^* = \left(\sqrt{2I(K^0)} + \sqrt{2EA(X)}\right)/2 \times R_c \tag{23}$$

All expressions are in atomic units, unless otherwise specified.

In the LZ model, the total transition probability for ion−pair formation can be calculated using the following expression:

$$P(b) = P_{COV} + P_{ION} = (1-p)p + p(1-p) \tag{24}$$

p is the non−adiabatic transition probability. It is worth noting that, p is considered the same at both crossing points. Here, in the Landau−Zener (LZ) model, the total cross section can be calculated by integrating the total probability P(b) for a given impact parameter b overall impact parameters, bs, from 0 to R_c.

$$Q = 2\pi \int_0^{R_c} P(b) b \, db = 2\pi \int_0^{R_c} 2p(1-p) b \, db = 4\pi R_c^2 \, F(\upsilon/\delta_0) \tag{25}$$

The function $F(\upsilon/\delta_0)$ is a universal function approaching zero at both very low and very high energies or collision velocities [75]. Here is the summary and key characteristics of some of the

models used previously for introducing the orientation effect of a molecule relative to the approaching projectile.

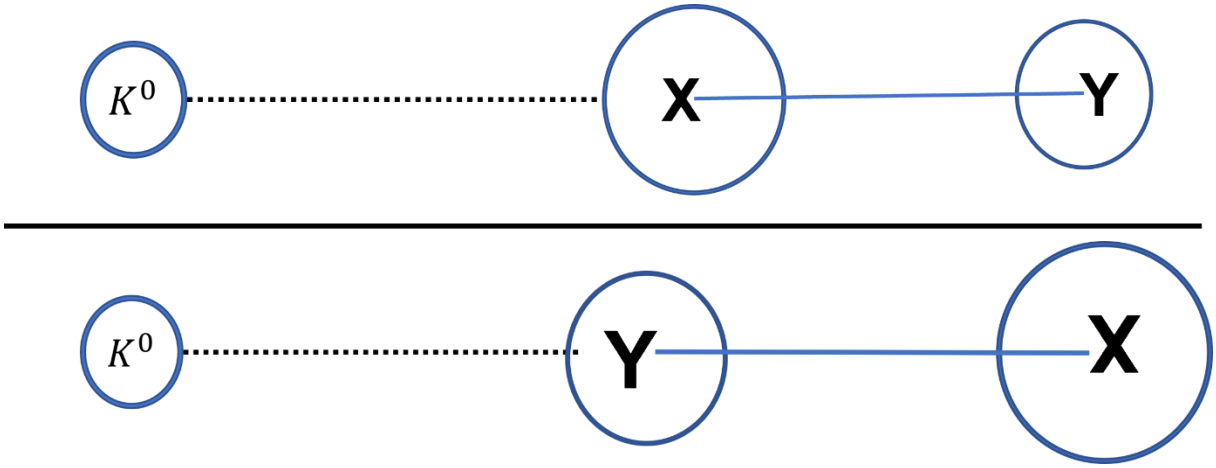

Figure 3 Geometric orientation of the XY molecule as potassium (K) approaches.

This spatial orientation can also affect the collision time; hence it can play a significant role in the electron transfer process at low collision energies.

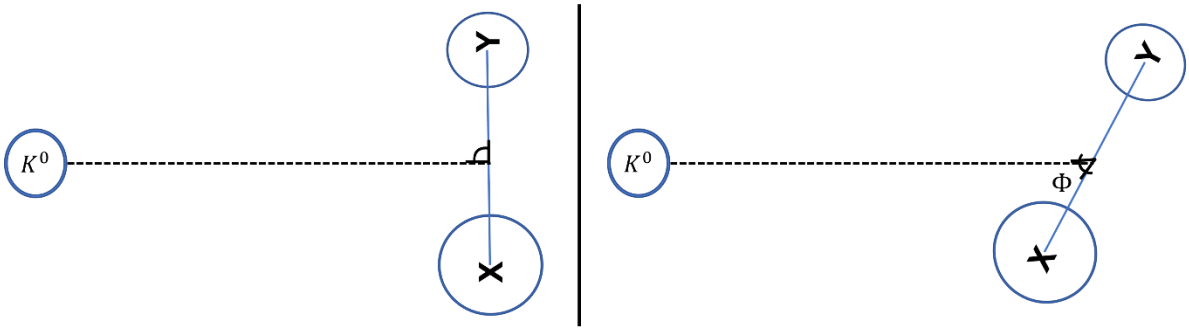

Figure 4 Various orientations of the XY molecule as potassium (K) approaches.

In such configurations, if the projectile's velocity of approach is slow, the molecule can continuously adjust, and the crossing seem can be crossed multiple times. The Projectile motion into continuously adjusted electronic configuration of the molecule, the perturbation to electron density will be significant in electron transfer occurs at the first crossing due to coulombic interaction [95], [99].

2.2.2 Rigid molecule method

In this method, the rotation and vibrational motions of the molecule are considered frozen and hence the molecule is treated like an atom during the collision. Such collisions were reported by M. M. Hubers in the higher collision energy range with shorter collision times, differing

from atom−atom case due to introduction of the coupling matrix element H_{12}, which depends on the spatial orientation of the molecule [77].

2.2.3 Born−Oppenheimer method

The diabatic and adiabatic states in two particle interaction, can be described quantum mechanically. In the Born−Oppenheimer (BO) approximation method it is assumed that there is significantly large mass difference between the projectile and the target's molecule, resulting in considerable velocity differences, hence the nuclear and the electronic motions can be separated, which does not hold for slow atom-molecule collisions below 100 eV collision energy in the lab frame. The BO method holds reasonably well for high energy collisions and has been successfully employed in the past, where electronic and internuclear potentials configurations can be decoupled using the BO method determining the nuclear motion. However, the BO method approximation breaks down when the nuclear kinetic energy is involved in the Hamiltonian, where adiabatic states of the same symmetry may cross each other in the so−called avoided crossing and forcing the corresponding wave functions to change their character considerably [75], [100], [101].

2.2.4 Impact Parameter method

This method works very well in agreement with the rigid molecule process in high energy collisions, and the system is considered to move along a straight-line trajectory given by:

$$R = \sqrt{b^2 + (\upsilon t)^2} \tag{26}$$

where, the reactant or product state, are not a concern. Here, b is the impact parameter, υ is relative velocity of the collision. This method was developed by Spalburg and Klomp [102] using potentials near the crossings according to LZ assumptions, for a single passage through the crossing region, i.e., for half collision. In this method the probability to find the system in lth vibrational level of the ionic state after passing the crossing zone e.g., the Franck-Condon overlap between the ground vibrational state of the molecule and lth vibration level of the molecular ion can be estimated:

$$|C_l|^2 = \left[1 - \exp\left[-2\pi H_{12}^2/\left(\hbar \Delta F \dot{Q}\right)\right]\right] \langle \upsilon_l | \upsilon_0 \rangle^2 \tag{27}$$

Here C_l, is the probability to find the system in the ℓth vibrational level after passing the crossing zone. $\langle \upsilon_l | \upsilon_0 \rangle$ denotes the Franck−Condon overlap between the vibrational ground state of the molecule υ_0 and ℓth vibrational level of the molecular ion υ_l. As such:

1. In the high velocity limit where the target molecule can be considered rigid, the transition probability is the product of a normal Landau−Zener transition probability and a Franck−Condon factor. The high velocity limit is defined by the requirement that the time to pass the dynamic width, dynamic width (ΔR_d) of the crossing region, which then determine the collision time [97]:

$$\Delta R_d = \sqrt{2\hbar\dot{Q}/\Delta F} \tag{28}$$

2. In the low velocity limit, the transition probability can be estimated by the following expression [97] which is identical to that obtained by Bauer, Fisher, and Gilmore [103], so:

$$|C_0|^2 = 1 - \exp\left(\frac{-2\pi H_{12}^2 \langle \upsilon_1 | \upsilon_0 \rangle^2}{\hbar \Delta F \dot{Q}}\right) \tag{29}$$

3. The low velocity limits the static width (ΔR_s, the measure of the change in effective internuclear separation due to electron transfer), and it is calculated using the following expression [97]:

$$\Delta R_s = 2H_{12}/\Delta F \tag{30}$$

By treating the vibrational degree of freedom classically, it can be incorporated in the surface hopping trajectory method. At very low velocities, this method reduces to the Bauer-Fisher-Gilmore model [103]. This model assigns a separate covalent potential surface to each vibrational level of the molecular target and separates the ionic potential's surface for each molecular anion for the ion−pair formation. Here each surface is a function of the internuclear distance R and the molecular orientation with respect to the projectile atom.
This is one of the most powerful methods to analyse vibronic excitation in curve crossing but fails to predict behaviour of transition probabilities at very low energy collisions [91] . However, in this method in the high velocity limit, the dynamic width underestimates the separation between the two crossing, and in the low velocity limit, the static width overestimates the separation between the two crossings.

2.2.5 Franck−Condon Principle

The Franck-Condon Principle, based on Born−Oppenheimer approximation, allows seperation of electronic and nuclear wave functions given the total wave function. Classically, the Franck-Condon principle is the approximation that an electronic transition is most likely to

occur without changes in the positions of the nuclei in the molecular system. Such resulting state called as Franck−Condon state, occurring vertical transition. In this case, electron transfer processes in atom-atom collisions or fast atom-molecule collisions in high energy collisions can be explained very well [12], [97].

Quantum mechanically, it states that vibronic transition intensity is proportional to the square of the overlap integral between the vibrational wavefunctions of the two states that are involved in the transition. However, if $t_{coll} \approx t_{vib}$, the effect the role of vibrational motion has been considered previously in diatomic molecules and their negative ion states.[102], [104], [105].

However, in diatomic molecules, change in bond length can occur through stretching and/or pre−stretching, considering 3N−5 (N being number of atoms in the molecule) degrees of freedom for a linear molecule[91]. When we consider the polyatomic molecules, there can be 3N−6 degree of freedom (non−linear molecule), resulting in increased molecular vibration in comparison to diatomic molecules, leading to change in bond length through various vibrational motions e.g., stretching, bending, rocking, wagging, twisting, and out−of−plane motions. It is with these vibrational motions that can influence the probability of ion−pair formation in polyatomic molecules, if the collision times are of same order as these vibrational motions, and cross−sections may carry imprints of such effects[76], [106].

2.2.6 Surface hopping trajectory method

In atom−molecule collisions, a two−state problem can be used, and considers that the electronic states under consideration have no influence from the other neighbouring electronic states. All nuclear motion is treated classically, and the transition probabilities are calculated quantum mechanically, and in doing so, the vibrations and /or rotations of the molecule are treated classically. This was implemented by Tully and Preston[107], [108] to account for loss of electron-nuclear correlation in Ehrenfest method[109], [110] In these cases, it leads to decoherence and recoherence/interference problems, resulting in the errors in the transfer of population between electronic states, thus in the dynamics of the nuclei[111], [112]. These issues are related to non-adiabatic dynamics, a recent review article explains this problem very well in section 2 of Nelson *et al* [113].

2.3 Summary

A summary of different approaches using various models has been presented along with their relevance regarding the collision energy region considered. Here in Figure 5, we depict the

reduced cross sections as a function of the ratio of velocities, v_{rel} and v_{cr}. Three different functions F_1 , F_2, and F_3 were used earlier to determine the nature of the cross sections of electron transfer yielding ion −pair. Here v_{cr} is critical velocity and defined as $v_{cr} = 4\pi H_{12}^2 R_C^2/\sqrt{2}$.[77] In such cross sections, F_1 represent atom-atom case, while F_2 represent atom−molecule collisions, F_3 is considered unity in the low collision energy region representing probability at second crossing when first crossing has been passed adiabatically.

I. F_1 represents the cross−section for ion−pair formation in the atom-atom case.
II. F_2 represents atom−molecule collisions, assuming no bond stretching.
III. F_3 represents, complete stretching of the molecular bond or dissociation of the XY^- ion, considering an ionic trajectory, leading to a probability at the second crossing $p_2 \approx 1$ at these low velocities.

It is with these effects that we will deal with some of the experimental data while analysing the results from electron transfer experiments in chlorinated unsaturated hydrocarbons. Such effects are not only relevant for dynamical stretching of the molecular bond in the femtosecond time scale but also for reactive collisions.

Reduced cross-sections, which are achieved by averaging orientational effects over 4π solid angle in atom−molecule collisions are defined as $Q = 4\pi R_c^2 F(K/v)$, where $F(K/v)$is a well-known function of reduced velocity[114], these F_1, F_2, and F_3 are derived from this universal function[77]. and assume that F_3 is unity (probability at second crossing when first crossing has been passed adiabatically) at low energy collisions.

According to the universal function $F(v/\delta)$, according to Faist and Levine[115] which states that in the very low and very high energies the cross−section should tend to zero, here however F_3 is constant, considering first crossing was crossed adiabatically. Which suggests either the possibility of first crossing being crossed diabatically needs to be considered, and/or interference of such crossings needs to be considered.

It is clearly visible with these assumptions that in atom-polyatomic molecule collisions, the probability of electron transfer cannot be considered like in the case of F_3, **where the effect of reneutralization of the projectile is completely ignored**. The shift in the peak of F_2 with respect to F_1 is explained as effective lowering of the H_{12} coupling by averaging it through all the molecular orientations. At the same time **the effect of close lying excited states on the adiabatic coupling** has been completely ignored. Such interference can be significant in the low velocity collision regime, leading to drastic variations in the cross sections as a function of the collision time. The mere existence of other neutral states due to interaction with excited atoms can introduce more intersections with the ionic state and the electron transfer can occur at any crossing. The switching between ionic and covalent configuration only occurs when the so-called adiabatic principle (continuous readjustment of electrons or electron cloud density

in the case of molecule with respect to approaching particle) is valid. This continuous adjustment involves transfer of the valence electron from the alkali atom to the molecule, which can be considered for the case for F_3. When the electronic configuration does not change, such can be considered for F_1 in a diabatic state. For further details on the analysis of these functions, a topical review by Kleyn and Moutinho serves as a very good starting point[75].

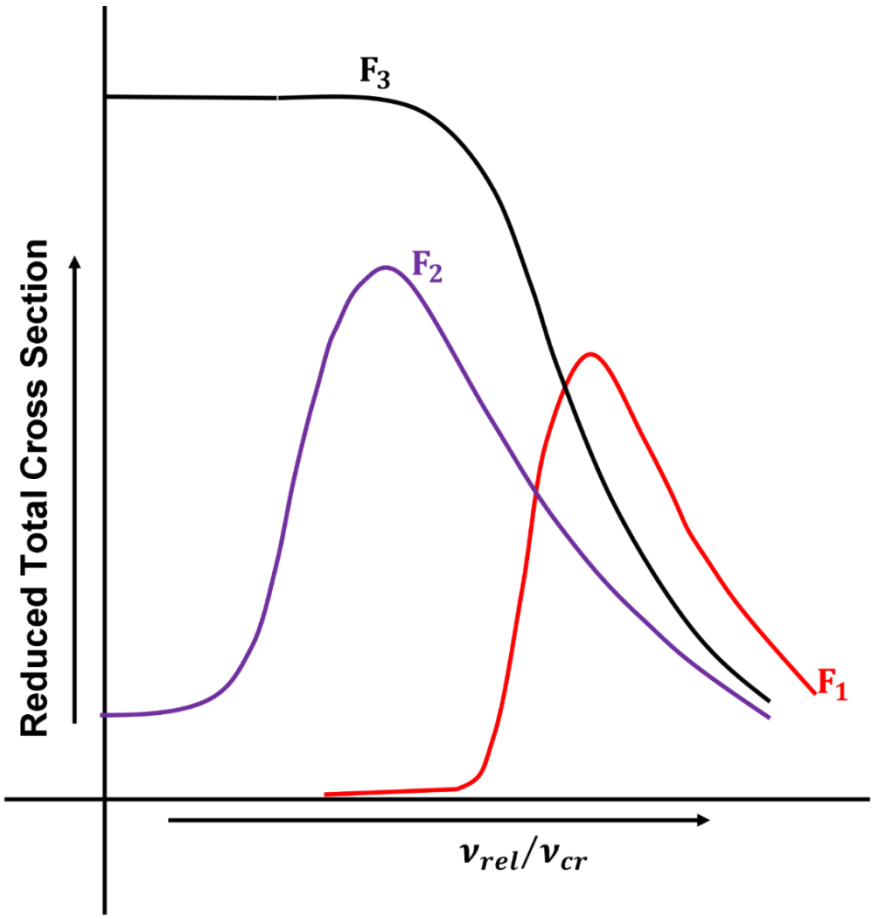

Figure 5 Representation of the reduced total cross sections for electron transfer in three different cases as a function of reduced velocity. Adapted from [75].

3.

EXPERIMENTAL SET UP

In this chapter, a detailed description of the experimental setup along with the procedures used to conduct the experiments and the methodology employed to analyse the results obtained at Laboratory for Atomic and Molecular Collisions (Laboratório de Colisões Atómicas e Moleculares, LCAM) at CEFITEC, Department of Physics, Universidade NOVA de Lisboa will be discussed.

3.1 Overview

The crossed molecular beam setup used to perform electron transfer experiments in neutral potassium (K) − neutral molecule collision experiments yielding ion−pair formation, is composed of two different high vacuum chambers interconnected by a manual interchamber valve. Both chambers are independently pumped to achieve high vacuum with base pressures of typically 2×10^{-7} mbar. The first chamber where the neutral alkali beam is produced is termed Beam Production Chamber and the second where the collision happens is termed Collision Chamber.

This crossed beam experimental setup is a modified and updated version of the one discussed previously [116]. The ion source and collision plane sit 417 mm apart from each other. A detailed solid works drawing of the setup can be found in the following figure, with main components indicated as following:

- Beam Production Chamber;
- Langmuir Taylor Detector;
- Collision Region;
- Molecular Oven;
- Energy Loss Analyzer;
- Collision Chamber.

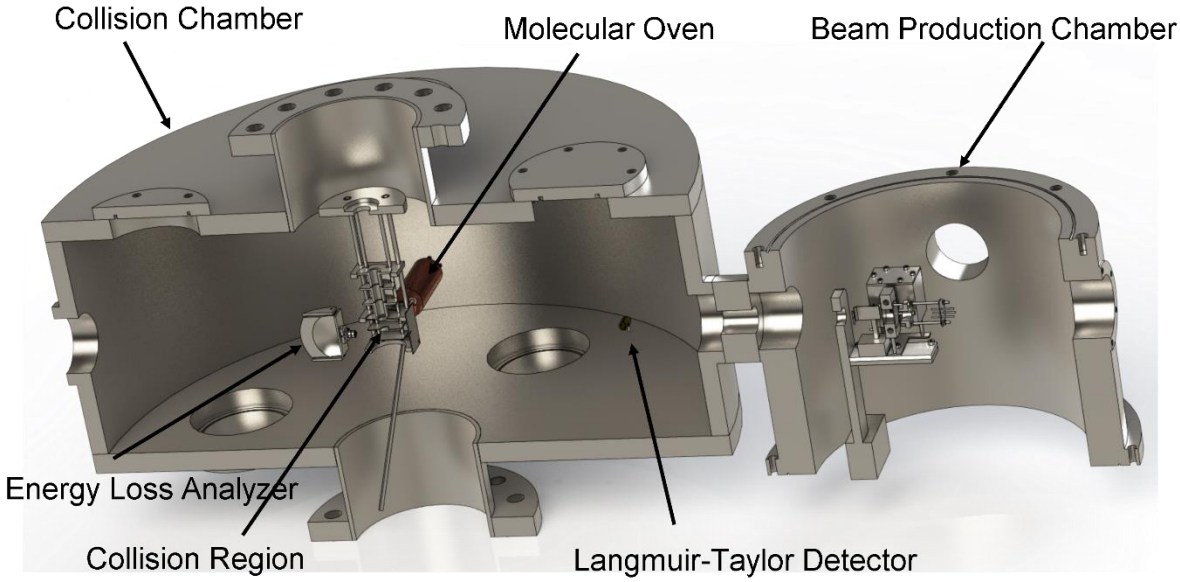

Figure 6 A Cross−Sectional drawing of the experimental setup with some of the main components in the potassium and collision chambers.

3.2 Beam Production Chamber

This chamber comprises a Varian 0184 diffusion pump backed by a two-stage rotary E2M18 Edwards pump to achieve 2×10^{-7} mbar. The diffusion pump is used due to potassium vapour in the chamber. The beam production chamber houses a commercial K^+ ion source, purchased from HeatWave Labs, used to generate a K^+ beam of a desired energy (from 9−10 eV up to 1keV).

The potassium oven houses a potassium chunk, which is resistively heated with a combination of two cylindrical resistors of 240 V, 200 Watts to vaporize the solid potassium. This vaporized potassium passes into the charge exchange chamber, where the K^+ beam passes through and resonantly charge exchanges. This charge exchange chamber is kept 20℃ higher than the temperature of the potassium oven, in order to avoid any potassium deposition thus blocking the 1 mm diameter appertures beam passage path.

In order to avoid any beam that did not resonantly charge exchanged, we employ a set of deflecting plates next to the charge exchange chamber exit to deflect all the K^+ beam and thus achieving the pure hyperthermal neutral potassium beam. The potassium beam can be accelerated from a few eV up to 1 keV, with a beam resolution at FWHM of ~0.5 eV.

The heating temperature in the potassium oven and charge exchange chamber is controlled through independent PID−Proportional−Integral−Derivate (CAL3300) units. The optimum temperatures in the potassium oven and charge exchange chamber are 120℃ and 140℃, respectively. The temperatures in both potassium oven and charge exchange chamber are

monitored using independent Pt100 type sensors. The charge exchange efficiency is extimated to be approx. 20 % relative to ionisation at 100 eV lab frame, with the K^+ ion source and the K^+ beam currents measured from the deflecting plates after charge exchange. This methodology has been very well established by Aten and Los[9]. The figure depicts from a top view all the main components in the beam's production chamber.

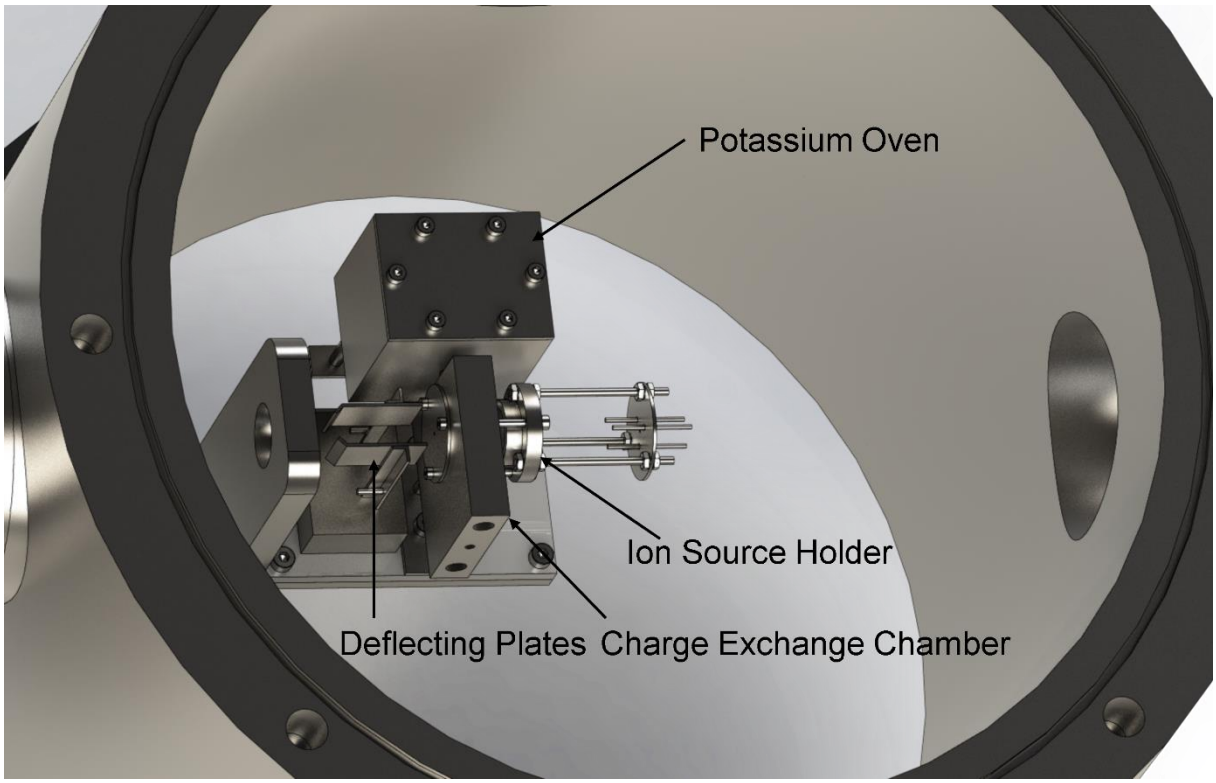

Figure 7 Main Components in the K Beam's Production Chamber.

3.3 Collision Chamber

The collision chamber is interconnected to the beam production chamber through an inter-chamber valve and is differentially pumped. Previously it was pumped through a set of diffusion Edwards E06 and Leroy Somer LS 90S51 Alcatel rotary pumps [10], yet a recent upgrade has now allowed to achieve an environment free of any oil contamination from the pumps. The diffusion pump was replaced by a Pfeiffer HiPace 2300 P06 302 with TC1200 turbo molecular pump, DN 250 CF−F with a pumping speed for Ar of ~1800 l/s [117], while the rotary pump was replaced by a dry scroll pump from Pfeiffer ACP 28 [118], allowing therefore to avoid oil contamination from the background. The collision chamber houses various sub systems needed to allow performing experiments. Some of these are listed as following.

3.3.1 Langmuir−Taylor Detector

It is the first instrument that encounters the neutral hyperthermal beam as it enters the collision chamber and measures the current of the neutral potassium beam. The detector is made of a cylindrical collector connected to an electrometer and an iridium filament of 0.125 mm thickness with 99% purity (Goodfelow). The iridium filament passes the collector longitudinally as is schematically depicted in Figure 8. The filament is biased with +60 V with respect to ground with a typical current of approx. 0.63 A reaching a temperature of $\sim 510\,K$. The neutrals that hit the filament are desorbed as positive ions and deflected towards the collector and measured as a current through a high sensitivity Keithley 6517A electrometer [119].

The choice of an iridium filament relative to a tungsten, resides on the fact that the former has a higher work function (approx. 5.8 eV)[120]. It increases the ionisation efficiency of the potassium to higher values (close to 1) and avoids negative ionisation that may occur for elements with large electron affinity [121], thus ensuring accurate measurements of the neutral beam current.

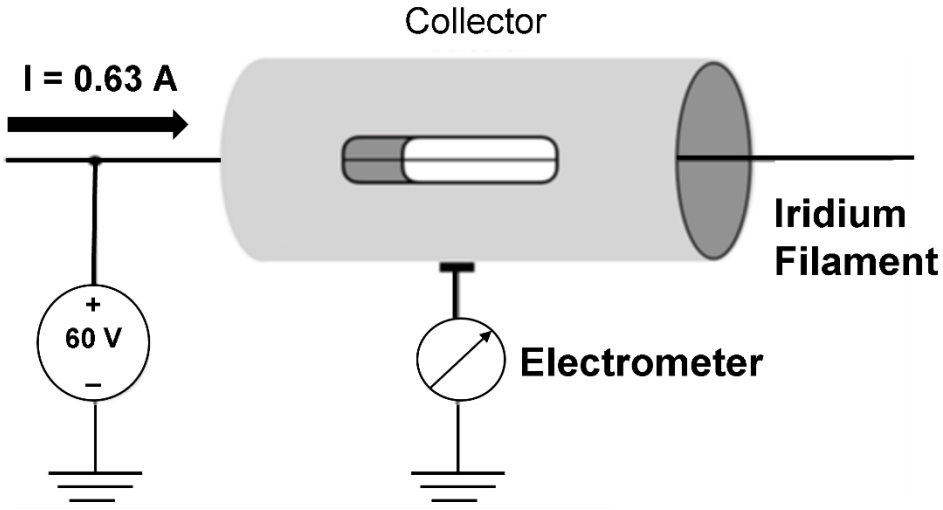

Figure 8 Schematic of the Langmuir Taylor Detector, adapted from [10]. The length of the opening in the collector is 5 mm with a height of 2 mm and the iridium filament passes through the centre of the collector.

3.3.2 Time-of-Flight Mass Spectrometers

The collision chamber can house two different kinds of mass spectrometers: a home built Linear Time−of−Flight Mass Spectrometer (L−TOF−MS) or a commercial reflectron Time−of−Flight Mass Spectrometer (r−TOF−MS) supplied by Kore Technologies, UK. Both TOF−MS cannot be accommodated at the same time, depending upon the type of molecules being investigated, yet they can be assembled prior to the sort of collision dynamics one wants to investigate. Note that these two TOF−MS have in total ~ 1.4 m flight path. The advantages

of using such spectrometers are several but most important features are the capability to obtain all ionic species simultaneously unlike quadrupole mass spectrometers. All other characteristics like mass resolution, working principles of this combination of the experimental set up has been established previously and thus will not be repeated further [10], [116].

3.3.2.1 Linear Time-of-Flight Mass Spectrometer

This is a Wiley McLaren[122] based dual−stage linear time−of−flight mass spectrometer. In the second stage, introduction of a second extraction region allowed modification of the space-focusing distance, achieving higher mass resolution in comparison to a single stage TOF−MS.

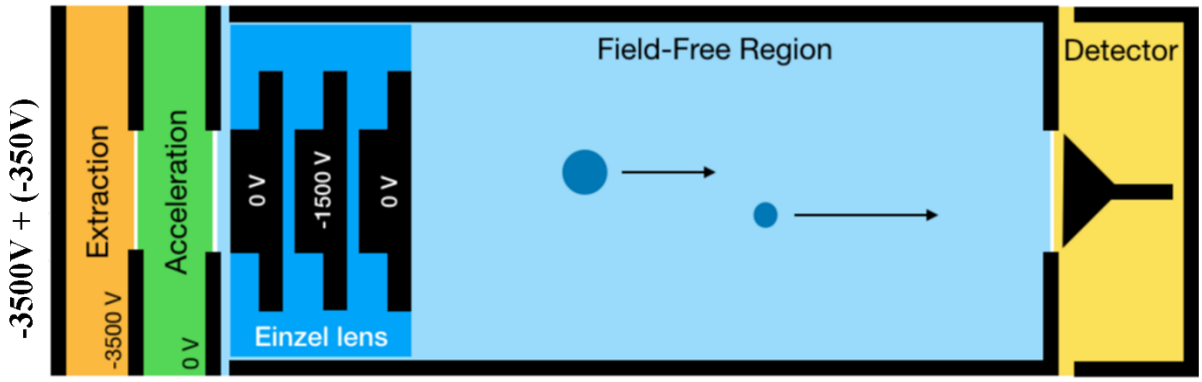

Figure 9 Linear Time-of-flight Schematic used in this thesis, adapted from Cunha[10].

In the present L−TOF−MS a total mass resolution of approx. 125 was achieved and was calibrated using the anionic species formed in collisions of neutral potassium atoms with neutral CH_3NO_2 molecules. This chemical compound was used due to its well−known negative ions formed in electron transfer experiments. All other parameters and characterization were similar as previously discussed in ref. [116], and the set of measurements shown in this thesis result from working on continuous mode of the potassium beam. One advantage of this type of TOF−MS over r−TOF−MS is the information one can obtain from the shape of the TOF mass peaks regarding kinetic energy release imparted to a fragment ion in the unimolecular decomposition of the temporary negative ion formed. In this configuration, such information is retained however in r−TOF−MS, where such is lost due to the reflectron geometry compensation effect. All the experiments on chlorinated benzene molecular compounds (C_6H_5Cl, C_6D_5Cl, $C_6H_{11}Cl$, and C_6Cl_6) were performed using the L−TOF−MS, where relevant information about the collision dynamics has been obtained from the kinetic energy release distributions (see Section 4.3.1).

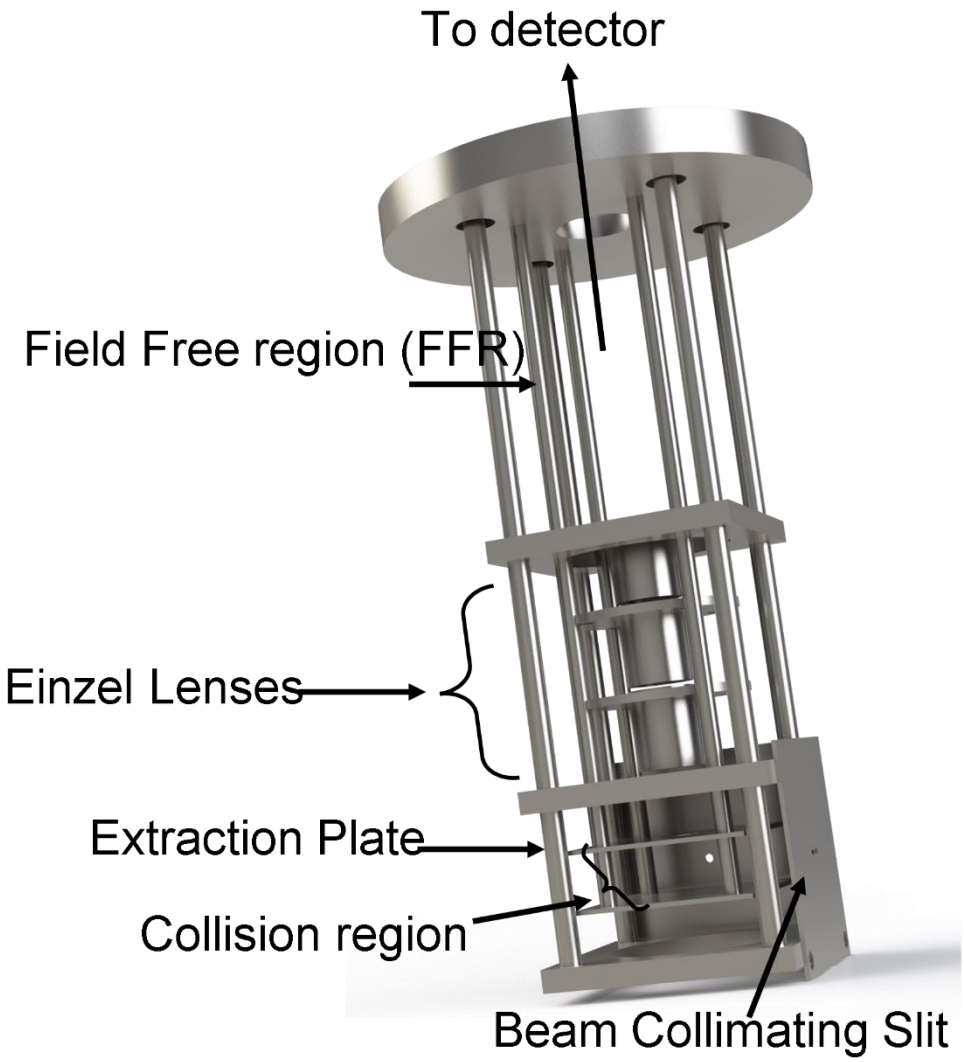

Figure 10 Custom built Wiley Mclaren type L−TOF−MS. The two plates in the collision region are 12 mm apart and the ions formed are extracted through a 10 mm aperture.

3.3.2.2 Reflectron Time-of-Flight Mass Spectrometer (r−TOF−MS)

A r−TOF−MS, first proposed by Mamyrin [123], [124] can achieve higher mass resolution in comparison to a L−TOF−MS due to the presence of an ion-mirror, which is comprised of a series of annular electrostatic lenses placed at the opposite end of the drift tube with respect to the optical bench. A repulsive voltage, V_r is applied to the lenses to deflect the ions into the detector, i.e., the ions are decelerated to zero velocity turn around and are accelerated backwards exiting the ion mirror with the same initial kinetic energy. Thus, with such configuration one loses information on the kinetic energy imparted upon formation of a negative ion. However, this improves the mass resolution significantly. Our current set−up, assembled in the crossed molecular beam experiment is a dual−stage reflectron−TOF mass spectrometer with an additional stage that decelerates the ions by a high electric field losing part of their

kinetic energy before entering the ion mirror. The detector in used is a Chevron micro channel plate with 25 mm diameter wide. Each micro channel is a continuous dynode electron multiplier. Currently, the maximum mass resolution achieved is around 1600, and further details of the setup can be found elsewhere [10].

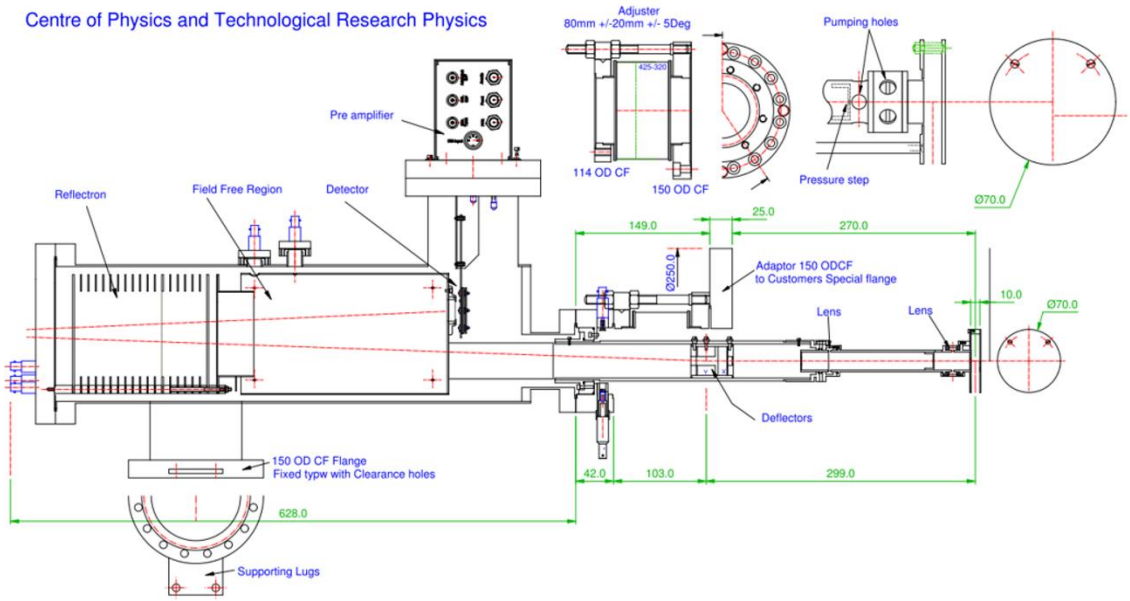

Figure 11 Schematics of the reflectron TOF−MS supplied by Kore technologies UK. Length values in mm.

3.3.3 Hemispherical Energy Loss Analyzer

The analyser (Figure 12) consists of two concentric hemispheres and by applying a potential difference between them acts as a narrow energy filter for charged particles. With this implemented energy loss analyser, it is possible to work in two energy modes: Sector field Sweep (SFS) and Constant Transmission. In SFS, a potential is scanned in one electrode, while the other is kept constant, sweeping the trajectory of the transmitted ion, keeping $\Delta E/E_0$ constant. In this case, the resolution ΔE (Full Width at Half Maximum) varies with respect to the energy of the entering ion at a given energy E_0.

In the second mode, a constant potential V_p, between the hemispheres is implemented and the centreline potential V_0 is scanned, thus, ensuring the constant resolution throughout the scan. This methodology was implemented to obtain all the results discussed in this thesis. The complete detail of the energy loss analyser can be found somewhere else [10]. In the present experimental configuration, a beam resolution (FWHM) of up to approx. 1 eV can be obtained.

In energy loss spectroscopy, commonly related with electron scattering experiments, the study of the energy distributions of electrons after being scattered from atoms or molecules can provide relevant insight about the electronic structure [125] and/or chemical information of the target atom/molecule being probed [126]. Further in our alkali energy loss spectroscopy measurements, we measure the K^+ ion energy distribution post collision in the forward scattering direction at ~0°. Such experiments have provided relevant information as to prevalent electronic transitions in the transient negative ion formation [127]. Note that such experiments were not performed in coincidence with TOF−MS experiments.

The outer hemisphere has a radius of 91 mm and the inner hemisphere 71 mm, thus providing an effective centre radius of 81 mm.

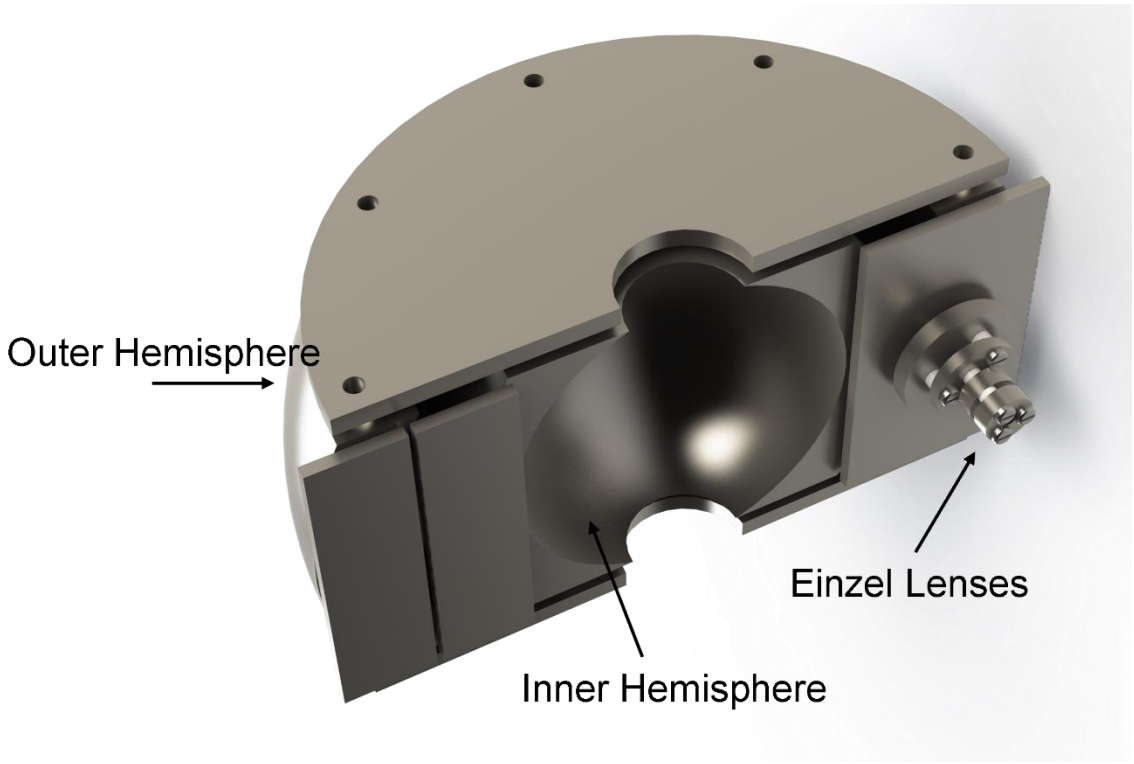

Figure 12 Hemispherical Energy Loss Analyzer installed in the Collision Chamber of the crossed molecular beam setup, LCAM.

3.4 Vacuum System

The configuration to efficiently pump the experimental setup and achieve high vacuum in both chambers is schematic depicted in Figure 12. Symbols are used according to the norm DIN 28401 (2008−03).

1) Rotary Pump	6) Gate valve	11) Vacuum gauge control unit with dial indicator
2) Electro-magnetic valve	7) Beam Production Chamber	12) Penning Gauge

3) Membrane valve	8) Collision chamber	13) Vacuum gauge control unit with dial indicator
4) Diffusion Pump	9) Turbo−molecular Pump	14) TOF−MS
5) Baffle	10) Flexible tube	15) Pirani Gauge

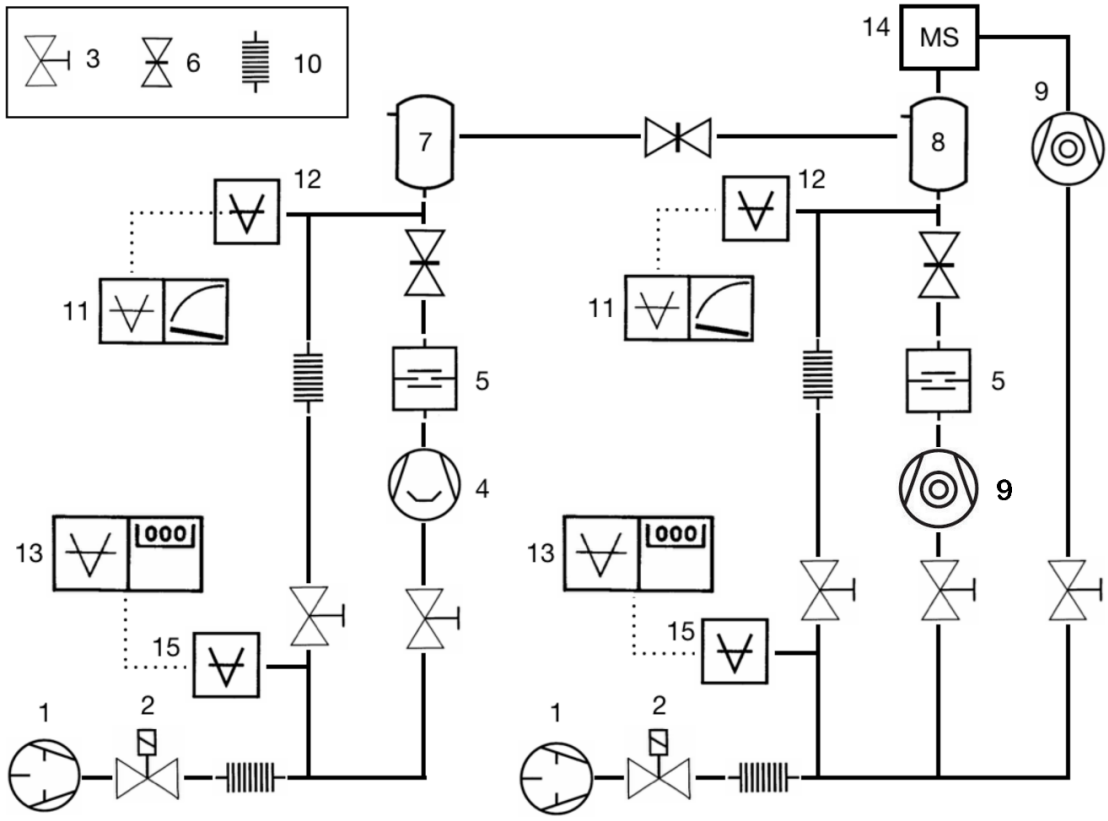

Figure 13 Schematic of pumping mechanism in experimental setup.

3.5 Summary

From these different combinations of the experimental apparatus, the following key information in ion-pair formation can be inferred:

- The ionic thresholds of formation can be obtained.
- Kinetic Energy Release imparted to ionic fragments in the case of L−TOF−MS have been thoroughly obtained.
- Branching ratios of various anionic fragments in charge−transfer experiments giving valuable insight into the competition mechanisms for anionic formation in a wide range of collision energies.
- Alkali energy loss spectroscopy provides, in some particular cases (e.g., in $K + C_6Cl_6$, $K + CCl_4$ collisions), detailed insight about the electronic as well as vibrational state spectroscopy.

- Relative probability of ion−pair formation (total relative cross sections) can be obtained in a wide energy range (from threshold up to 1 keV).

4.

COLLISION DYNAMICS OF CHLORINATED BENZENES

In this chapter a detailed overview of charge transfer processes in 4 different chlorinated benzenes will be provided in an extended collision energy range. Such experiments are accompanied with kinetic energy release distribution (KERD) studies and relative cross-section for Cl^- formation from chlorinated benzenes upon potassium impact. This chapter is also based on **"Cl^- Kinetic-energy release distributions from chlorobenzene and related molecules in electron transfer experiments"** published in *Eur. Phys. J. D (2021)* **75**:*294*. as a special issue dedicated to the late Prof. Vincent McKoy.

4.1 Introduction

Electron transfer from neutral potassium (K) atoms in collisions with neutral molecules (M) yielding ion-pair formation, generates a cation (K^+) and a metastable temporary negative ion (TNI) with an excess of internal energy $(M^-)^\#$ that may result in further fragmentation. In such collision induced dissociation processes, since the energy can be chosen larger than the threshold of electron transfer, i.e., ΔE = IE(K) – EA(M), with IE(K) the ionisation energy of the potassium atom and EA(M) the electron affinity of the molecule, a fragment anion and a neutral radical may be formed. Yet if the lifetime of the TNI is long enough, intramolecular energy redistribution may occur competing with dissociation, the latter being classified either statistical or direct. Such processes have been reported in our laboratory in different molecular targets investigated in a wide collision energy range, typically from a few eV up to 1 keV. For the sake of example, we note particular attention to cyclic and non-cyclic polyatomic molecules. In case of the cyclic chemical compounds an efficient redistribution of the excess energy through the different internal degrees of freedom was observed in radiosensitizers, e.g., nitroimidazoles[57], [58] and pyrimidine[128]. Regarding non−cyclic molecules these have

shown to serve as efficient doorway for enhanced bond excision due to the mainly repulsive nature of their lowest-lying anionic potential energy surfaces, as are the cases of nitromethane[17] and tetrachloromethane[129].

From the time-of flight (TOF) analysis of fragment anions formed in electron transfer experiments, the shape and width of detected features contain relevant information on the collision dynamics. In particular, the kinetic energy gained by a given negative ion resulting from bond breaking of the TNI can be derived. As a result of a methodology used to explore the underlying molecular mechanisms resulting in dissociation of chlorobenzene and chlorinated related molecules, we present for the first time a comprehensive investigation of Cl^- kinetic−energy release distributions (KERDs) from C_6H_5Cl, C_6D_5Cl, $C_6H_{11}Cl$ and C_6Cl_6 in electron transfer experiments in a wide collision energy range.

The formation of chlorobenzene–h_5 negative ions has been reported on several occasions either in dissociative electron attachment (DEA)[130]–[137] or electron transmission spectroscopy experiments[138]–[141]. This molecular anion has been considered as a prototype for radiosensitisation due to its closely related resemblance to halo pyrimidine molecules[56], [142], [143]. Other studies on C_6H_5Cl relevant to the present work are electron impact spectroscopic experiments[144]–[146], theoretical investigations on potential energy surfaces[147] and electronic structure[148], as well as references therein. Regarding chlorobenzene–d_5, we are only aware of a DEA study yielding Cl^-, where a close comparison with its hydrogenated analogue (C_6H_5Cl) revealed that deuteration has no appreciable effect in the magnitude of the cross-section[149].

As far as the formation of Chlorocyclohexane and hexachlorobenzene negative ions is concerned, a literature survey revealed no information for the former, whereas for the latter just the formation of $C_6Cl_6^-$ has been reported[150], [151]. Nonetheless, we have recently performed in our laboratory a thorough investigation on the formation of anionic states of C_6Cl_6 probed in electron transfer experiments for the energy range 10–150 eV (laboratory frame), with such study being supported by state-of-the art quantum chemical calculations[127].

4.2 Experimental Method

Time-of-flight (TOF) mass spectra of product anions formed in electron transfer experiments in collisions of neutral potassium (K) atoms with target molecules (C_6H_5Cl, C_6D_5Cl, $C_6H_{11}Cl$ and C_6Cl_6), were recorded at different lab frame energies. The spectra have been obtained in a crossed molecular beam setup which was previously described elsewhere.[152] Briefly, a projectile beam of neutral hyperthermal K atoms crosses at right angles an effusive target molecular beam and the product anions formed in the electron transfer process are TOF

mass analysed. The hyperthermal K beam is produced in a charge exchange chamber from the interaction of accelerated K^+ ions emitted from a commercial ion source (HeatWave, US) in the range of 10 to 150 eV in the lab frame with gas-phase neutral potassium atoms from an oven source. The intensity of the neutral K beam prior to collisions with the target molecules is monitored using a Langmuir−Taylor type ionisation detector, before and after collecting the mass spectra. The TOF mass spectrometer used is a dual−stage Wiley−McLaren type, where the extraction region is formed by two parallel plates (one of it is a tungsten mesh with high transparency) placed 12 mm apart and operated at an extraction voltage of 292 Vcm^{-1} with a time duration of 1 μs in an 80 μs duty cycle. Anions are detected by a channel electron multiplier (CEM) with an effective area of 1 cm diameter. The TOF anion yield is normalized considering the primary beam current, pressure, and acquisition time. The typical base pressure in the collision chamber was 4×10^{-5} Pa and the working pressure was 1×10^{-3} Pa. TOF mass calibration was performed based on the well-known anionic species formed after potassium collisions with nitromethane[153] and tetrachloromethane[129].

Chlorobenzene–h_5 and –d_5, chlorocyclohexane and hexachlorobenzene samples were supplied by Sigma Aldrich with a stated purity of 99.9%, 99%, 99% and ≥ 98%, respectively. C_6H_5Cl, C_6D_5Cl, and $C_6H_{11}Cl$ were degassed through repeated freeze-pump-thaw cycles. C_6Cl_6 solid sample was used as delivered and gently heated up to 340 K through a temperature PID (proportional-integral-derivate controller) unit. To test for any thermal decomposition products from hexachlorobenzene molecular beam, TOF mass spectra were recorded at different temperatures and no differences in the relative peak intensities as a function of temperature were observed.

4.3 Results and Discussion

In this chapter two kind of results are reported, based on the two different categories.

- Kinetic energy release distributions
- Total relative cross-sections for Cl^- formation.

4.3.1 Kinetic-energy release distributions (KERDs)

In this sub−section we present a concise description of the methodology used to extract the kinetic−energy release from the width and shape of the TOF mass spectra of chlorine anions formed in electron transfer experiments. This approach has been used before where a comprehensive description can be found in Limão-Vieira et al.[154] and Rebelo et al.[155] Briefly, in the unimolecular dissociation mechanism of a temporary negative ion (TNI) yielding two

fragments with masses m_1 and m_2, the kinetic-energy release ε_d of a fragment anion formed with an isotropic velocity distribution is given by:

$$\varepsilon_d = \frac{1}{8\mu}(F.\Delta t)^2 \tag{31}$$

with μ being the reduced mass of the system, F being the electrostatic extraction field and Δt the difference in extraction time between two fragments emitted in forward and backward directions.

The kinetic-energy release distribution, $D(\varepsilon_d)$, is closely related to the intensity and velocity of the primary K beam, the density of the target molecular beam, the dimensions of the interaction volume and $Q(v)$ the velocity dependent emission of the anionic fragments per solid angle. The maximum velocity component (v) of a fragment anion impinging on the detector is reached by those ions which are well-aligned with the extraction field, i.e., $v \approx v_0$ (v_0 the initial velocity). The maximum velocity component normal to the TOF axis (v_m) is given by $v_m = \frac{r}{t}$, with r the detector radii and t the total flight time. The flight time is proportional to $\sqrt{m}$ so the maximum $\frac{1}{2}mv_m^2$ is constant and independent of m or v_0.

The current TOF configuration yields $\varepsilon_m = \frac{1}{2}mv_m^2 \approx 0.03$ eV. We can now express $Q(v_0)$ as a function of the experimental Δt and $I(\Delta t)$ functions, the latter obtained by measuring the intensity of the TOF mass feature, according to ref.[156] as:

$$Q(v_0) = \frac{F}{2A}\left\{1 + \frac{3}{4}\frac{v_m^2}{v_o^2} + \cdots\right\}\Delta t^2.I(\Delta t) \tag{32}$$

where the constant A is a function of ε_m[156], and so the KERD can now be given as:

$$D(\varepsilon_d) = \frac{1}{A}\left\{1 + \frac{3}{4}\frac{v_m^2}{v_o^2} + \cdots\right\}\Delta t.I(\Delta t) \tag{33}$$

this provided that $\frac{v_m^2}{v_o^2} \ll 1$. The quadratic term in equation (33) can be ignored for $\varepsilon_d >$ 0.1 eV, thus $D(\varepsilon_d)$ is given as:

$$D(\varepsilon_d) = \frac{1}{A}.\Delta t.I(\Delta t) \tag{34}$$

Negative ion formation in potassium collisions with C_6H_5Cl, C_6D_5Cl, and $C_6H_{11}Cl$ yields only chlorine anions, whereas in the case of C_6Cl_6 the main anion signal intensities have been assigned to the undissociated parent anion ($C_6Cl_6^-$) and the formation of $C_6Cl_5^-$ and Cl^-, with

other minor contributions from ions resulting from the loss of Cl units and ring breaking due complex internal reactions within the TNI[127].

Kinetic-energy release distributions for the dominant fragment anion Cl^- have been obtained from the TOF mass spectra induced by potassium electron transfer to chlorobenzene–h_5 and –d_5, chlorocyclohexane and hexachlorobenzene Figure 14 at collision energies, in the centre-of-mass frame, of about 12, 40 and 118 eV.

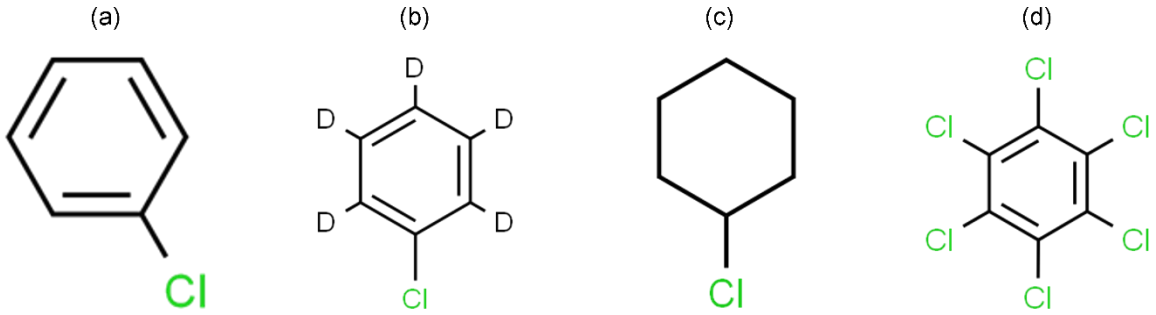

Figure 14 Molecular structure schematics of C_6H_5Cl, C_6D_5Cl, $C_6H_{11}Cl$ and C_6Cl_6.

Note that in the present arrangement, the associated collision energy uncertainties are 0.34 eV for C_6H_5Cl, C_6D_5Cl, and $C_6H_{11}Cl$, while for C_6Cl_6 is 0.4 eV.

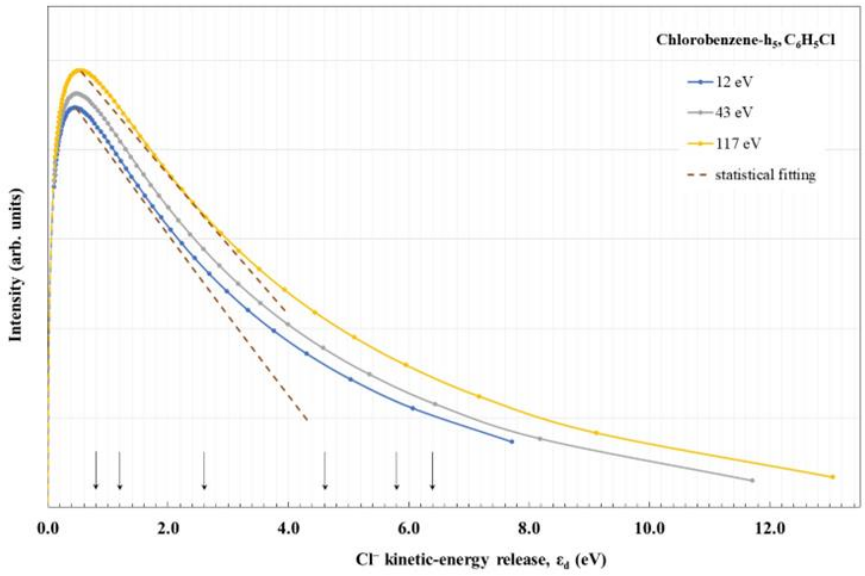

Figure 15 Kinetic-energy release distributions $D(\varepsilon_d)$ in collisions of K + C_6H_5Cl obtained from the TOF spectra of Cl^- at 12, 43 and 117 eV collision energy in the centre-of-mass frame. Statistical fitting procedure for 12 and 117 eV (see text for details).

The shape of an asymmetric TOF mass peak is related to the fragment anion velocity in the extraction region, where the maximum intensity corresponds to ions formed with no initial velocity, while the left and right flanks of such peaks are related to the extraction of ions with

a velocity component in the forward and backward directions, respectively. From the height of Cl^- TOF mass peaks at different widths, one obtains the kinetic-energy release distribution (KERD).

Figure **15**,

Figure **16**, Figure 17, and Figure 18 depict the KERDs, $D(\varepsilon_d)$, obtained from equation (34) for C_6H_5Cl, C_6D_5Cl, $C_6H_{11}Cl$ and C_6Cl_6, respectively. For values of $\varepsilon_d < 0.1$ eV the distributions are plotted with dashed lines, meaning the less accuracy of such data due to neglecting, as already noted, the quadratic term contribution in equation (33). The uncertainty limits associated to each experimental data point do not change the shape of the distributions, within ±5%, so these have not been included in the figures to avoid congestion.

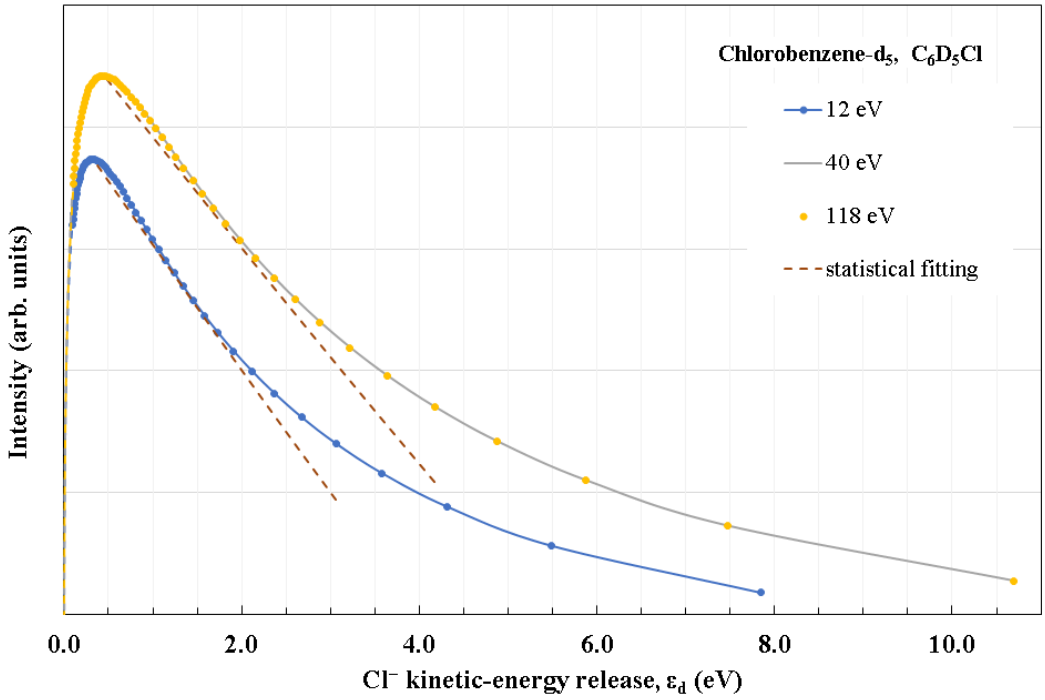

Figure 16 Kinetic−energy release distributions D(εd) in collisions of K + C_6D_5Cl obtained from the TOF spectra of Cl^- at 12, 40 and 118 eV collision energy in the centre-of-mass frame. Statistical fitting procedure for 12 and 40/118 eV (see text for details).

Figure 19 shows Cl^- kinetic−energy release maximum from chlorobenzene−h_5 and −d_5, chlorocyclohexane and hexachlorobenzene at 12, 40 and 118 eV collision energy in the centre−of−mass frame. The KERDs of Cl^- are limited to ~ 14 eV for K + C_6H_5Cl, K + C_6D_5Cl and K + $C_6H_{11}Cl$ reaching this value at 118 eV collision energy (

Figure **15** to Figure 17) whereas those for K + C_6Cl_6 are within ~ 8.0 eV with the maximum value at 40 eV (Figure 18). The shape of the distribution does not change appreciably with the 5% error bars, so these have not been included to avoid congestion of the figure. The anion states are marked as arrows.

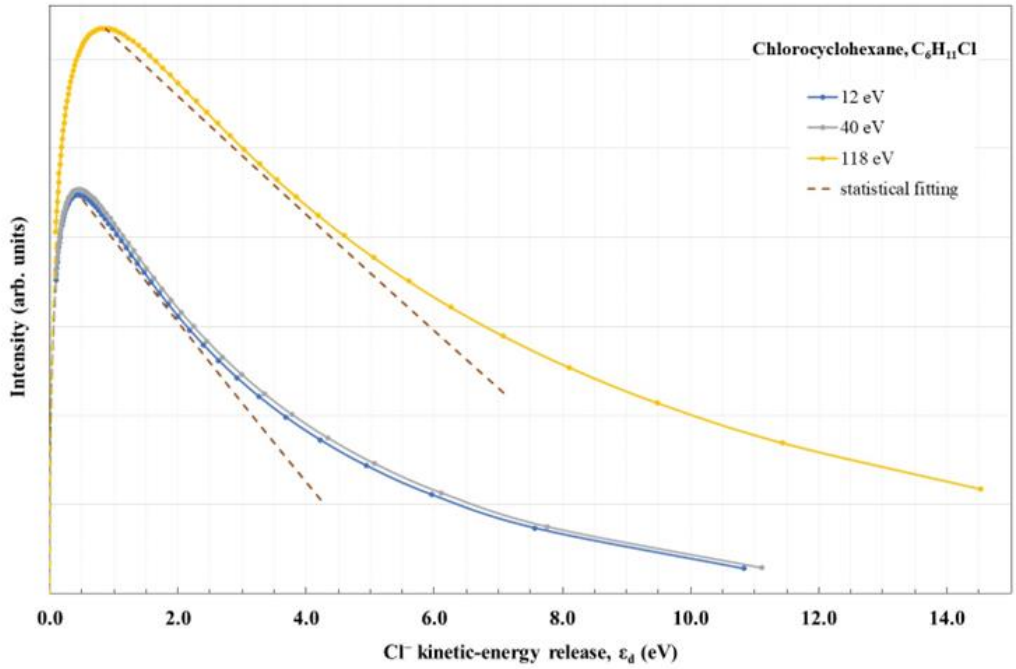

Figure 17 Kinetic–energy release distributions D(εd) in collisions of K + $C_6H_{11}Cl$ obtained from the TOF spectra of Cl^- at 12, 40 and 1118 eV collision energy in the centre–of–mass frame. Statistical fitting procedure for 12/40 and 118 eV (see text for details).

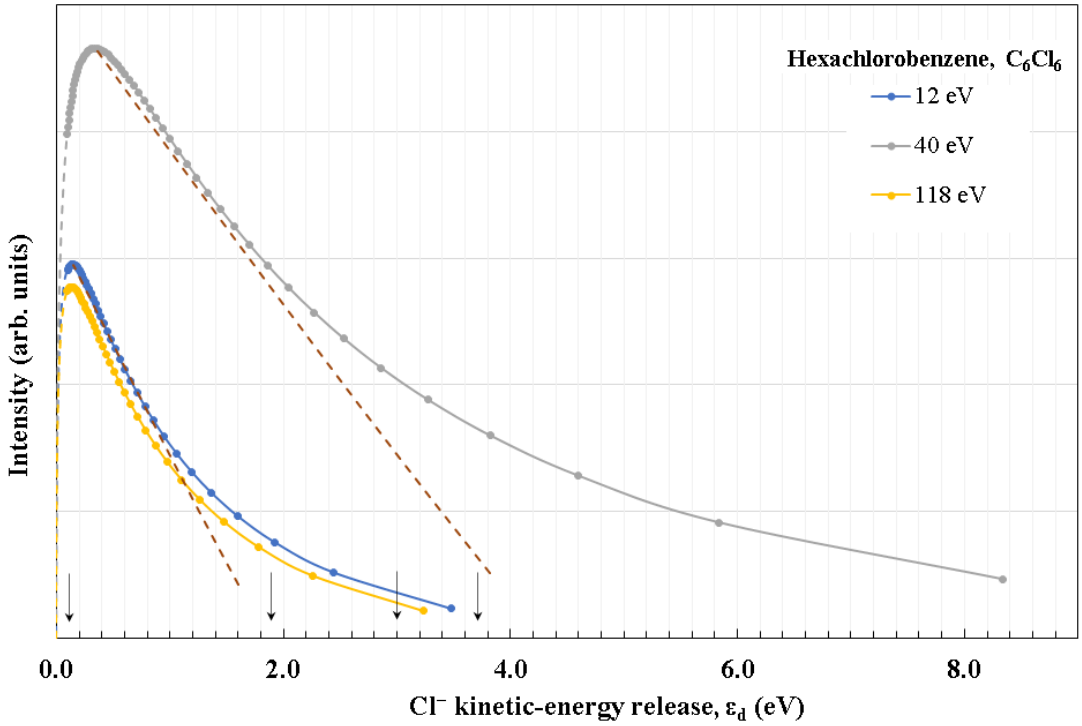

Figure 18 Kinetic – energy release distributions D(εd) in collisions of K + C_6Cl_6 obtained from the TOF spectra of Cl^- at 12, 40 and 118 eV collision energy in the centre – of – mass frame. Statistical fitting procedure for 12 and 40 eV (see text for details).

Regarding DEA experiments in chlorobenzene–h_5, Khatymov et al.[134] report anion formation with masses of 111, 75, 25 and 35 u, being Cl^- (35 u) the most abundant. From the resonance profiles obtained through the different DEA[132], [134], [157], [158] and ETS[138]–[141], [159] data, a general consensus has been reached to assign the Cl^- formation to the prominent feature found at ~ 0.8 eV electron impact energy, as a shape resonance of π* character (Table 1).

Table 1 Resonance positions (in eV) and their assignments from dissociative electron attachment, electron transmission spectroscopy (ETS) and electron scattering from C_6H_5Cl.

Reference	Resonance positions (eV)							
Asfandiarov et.al.[137]	0.74							
Barbosa et.al.[148]	0.76, 0.70		2.80		5.20			
Burrow et.al[138]	0.75		2.42		4.39			
Christophorou et.al.[160]	0.60							
Khatymov et.al.[134]	0.69	0.96			5.00	5.80	6.40	
Lunt et.al.[146]	0.75							
Makochekanwa et.al.[145]	0.80		2.50					8.50
Mathur and Hasted[139]	0.90		1.74	3.10	4.68			8.22
Milhaud[157]	0.77				4.90	5.82		7.17
Nae et.al.[132]	0.70							
Olthoff et.al.[140]	0.73		2.50		4.50			
Shimamori et.al.[158]	0.70							
Skalicky et.al.[144]	~0.80	1.20	2.60		4.50			
Stricklett et al.[141]	0.72		2.44					
Assignment (C_{2v})[138]	$\pi^*(a_2, b_1)$[1]		$\sigma^*_{C-Cl}(a_1)$		$\pi^*(b_1)$			

The grand total cross section for electron scattering measurements reports the main resonance peak at 8.5 eV[145] in good agreement with the electron transmission value of 8.22 eV[139]. The resonance features above 5.0 eV are related to core-excited resonances given the lowest-lying excited states of chlorobenzene which are discernible at photon energies > 5.5 eV[161].

[1]Selectivity of vibrational excitation in electron impact spectroscopy excitation functions suggests the symmetry ordering to be b_1 and a_2, at the geometry of the neutral molecule, yet with no conclusive evidence[144].

In the case of chlorobenzene–h_5, the main anion states' positions from DEA[134] and/or electron impact spectroscopy[144] experiments are marked in
Figure 15 with arrows and the corresponding values are shown in Table 1. The lowest resonance π_1^* at ~ 0.8 eV, and presumably π_2^* at 1.2 eV, give rise to Cl^- formation provided a C_{2v} symmetry lowering induced by vibronic coupling of the $\pi_1^*(b_1)$ and $\pi_2^*(a_2)$ with the $\sigma^*(a_1)$ anion states prevail[144]. Though, strong excitation of out−of−plane (a_2) and in-plane non-totally symmetric vibrations (b_2) are the effective path for C−Cl bond excision[144]. Moreover, the broad resonance feature at 2.6 eV has been assigned to a temporary electron capture into the $\sigma^*_{C-Cl}(a_1)$ molecular orbital, the band at 4.50 eV to a $\pi_3^*(b_1)$ of the anion[144], while the features at 5.8 and 6.4 eV to inter-shell resonances of core-excited character[134]. Note that Palmer et al.[162] report vertical excitation energies for neutral chlorobenzene at 5.807 ($^1A_1$) and 6.724 eV ($^1A_1$) yielding C−Cl bond excision, in good agreement with the values of 5.91 and 6.77 eV from Ari *et al* [163].From the KERD profile in
Figure 15, the first and second resonances at 0.8 and 1.2 eV are the dominant reaction paths for Cl^- formation. The distributions maxima peak at 0.47 eV and 0.55 eV for the 12 (and 43 eV) and 117 eV collision experiments (Figure 19).

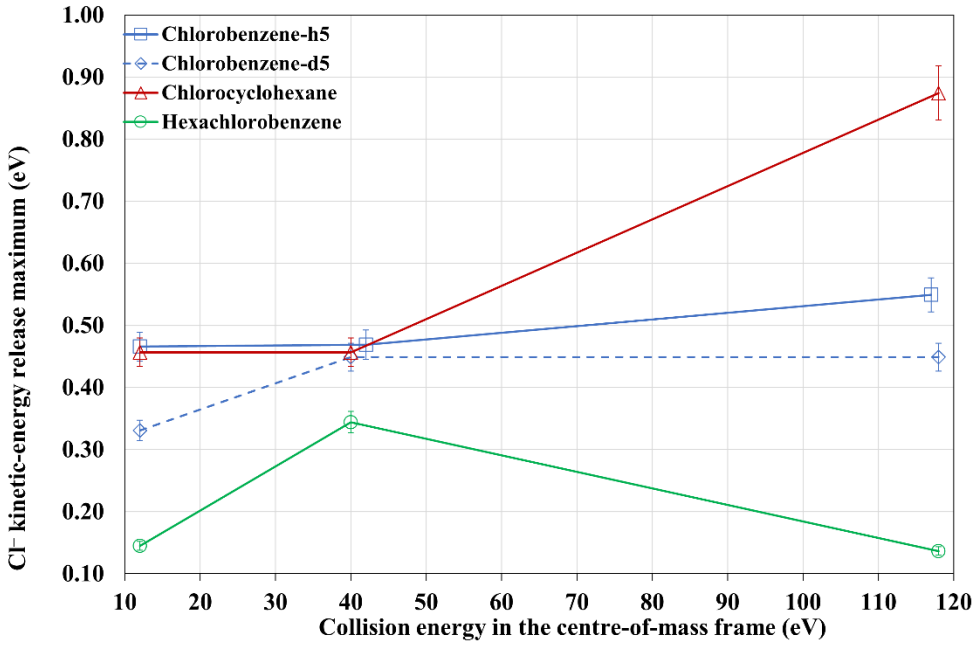

Figure 19 Cl^- kinetic-energy release maximum in collisions of K atoms with C_6H_5Cl, C_6D_5Cl, $C_6H_{11}Cl$, and C_6Cl_6 at 12, 40 and 118 eV in the centre−of−mass frame. Error bars have been added and account for ±5%.

Note that at 12 and 43 eV the downward slope shows a tendency to change at ≳ 2.6 eV which may be reminiscent of the excess energy in the TNI character changing relative to

$C_6H_5 - Cl^-$ dissociation level, i.e., at lower energies is due to a statistical process and at higher energies to direct dissociation.

At 2.6 eV, Cl^- is formed through a $\sigma^*_{C-Cl}(a_1)$ resonance, so the broad contribution at higher kinetic energies, ε_d, is due to direct dissociation with the excess energy converted into translational energy of the fragment. A close inspection of

Figure **15** also reveals that the downward slope of the distribution at 117 eV seems to level off at ~ 8 eV with character changing $\gtrsim$ 6.0 eV. This is due to the contribution of two additional resonances at 5.80 and 6.40 eV (Table 1) that are associated to core-excited resonances. We now detain ourselves to the lower kinetic energy release region where the distribution profile has been fitted with a statistical fitting in

Figure 15 to Figure 18 (dashed lines), as thoroughly described before[164]:

$$D(\varepsilon_d) = C\left(1 - \frac{\varepsilon_d}{E_e}\right)^{s-2} \quad (35)$$

with *C* a constant independent of the energy, *s* the adapted degree of freedom of the anion and E_e the available access energy. In the specific case of C_6H_5Cl, for 12 eV and 117 eV collision energy, E_e = 6 eV and E_e = 7.5 eV. The reasonably good fitting accord with the distributions yield *C* and *s* values of 2.65×10^{-6} and 3.0, and 2.86×10^{-6} and 3.0, respectively. Given the arbitrary units of the KERD intensities, constant *C* has no physical meaning. At this stage is relevant to comment on the *s* values. Actually, three degrees of freedom rather than 30 internal modes in chlorobenzene, is rather small, this meaning that only part of the reaction pathway leading to dissociation is channelled through a particular isolated state of the TNI, whereas the remaining is certainly going through direct bond breaking.

As noted previously, we have no information related to the electron affinities of the lowest-lying electronic states of chlorobenzene–d_5 and chlorocyclohexane. Yet, we have plotted in

Figure **16** and Figure 17 the KERDs of both molecules at 12, 40 and 118 eV collision energy in the centre-of mass frame. The Cl^- distributions from C_6D_5Cl peak at 0.33 eV and shift to slightly higher energy at 0.45 eV, while for $C_6H_{11}Cl$, the maximum appears at 0.33 eV and shifts to 0.87 eV as the collision energy is increased (Figure 19). Of relevance the trending of such peak maxima as a function of the collision energy relative to C_6H_5Cl (see Figure 19). We note in the case of the chlorobenzenes (–h_5 and –d_5) that above 40 eV, the peak maximum distribution is, roughly speaking, insensitive to the increasing collision energy.

Such seems reasonable given the role of the σ^*_{C-Cl} resonances and even core-excited resonances that are mainly dissociative in character. Above 40 eV, the difference in Cl^- kinetic-energy release maximum is not particularly significant for C_6D_5Cl against C_6H_5Cl, yet below 40 eV that

becomes noticeable. Such is certainly related to the lifetime of the low-lying resonances, where in case of C_6D_5Cl, autodetachment strongly competes with dissociation and rejection of the extra electron may prevail in the deuterated compound. Moreover, the statistical fittings in Figure **16** have been obtained by using Eq. (35) for 12 eV and 118 eV collision energy with excess energies of E_e = 4.5 eV and E_e = 6.0 eV, certainly lower than the related values of C_6H_5Cl.

In case of chlorocyclohexane, the striking difference to C_6H_5Cl is noted above 40 eV (Figure 19). Note that $C_6H_{11}Cl$ does not have any π delocalized electrons over the ring, so any π*/σ* mixing does not hold, and the dissociation mechanism may certainly be dictated by relevant σ* antibonding character along the C–Cl coordinate resulting in higher kinetic energy of the fragment anion.

This is in contrast with chlorobenzene, where Skalicky et al.[144] have shown that the SOMO (singly occupied molecular orbital) of the negative ion has a π*(a_2)-like molecular orbital character strongly mixing with $\sigma^*_{C-Cl}(a_1)$ MO favouring π*/σ* mixing with relevant implications regarding the dissociation mechanism as the nuclear wave packet moves along the potential energy surface. The statistical fittings in Figure 17 result from equation (35) for 12 eV and 118 eV collision energy, and with values of E_e = 6.0 eV and E_e = 11.5 eV, respectively.

As far as hexachlorobenzene is concerned, the ground-state character has been assigned to valence π* in $C_6Cl_6^-$ from generalized Kohn-Sham semicanonical projected random phase approximation at different levels of accuracy.[165]

Recently we have calculated at the RKS/B3LYP+D3/aug-cc-pvtz level of theory a vertical electron affinity of –0.14 eV (π*) and obtained from the K^+ energy loss spectrum in collisions of potassium with C_6Cl_6, vertical electron affinities for the different anion states at (–1.86 ± 0.30), (–2.96 ± 0.20) and (–3.76 ± 0.20) eV[127]. These have been assigned to σ^*_{C-Cl}, $\pi^*_{CC}/\sigma^*_{CC} + \sigma^*_{C-Cl}$ and σ^*_{C-Cl} states, respectively, and are marked as arrows in Figure 18. From the time-of-flight mass spectrometry and energy loss data[127], the first resonance is not the dominant reaction path for Cl^- formation.

Moreover, we have reported that for collision energies below 30 eV, the extra electron is captured by the LUMO with mostly π^*_{CC} character. Note that in C_6Cl_6 with relevant ring delocalized π system, the six identical Cl atoms are "highly competitive" among each other for the extra charge. In such K– C_6Cl_6 collisions at energies above the threshold of ion−pair formation, the excess energy may be channelled into the available degrees of freedom, resulting mainly in a stable $C_6Cl_6^-$ ion rather than prevalent bond breaking. However, the SOMO of the negative ion has π^*_{C-Cl} character while the closest MO shows a strong σ^*_{C-Cl} antibonding nature. Therefore, C–Cl bond breaking resulting in Cl^- formation, may be only operative by efficient diabatic curve crossing between π^*_{C-Cl} and σ^*_{C-Cl}, if the nuclear wave packet survives long enough along the C–Cl coordinate to yield the chlorine anion. From the KERD profiles in

Figure 18, the second, third and fourth resonances are the dominant reaction paths for Cl^- formation. Note that at 12 and 118 eV the downward slope shows a tendency to change at ≳ 1.86 eV, while at 40 eV such is certainly visible at higher kinetic energies closely related to the anionic states at 2.96 and 3.76 eV.

Thus, the excess energy in the TNI at lower energies is dictated by a statistical process and at higher energies to direct dissociation. Of relevance the fact that at 1.86 eV, Cl^- is formed through a σ^*_{C-Cl} resonance. The statistical fitting for 12 eV and 40 eV collision energy, results in E_e = 2 eV and E_e = 4.5 eV, respectively and with s = 3.0 in both cases.

Finally, the distributions maxima in Figure 19 peak at 0.14 eV and 0.34 eV for 12 (and 118 eV) and 40 eV collision energies. From the chlorinated molecules investigated, C_6Cl_6 shows the Cl^- kinetic−energy release maximum with the lowest values (Figure 19). In this comparison, such does not seem to be unexpected given that Cl^- is the only anion formed from electron transfer to chlorobenzene–h_5 and –d_5 and chlorocyclohexane. In hexachlorobenzene the parent anion formation strongly competes with the chlorine anion, the former accounting for a significant branching ratio at low collision energies, i.e., more than 70% below 10 eV[127]. At intermediate energies, 40 eV, $C_6Cl_6^-$ amounts 30% and Cl^- 60%, while at higher energies other fragments stemming from ring breaking amount to 25% of the total anion yield, although the role of the σ^*_{C-Cl} resonances and even core-excited resonances that are mainly dissociative in character [127].

4.3.2 Total relative cross-sections for Cl^- formation

The negative ion Time−of−Flight mass spectra were recorded for Cl^- formation from chlorinated benzenes namely C_6H_5Cl, C_6D_5Cl, $C_6H_{11}Cl$, and C_6Cl_6. Upon collisions with neutral potassium atoms, C_6H_5Cl, C_6D_5Cl, $C_6H_{11}Cl$ only yield Cl^- negative ion in their TOF-MS. In the case of C_6Cl_6, apart from the undissociated parent anion $C_6Cl_6^-$, $C_6Cl_5^-$ and Cl^- formation, other fragment anions that require complex internal reactions within the temporary negative ion formed, have been assigned to $C_6Cl_4^-$, $C_3Cl_2^-$, C_2Cl^-, and Cl_2^- [127], [166]. The Cl^- yield of formation was normalized with respect to the total anion yield in TOF−MS. To compare the Cl^- formation, a normalization of the TOF−MS with respect to the accumulation time, projectile beam current and operating pressure was done. However, only total relative cross-sections for Cl^- formation are being reported because we are not able to estimate the density of the molecular beam in the collision region.

The Cl^- yield has been recorded in a wide collision energy range (from approx. 10 eV to 700 eV in CM frame), and the Cl^- cross−sections will be scrutinized in terms of the parameters

given in the next sections. This scrutiny may help us interpret some of the interesting features in the wide energy range. All the parameterization is based on the chapter 2.

I. Crossing radius (R_C)

The crossing radius as described and defined in chapter 2 , classically is a function of the ionization energy of the potassium atom and the electron affinity of molecule under investigation[77].

II. Coupling Matrix element (H_{12}).

The coupling matrix element H_{12} represents the coupling of two neighbouring diabatic states for electron transfer process [77], where large H_{12} values represent adiabatic electron transfer and a small H_{12}, a diabatic behaviour [12], [86], [102]. Here small H_{12} value also represents weak coupling, implying smaller vibronic transition probabilities, hence effects of weak long-range interactions.

III. Velocity of collision (v_{rel}, v_{rad}, and v_{cr},).

Relative, radial, and critical velocity can be used to identify the location of the type of probability occurring using functions F_1, F_2 and F_3 approach. Thus, categorizing the velocity region into three main regions[77]:

- Threshold region;
- Post-threshold region;
- High velocity region.

IV. Collision time (t_{coll}).

The collision time is defined as the classical time that the projectile atom (K) spends in the vicinity of the molecule, i.e., in a crude approximation, the time taken by the projectile to complete a $2R_c$ distance. Hence, the collision time becomes inverse of the collision energy, i.e., higher the energy smaller the collision time [12]. We will also use the collision time to compare it with the vibrational time of a given vibrational motion. The collision time can also be classified in three categories relating to the collision velocity [77]:

- Threshold region (collisional time $\gtrsim$ vibrational time);
- Post-threshold region (collisional time $\approx$ vibrational time);
- High velocity region (collisional time $\ll$vibrational time).

V. Vertical Electron affinity (EA_v or VEA)

The threshold of parent anion formation corresponds with the adiabatic electron affinity[167]. The distribution of electron affinities takes account of the vibrational motion of the molecule before the collision, determined by the wave function of the vibrational ground state of the XY molecule as shown by the Franck−Condon overlap calculations [168] [77].

It is clear from chapter 2 that the collision time is dependent on R_c. R_c depends on the electronic affinity, and the electron affinity depends on the vibrational motion.

In the threshold region where the collisional time ≳ the vibrational time, the vibrationally excited molecular ion can be effectively quenched by the alkali ion during the passage of the crossing region [77] resulting in smaller cross−section.

Thus, implying that the vibrational motion of the molecule may govern the electron transfer processes where the collision time and the vibration time of the molecule are of the same order i.e., for collisional time ≈ vibrational time in post threshold region. Here stretching of the internuclear bond shifts the crossing radius outwards, thus strongly enhancing the diabatic transition probability, and may conceal a Landau−Zener type of behaviour of the collision[77], [169].Meaning the cross-section in this region may not have visible features like Landau-Zener cross−section curve.

Finally, in the high velocity region, the molecules can be considered rigid and molecular ion state may reflect original neutral molecular vibrational state distribution in agreement with the Franck−Condon principle[77], [86], [114], [169].

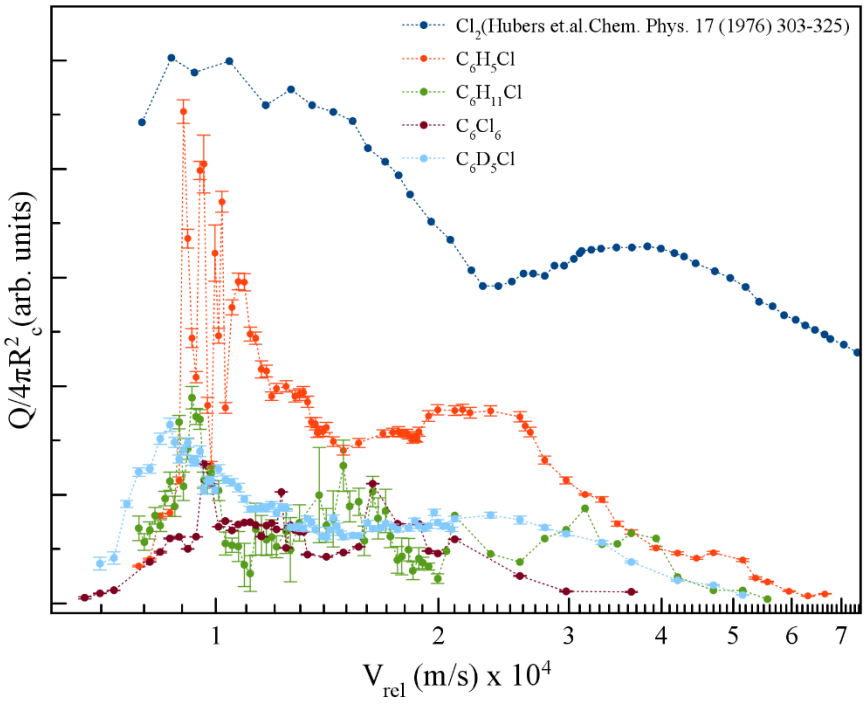

Figure 20 Relative cross−section for Cl^- formation from different chlorinated benzenes in extended velocity region.

In Figure 20, a comparative study of the relative cross-sections in alkali atom-molecule collisions are presented and compared with $K+Cl_2$ collision results of Hubers et al. [77]. In the low relative velocity collision region, the effects of stretching of the bond are clearly visible

(intensities are not normalized, so cannot be compared directly) in Cl_2 and conceals the Franck–Condon region, enhancing the diabatic transition probability significantly [77]. Investigation of these results with respect to the collision time, may provide indication of some possible underlying mechanisms responsible for the chlorine anion formation in such polyatomic molecules. In the case of chlorinated benzene C_6H_5Cl (Figure 21) , the first maximum is at approx. 1.1×10^4 m/s velocity, and the second maximum is shifted (Figure 20) with respect to Cl results from K+Cl_2 experiments. In the case of C_6Cl_6 and $C_6H_{11}Cl$ it is almost suppressed.

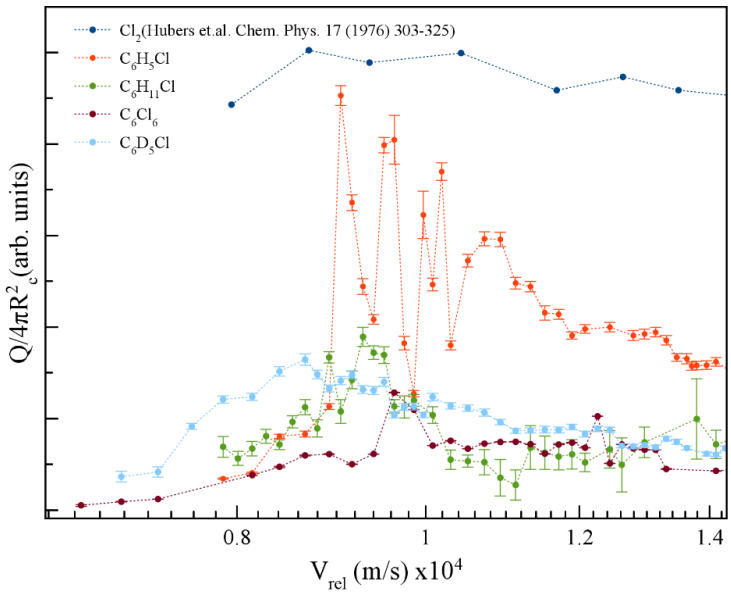

Figure 21 Relative cross–section for Cl^- formation from different chlorinated benzenes in the F3 region according to Hubers et al. [77], [91].

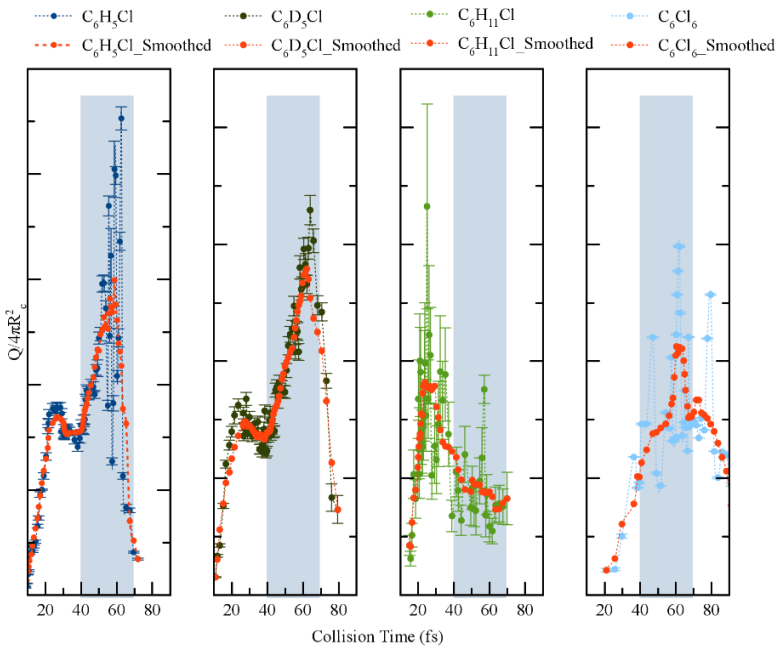

Figure 22 Relative cross−section for Cl^- formation from different chlorinated benzenes in terms of collision time (in fs). Smoothed data is adjacent averaged to guide the eye.

If we consider collisional time ≳ vibrational time, in

Figure **22**, (highlighted part shows when we can consider molecular vibration dominates the cross-section) above 70 fs collision time, in C_6H_5Cl, C_6D_5Cl and C_6Cl_6, the presence of the quenching effect is visible according to ref. [77] reducing the cross−section significantly. Between 40 and 70 fs collision time, the effects of vibrational motion, conceal the Franck−Condon overlap, and the vibrational motion may dominate the cross-section through diabatic transitions. However, the effects of internuclear separation, crossing radius, and electron affinities cannot be neglected [91], [102], [115], [167], [168].

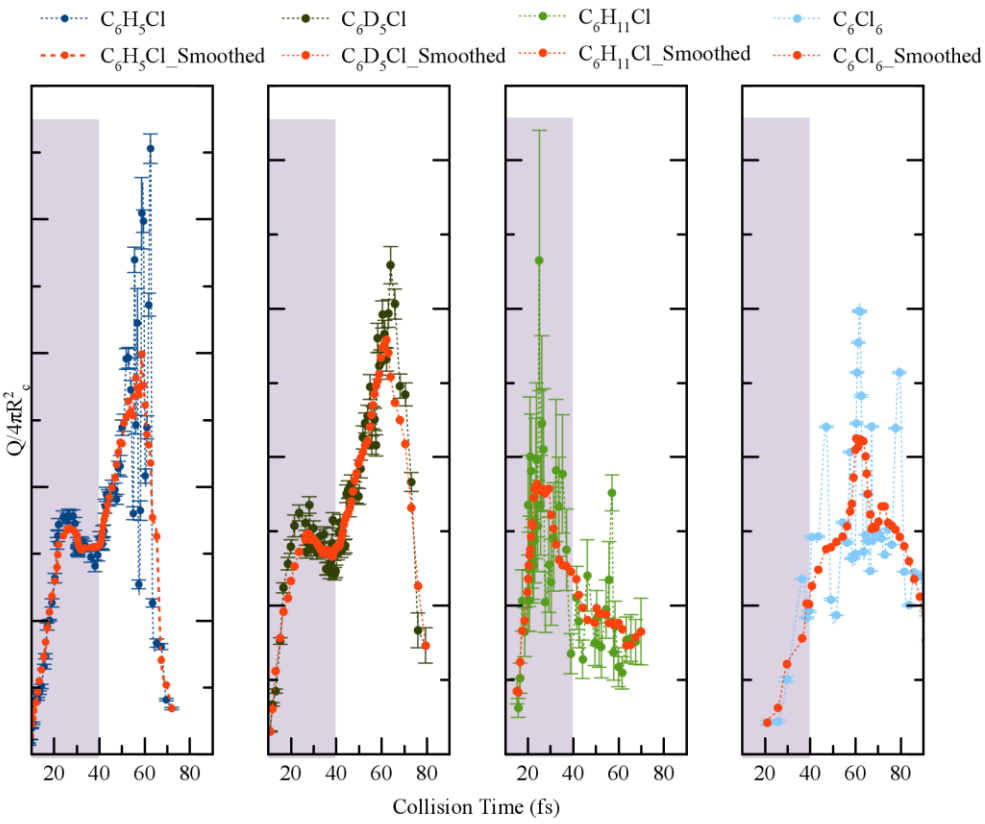

Figure 23 Relative cross-section for Cl^- formation from different chlorinated benzenes in terms of collision time (in fs). Highlighted part shows when we can consider molecular vibration frozen. Smoothed data is adjacent averaged to guide the eye.

In Figure 23 , the collision times between 20 and 40 fs indicates that these are fast (highlighted in grey), and the molecule can be considered rigid thus vibrational motion is assumed frozen [77],hence resembling the second maximum in diatomic molecules [77], [91], [170].

4.4 Summary

We have reported a comprehensive investigation into the kinetic-energy release distributions of chlorobenzene–h_5 and –d_5, chlorocyclohexane and hexachlorobenzene at collision energies in the centre-of-mass frame of about 12, 40 and 118 eV. Such distributions have been obtained from the shape and width of the time-of-flight mass spectra of Cl^-ions. Collision induced dissociation results in an energy redistribution either through the different internal degrees of freedom (via vibrational excitation) or direct transformation of the excess energy via translational motion of the fragment anions involved. The statistical fittings of Cl^-distributions at low kinetic-energy release, ε_d, reveal at least three effective degrees of freedom, while the role of statistical and direct dissociation has been thoroughly discussed according to the nature of the different resonances obtained by dissociative electron attachment and/or electron transmission spectroscopy, where applicable. Additionally, we have made some considerations on the collision dynamics for the set of chosen molecules, and the conclusions drawn lend support to previous investigations of hexachlorobenzene negative ion formation in electron transfer experiments, while for the remaining molecular systems the present results will serve to help interpreting the underlying molecular mechanisms within electron transfer induced fragmentation.

In case of Cl^-formation from chlorinated benzenes influence of vibration motion upon cross section is significant in low energy collisions where t_{coll} is of order of t_{vib}. the structures in the cross sections significant predict the vibration motion and its influence on the cross-sections with changing collision time.

5.

COLLISION DYNAMICS OF HEXACHLORO-BENZENE UPON ELECTRON TRANSFER

In this chapter a detailed overview of charge transfer processes in hexachlorobenzene will be discussed. various anionic states of C_6Cl_6 have been probed and detailed fragmentation of C_6Cl_6 upon potassium impact has been reported. This chapter is based on **"Anionic states of C_6Cl_6 probed in electron transfer experiments"** published in *Phys. Chem. Chem. Phys. (2022),* **24**,*366-374*, another manuscript based on this chapter **"Sensing the *ortho* Positions in C_6Cl_6 and $C_6H_4Cl_2$ from Cl_2^- Formation upon Molecular Reduction"** is published in *Molecules (2022)* **27**,*15, 4820.*

5.1 Introduction

Hexachlorobenzene (C_6Cl_6), as part of a large group of volatile organochloride compounds, has been used as a pesticide across the globe,[171], [172] and found to be a prevailing environmental pollutant.[173] Its global distribution revealed it moves through the atmosphere from warmer source regions (where it is volatilized) and tend to condense at colder regions,[174]–[176] undergoing a process known as global distillation.[171], [174] In the atmosphere, reactions with $OH^{\bullet}$ radicals have been identified as a sink mechanism,[171] yet the relative low rate constant, 0.27×10^{-13} cm^3 $molecules^{-1}$ s^{-1} at 298K, favours such global distillation process.[171] C_6Cl_6 can be eliminated by ozone coupled with hydrogen peroxide processes and these can be enhanced by combination with active carbon absorption methods.[172], [177] Additionally, the lack of comprehensive photolysis rates in the literature do not allow identifying ultra-violet photo absorption as a route to remove and/or chemically change these molecular compounds in the Earth's atmosphere.

Hexachlorobenzene has been investigated by experimental and theoretical methods, the former dealing with ultraviolet photo absorption,[178], [179] infrared photo absorption[180],

[181], photoelectron spectroscopy,[182] gas-phase reactions with molecular oxygen[150] and reduction potentials with an electron capture detector (ECD)[183]; the latter on vibronic interactions and charge transfer[184] and electron affinities of chlorinated benzene molecules.[165], [185], [186] Photodegradation of C_6Cl_6 and theoretical prediction of its pathways using quantum chemical calculation has been reported by Yamada et al.[187] As far as negative ion formation is concerned, a comprehensive literature survey reveals only the parent anion from resonance electron capture mass spectrometry, allowing to determine an adiabatic electron affinity of 0.91 eV,[150] whereas a value of 0.98 eV has been reported by Wiley and co-workers.[185] Moreover, the generalized Kohn-Sham semicanonical projected random phase approximation method, predicts a valence π* character for $C_6Cl_6^-$ ground-state,[165] while Robin[179] has noted that the most relevant absorption features at 42500 cm^{-1} ($^1A_{1g} \rightarrow {}^1B_{1u}$) and 46000 cm^{-1} ($^1A_{1g} \rightarrow {}^1E_{1u}$) in neutral C_6Cl_6 have been assigned to intense halogen np → π* charge transfer transitions.

The molecular orbitals configuration of C_6Cl_6 in D_{6h} symmetry yields for the outer valence … $(e_{1g})^4$ corresponding to the $^1A_{1g}$ sate, while the parent anion results from electron capture into the non-degenerate a_{1g} lowest unoccupied molecular orbital with configuration … $(e_{1g})^4$ $(a_{1g})^1$ which corresponds to $^2A_{1g}$ state, with no appreciable Jahn-Teller effect.[184] Given the lack of any other relevant information on negative ion formation from hexachlorobenzene either by dissociative electron attachment or charge transfer processes, a comprehensive investigation of the underlying molecular mechanisms yielding $C_6Cl_6^-$ and its fragment anions is necessary for getting further knowledge on the electronic structure of such chemical compound.

5.2 Experimental methods

The crossed molecular beam setup used to investigate negative ion formation in collisions of neutral potassium (K) atoms with hexachlorobenzene (C_6Cl_6) molecules was previously described elsewhere,[188] therefore only a general description is given here. Briefly, an effusive target molecular beam crosses a projectile beam of neutral hyperthermal K atoms and the product anions formed in the electron transfer process are analysed by a dual-stage linear time-of-flight (TOF) mass spectrometer. The K beam is produced in a charge exchange chamber from the interaction of gas-phase neutral potassium atoms from an oven source with accelerated K^+ ions emitted from a commercial ion source (HeatWave, US) in the range of 10 to 100 eV in the lab frame. The intensity of the neutral potassium beam is monitored using a Langmuir−Taylor ionisation detector, before and after collecting the mass spectra. The TOF anion yield is normalized considering the primary beam current, pressure, and acquisition

time. The typical base pressure in the collision chamber was 4×10^{-5} Pa and the working pressure was 1×10^{-3} Pa. Mass calibration was performed based on the well−known anionic species formed after potassium collisions with nitromethane[188] and tetrachloromethane.[189] A hemispherical energy loss analyser was used to obtain the K^+ signal post-collision in the forward scattering direction with the beam's optical path, where such experiments were not performed in coincidence with TOF mass spectrometry. The analyser was operated in constant transmission mode, hence keeping the resolution constant throughout the entire scans. The estimated energy resolution during the experiments was ~1.2 ± 0.2 eV. The energy loss scale was calibrated using the K^+ beam profile from the potassium ion source serving as the *elastic* peak. Hexachlorobenzene (C_6Cl_6) was supplied by Sigma Aldrich with a stated purity of ≥ 98%. The solid sample was used as delivered and gently heated up to 340 K through a temperature PID (proportional-integral-derivate controller) unit. To test for any thermal decomposition products within the hexachlorobenzene beam, mass spectra were recorded at different temperatures and no differences in the relative peak intensities as a function of temperature were observed.

5.3 Theoretical methods

Charge transfer processes are described with the aid of *ab initio* calculations, based on the evolution of the quasi-molecular system, formed by the potassium projectile and the molecular target along the reaction coordinate within the framework of the molecular representation. This methodology has been successfully used for diatomic systems and tested in ion-neutral molecule collisions,[190]–[194] later extended to atom-molecule interactions[128], [129], [195] where the system evolves along the reaction coordinate corresponding to the distance R between the impact atom and the molecular target.[196]–[199] In such approximation, we do not include the internal degrees of freedom of the molecular target explicitly, which is reasonable since collisional processes are very fast and thus nuclear vibrational and rotational motions are much slower than the collision time and can be considered frozen during the collision.

The geometry of hexachlorobenzene at D_{2h} symmetry was optimized at the MP2/def2-TVZP level of theory[200] while in the presence of potassium atom the C_{2v} symmetry was used. All calculations have been performed by means of the ORCA and MOLPRO packages of *ab initio* programmes.[201], [202]

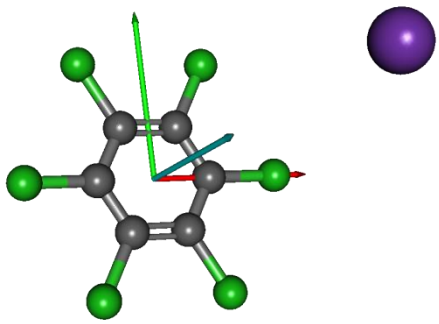

Figure 24 Molecular structure of C_6Cl_6 and orientation of the $K-C_6Cl_6$ collisional system; K, purple, x, red; y, green; z, blue.

The potassium atom has been placed along the y axis as shown in **Figure 24** and the C_6Cl_6 target is kept frozen in its ground state ($\tilde{X}$: $^1A'$) geometry during the collision process. A detailed analysis of the $K-C_6Cl_6$ interaction at R = [2.5, 5, 7.5, 10] Å, occurring between molecular states involved in this process, has been made to precisely determine asymptotic molecular configurations of the calculated states. The calculation has been carried out in Cartesian coordinates, with no symmetries. All electrons of carbon and chlorine atoms have been included in the calculations and their 1s orbitals were treated as frozen core. For the potassium atom, the ECP18SDF core−electron pseudopotential[203] with the associated basis set has been chosen. The natural molecular orbitals for $K-C_6Cl_6$ (see appendix A Fig. A1 and Table A1) have been obtained at state-averaged Complete Active Space Self Consistent Field (CASSCF)[204]–[206] level of theory considering the static electron correlation for the reaction coordinate $K-C_6Cl_6$ at R = 5 Å distance, corresponding to the asymptotic region. The resultant highest occupied (HOMOs) and the lowest unoccupied molecular orbitals (LUMOs) for $K-C_6Cl_6$ are shown in Figure 25 and Fig. A1 together with the corresponding orbitals without the presence of the potassium atom (see Fig. A2 and Table A2). Finally, Fig. A3 depicts $C_6Cl_6^-$ highest doubly occupied, singly occupied (SOMO) as well as the lowest unoccupied molecular orbitals (RKS, B3LYP+D3).

To determine the ionisation energy, electron affinity and vertical detachment energy (see Table A3) and to look closely at the anion where the symmetry is broken, DFT calculations have been performed where Kohn-Sham orbitals were used rather than canonical HF orbitals, since the former improve the agreement with the experimental electron affinity of C_6Cl_6 by 0.08 eV. To describe an extra electron, diffuse functions with additional augmented basis functions were used at the restricted open shell Kohn-Sham, B3LYP+D3 level of theory.[207] Energies of the neutral, the anion and the cation are -2989.57786, -2989.61393 and -2989.25288 Hartree, respectively and resign from Table A4 in appendix A.

	C_6Cl_6	$K + C_6Cl_6$
HOMOs	$\bar{n}_{Cl}$ (in-plane) -11.9 eV 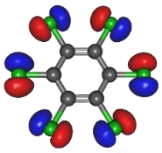 π_{CCl} -10.5 eV 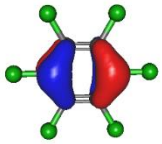	$\bar{n}_{Cl}$ (in-plane) -12.0 eV 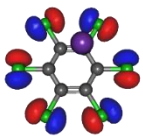 π_{CC} -10.6 eV 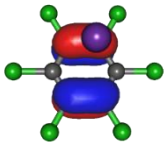
LUMOs	π_{CC}* 2.89 eV 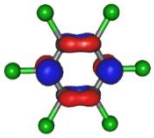	π_{CC}* 2.89 eV 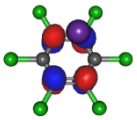
	π_{CC}* 2.96 eV 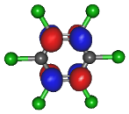	π_{CC}*/σ_{CC}* + σ_{CCl}* 3.09 eV 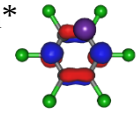
	π_{CC}* 9.72 eV 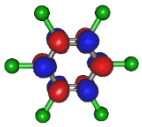	π_{CC}* 9.84 eV 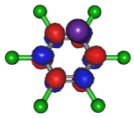
	σ_{CC}* 17.0 eV 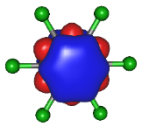	σ_{CC}* 15.8 eV 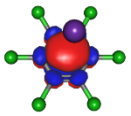
	σ_{CC}* 17.2 eV 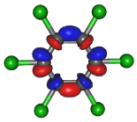	σ_{CC}* 16.2 eV 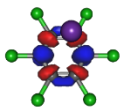
	σ_{CC}* 17.5 eV 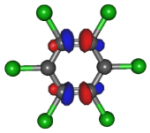	σ_{CC}*+ σ_{CCl}* 16.6 eV 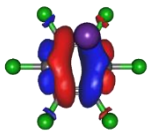

Figure 25 Calculated highest occupied molecular orbitals (HOMOs) and lowest unoccupied molecular orbitals (LUMOs) for C_6Cl_6 and $K + C_6Cl_6$. Energies in eV.

5.4 Results and discussion

TOF mass spectra have been recorded in a wide range of lab−frame collision energies from 10 up to 100 eV (7.9 to 79.1 eV in the centre−of−mass frame), yielding negative ions assigned to

Cl^-, Cl_2^-, C_2Cl^-, $C_3Cl_2^-$, $C_6Cl_4^-$, $C_6Cl_5^-$ and $C_6Cl_6^-$ along with their respective isotopes. Figure 26 shows a typical mass spectrum recorded at 100 eV (E_{CM} = 79.1 eV), where the inset depicts the parent anion signal fitted with Gaussian functions to reproduce its isotope contributions at 282 u (51%), 284 u (100%), 286 u (81%) and 288 u (35%). Note that a TOF mass peak shows an apparent asymmetry relative to its maximum position, with typically the left-hand branch much steeper that the right-hand [183]. Yet, for the sake of example, the Gaussian fitting used reproduces quite well in magnitude and in shape the TOF mass signal.

Another relevant aspect pertains to the Cl_2^- TOF mass contribution, where the peak should show its isotope contributions at 70 u (100%), 72 u (~65%), 74 u (~11%). A close inspection of this anion feature in Figure 26 reveals that the peak contains three contributions but not in the expected intensity. Given the limited TOF mass resolution ($m/\Delta m \approx 125$) that does not allow to clearly resolve close fragment anions, yet a proper peak fitting, as that used for $C_6Cl_6^-$, reproduces perfectly well the expected isotope distribution intensities (see

Fig. A4 in appendix A).

The energy loss spectrum of the potassium cations formed in the forward direction ($\theta \cong 0°$) of K atoms in collisions with C_6Cl_6 at 205 eV lab frame energy (E_{CM} = 162 eV), is shown in Figure 27. Hexachlorobenzene branching ratios (fragment anion yield/total anion yield) of the main negative ions formed as a function of the collision energy in the centre-of-mass frame are depicted in Figure 28. From a close inspection of Figure 26 TOF mass spectrum, the prevalent anion is assigned to Cl^-, followed by the undissociated parent anion and Cl_2^-, while other fragment ions are considerably less intense, *viz*. those resulting from the loss of Cl units and ring breaking. We have performed additional calculations on $C_6Cl_6^-$ to obtain the energy values of the orbitals with the restricted open shell Kohn-Sham B3LYP+D3 level of theory (see Fig. A3), where the electron spin densities show a preferential C–Cl bond excision yielding the chlorine anion (see discussion below).

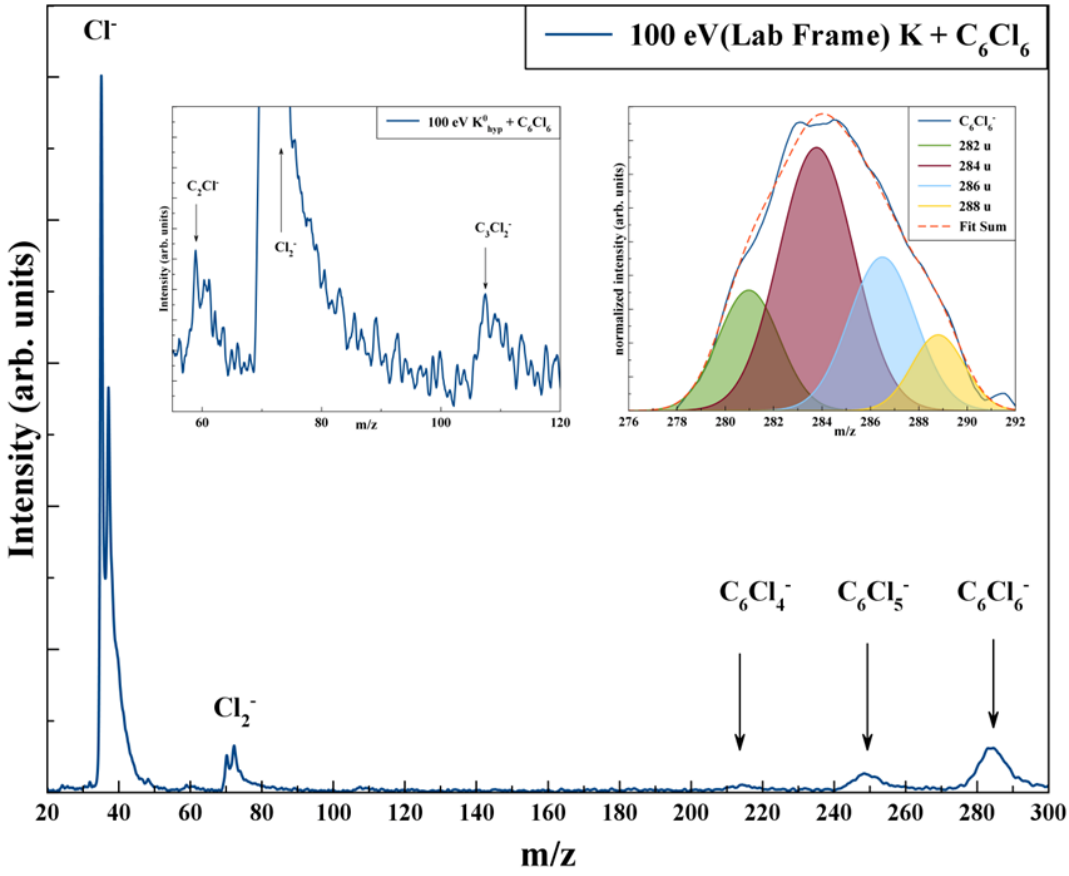

Figure 26 Time−of−flight negative ion mass spectra in potassium (K)–hexachlorobenzene (C_6Cl_6) collisions at 100 eV lab frame energy (79.1 eV in the centre−of−mass frame). See text for details.

The calculated lowest unoccupied molecular orbitals in Figure 25 show that the LUMO+4 and LUMO+5 σ* states are slightly shifted to lower energies (0.8–1.0 eV) in comparison to respective calculated MOs without the presence of the potassium atom.

5.4.1 K^+ energy loss data

The energy loss spectrum of K^+ ions formed in collisions of potassium atoms with hexachlorobenzene, has been obtained at 162.2 eV in the centre−of−mass frame (205 eV lab frame) in the forward direction ($\theta \cong 0°$) and is depicted in Figure 27. We observe for the first time some low-intensity features and a main peak with maximum intensity (I_{max}) at (8.1 ± 0.2) eV. Electron transfer processes triggered by the collision of neutral potassium atoms (K) with neutral target molecules and yielding ion-pair formation, the energy loss required to access an electronic state, $\Delta E = IE(K) - EA(I_{max})$, with the difference between the potassium atom ionisation energy and the target molecule's electron affinity for that state,[208] which results on a vertical electron affinity of (–3.76 ± 0.20) eV.

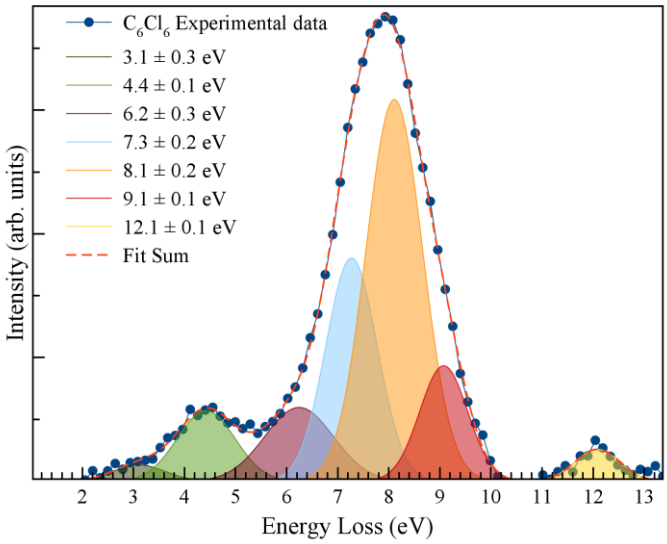

Figure 27 Energy loss spectrum of K^+ ions formed in the forward direction of K atoms in collisions with C_6Cl_6 at 205 eV lab frame energy (162 eV in the centre−of−mass frame). See text for details. Error bars are within experimental data points and within 10% associated with the fitting.

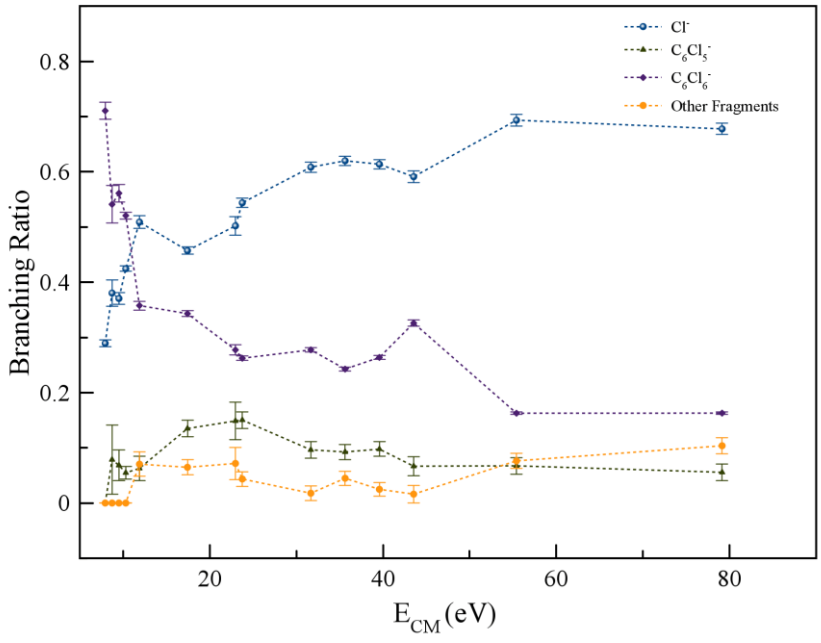

Figure 28 Hexachlorobenzene (C_6Cl_6) branching ratios (fragment anion yield/total anion yield) of the main negative ions formed as a function of the collision energy in the centre-of-mass frame. Error bars related to the experimental uncertainty associated with the ion yields

have been added to a few data points in order to avoid congestion of the figure. The lines are just to guide the eye. See text for details.

Gaussian fittings have been used to decompose the energy loss spectrum main peak, indicating the presence of adjacent contributions, as well as other low-intensity less resolved features with their vertical electron affinities listed in Table 2. Note that Voora[165] has assigned the lowest-lying character of $C_6Cl_6^-$ to a valence-bound (vb) π* state with an electron affinity EA (C_6Cl_6) varying from 0.03 up to 0.30 eV, depending on the basis set used, and an associated error of 0.13 eV.

5.4.2 $C_6Cl_6^-$ formation

The TOF mass spectra recorded in the wide collision energy range show that the undissociated parent anion accounts for more than 70% of the total ion yield for E_{CM} < 10 eV, whereas above 50 eV its BR is ~ 20% (Figure 28). These results indicate that electron transfer is very efficiently captured by hexachlorobenzene, and the process may proceed according to the reaction:

$$K + C_6Cl_6 \rightarrow (K^+C_6Cl_6^-) \rightarrow K^+ + (C_6Cl_6^-)^{\#} \rightarrow K^+ + C_6Cl_6^- \quad (36)$$

with $(C_6Cl_6^-)^{\#}$ formation of a temporary negative ion (TNI) with an excess of internal energy.

Table 2 Assignment of different features from Gaussian fitting to K^+ energy loss spectrum from potassium collisions with hexachlorobenzene 205 eV lab frame energy (162 eV in the centre-of-mass frame). The uncertainties result from the Gaussian fitting procedure. See text for details.

K^+ Energy Loss Features (eV)	Vertical Electron Affinity (eV)	Calculated Vertical Energy of MO (eV)	Assignment	Ref.[165]	Adiabatic Electron Affinity (eV)[150], [151]
3.1 ± 0.3	1.24 ± 0.30	0.98[a]			0.91; 0.98
4.4 ± 0.1	–0.06 ± 0.10		π*	vb[b]-π*	
6.2 ± 0.3	–1.86 ± 0.30	–1.92	71, σ_{CCl}*		
7.3 ± 0.2	–2.96 ± 0.20	–3.10	LUMO+1		
8.1 ± 0.2	–3.76 ± 0.20		σ_{CCl}*		
9.1 ± 0.1	–4.76 ± 0.10		π*		
12.1 ± 0.1	–7.76 ± 0.10		$n_{Cl} \rightarrow (n+1)s$ $n_{Cl} \rightarrow (n+2)s$		

[a] adiabatic electron affinity;

[b] valence-bound state, with calculated electron affinities of 0.03 eV (aug-cc-pVDZ+7S7P), 0.30 eV (aug-cc-pVTZ+7S7P) and 0.29 eV(aug-cc-pVTZ). See Voora[165] for details.

Attachment of an electron is accompanied by significant energy release comprising the kinetic energy of the incoming electron and the molecule's electron affinity, which was calculated to be –0.14 eV (vertical) and 0.98 eV (adiabatic) at the RKS/B3LYP+D3/aug-cc-pVTZ level of theory (Table A3), the latter in good agreement with 0.91 eV and 0.98 eV from Knighton et al.[150] and Wiley et al.,[151] respectively. Since the collision energy is always above the threshold of ion-pair formation, the excess energy of the TNI (metastable) can lead to statistical and/or direct dissociation[209]. Formation of metastable parent anions and their detection within the TOF mass window (< 80 µs), has been observed in electron transfer experiments to cyclic and non-cyclic molecular compounds. The former may enable an efficient redistribution of the excess energy through the different internal degrees of freedom, e.g., nitroimidazoles,[57], [58] the latter can be rationalised in terms of an efficient doorway for enhanced bond breaking such as nitromethane.[188] Hexachlorobenzene is a highly symmetric molecule with 30 vibrational degrees of freedom, thus providing an effective mean for energy redistribution, enhancing $C_6Cl_6^-$ yield in the low−energy collision range. As the collision energy is further increased, the parent anion yield decreases, meaning that in such energy range more energy is transferred to the target molecule enhancing fragmentation.

In the energy loss data of Figure 27, the weak feature peaking at (3.1 ± 0.3) eV, yields a positive electron affinity of (1.24 ± 0.3) eV. Note that the asymptotic limit of $C_6Cl_5 + Cl^-$ is 0.56 eV, i.e., 0.35 eV below the ground state of the neutral[184], [187] (C_6Cl_6) meaning that the feature at 1.24 eV does not lead to bond breaking resulting in $C_6Cl_6^-$ formation. There is no available information in the literature on the precise energy value of C–Cl stretching mode of the parent anion (372 cm^{-1} for the neutral ground state[182]), thus the lower limit of the electron affinity (0.94 eV) is in very good agreement with the adiabatic values reported by Knighton et al.[150] and Wiley et al.,[151] 0.91 and 0.98 eV, respectively, as well as the calculated value at the RKS/B3LYP+D3/aug-cc-pVTZ level of theory (see Table 2 and Table A3).

5.4.3 $C_6Cl_5^-$ and Cl^- formation

The TOF mass spectra in Figure 26 is dominated by Cl^- formation in the collision energy range above 10 eV, amounting to ~ 70% of the total anion yield above 40 eV (see BRs in Figure 28). The dominance of such anion formation does not seem unexpected given the considerable high electron affinity of Cl (3.6131 eV[8]). Moreover, in the energy range above 40 eV, the Cl^- branching ratio shows a rather constant behaviour which is reminiscent of the fast collision dynamics (collision time < 37 fs) dictated by direct vertical access within the Franck−Condon region to the ionic states. Hence, those prominent strong antibonding character potential energy surfaces above the ground state are attainable. The collision is therefore mostly dictated by electron promotion into a σ^*_{C-Cl} molecular orbital as depicted in Figure 25 (LUMO+5).

Formation of $C_6Cl_5^-$ and/or Cl^- occurs after cleavage of a C–Cl bond in the TNI and results from a complementary reaction with respect to the negative charge:

$$K + C_6Cl_6 \rightarrow (K^+C_6Cl_6^-) \rightarrow K^+ + (C_6Cl_6^-)^{\#} \rightarrow K^+ + C_6Cl_5^- + Cl \quad (37)$$

$$K + C_6Cl_6 \rightarrow (K^+C_6Cl_6^-) \rightarrow K^+ + (C_6Cl_6^-)^{\#} \rightarrow K^+ + C_6Cl_5 + Cl^- \quad (38)$$

where (C_6Cl_5 −Cl) represents a direct bond breaking and the extra charge sitting on one of the radicals, either on $C_6Cl_5^{\bullet}$ or on $Cl^{\bullet}$. Note that the EA(Cl) = 3.6131 eV[8] and the EA(C_6Cl_5) = 3.10 ± 0.24 eV[8] are essentially identical, yet the Cl^- yield is approximately 3 to 4 times higher than $C_6Cl_5^-$ for E_{CM} < 30 eV and 6 to 7 times higher for E_{CM} > 30 eV collision energy (see BRs in Figure 28). Such behaviour seems plausible given the electronic structure of the hexachlorobenzene molecule. For E_{CM} < 30 eV, the extra electron could attach and occupy the LUMO (Fig. A1) with mostly π^*_{C-C} character.

In such a delocalized system, all six identical chlorine atoms compete for the extra charge, with the excess energy being channelled into the available degrees of freedom, resulting in a stable parent anion rather than prevalent bond breaking. The shape of a selection of $C_6Cl_6^-$ molecular orbitals calculated at the RKS/ B3LYP+D3 level of theory (see Fig. A3) reveal that the SOMO has π_{CCl} character while the next MO shows a strong σ^*_{C-Cl} antibonding nature.

Effective bond breaking yielding Cl^- can only be achieved by efficient non-adiabatic curve crossing between π^*_{C-Cl} and σ^*_{C-Cl} (see Fig. A1 and 72, π* and 73, σ^*_{C-Cl} in Fig. A3), providing that the nuclear wave packet in the C–Cl coordinate survives long enough for the system to change its character, resulting in the formation of a chlorine anion. However, as the collision energy is increased, the number of electronic excited states being accessed also increases, the MOs are mostly σ^*_{C-Cl} in character (Fig. A3) and so direct bond cleavage resulting in Cl^- formation is expected to be more favourable.

The Cl^- BR in Figure 28 shows clearly that trending behaviour as the collision energy is increased above E_{CM} = 20 eV. Moreover, in the high energy collision region, one should not discard that such anion formation can also proceed through shape and/or core-excited resonances, the latter e.g., relaxing into a dissociative state by internal conversion.

The K^+ energy loss spectrum obtained in the forward direction, shows the main feature at (8.1 ± 0.2) eV (Figure 27) with a vertical electron affinity of (–3.76 ± 0.20) eV. This can be assigned to a purely repulsive transition from C_6Cl_6 ground state to a σ^*_{C-Cl} state of the temporary negative ion yielding Cl^- formation, given that this is the most intense fragment anion formed in potassium–hexachlorobenzene collisions above 10 eV.

The energy loss feature peaking at 6.2 ± 0.3 eV (Figure 27), results from accessing an electronic state at 1.86 ± 0.30 eV above the neutral molecule. The calculated molecular orbital for hexachlorobenzene anion at 1.92 eV (Fig. A3), shows a remarkable σ^*_{C-Cl} antibonding character with the extra charge sitting on the C_6Cl_5 radical (Fig. A3). If we now take the ionisation

energy of the potassium atom as 4.34 eV[8] and the C_6Cl_5 electron affinity (see above), from the appearance energy (*AE*) in the energy loss spectrum (~4.5 eV), we can estimate the C_6Cl_5 −Cl bond dissociation energy. Thus, D(C_6Cl_5 −Cl) = AE ($C_6Cl_5^-$) – IE(K) + EA (C_6Cl_5) = (3.26 ± 0.30) eV, which is in excellent accord with Yamada and co-workers[187] calculated value of 3.297 eV (318.1 kJ/mol).

5.4.4 Other fragments

The branching ratios in Figure 28 show that other fragment anions account for ≤ 20% of the total anion yield and these have been assigned to $C_6Cl_4^-$, $C_3Cl_2^-$, C_2Cl^- and Cl_2^-. The possible reaction mechanisms that can be involved in such anions' formation are:

$$K + C_6Cl_6 \rightarrow (K^+C_6Cl_6^-) \rightarrow K^+ + (C_6Cl_6^-)^{\#} \rightarrow K^+ + C_6Cl_4^- + Cl_2 \quad (39)$$

$$K + C_6Cl_6 \rightarrow (K^+C_6Cl_6^-) \rightarrow K^+ + (C_6Cl_6^-)^{\#} \rightarrow K^+ + C_6Cl_4^- + 2Cl \quad (40)$$

$$K + C_6Cl_6 \rightarrow (K^+C_6Cl_6^-) \rightarrow K^+ + (C_6Cl_6^-)^{\#} \rightarrow K^+ + C_3Cl_2^- + C_3Cl_2 \quad (41)$$

$$K + C_6Cl_6 \rightarrow (K^+C_6Cl_6^-) \rightarrow K^+ + (C_6Cl_6^-)^{\#} \rightarrow K^+ + C_2Cl^- + C_4Cl_4 + Cl \quad (42)$$

$$K + C_6Cl_6 \rightarrow (K^+C_6Cl_6^-) \rightarrow K^+ + (C_6Cl_6^-)^{\#} \rightarrow K^+ + Cl_2^- + C_6Cl_4 \quad (43)$$

Note that in eq. (39) and (40), the loss of two chlorine atoms may proceed through reactions yielding Cl + Cl and/or Cl_2. A literature survey reveals neither information on dissociative electron attachment experiments to hexachlorobenzene nor $C_6Cl_4^-$ electron affinity, so no comparative studies as to such neutral radical formation is possible to establish.

The TOF mass spectrum inset in Figure 26 shows two weak signals that have been assigned to $C_3Cl_2^-$ and C_2Cl^- with proposed mechanisms in eq. (41) and (42). We note that these anions are only formed at 100 eV collision energy lab frame, the latter has been reported by MacNeil and Thynne[209] in ion-pair formation from ionisation of tetrachloroethylene. Due to the lack of any other relevant information in the literature regarding either resonances from dissociative electron attachment or any gas-phase thermochemistry data, it is impossible to estimate any thermodynamic thresholds for eq. (41) and (42) producing $C_3Cl_2^-$ and C_2Cl^- and their associated neutral radicals.

Finally, we detain ourselves with Cl_2^- formation from eq. (43) where two C − Cl bonds must be broken, and a molecular chlorine anion has to be formed. From the electron affinity value of Cl_2 to be (2.5 ± 0.2) eV,[8] the above bond dissociation energy D(C_6Cl_5 − Cl) = (3.26 ± 0.30) eV, and taking the available data on D(C − Cl) = (3.3 ± 0.3) eV[210] and D(Cl − Cl)= 2.52 eV,[211] after adding the potassium ionisation energy, the appearance energy of eq. (43) is given by:

$$\begin{aligned}\Delta_f H_g^0(Cl_2^-) &= D(C_6Cl_5 - Cl) + D(C - Cl) - D(Cl - Cl) - EA(Cl_2) + IE(K) \\ &= (5.88 \pm 0.30\ \text{eV})\end{aligned} \quad (44)$$

In the energy loss data of Figure 27, the feature peaking at (7.3 ± 0.2 eV), shows an estimated appearance energy of (5.8 ± 0.2) eV, in good agreement with Cl_2^- formation that may result from eq. (43) with a threshold calculated in (44).The K^+ energy loss features at (9.1 ± 0.1) and (12.1 ± 0.1) eV (Figure 27) with vertical electron affinities of (−4.76 ± 0.10) and (−7.76 ± 0.10) eV are tentatively assigned to core−excited resonances of π^* character and Rydberg excitations, respectively (Table 2). The former is closely related to electronic excitation of the neutral molecule at 4.96 eV to $^1B_{1u}$ state,[178] while Robin reports a value of 5.27 eV;[179] the latter can be assigned to the series $n_{Cl} \rightarrow ns$ converging to (e_{1g}^{-1}) at 9.19 eV[182]. Due to the large number of states which occur in this high energy region, Rydberg assignment is rather difficult to perform, so the series are labelled either as (n+1) or (n+2).

5.5 Cl_2^- Formation upon Molecular Reduction

We investigated hexachlorobenzene reduction in electron transfer experiments to determine the role of chlorine atom positions around the aromatic ring and compared with ortho, meta− and para−dichlorobenzene molecules. This has been achieved by combining gas-phase experiments to determine the reaction threshold by means of mass spectrometry together with quantum chemical calculations. We also observed that Cl_2^- formation can only occur in $1,2-C_6H_4Cl_2$ where the two closest $C-Cl$ bonds are cleaved while the chlorine atoms are brought together within the ring framework excess energy dissipation. These results show that a strong coupling between electronic and $C-Cl$ bending motion is responsible for a positional isomeric effect where molecular recognition is a determining factor in chlorine anion formation.

This is the first combined electron transfer investigation on hexachlorobenzene (C_6Cl_6) and dichlorobenzene isomers ($o-, m-,$ and $p-C_6H_4Cl_2$) yielding a fragment anion at m/z 70, corresponding to the loss of 1,2,3,4−tetrachloro-1,3-cyclohexadien−5−yne, $K + C_6Cl_6 \rightarrow K^+ + C_6Cl_4^{\bullet -} \rightarrow K^+ + Cl_2^- + C_6Cl_4^{\bullet}$ and benzyne $K + C_6H_4Cl_2 \rightarrow K^+ + C_6H_4Cl_2^{\bullet -} \rightarrow K^+ + Cl_2^- + C_6H_4^{\bullet}$radicals from the TNIs.

The TNIs are formed by accommodation of the extra electron into π^* antibonding molecular orbitals of the neutral molecules, while internal rearrangement and efficient intramolecular electron transfer via diabatic curve crossing with $\sigma^*(C-Cl)$, may yield a radical and a negative ion.

We show that the collision induced dissociation mechanism is strongly dependent on the geometrical position of each Cl atom participating in Cl_2^- formation allowing the control of specific bonds to be cleaved upon electron transfer, i.e., a selective molecular bond excision

just in *ortho* positions are favored by capture of an extra electron coupled with relevant internal degrees of freedom along the $C-Cl$ bond. Figure 29 shows the time−of−flight (TOF) mass spectrum with the m/z most intense anions formed in electron transfer from K to C_6Cl_6 at 55 eV lab frame energy (43.5 eV in the centre−of−mass frame), while a discernible less intense anion at m/z 70 is formed. Such anion formation involves a concerted intramolecular rearrangement mechanism within the TNI, where two $C-Cl$ bonds have to be cleaved and a Cl_2 molecule formed with the extra charge. The detection of the parent anion in the present experiments means that hexachlorobenzene has a positive electron affinity (EA), i.e., the anionic state lies energetically below the neutral state. The present quantum chemical calculations at the CBS−QB3 level of theory predict a value of +1.022 eV, thus supporting the experimental observation and in good accord with +1.07 eV from the ωB97XD/aug−cc−pVDZ level of theory of Kumar et al[166].

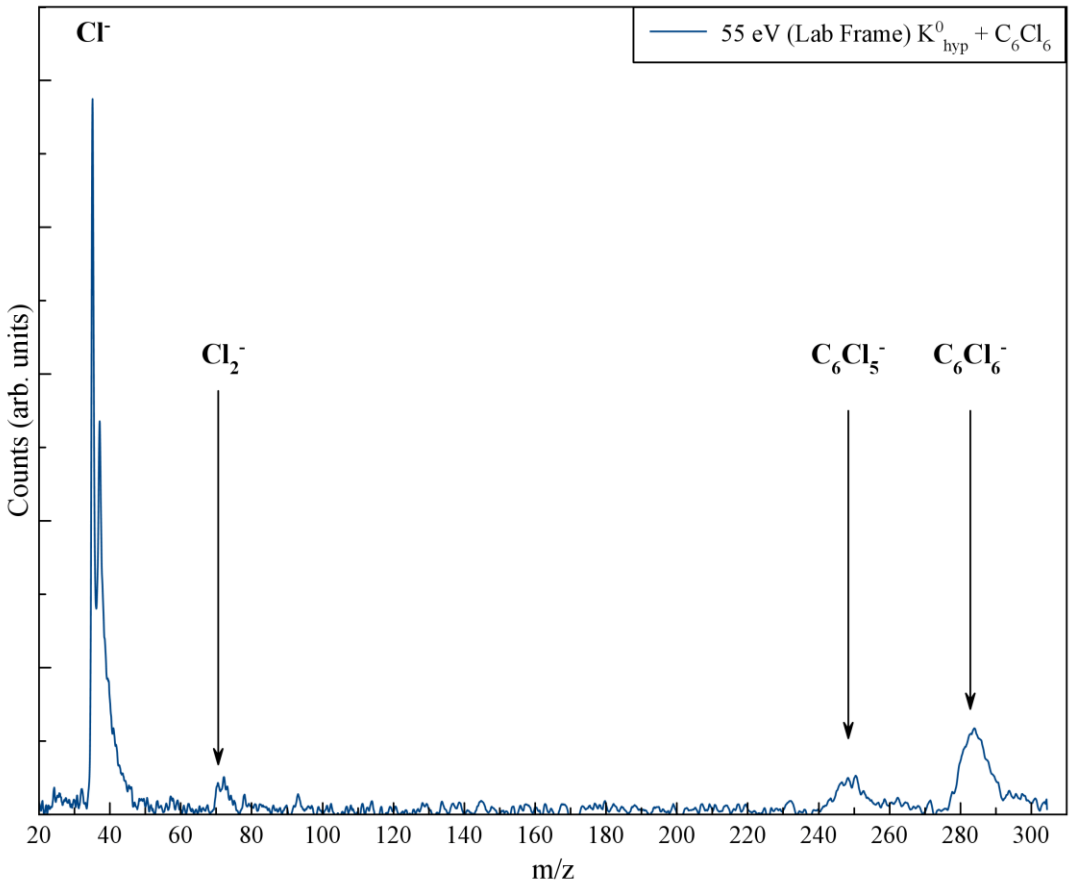

Figure 29 Time-of-flight negative ion mass spectrum in $K-C_6Cl_6$ collisions at 55 eV lab frame energy (43.5 eV in the centre−of−mass frame). The spectrum shows the intensity of m/z anions.

The branching ratios in Figure 30 show that the chlorine molecular anion formation is restricted to less than 10% of the total anions recorded in the wide range of collision energies,

yet above 45 eV it gains some intensity on the expense of $C_6Cl_6^-$ decreasing tendency. The rather constant behaviour above 55 eV is reminiscent of the fast collision dynamics ($t_{collision}$ < 40 fs), where electron promotion into strongly antibonding σ^*_{C-Cl} potential energy surfaces above the ground state is prevalent.

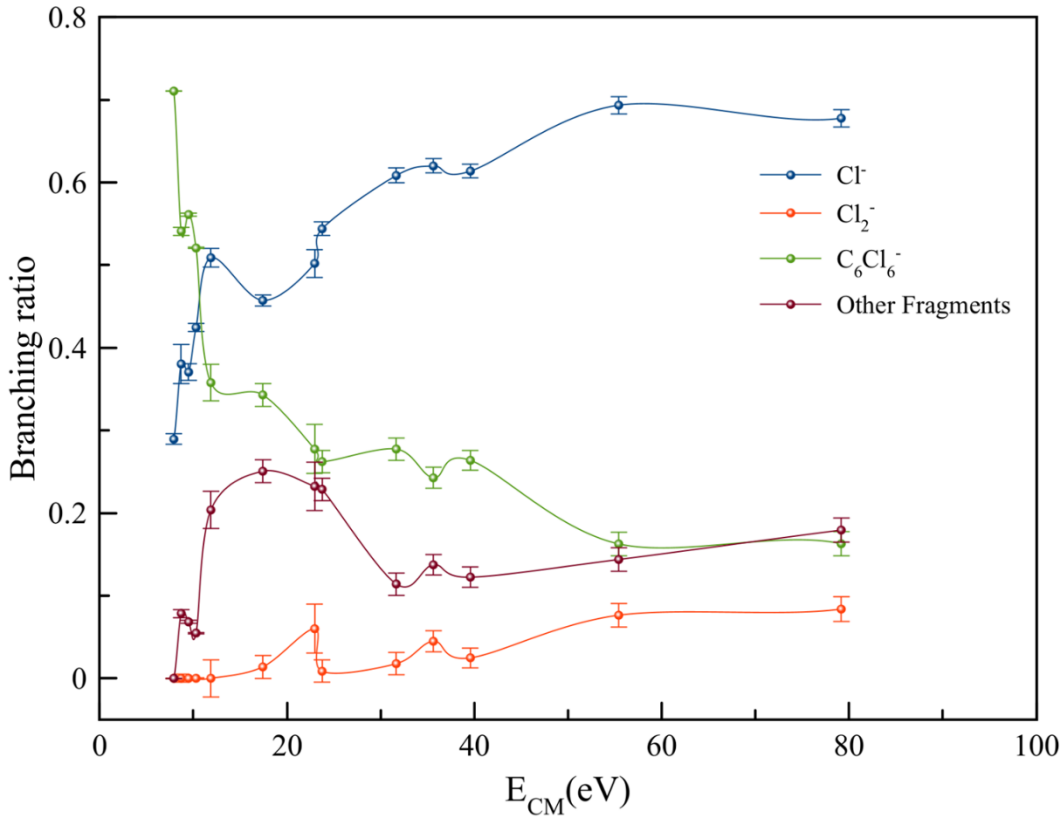

Figure 30 Hexachlorobenzene BRs (fragment anion yield/total anion yield) of $C_6Cl_6^-$, Cl_2^- and Cl^- ions formed as a function of the collision energy in the CM frame. Error bars are related to the experimental uncertainty associated with the ion yields. The lines are just to guide the eye.

We have calculated at the CBS-QB3 (and G4MP2) level of theory the thermodynamic thresholds of Cl_2^-, by taking the bond dissociation energies of $C_6Cl_5 - Cl$, $C_6Cl_4 - Cl$, Cl–Cl and Cl_2 electron affinity, with energies of 1.97, 2.39 and 3.66 eV for *o*-, *m*- and $p - C_6Cl_6$, respectively (**Error! Not a valid bookmark self-reference.**). The reaction threshold has been obtained at (5.88 ± 0.30) eV from the K^+ energy loss experimental data of Kumar et al [127]. If we subtract the potassium ionization energy (4.34 eV), the threshold is now expected at (1.54 ± 0.30) eV. Thus, we assign Cl_2^- formation to exclusive cleavage of two close-lying C–Cl bonds from C_6Cl_6 upon electron transfer and the experimental value is in good accord with the quantum chemical calculations for the $o - C_6Cl_6$ configuration (**Error! Not a valid bookmark self-reference.**). We also investigated, with M06-2X density functional and the 6−31G (d, p) basis set, Cl_2^- (and

Cl_2) detachment reactions via *para*-Cl migration, and concluded that it is an unlikely mechanism, see appendix A.4.

Table 3 Calculated Cl_2^- appearance energies (AE), bond dissociation energies (D) and electron affinity (EA) for hexachlorobenzene at different levels of theory. Values are in (eV).

	CBS−QB3 (eV)	G4MP2 (eV)
AE (Cl_2^-), $o-C_6Cl_6$	1.97	1.96
AE (Cl_2^-), $m-C_6Cl_6$	2.39	2.39
AE (Cl_2^-), $p-C_6Cl_6$	3.66	3.65
D (C_6Cl_5-Cl)	4.38	4.18
D ($o-C_6Cl_4-Cl$)	2.66	2.64
D ($m-C_6Cl_4-Cl$)	3.07	3.08
D ($p-C_6Cl_4-Cl$)	4.35	4.34
D (Cl–Cl)	2.57	2.51
EA (Cl_2)	2.50	2.36

In electron transfer to hexachlorobenzene, the minimum energy required to break a second C–Cl bond ($o-C_6Cl_4-Cl$, $m-C_6Cl_4-Cl$ and $p-C_6Cl_4-Cl$) lies between 2.7 and 4.4 eV (We have calculated at the CBS-QB3 (and G4MP2) level of theory the thermodynamic thresholds of Cl_2^-, by taking the bond dissociation energies of C_6Cl_5-Cl, C_6Cl_4-Cl, Cl–Cl and Cl_2 electron affinity, with energies of 1.97, 2.39 and 3.66 eV for *o*-, *m*- and $p-C_6Cl_6$, respectively (**Error! Not a valid bookmark self-reference.**). The reaction threshold has been obtained at (5.88 ± 0.30) eV from the K^+ energy loss experimental data of Kumar et al [127]. If we subtract the potassium ionization energy (4.34 eV), the threshold is now expected at (1.54 ± 0.30) eV. Thus, we assign Cl_2^- formation to exclusive cleavage of two close-lying C–Cl bonds from C_6Cl_6 upon electron transfer and the experimental value is in good accord with the quantum chemical calculations for the $o-C_6Cl_6$ configuration (**Error! Not a valid bookmark self-reference.**). We also investigated, with M06-2X density functional and the 6−31G (d, p) basis set, Cl_2^- (and Cl_2) detachment reactions via *para*-Cl migration, and concluded that it is an unlikely mechanism, see appendix A.4.

Table 3), so site selectivity yielding Cl_2^- does not result from any particular energy constraint. The electronic structure of the associated TNIs accessed in the collision process must play a significant role on the intramolecular mechanisms responsible for channelling the excess energy through the different available degrees of freedom that will lead to molecular dissociation. To investigate this, we have conducted a comprehensive dynamical investigation on the role of C–Cl stretching in the TNI.

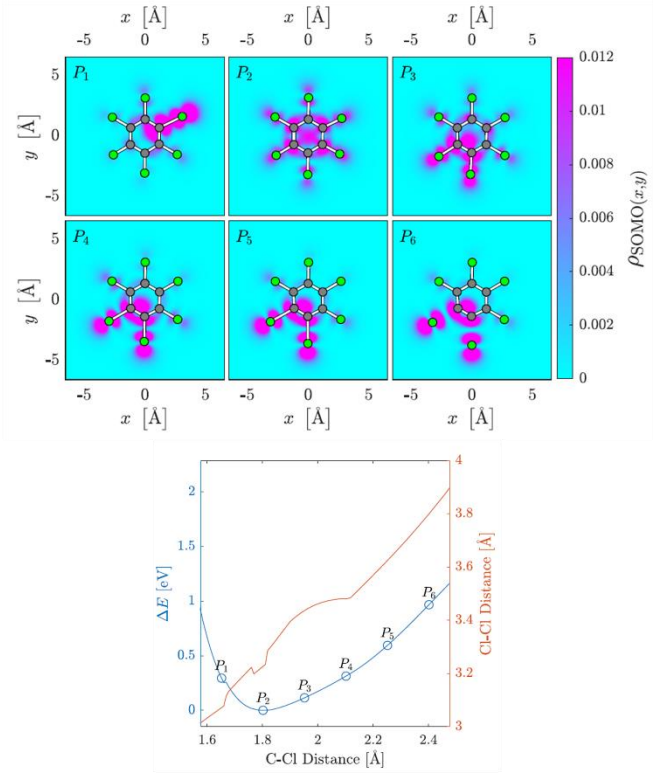

Figure 31 SOMO densities at six different C–Cl internuclear stretching distances and the corresponding potential energy curve.

Figure 31 shows the change in energy (ΔE), in the Cl–Cl distance and the shape of $C_6Cl_6^-$ singly occupied molecular orbital (SOMO), as the C–Cl bond stretching distances of two Cl atoms in the *ortho* isomer are varied while keeping all other geometric parameters relaxed. The color maps show the electron density of the SOMO, squared, and integrated along the z-coordinate perpendicular to the molecular plane. A close inspection of this figure shows that the equilibrium geometry is found at 1.802 Å, while at P1 the C–Cl distance is considerably shorter. At P2 the SOMO is delocalized over the whole anion whereas from P3 to P6, the C–Cl bond elongation causes a SOMO displacement to two neighbouring C–Cl bonds. The energy increases, although at 2.4 Å there is no evidence of bond breaking, from which the Cl atoms do not move together and there is not yet an indication of a bond being formed between the two adjacent chlorine atoms.

The other possible mechanism is related to the change in the Cl–Cl distance of two adjacent Cl atoms as the C–Cl bending distances are changed while relaxing the other geometric parameters within the TNI (Figure 32). The Cl–Cl distance of the two upper Cl atoms is increased from P1 to P6. The equilibrium geometry is found at 3.246 Å, while from P1 to P5 the SOMO is delocalized and does not appreciably change upon increasing the Cl–Cl distance. In P6, the occupied MO moves to the elongated C–Cl bonds and their Cl atoms. The Cl–Cl distance increases further, in line with the observation from the scan of the C–Cl coordinate

whereas the C–C–Cl angles are kept at 120°. However, as the Cl–Cl distance is decreased, at ~ 2 Å, a bond is formed between two adjacent chlorine atoms and these detach from the neutral ring carrying the extra charge, as confirmed from the atomic charge populations.

The electron transfer TOF mass spectra of negative ions formed in potassium collisions with dichlorobenzene isomers, do not show a parent anion formation, but are dominated by Cl^-, with Cl_2^- only formed from 1,2−$C_6H_4Cl_2$ (see Appendix A.4). The absence of a non-dissociated anion does not seem surprisingly given their negative EA values (at the CBS-QB3 level of theory) of −0.20, −0.21, and −0.44 eV for o−$C_6H_4Cl_2$, m−$C_6H_4Cl_2$, and p−$C_6H_4Cl_2$ meaning no thermodynamically stable anions exist.

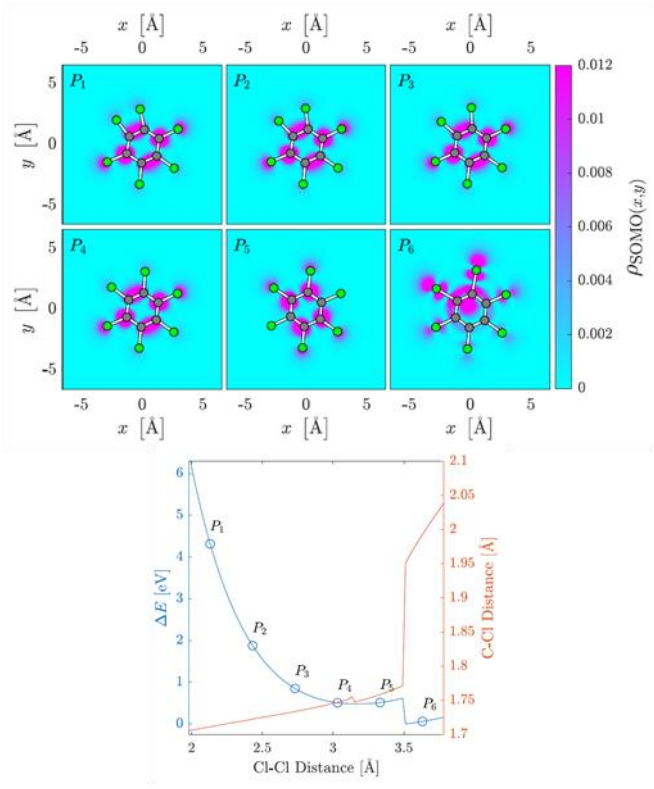

Figure 32 SOMO densities at six different C–Cl internuclear bending distances and the corresponding potential energy curve.

Another interesting aspect of dichlorobenzene isomers fragmentation pattern pertains to the absence of a $C_6H_4^-$ ion despite the benzyne radical electron affinity (EA = 1.265 ± 0.008 eV [212]). Upon reduction of $C_6H_4Cl_2$ molecules in the low-energy collision regime (typically below 100 eV), the extra charge is accommodated in the π* antibonding MOs of the ring. As long as an efficient diabatic curve crossing enables a fast-intramolecular electron transfer to a σ*(C–Cl) bond, the collision induced dissociation favours formation of fragments with higher electron affinities (EA(Cl) = 3.6131 eV [213], EA(Cl_2) = 2.50 eV (We have calculated at the CBS-QB3 (and G4MP2) level of theory the thermodynamic thresholds of Cl_2^-, by taking the bond

dissociation energies of $C_6Cl_5 - Cl$, $C_6Cl_4 - Cl$, Cl–Cl and Cl_2 electron affinity, with energies of 1.97, 2.39 and 3.66 eV for *o*-, *m*- and $p - C_6Cl_6$, respectively (**Error! Not a valid bookmark self-reference.**). The reaction threshold has been obtained at (5.88 ± 0.30) eV from the K^+ energy loss experimental data of Kumar et al [127]. If we subtract the potassium ionization energy (4.34 eV), the threshold is now expected at (1.54 ± 0.30) eV. Thus, we assign Cl_2^- formation to exclusive cleavage of two close-lying C–Cl bonds from C_6Cl_6 upon electron transfer and the experimental value is in good accord with the quantum chemical calculations for the $o - C_6Cl_6$ configuration (**Error! Not a valid bookmark self-reference.**). We also investigated, with M06-2X density functional and the 6−31G (d, p) basis set, Cl_2^- (and Cl_2) detachment reactions via *para*-Cl migration, and concluded that it is an unlikely mechanism, see appendix A.4.

Table 3)), *viz.* Cl^- and Cl_2^-. Note that the formation relative efficiency of the latter relative to the former anion is lower because two C–Cl bonds have to be excised and a molecular ion formed. This certainly requires a concerted mechanism within the TNI and energy redistribution through the available degrees of freedom.

The CBS-QB3 (and G4MP2) level of theory calculations in Table 4, show the Cl_2^- thermodynamic thresholds for *o*-, *m*- and *p*-$C_6H_4Cl_2$, to be 2.08, 2.78 and 3.29 eV, respectively, by taking the bond dissociation energies of $C_6H_4Cl - Cl$, $C_6H_4 - Cl$, Cl–Cl (We have calculated at the CBS-QB3 (and G4MP2) level of theory the thermodynamic thresholds of Cl_2^-, by taking the bond dissociation energies of $C_6Cl_5 - Cl$, $C_6Cl_4 - Cl$, Cl–Cl and Cl_2 electron affinity, with energies of 1.97, 2.39 and 3.66 eV for *o*-, *m*- and $p - C_6Cl_6$, respectively (**Error! Not a valid bookmark self-reference.**). The reaction threshold has been obtained at (5.88 ± 0.30) eV from the K^+ energy loss experimental data of Kumar et al [127]. If we subtract the potassium ionization energy (4.34 eV), the threshold is now expected at (1.54 ± 0.30) eV. Thus, we assign Cl_2^- formation to exclusive cleavage of two close-lying C–Cl bonds from C_6Cl_6 upon electron transfer and the experimental value is in good accord with the quantum chemical calculations for the $o - C_6Cl_6$ configuration (**Error! Not a valid bookmark self-reference.**). We also investigated, with M06-2X density functional and the 6−31G (d, p) basis set, Cl_2^- (and Cl_2) detachment reactions via *para*-Cl migration, and concluded that it is an unlikely mechanism, see appendix A.4.

Table 3) and Cl_2 electron affinity (We have calculated at the CBS-QB3 (and G4MP2) level of theory the thermodynamic thresholds of Cl_2^-, by taking the bond dissociation energies of $C_6Cl_5 - Cl$, $C_6Cl_4 - Cl$, Cl–Cl and Cl_2 electron affinity, with energies of 1.97, 2.39 and 3.66 eV for *o*-, *m*- and $p - C_6Cl_6$, respectively (**Error! Not a valid bookmark self-reference.**). The reaction threshold has been obtained at (5.88 ± 0.30) eV from the K^+ energy loss experimental data of Kumar et al [127]. If we subtract the potassium ionization energy (4.34 eV), the threshold is now expected at (1.54 ± 0.30) eV. Thus, we assign Cl_2^- formation to exclusive cleavage of two close-lying C–Cl bonds from C_6Cl_6 upon electron transfer and the experimental value is in

good accord with the quantum chemical calculations for the o $-C_6Cl_6$ configuration (**Error! Not a valid bookmark self-reference.**). We also investigated, with M06-2X density functional and the 6−31G (d, p) basis set, Cl_2^- (and Cl_2) detachment reactions via *para*-Cl migration, and concluded that it is an unlikely mechanism, see appendix A.4.

Table 3). Thus, the proximity of two chlorine atoms in the ring as is the *o*-$C_6H_4Cl_2$ case, indicates that Cl_2^- formation requires the lowest energy within the three dichlorobenzene isomers, ~ 2.1 eV, while in *m*-$C_6H_4Cl_2$ and *p*-$C_6H_4Cl_2$, the calculated reactions have energies in excess of 2.8 eV, yet Cl_2^- formation from these molecules was not observed in the experiment. As it happens in *o*−C_6Cl_6, the geometrical proximity of Cl atoms is pivotal to guarantee formation of such anion, although Cl motion from other positions within the ring are very unlikely, see appendix A.4.

Table 4 Calculated Cl_2^- appearance energies (AE) and bond dissociation energies (D) for dichlorobenzenes at different levels of theory. Values in (eV).

	CBS−QB3 (eV)	G4MP2 (eV)
AE (Cl_2^-), *o*−$C_6H_4Cl_2$	2.08	2.07
AE (Cl_2^-), *m*−$C_6H_4Cl_2$	2.78	2.79
AE (Cl_2^-), *p*−$C_6H_4Cl_2$	3.29	3.29
D(*o*−C_6H_4Cl-Cl)	4.41	4.23
D(*m*−C_6H_4Cl-Cl)	4.38	4.22
D(*p*−C_6H_4Cl-Cl)	4.41	4.25
D(*o*−C_6H_4-Cl)	2.74	2.71
D(*m*−C_6H_4-Cl)	3.46	3.44
D(*p*−C_6H_4-Cl)	3.95	3.91

Comparing now the negative ion formation from C_6Cl_6 and $C_6H_4Cl_2$ molecules, the remarkable *ortho* position sensitization in the presence of an electron donor, triggers a specific electron transfer process with the same consecutive C–Cl bond excision leading to formation of a neutral radical and the corresponding molecular fragment anion. The calculated energy thresholds indicate no appreciable difference in the exclusive reaction yielding Cl_2^- from *o*−C_6Cl_6 and *o*-$C_6H_4Cl_2$, where in the case of the former molecule is evident by the experimental value obtained. The preferred selectivity of the bond excision position in these molecules is not particularly enhanced because the electron transfer reaction proceeds in the presence of barriers (transition states), leading therefore to comparably low abundance of the fragment chlorine molecular anion formed, see appendix A.4. Notwithstanding, the process investigated here can be of relevance on key selected molecular compounds playing a specific role in catalysis, enzymatic reactions, or more generally in chemical reactions where a transition state is prevalent in bond breaking and bond making [214].

5.6 Summary

We have presented a novel comprehensive study on TOF mass spectrometry negative ion formation in neutral potassium atom collisions with neutral hexachlorobenzene molecules in the lab frame energy range from 10 up to 100 eV. The TOF mass spectra are dominated by the undissociated parent anion $C_6Cl_6^-$, and Cl^- and together with $C_6Cl_5^-$ these anions contribute to more than 80% of the ions recorded, where other fragments assigned to $C_6Cl_4^-$, $C_3Cl_2^-$, C_2Cl^- and Cl_2^-, amounting to less than 20% of the total anion yield. Theoretical calculations on the vertical excitation energies were performed at different levels of theory to help us in assigning the electronic transitions.

Potassium cation post-collision energy loss data has been obtained in the forward direction ($\theta \cong 0°$) at 162.2 eV in the centre-of-mass frame (205 eV lab frame), with a dominant feature assigned to an electronic transition with a vertical electron affinity of (–3.76 ± 0.20) eV. This has been assigned to a purely repulsive transition from C_6Cl_6 ground state to a σ^*_{C-Cl} state of the temporary negative ion yielding Cl^- formation. The energy loss data has revealed a weak feature at (3.1 ± 0.3) eV, yielding a positive electron affinity of (1.24 ± 0.3) eV, where its lower limit value (0.94 eV) was assigned to C_6Cl_6 adiabatic electron affinity and is in very good agreement with the values reported in the literature. Moreover, the $C_6Cl_5^-$ and Cl_2^- thresholds of formation have been obtained from the experimental energy loss data, the former allowing to estimate a bond dissociation energy D $(C_6Cl_5 - Cl)$ = (3.26 ± 0.30) eV. We have also comprehensively investigated the reduction of hexachlorobenzene and dichlorobenzene isomers in electron transfer processes and obtained selective C–Cl bond excisions to both molecular compounds in the gas-phase. This is achieved by the combined balance between bond dissociation energies and electron affinity of the chlorine molecule. The reactions are all endothermic and, corresponding to the different isomers, the presence of a barrier results in an energy balance that favours the *ortho* configuration. Although the efficiency in producing Cl_2^- is not particularly significant from the TOF negative ions branching ratios relative to other fragment anions, this is due to a relevant energy redistribution within the TNI upon electron capture that involves the different internal degrees of freedom through relevant vibronic coupling. The present findings may have implications in the role of a transition state in chemical reactions which are prevalent in different environments not only in the gas but in bulk systems. The sensitization of *ortho* positions in C_6Cl_6 and $C_6H_4Cl_2$ can be achieved upon molecular reduction, which in the present case is obtained through a potassium atom, making these geometrical effects in polyatomic molecules important in single electron transfer reactions. We can anticipate that within the scope of redox reactions, the effect of an electron donor (oxidized species) and an

electron acceptor (reduced species), may offer in solution a particular selectivity as to the role of reactants and products.

6.

BOUND ELECTRON ENHANCED RADIOSENSITISATION OF NIMORAZOLE UPON CHARGE TRANSFER

This chapter describes nimorazole (NIMO) radiosensitizer reduction upon electron transfer in collisions with neutral potassium (K) atoms in the lab frame energy range of $10 - 400$ eV. The negative ions formed in this energy range were time−of−flight mass analysed, and branching ratios obtained. Assignment of different anions shows that more than 80% is due to formation of the non−dissociated parent anion $NIMO^{\bullet -}$ at 226 u and nitrogen dioxide anion NO_2^- at 46 u. The rich fragmentation pattern reveals significant collision induced decomposition of the 4−nitroimidazole ring as well as other complex internal reactions within the temporary negative ion formed after electron transfer to neutral NIMO. Other fragment anions are only responsible for less than 20% of the total ion yield. Additional information on the electronic state spectroscopy of nimorazole has been obtained by recording a K^+ energy loss spectrum in the forward scattering direction ($\theta \approx 0°$) allowing to determine the most accessible electronic states within the temporary negative ion. Quantum chemical calculations on the electronic structure of NIMO in the presence of a potassium atom have been performed to help assigning the most significant lowest unoccupied molecular orbitals participating in the collision process. Electron transfer is shown to be a relevant process for nimorazole radiosensitisation through efficient and prevalent non-dissociated parent anion formation. This chapter has been submitted for peer review publication.

6.1 Introduction

In the atmosphere, reactions with •OH radicals have been identified as a yet the relative can be eliminated by ozone coupled with hydrogen peroxide processes and Nimorazole (NIMO ≡ $C_9H_{14}N_4O_3$), is a chemical compound that has been widely used as an efficient

hypoxic (deficient in oxygen) cell radiosensitizer in head and neck squamous carcinoma due to its low toxicity [41]. In its composition, NIMO contains a 4−nitroimidazole and a morpholine rings bonded by their nitrogen atoms (N1) through a $-H_2C-CH_2-$ side group (Figure 33).

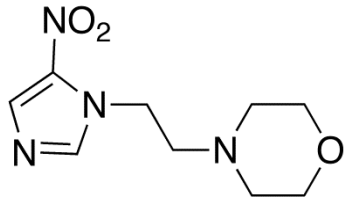

Figure 33 Chemical structure of nimorazole (NIMO),$C_9H_{14}N_4O_3$.

NIMO's ability to scavenge low-energy electrons has been recently shown to be very efficient in producing a non−dissociated parent anion with a considerable large cross−section of $\sim 3 \times 10^{-18}$ m^2 (at ~ 0 eV) [43], [215], while dissociative electron attachment to be a minor reaction channel which is suppressed upon hydration [215]. Although the detailed mechanisms by which radiosensitisation operates are still unknown, it is believed that radiosensitisers are chemical compounds subject to redox reactions inside the hypoxic cells [44], and in case of nitroimidazoles, the ring facilitates reduction through reactive anion radicals' formation [45]–[47]. Nitroimidazole radiosensitisers have been thoroughly investigated by experimental methods on low-energy electron interactions [48]–[52] and together with nimorazole probed by electrospray ionization mass spectrometry [53]–[55]. While associative electron attachment may contribute to NIMO's radiosensitising effect, within the biological environment, electron transfer processes (redox reactions) may prevail and so these may seem more appropriate to describe the underlying molecular mechanisms of such chemical compounds and their role as radiosensitisers. Thus, we have initiated more than a decade ago an investigation methodology to explore key selected radiosensitisers by charge transfer in atom-molecule collision experiments, *viz*. halogenated uracil [56] and more recently nitroimidazoles [57], [58]. In the former case, the decomposition yields significant ring breaking with appreciable NCO^- intensities (in 5-FU) and halogen anion formation (in 6-ClU), thus compromising the integrity of viral RNA where the neutral molecules bind. For the latter, the collision induced dissociation results in formation of several radicals, with particular attention to $NO^\bullet$ and $OH^\bullet$. These radicals act as an indirect DNA damage agent triggered by ionising radiation, while nitric oxide has been noted for sensitizing hypoxic solid tumours in radiotherapy and chemotherapy treatments [59]. Another relevant aspect pertains to the role of site and bond-selectivity in electron transfer processes to DNA/RNA nucleotides yielding bond cleavage [11], [16], which have been shown to be pivotal in controlling chemical reactions. As recently shown [57], [58], such

control of a given bond breaking may have relevance to tailor chemical control for different applications such as tumour radiation therapy through nitroimidazole-based radiosensitisation.

6.2 Materials and Methods

6.2.1 The crossed molecular beam setup

The crossed molecular beam setup used to investigate collisions of neutral potassium (K) atoms with neutral nimorazole (NIMO) molecules, has been described in detail elsewhere [57], [188]. Briefly, an effusive molecular beam target crosses a primary beam of fast neutral K atoms, and the product anions are analysed using a reflectron (KORE R-500-6) time-of-flight (r−TOF) mass spectrometer. The K beam is produced in a resonant charge exchange chamber from the interaction of K^+ ions from a commercial potassium ion source (HeatWave, USA), in the range of 10 up to 400 eV in the lab frame, with gas-phase neutral potassium atoms from an oven source. The TOF anion yield is normalized considering the primary beam current, pressure, and acquisition time. Negative ions formed in the collision region were extracted by a ~380 V/cm pulsed electrostatic field. The typical base pressure in the collision chamber was 6×10^{-5} Pa and the working pressure was 2×10^{-4} Pa. Mass spectra (resolution $m/\Delta m \approx 800$) were obtained by subtracting background measurements (without the sample) from the sample measurements. Mass calibration was performed based on the well-known anionic species formed after potassium collisions with nitromethane [188] and tetrachloromethane [189].

Post−collision potassium cation (K^+) energy loss spectra in the forward scattering direction ($\theta \approx 0°$) with the beam's optical path have been recorded in a hemispherical energy loss analyser. These experiments were not performed in coincidence with TOF mass spectrometry. The analyser was operated in constant transmission mode, hence keeping the resolution constant throughout the entire scans. The energy resolution during the experiments was (1.2 ± 0.2) eV, and the energy loss scale was calibrated using the K^+ beam profile from the potassium ion source serving as the elastic peak.

The molecular sample of NIMO was supplied by Toronto Research Chemicals with a stated purity of ≥ 97%. The solid sample was used as delivered and gently heated up to 343 K using a temperature PID (proportional-integral-derivate controller) unit. Special procedure was taken to test for any thermal decomposition products within the NIMO beam. Thus, mass spectra were recorded at different temperatures and no differences in the relative peak intensities as a function of temperature were observed.

6.2.2 Theoretical Methods

The electronic structure investigations of the molecular orbitals (MOs) formed in collisions between potassium (K) atoms and NIMO have been performed to provide insight into the electron transfer process up to 10 eV. Focus on the analysis of the computed lowest unoccupied molecular orbitals (LUMOs) was considered to assess the nature of the different electronic states that result in the detected negative ions of the current experiments.

The geometries of both NIMO in its ground state, and NIMO + K were initially fully optimized at the M06-2X/6-311++g (d, p) level of theory [216]. We start the calculations by positioning the potassium atom at 5 Å from morpholine and 4-nitromidazole moieties. The resulting optimized system upon the collision of the K atoms with NIMO resulted in the structure shown in Figure 37.

All quantum chemical computations have been performed with the Gaussian 16 program package [217]. The calculation has been carried out in Cartesian coordinates, with no symmetries. All electrons have been considered for carbon, oxygen, nitrogen, hydrogen, and potassium atoms with the 6-311++g (d, p) basis set [218], [219]. The natural molecular orbitals for K−NIMO have been calculated by Time-Dependent Density Functional Theory (TD-DFT/M06-2X) methods [220].

6.3 Results

Negative ion yields of NIMO have been obtained as a function of the collision energy from 10 − 400 eV in the lab frame (7.7 − 310 eV in the centre−of−mass frame), with their proposed assignments in Table 5. Note that the observed relative isotopic yields are in accordance with the expected natural abundances for the cyanide anion (CN^-) at 26 u (100%) and 27 u (1.44%), the nitrogen dioxide anion (NO_2^-) at 46 u (100%), 47 u (0.44%) and 48 (0.4%), and the non-dissociated parent anion $NIMO^{\bullet-}$ at 226 u (100%), 227 u (11.5%), 228 u (1.2%) and 229 u (~0.1%). In Table 5 we also list the anions formed in (dissociative) electron attachment experiments [43], [215], noting that in the present investigation the fragmentation pattern is much richer. Such is certainly not unexpected given the different collision dynamics in electron transfer to a free electron process. The two most intense signals are assigned to the non-dissociated parent anion $NIMO^{\bullet-}$ at 226 u and the nitrogen dioxide anion NO_2^- at 46 u (see Figure 34), amounting, on average more than 90% of the total anion yield. The rich fragmentation pattern, which is more enhanced at higher collision energies (above 40 eV in Figure 34), reveals significant collision induced decomposition of the 4−nitroimidazole ring as well as other complex internal reactions within the temporary negative ion formed after electron transfer to neutral NIMO. Yet, these fragment anions are only responsible for less than ~10% of the total ion yield. The

branching ratios (BRs) for the most intense anions from NIMO are shown in Figure 35, where a strong energy dependence is discernible. These have been obtained from the integrated time-of-flight mass peak divided by the total anion yield at a given collision energy. This means that, although the non-dissociated parent anion yield in the TOF mass spectra is lower than NO_2^- (Figure 34), its integrated signal comprises 226 u and its isotopes yield a branching ratio value that is dominant over all the other fragment anions across the entire collision energy range investigated.

The vertical electron affinities and assignments of the most typical molecular orbitals are shown in Table 6. The energy loss needed to access an electronic state is given by:

$$\Delta E = IE(K) - EA(I_{max}) \tag{45}$$

with IE(K) the ionization energy of the potassium atom (4.34 eV [221]) and EA(I_{max}) the target's molecule electron affinity for that state [208]. Figure 36 shows a main feature with a maximum intensity (I_{max}) cantered at (7.21 ± 0.03) eV, yielding a vertical electron affinity of (−2.87 ± 0.03) eV, in good accord with the dissociative electron attachment resonance at ~ 2.97 eV [43] (see discussion further down).

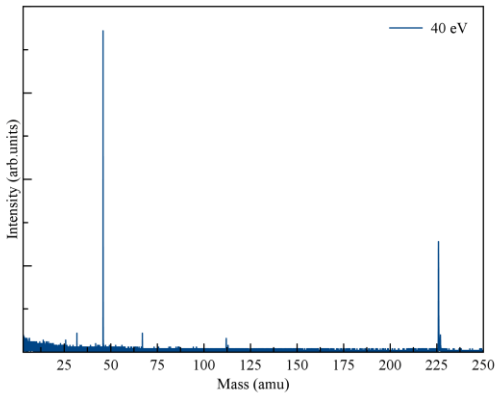

(a)

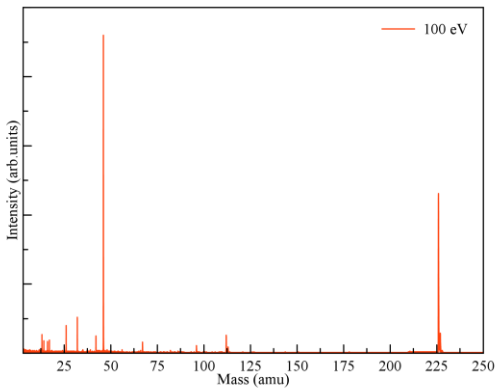

(b)

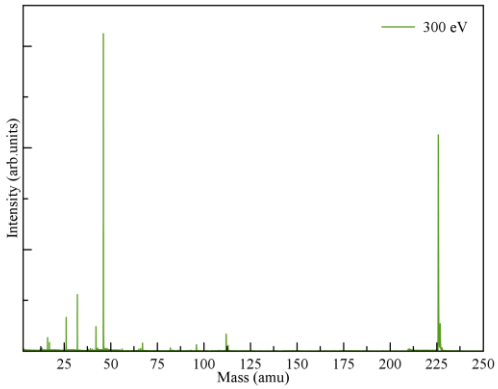

(c)

Figure 34 Time-of-flight negative ions mass spectra in neutral potassium collisions with neutral nimorazole at: (a) 40 eV lab frame (30.7 eV centre–of–mass); (b) 100 eV lab frame (76.7 eV centre–of–mass); (c) 300 eV lab frame (230.2 eV centre–of–mass). See text for details and Table 1 for assignments.

Table 5 Proposed assignment of negative ions formed in electron transfer in potassium collisions with nimorazole (NIMO) compared with electron attachment experiments[42], [43]

Mass (u)	Mass (u) [42], [43]	Assignment	Major source of fragmentation
26, 27	26	CN^-, $^{13}CN^-$	4–nitromidazole ring
30	–	NO^-	4–nitromidazole ring
38	–	$C_2N^-/C_3H_2^-$	
39	–	$C_2HN^-/C_3H_3^-$	
40	–	$C_2H_2N^-$	
41	–	$C_2H_3N^-/CHN_2^-$	
42	42	CNO^-	4–nitromidazole ring
43	–	$CHNO^-$	
46, 47, 48	46, 48	NO_2^-, $^{15}NO_2^-$, $^{14}N^{18}OO^-$	4–nitromidazole ring
52	–	$C_3H_2N^-$	

56	–	$C_2H_2NO^-$ / $C_3H_6N^-$	4−nitromidazole ring
64	–	$C_3N_2^-$	
65	65	$C_3HN_2^-$	
66	–	$C_3H_2N_2^-$	
67	67	$C_3H_3N_2^-$	
68	–	$C_3H_4N_2^-$	
69	–	$C_3H_5N_2^-$	
79	–	$C_4H_3N_2^-$	
80	–	$C_4H_2NO^-$	
81	–	$C_3HN_2O^-$ / $C_4H_3NO^-$	morpholine ring
82	82	$C_3H_2N_2O^-$ / $C_4H_4NO^-$	
83	83	$C_3H_3N_2O^-$ / $C_4H_5NO^-$	
84	–	$C_3H_4N_2O^-$ / $C_4H_6NO^-$	
86	–	$C_4H_8NO^-$	
93	–	$C_4HN_2O^-$	
94	–	$C_3N_3O^-$	
95	–	$C_4H_3N_2O^-$	
96	–	$C_3H_2N_3O^-$	
97	97	$C_3H_3N_3O^-$	
108	–	$C_4H_2N_3O^-$	
109	–	$C_4HN_2O_2^-$	
111	–	$C_4H_3N_2O_2^-$	
112	112	$C_3H_2N_3O_2^-$	
113	–	$C_4H_5N_2O_2^-$	
114	–	$C_3H_4N_3O_2^-$	
126	–	$C_4H_4N_3O_2^-$	
134	–	$C_5N_3O^-$	
138	–	$C_5H_4N_3O_2^-$	
139	–	$C_4H_3N_4O_2^-$	
–	178	$(NIMO - NO_2 - 2H)^-$	
196	196	$(NIMO - NO)^-$	
–	208	$(NIMO - H_2O)^-$	
–	209	$(NIMO - OH)^-$	
210	210	$(NIMO - O)^-$	
225	225	$(NIMO - H)^-$	
226, 227, 228, 229	226	$NIMO^{\bullet -}$ and its isotopes	

The electronic structure of NIMO in presence of a potassium atom has also been investigated by theoretical methods (see 6.2.2), where the shape and energy of the different molecular orbitals (MOs) have been obtained up to 10 eV (see appendix B). The information gained from the lowest unoccupied molecular orbitals (LUMOs) has been critical to assign the different electronic states attained in the electron transfer process. The geometry of nimorazole was optimized at the M06-2X/6-311++g (d, p) level of theory. Upon collision with the potassium atom, the system K + NIMO was also optimized at the M06-2X/6-311++g (d, p) level of theory.

The optimized geometry led to a distance of ≈ 5.1 Å between K and O atoms from the 4-nitroimidazole ring (see Figure 37).

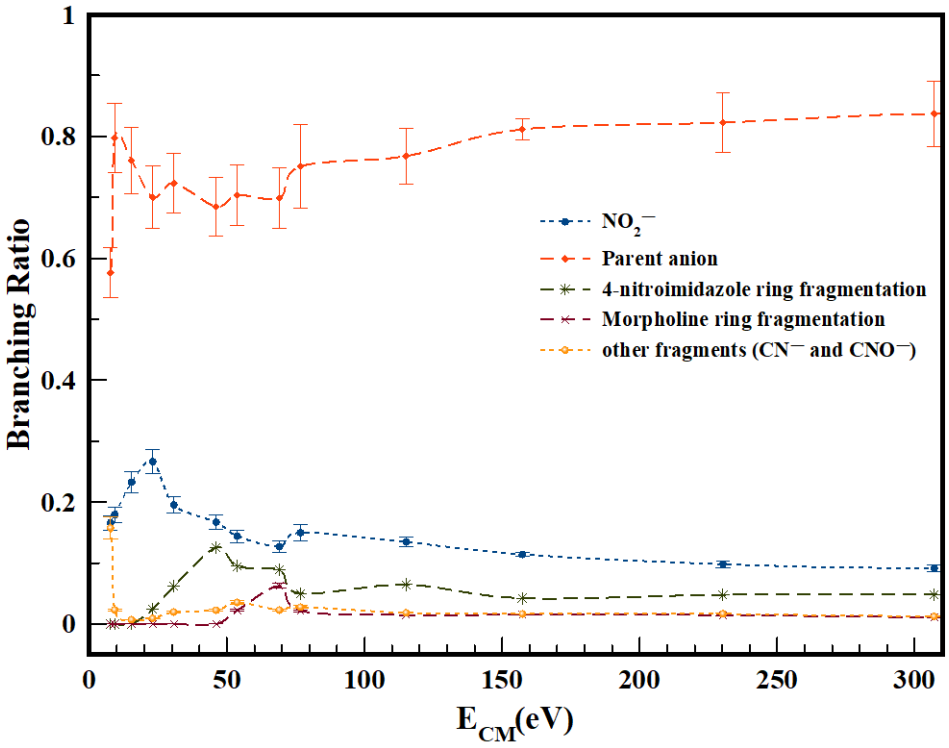

Figure 35 NIMO branching ratios (fragment anion yield/total anion yield) of the main anions formed as a function of the collision energy in the centre–of–mass frame. Error bars are related to the experimental uncertainty associated with the ion yields. The lines were just to guide the eye.

Table 6 Assignment of different features from the Gaussian fitting to K^+ energy loss spectrum from potassium collisions with NIMO at 205 eV lab frame energy (157 eV in the centre–of–mass frame). VEA (Vertical Electron Affinity), VE (Vertical Energy)[2].

K^+ energy loss feature (eV)	VEA (eV)	Calculated VE of MO (eV)	Assignment	DEA resonances[42], [43]
4.74 ± 0.07	− 0.40 ± 0.07	4.81	LUMO+50	0.41
6.11 ± 0.04	− 1.77 ± 0.04	5.69	LUMO+60	1.49, 1.93
7.21 ± 0.03	− 2.87 ± 0.03	7.01	LUMO+70	2.97
8.17 ± 0.06	− 3.83 ± 0.06	8.28	LUMO+80	3.53, 3.6
9.55 ± 0.11	− 5.21 ± 0.11	9.17	LUMO+90	–

[2] The uncertainties result from the Gaussian fitting procedure used.

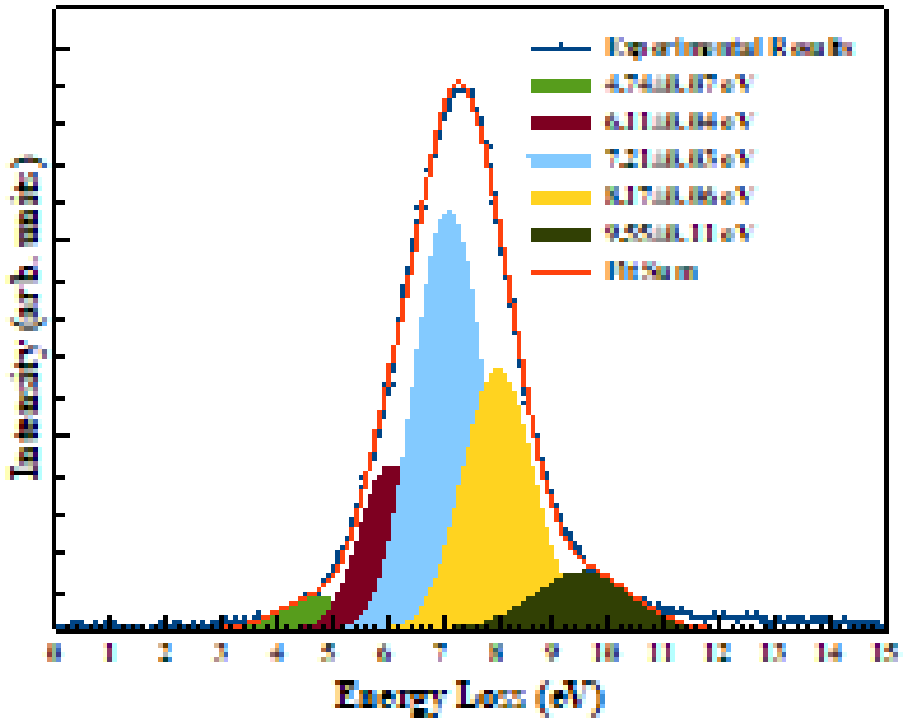

Figure 36 Post–collision potassium cation (K^+) energy loss spectrum at 157 eV in the centre-of–mass frame (205 eV in the lab frame) in the forward scattering direction ($\theta \approx 0°$). The peaks' uncertainty result from the Gaussian fitting procedure. See text for details.

Note that in K + NIMO collisions the major fragment anion yield is assigned to NO_2^- and so the calculations have been performed with the potassium atom pointing at the $-NO_2$ end group from the 4–nitroimidazole ring as shown in Figure 37.

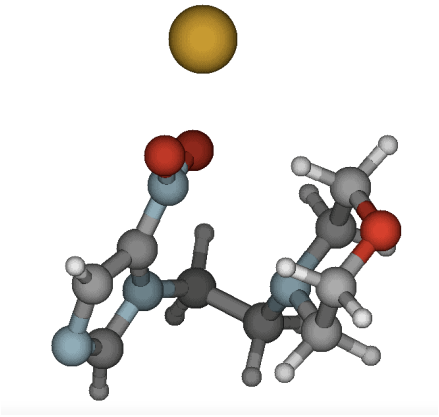

Figure 37 Optimized molecular structure of nimorazole, and orientation of the K + NIMO collisional system K–O ≈ 5.1 Å. K: yellow, O: red, C: grey, N: light blue, and H: white. See text for details.

6.4 Discussion

In potassium (K) −molecule (M) collision experiments, yielding ion− pair formation, the collision complex is formed by the oxidized and the reduced species, i.e., K^+ and $M^{-\#}$. While K^+ is still in the vicinity of the metastable parent anion ($M^{-\#}$), a strong Coulomb interaction can delay autodetachment long enough allowing therefore a stabilization of the negative ion via intramolecular energy redistribution through the different available degrees of freedom resulting either on a stable parent anion or on fragmentation channels (via direct or statistical dissociation). Relative to dissociative electron attachment, in electron transfer experiments one can attain identical anions' formation, yet with different yields, as well as other exit channels yielding different anionic species. This has been reported several times in the past (see e.g. [15], [222]–[229] and references therein) and is solely due to the different collision dynamics dictating the underlying molecular mechanism responsible for negative ion formation [230]. Briefly, in atom−molecule collisions, in the vicinity of the crossing between the ionic and covalent potential energy curves governing the electron transfer process, electrons follow adiabatically the nuclear motion. The endoergicity (ΔE) of the process yielding ion− pair formation is given by the difference between the ionization energy of the electron donor and the electron affinity of the target molecule [231], [232] (see Eq. (45)). Since the collision energy is typically set above the threshold of ion-pair formation, the metastable parent anion is formed with an excess of internal energy.

Anion yields from time-of-flight (TOF) mass spectra as a function of the K + NIMO collision energy have been obtained from 10 to 400 eV in the lab frame (7.7 − 310 eV in the centre−of−mass frame), where a rich fragmentation pattern is observed (assignments in Table 5) mainly at higher energies (see Figure 34). The major ion signal is due to the non−dissociated molecular anion $NIMO^{\bullet-}$ followed by NO_2^- formation. Based on the present experimental results and theoretical calculations, we now discuss in detail the electronic state spectroscopy of the most representative anions formed in collisions of neutral potassium atoms with neutral nimorazole molecules, *viz*. $NIMO^{\bullet-}$, NO_2^-, 4−nitroimidazole and morpholine rings fragmentation, CN^-, CNO^- and $(NIMO - NO)^-$

6.4.1 Parent Anion

The TOF mass spectra recorded in a wide collision energy range shows that the non−dissociated parent anion contributes to more than 60% of the total ion yield for E_{CM} < 10 eV, while above 100 eV, its branching ratio is ~80 % (see Figure 35). This is a strong indication that NIMO

is extremely efficient in scavenging an electron being transferred from the potassium donor. The reaction that yields the parent anion is given by:

$$K + NIMO \rightarrow \left(K^{+}NIMO^{\bullet -\#}\right) \rightarrow K^{+} + (NIMO^{\bullet -})^{\#} \rightarrow K^{+} + NIMO^{\bullet -} \quad (46)$$

with $(NIMO^{\bullet -})^{\#}$ the temporary negative ion (TNI) formed with an excess of internal energy. Formation of the non−dissociated parent anion may strongly compete with either autodetachment or molecular dissociation, the latter clearly visible from the fragmentation pattern obtained from 10 to 50 eV (Figure 35). However, owing to the different internal degrees of freedom, efficient intramolecular energy redistribution may occur living the parent anion intact within the 80 μs time detection of the present experiment.

The calculated highest occupied molecular orbitals in the presence of a potassium atom, show a delocalized spin density over the entire molecule (HOMO—1) with a prevalent character around the 4 −nitroimidazole and morpholine rings (HOMO) (Figure 38). This is also the case in the bare NIMO molecule (Fig. B3). As far as the lowest unoccupied molecular orbitals are concerned (see Fig. B2 and Fig. B3), in the presence of a potassium atom, a significant delocalization over the molecule is observed which can be responsible for $NIMO^{\bullet -}$ formation (e.g., LUMO+50 in Figure 38). As the collision energy is increased, one would expect more energy deposited in the NIMO molecule, thus increasing its fragmentation yield and a decrease in the non-dissociated parent anion signal. However, $NIMO^{\bullet -}$ becomes dominant for the entire collision energy range albeit the modest increase of fragment anion yields from 7.7 up to ~50 eV in the center— of— mass (Figure 38). This tendency of the $NIMO^{\bullet -}$ yield pertains to the role of the electronic structure, where a more enhanced delocalized spin density over all molecule is discernible from the high energy LUMOs (appendix B). Above ~70 eV, the parent anion BR, as well as the other fragment anions, are insensitive to the collision energy, the former contributing to 80 % of the total anion yield. This means that the electron transfer process may occur when the potassium atom flies apart from the NIMO molecule leaving the TNI with an excess of internal energy that is not efficiently channelled into the fragmentation channels. In such energy range, the collision time is faster, < 23 fs, and the efficient Coulomb stabilization of the collision complex ($K^{+}NIMO^{\bullet -\#}$) no longer efficiently holds.

Within the scope of electron transfer, we note a set of molecular systems where a non-dissociated parent anion is formed in e.g., highly symmetric molecules such as hexachlorobenzene C_6Cl_6[127] (six identical $C-Cl$ bonds) and in cyclic chemical compounds like nitroimidazoles [57] (strong competition between the ring and the $-NO_2$ end). Other molecular targets where strong evidence of effective bond breaking and rearrangement are operative further to the excess energy deposited within the TNI, are the cases of thymine $C_5H_6N_2O_2$ and uracil $C_4H_4N_2O_2$ [13], nitromethane CH_3NO_2 [17] and acetic acid CH_3COOH [233], just to mention a few.

Interesting to note that electron attachment studies have revealed that $NIMO^{\bullet-}$ is by far the dominant anion with a very narrow feature at ~0 eV with an absolute cross-section value of $\sim 3 \times 10^{-18}$ m^2[215]. The shape of the molecular orbitals in Fig. B3 (LUMO to LUMO+7) clearly show the predominant character over the entire molecule to attach an extra electron. Although nimorazole is of low symmetry, its 84 different vibrational degrees of freedom have been suggested to provide the effective means of dissipating the excess energy leading to a stable $NIMO^{\bullet-}$ anion within the detection time window of few hundred microseconds [215]. The post-collision potassium cation (K^+) energy loss spectrum at 157 eV in the center-of-mass frame (205 eV in the lab frame) in the forward scattering direction ($\theta \approx 0°$) is shown in Figure 36. The lowest energy−loss feature peaks at (4.74 ± 0.07) eV and results on an electron affinity of (-0.40 ± 0.07) eV (Table 6). Taking the $C-NO_2$ bond dissociation energy in 4−nitroimidazole to be 3.19 eV [234], the NO_2 electron affinity of (2.2730 ± 0.0050) eV [235], and a calculated adiabatic electron affinity of 1.31 eV at the M062x/6-311+G(d,p) level of theory [45], the asymptotic limit of $(NIMO - NO_2) + NO_2^-$ is now obtained at 2.227 eV, i.e., 0.917 eV above the ground state of the neutral molecule. This means that the 4.74 eV feature does not lead to bond excision but rather $NIMO^{\bullet-}$ formation.

6.4.2 NO_2^- formation

The nitrogen dioxide anion BR is the second most intense in K + NIMO collisions, contributing to more than 20% of the total ion yield for E_{CM} < 50 eV, while above 80 eV, its value accounts on average for 15 % (see Figure 35). Electron promotion to NIMO via the 4−nitroimidazole ring may yield the nitrogen dioxide anion given the high electron affinity of NO_2. In the unimolecular decomposition of the TNI, the reaction involves cleavage of the $C-NO_2$ bond from the nitroimidazole ring, with the extra charge on the NO_2 radical, and can be given by:

$$\begin{aligned} K + NIMO \rightarrow \left(K^+ NIMO^{\bullet -\#}\right) &\rightarrow K^+ + (NIMO^{\bullet -})^{\#} \\ &\rightarrow K^+ + NO_2^- + (NIMO - NO_2) \end{aligned} \tag{47}$$

As far as the lowest unoccupied molecular orbitals are concerned, a significant delocalization over the molecule together with considerable $\sigma^*(N-C)$ antibonding character between the 4−nitroimidazole ring and the $-H_2C-CH_2-$ side group (LUMO+50), are responsible for $NIMO^-$ and NO_2^- formation, respectively. From the BRs in Figure 35, we note that the relative intensity of NO_2^- has a maximum at ~30 eV, decreases from 30 up to 70 eV and its yield remains somehow constant (~15%) with increasing collision energy.

We have obtained the asymptotic limit of $(NIMO-NO_2) + NO_2^-$ at ~0.92 eV above the ground state of the neutral NIMO molecule and determined that the first energy loss feature at 4.74 eV (Figure 36), is mainly due to the non-dissociated parent anion formation (see 6.4.1).

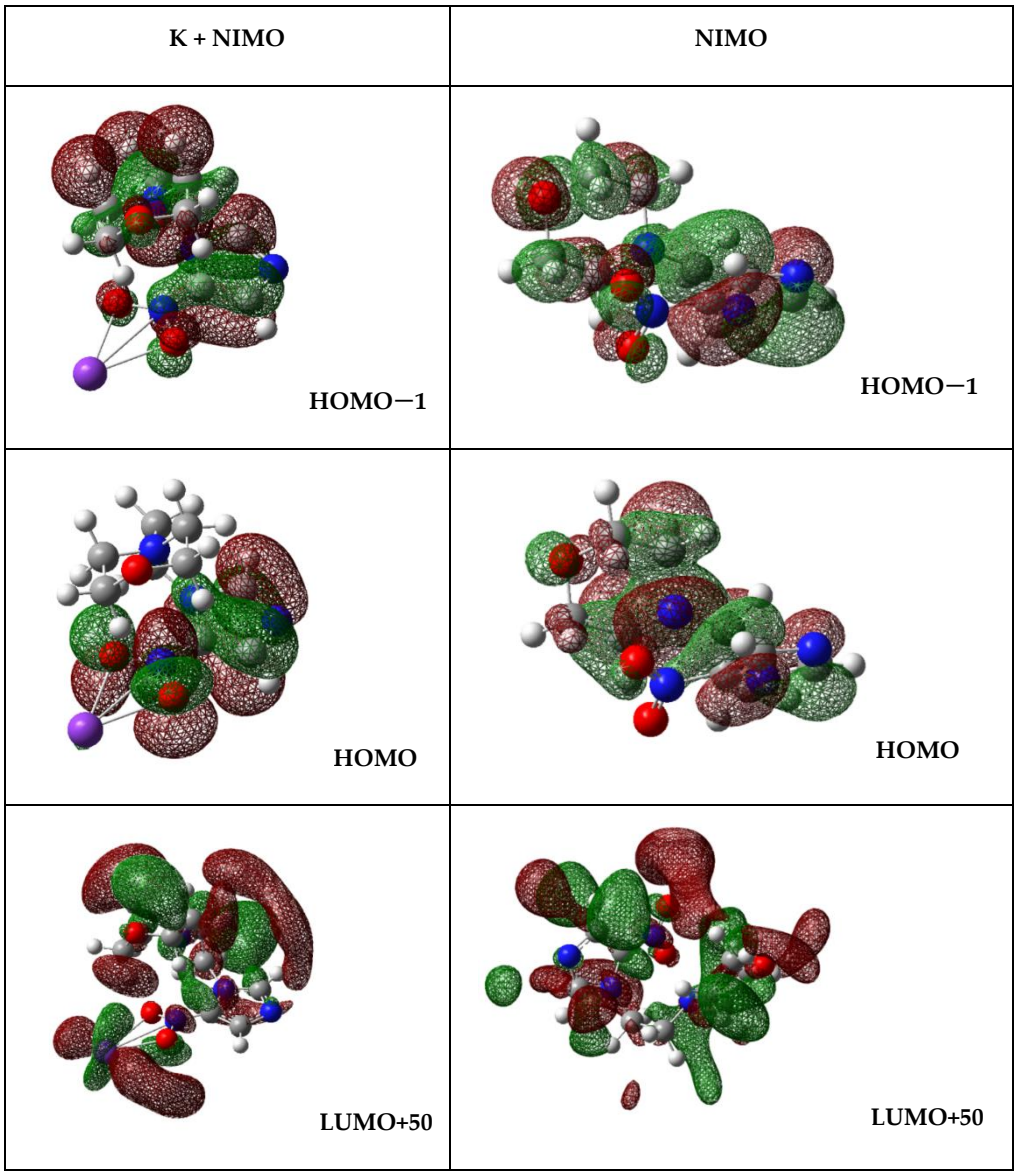

Figure 38 Calculated highest occupied molecular orbitals (HOMO−1 and HOMO) and lowest unoccupied molecular orbital (LUMO+50) for K + NIMO and NIMO (K: purple, C: grey, N: blue, O: red, and H: white). The straight lines between the K atom and the $-NO_2$ end in the 4−nitroimidazole ring are just to indicate the spatial mutual position. For a complete set of MOs see Fig. B2 and Fig. B3.

However, the DEA data of Meißner et al. [43] shows a weak NO_2^- feature at 0.41 eV which was assigned to the excitation of the symmetric stretching vibration mode of NO_2 with an energy of 0.163 eV (1318 cm^{-1}) in the neutral ground and 0.159 eV (1284 cm^{-1}) in the negative ion states [235]. Thus, a possible operative mechanism can be related to the role of vibrationally excited neutral molecules, even with modest population at 374 K heating temperature of

NIMO. Notwithstanding, a more plausible explanation can reside on the nature of the multi-dimensional potential energy surfaces of NIMO in respect to the reaction coordinate leading to $C-NO_2$ bond excision. Meißner et al. [215] have reported a weak NO_2^- signal at electron energies close to 0 eV and is due to an exothermic reaction with ΔG = −0.26 eV corresponding to the release of $C_3H_3N_2 + C_6H_{11}NO$.

The energy loss feature at (6.11 ± 0.04) eV (Figure 36) is closely related to accessing an electronic state at 1.77 eV. The calculated MOs (LUMO+60 in Fig. B2) show a σ^*_{CN} antibonding character in the 4-nitroimidazole ring with the extra electron sitting on NO_2, although we should not discard the possibility of other fragment anions stemming from the nitroimidazole ring being formed, *viz.* CN^-. Yet, and according to the DEA data [43], other close lying resonance at 1.93 eV can be responsible for the cyano radical anion formation which is clearly visible from the LUMO+15 in Fig. B3. The next energy loss feature peaking at (7.21 ± 0.03) eV yields a vertical electron affinity of (−2.87 ± 0.03) eV which can be assigned to the DEA resonance at 2.97 eV resulting in NO_2^- formation [43]. The calculated MOs show that LUMO+70 (Fig. B2) at 7.01 eV depicts a strong σ^*_{CN} antibonding character in the 4-nitroimidazole ring. A close inspection of Figure 36 reveals that this energy loss feature has a threshold at ~ 5 eV which is in excellent accord, within the energy resolution of the K^+ energy loss data, with the obtained value of 0.92 eV if we now add the potassium ionization energy of 4.34 eV.

6.4.3 Other fragment anions

Figure 35 shows that fragment anions stemming from the 4−nitroimidazole ring, the morpholine ring and other anions (CN^- and CNO^-) in K + NIMO collisions, contribute to less than 15% of the total ion yield for E_{CM} ~ 50 eV, while above this energy they account only for just ~10 %. Such ion yields decrease at higher energies, which is related to fast collisions where the strong Coulomb stabilization within the collision complex is no longer efficient enough to allow opening the different accessible dissociation channels.

At 10 eV centre−of−mass frame (Figure 35), CN^- and CNO^- contribute to ~20% of the total anion yield. The neutral species are known to be pseudo halogens considering their electron affinities, EA(CN) = 3.86 eV and EA(CNO) = 3.61 eV [221], exceeding those of the halogen atoms. Interesting to note that such high electron affinities do not mean higher yields of the fragment anions, which has also been reported in electron transfer experiments to nitroimidazoles [236], [237], pyrimidine [227], adenine [11], [238], thymine and uracil [13], [14]. CN^- and CNO^- are mostly formed from the decomposition of the 4−nitroimidazole ring upon electron transfer to NIMO. Such is in assertion of the similarity found in the resonance shapes and positions of these anions together with NO_2 in DEA experiments[43] The reactions yielding such anions' formation involve several bonds being broken, the former from the loss of an O

atom from NO_2 and excision of two $C-N$ bonds within the (4−nitro) imidazole ring, whereas the latter through the loss of an N atom from the NO_2 or by multiple bond breaking directly from the imidazole ring. A close inspection of the molecular orbitals in **Fig. B2** (see appendix B), show a modest antibonding character within the 4−nitroimidazole ring involving the $C-N$ bonds which may related to the lowest ionic yields obtained in the different TOF mass spectra as a function of the collision energy (see e.g., from LUMO+50 to LUMO +100).

The loss of a neutral $NO^{\bullet}$ (196 u) belongs to the set of trace anions with a branching ratio < 5%, and can be formed through the following reaction:

$$\begin{aligned} K + NIMO \rightarrow \left(K^{+}NIMO^{\bullet -\#}\right) \rightarrow K^{+} + (NIMO^{\bullet -})^{\#} \\ \rightarrow K^{+} + (NIMO - NO)^{-} + NO^{\bullet} \end{aligned} \tag{48}$$

The formation of $(NIMO-NO)^{-}$ ion requires the cleavage of $C-N$ and $N-O$ bonds if proceeding from the 4-nitroimidazole ring or even through other more complex reactions involving the morpholine ring. Nonetheless, the similarity between the DEA resonance profiles and energy positions from NO_2^- and $(NIMO-NO)^{-}$ [43], suggest that these anions have common precursor anion states and so the reaction leading to the loss of a neutral $NO^{\bullet}$ stems from the 4-nitroimidazole ring. Within the cellular environment, such reaction is particularly relevant as to the reactive nature of $NO^{\bullet}$ [239]–[242], though producing relevant damage of key biological units including DNA. Yet if charge transfer is a prevalent mechanism upon irradiation of biological material rather than single electron attachment, such radical formation from NIMO may certainly not play a relevant role.

The energy feature in Figure 36 at (8.17 ± 0.06) eV yields a vertical electron affinity of (−3.83 ± 0.06) eV. DEA experiments to NIMO have assigned the main resonance features at 3.53 and 3.6 eV to CN^- and CNO^- formation [43]. Given the resonance profiles resemblance between CN^- (26 u) and CNO^- (42 u) with fragment anions $C_3HN_2^-$ (65 u) and $C_3H_3N_2^-$ (67 u), Meißner et al. [43] have concluded that these stem from the imidazole ring. These fragment anions in Table 5 have also been assigned to result from bond breaking within the 4−nitroimidazole ring in particular from the $C-NO_2$ site in the corresponding unimolecular decomposition of the TNI upon electron transfer. Following Meißner et al.'s assignment [43], CN^- can proceed from a dissociative mechanism where the electron transferred to NIMO molecule sits on a π^*_{CN} antibonding orbital with efficient energy transfer from CN to the $C-CN$ reaction coordinate. Such is in assertion with the LUMO+80 character in Fig. B2. A close inspection of such MO reveals, apart from the π^* character in the 4-nitroimidazole ring, a relevant σ^*antibonding character along the $C-CN$ bond. This intramolecular mechanism within the TNI can solely be explained in terms of vibrational predissociation, which can hold as long as the nuclear wave packet survives long enough for the π^*_{CN} system diabatically cross with the σ^*

antibonding state. The morpholine ring fragmentation has been assigned in Table 5 to fragment anions from 81 u to 86 u.

The K^+ energy loss features at (9.55 ± 0.11) eV (Figure 36) with a vertical electron affinity of (−5.21 ± 0.11) eV is tentatively assigned to a Rydberg excitation. The MOs calculation in Figure S2 shows the LUMO+90 with a delocalized spin density resembling a ns Rydberg shape normal to the 4−nitroimidazole ring plane. This feature can be due to an electronic excitation of the series $n_o \rightarrow n_s$ converging to NIMO ionization energy at 8.15 eV [43]. We tentatively assign it to (n + 1) s or (n + 2) s due to the large number of states which occur in this high energy region.

6.5 Summary

The current comprehensive study on collisions of neutral potassium atoms with neutral NIMO molecules, constitutes the most detailed and unique assignments on electron transfer experiments. Here we combine experimental TOF mass spectrometry and energy loss spectroscopy, together with state-of-the art theoretical calculations at different levels of accuracy. The information obtained has allowed to investigate the formation of the most representative anions in a wide collision energy range from 10 up to 400 eV in the laboratory frame. Special attention has been paid to the non-dissociated parent anion, $NIMO^{\bullet -}$, NO_2^- and other fragment anions stemming from the 4-nitroimidazole and morpholine rings. Although we observe a rich fragmentation pattern related to both rings multiple bond breaking, their yields are not significant when compared to $NIMO^{\bullet -}$at 226 u and NO_2^- at 46 u. The role of K^+ in the collision complex ($K^+NIMO^{\bullet -\#}$) seems to be a relevant stabilizing effect at low-energies (E_{CM} < 70 eV) opening up different fragmentation channels, despite their lowest BRs, whereas at higher energies the collision dynamics is mostly dictated by the efficient energy redistribution within the different degrees of freedom of NIMO temporary negative ion, resulting mostly in a stable non-dissociated parent anion and a minor fragmentation yield (~15%).

Potassium cation energy loss spectrum in the forward scattering direction ($\theta \approx 0°$) at 157 eV in the centre-of-mass frame (205 eV in the lab frame), shows a dominant feature with a vertical electron affinity of (7.21 ± 0.03) eV, and assigned to a transition from NIMO neutral ground state to a repulsive σ^*_{CN} antibonding state of the TNI resulting in NO_2^- formation. This energy loss feature shows a threshold at ~ 5 eV which is in excellent agreement with the obtained value of 5.26 eV.

We also note some differences in the rich fragmentation pattern and the anion yields obtained from the present experiments, and those from electron attachment studies. Yet,

NIMO is extremely efficient in capturing an extra electron either from a bound atomic compound via an electron transfer process or from a simple associate electron attachment mechanism. The present results also give relevant information as to the underlying molecular mechanisms governing the electron transfer process, showing the strong ability of this molecule to scavenge an electron supporting therefore the premise that NIMO is selectively cytotoxic to tumour cells via its reduction as a requirement for accumulation in the cell [243]. Thus, radical formation upon electron capture has been identified to be a pivotal mechanism for radiosensitisation of hypoxic cells by using nitroimidazoles' compounds as is the case of NIMO. The radiosensitisation effect is only operative if these chemical compounds are incorporated in cells prior to irradiation of the biological material [244]. Upon redox reactions in cells, formation of a non-dissociated parent anion (radical anion) is not responsible for cytotoxicity to DNA. The mechanism that seems to be operative in hypoxic cells, requires a proton transfer to the reduced chemical compound yielding a neutral radical species that will bind to DNA resulting in strand breaks [245]. Also, interesting to note is the relevance of OH° radicals from water radiolysis which attack DNA at specific sites where nitroimidazoles' agents bind to DNA, making these chemical compounds well-attuned to mimicking oxygen in hypoxic tumours. Finally, we believe that the present investigation is relevant to understand how NIMO accumulating in tumour cells can be used for further formulation of new radiopharmaceutical compounds.

7.

ELECTRON TRANSFER PROCESSES IN BIOLOGICALLY RELEVANT H_2O AND D_2O

In this chapter an attempt to electron transfer processes in H_2O and D_2O will be given with the aid of experimental results from the crossed molecular beam setup. TOF−MS of the different anions formed have been recorded and the post collision energy loss of the projectile have been obtained in the forward scattering direction. A manuscript about these results is under preparation to be submitted soon to an international peer review journal.

7.1 Introduction

H_2O is a triatomic and key biological molecule and yet it still gets the attention of the international scientific community. A literature survey reveals that within the community there is still no general agreement as to the position of some of water's resonances related to its anionic fragments [246].

7.2 Results and discussion

A comprehensive crossed beam experimental study on potassium collisions with H_2O and D_2O has been performed, where the dissociation dynamics in a wide energy range has been investigated. As a normal procedure successfully implemented with other molecules, alkali energy loss spectroscopy in post collision experiments in the forward direction gives valuable insight into the accessible electronic states upon formation of a transient negative ion.
Negative ion formation in $K + H_2O$ collisions was investigated using the r−TOF−MS, where all previously reported anions (H^-, O^-, and OH^-) were observed. Thresholds of formation for each fragment anion were obtained, with values higher than the thermodynamically

calculated energies. Such difference can be due to kinetic energy imparted to fragment anions upon the collision induced dissociation process.

From the branching ratios obtained (Figure 39), we can infer that the OH^- anion is the most dominant and has the lowest threshold of formation in such electron transfer experiments. OH^- anion accounts for almost 80% of the total fragment anion yield in the collision energy range probed, i.e., from ~9 up to 200 eV in the centre−of−mass frame.

The alkali-energy loss K^+ in the forward direction upon collision with H_2O and D_2O, allows to obtain the different vertical electron affinities attained. A comparative study of H_2O and D_2O energy loss data shows that up to 21 eV energy loss (Figures 42 and 43), both H_2O and D_2O have similar features as to their energy positions. However, D_2O energy loss differs from H_2O for an energy loss above 16 eV. The energy loss spectrum for D_2O between 16 and 20 eV are enhanced in comparison to H_2O and the former extends to higher energies that the latter. At the moment the solely explanation for that can be related to dipolar dissociation. However, the on-going theoretical calculations from our close collaborations may give further insight about the collision dynamics of the process at these energies.

7.2.1 Electron transfer processes in H_2O

Upon electron transfer in potassium $K - H_2O$ collisions, negative ion mass-spectrometry was performed, with H^-, O^-, and OH^- just the three fragment anions formed.

7.2.1.1 OH^- formation

OH^- formation dominates the TOF-MS in the whole collision energy range and accounts for approx. 80% of the total anion yield. The formation of such anion in potassium water collisions can proceed through the following reaction:

$$K + H_2O \rightarrow \left(K^+H_2O^{-\#}\right) \rightarrow K^+ + H + OH^- \quad (49)$$

where, the $OH - H$ bond has to be cleaved. In the unimolecular decomposition of the water temporary negative ion, the extra charge is delocalized to the OH end. The enthalpy of formation from the above reaction pathway can be estimated thermodynamically:

$$\Delta\left(H_R{}^0\right) = \sum \Delta H_f(\text{Products}) - \sum \Delta H_f(\text{Reactants}) \quad (50)$$

and if the enthalpy of formation of a negative ion is not available, then:

$$\Delta H_f(\text{Anion}) = \Delta H_f(\text{Neutral}) - \text{VEA}(\text{Neutral}) \quad (51)$$

Hence, the thermodynamic threshold of formation $E_{th}(OH^-)$ can be estimated as:

$$E_{th}(OH^-) = D(OH - H) - \text{VEA}(OH) \quad (52)$$

Note that Equation (52) is considered to proceed with no excess of energy. Taking IE(K) = 4.34 eV[8], the EA(OH) = 1.83 eV[247], and the bond dissociation energy D $(H - OH)$ = 498 kJ/mol (5.16 eV), then $E_{th}(OH^-)$ = 7.67 eV. Here, the experimental observed threshold for OH^- is

approx. 9.38 eV. The difference of 1.71 eV can be attributed considering the possibility of kinetic energy imparted to OH^- during the collision. Although we have not yet accurately determined such KERD, such assumption seems reasonable given the recent data on the hydroxyl anion produced from methanol in electron transfer experiments[248].

7.2.1.2 H^- formation

The H^- anion can proceed through the following reaction to water upon electron transfer:

$$K + H_2O \rightarrow \left(K^+H_2O^{-\#}\right) \rightarrow K^+ + OH + H^- \quad (53)$$

The hydrogen anion BR in Figure 39 shows that is the lowest yield across the entire collision energy range investigated and on average it contributes to a constant value of approx. 10 % of the total anion yield. Such does seem reasonable given the lowest electron affinity of water fragments, EA(H) = 0.76 eV [235]. From the bond dissociation energy D (H − OH) = 498 kJ/mol (5.16 eV), the threshold of formation is obtained as E_{th} (H^-) = 4.4 eV.

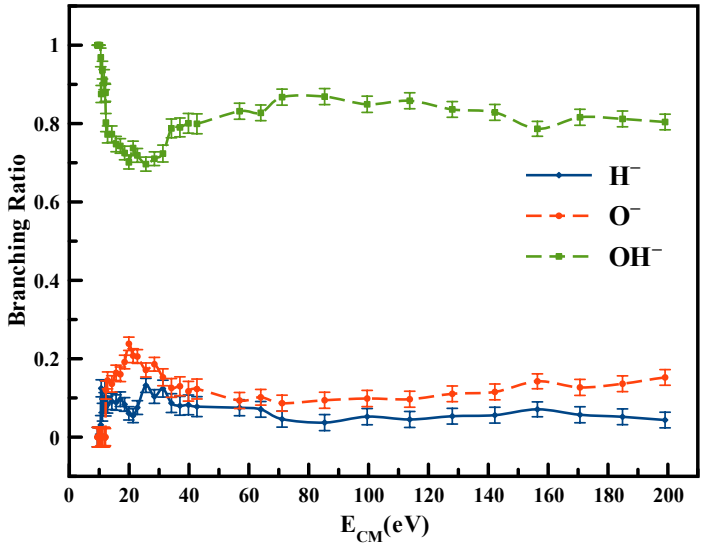

Figure 39 Branching ratio for H^-, O^-, and OH^- formation from threshold up to 200 eV in the centre-of-mass frame.

Adding the potassium ionization energy, we reach a value of 8.74 eV. The experimental threshold is obtained at 10.52 eV, 1.78 eV above the expected value. Given that H^- is the lighter fragment anion stemming from water negative ion, the excess energy can certainly be accommodated as kinetic energy of the fragment anion. This result is in good agreement with 1.55 eV kinetic energy released when accessing the $^2A_1$ resonance[249].

7.2.1.3 O^- formation

A close look at the oxygen anion branching ratio indicates that as soon as it is formed the intensity of the H^- anion is reduced, suggesting that the O^- formation channel dominates the formation of H^-. In collision energies above 40 eV (in CM frame) the branching ratios are almost insensitive to the collision energy. The formation of O^- in potassium water collisions can proceed through the following reactions:

$$K + H_2O \rightarrow \left(K^+H_2O^{-\#}\right) \rightarrow K^+ + 2H + O^- \quad (54)$$

$$K + H_2O \rightarrow \left(K^+H_2O^{-\#}\right) \rightarrow K^+ + H_2 + O^- \quad (55)$$

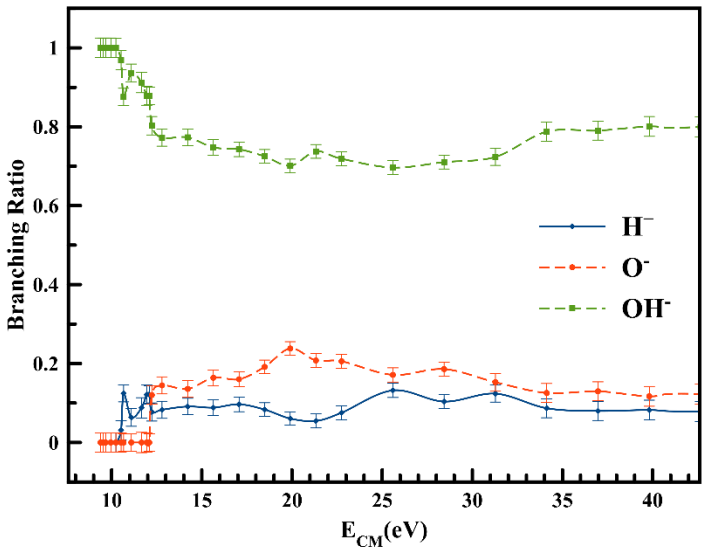

Figure 40 Branching ratio for H^-, O^-, and OH^- formation from threshold up to 40 eV.

Formation of the oxygen anion requires the excision of $H-OH$ and $O-H$ bonds and electron capture from the oxygen atom. If we take the bond dissociation energies, D $(H-OH)$ = 498 kJ/mol (5.16 eV) and D $(O-H)$ = 428 kJ/mol (4.436 eV), and EA(O) = 1.44 eV[235] the expected threshold is E_{th} (O^-) = 8.156 eV. Now adding the potassium ionization energy, we obtain a value of 12.50 eV. We note that the experimental threshold value is 12.08 eV. This value is in good agreement with 0.12 and 0.19 eV kinetic energy released when accessing the $^2B_1$ and $^2A_1$ resonances, respectively[249].

7.2.2 Electron transfer processes in D_2O

In the case of electron transfer to D_2O yielding negative ion formation, the process is identical as in the case of H_2O. Although, the heavier mass of D relative to H, one would expect that in the unimolecular decomposition of the temporary negative ion formed in electron transfer experiments, autodetachment may strongly compete with dissociation. We have noted that

under the same experimental conditions, the energy loss spectra of H_2O relative to D_2O, yielded a much higher signal in the accumulation time window used to record such data. If we compare the branching ratios from H_2O (Figure 40) and D_2O (Figure 41), above threshold in the former O^- is ~ 20% whereas in the latter amounts to ~ 30%.

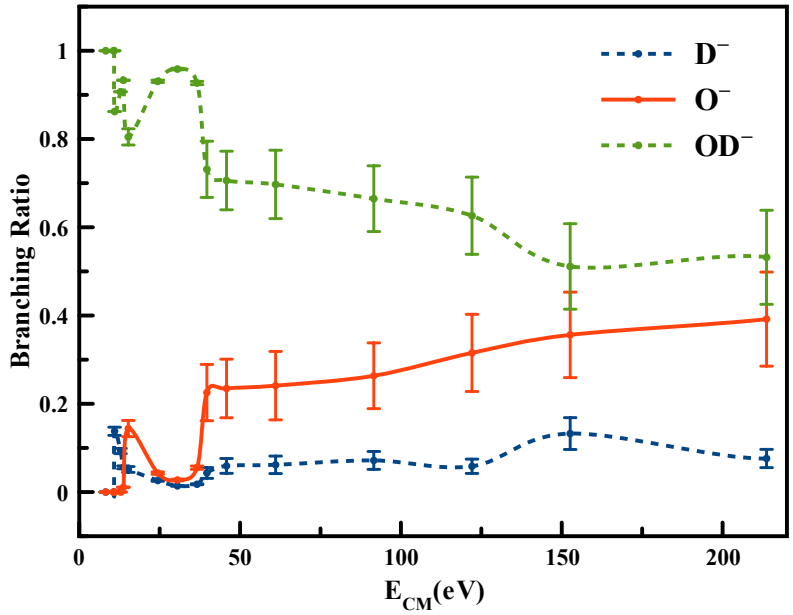

Figure 41 Branching ratio of D^-, O^- and OD^-formation upon electron transfer in potassium collision from threshold up to 220 eV in the centre–of–mass frame.

7.2.2.1 OD^- formation

In D_2O negative ion formation, as expected OD^- is the most dominant fragment anion given the electron affinity of OD relative to the other fragments. A close inspection of the branching ratio (Figure 41) indicates that O^- formation in D_2O has an increasing trend in higher energies which directly competes with OD^- formation. This indicates an interplay of different electron-transfer mechanism for ion-pair formation in D_2O than H_2O. Another interesting fact is the difference in threshold of formation for D^- from D_2O, in comparison to H^- from H_2O. The formation of OD^- in potassium D_2O collisions can proceed through the following reaction:

$$K + D_2O \rightarrow \left(K^+D_2O^{-\#}\right) \rightarrow K^+ + D + OD^- \qquad (56)$$

Taking the IE(K) = 4.34 eV[8], the EA(OD) = 1.83 eV[247], and the bond dissociation energy D $(D - OD)$ = D $(H - OH)$ = 498 kJ/mol (5.16 eV), then $E_{th}(OD^-)$ = 7.67 eV. Here, the experimental observed threshold for OH^- is approx. 9.92 eV. The difference of 2.15 eV can be attributed considering the possibility of kinetic energy imparted to OD^- during the collision. Yet, this will need to be proved through the KERD of the fragment anion in a L–TOF–MS.

7.2.2.2 O^- formation

A detailed study of the branching ratio of D_2O also indicate that O^- formation in D_2O has an increasing trend in higher energies which directly competes with OD^- formation. The formation of O^- in potassium D_2O collisions can proceed through the following two reaction:

$$K + D_2O \rightarrow \left(K^+D_2O^{-\#}\right) \rightarrow K^+ + 2D + O^- \quad (57)$$

$$K + D_2O \rightarrow \left(K^+D_2O^{-\#}\right) \rightarrow K^+ + D_2 + O^- \quad (58)$$

Now taking the bond dissociation energies, D $(D - OD)$ = D $(H - OH)$= 498 kJ/mol (5.16 eV) and D $(O - D)$ = D $(O - H)$ = 428 kJ/mol (4.436 eV), and EA(O) = 1.44 eV[235] the expected threshold is $E_{th}\,(O^-)$ = 8.156 eV. Now adding the potassium ionization energy, we obtain a value of 12.50 eV. We note that the experimental threshold value is 12.08 eV. This value is in good agreement with 0.14 and 0.31 eV kinetic energy released when accessing the $^2B_1$ and $^2A_1$ resonances, respectively[249].

7.2.2.3 D^- formation

The D^- branching ratio is above 50 eV, as in the case of H_2O, just ~10% of the total anion yield (Figure 41). Currently the calculated and experimental theresholds show a considerable difference in energy which cannot solely be expoleined in terms of kinetic energy release. We do not have an explanation for that, yet at collision energies as those probed here, in particular above 30 eV, dipolar dissociation can be operative.

7.3 Alkali energy loss data of H_2O and D_2O

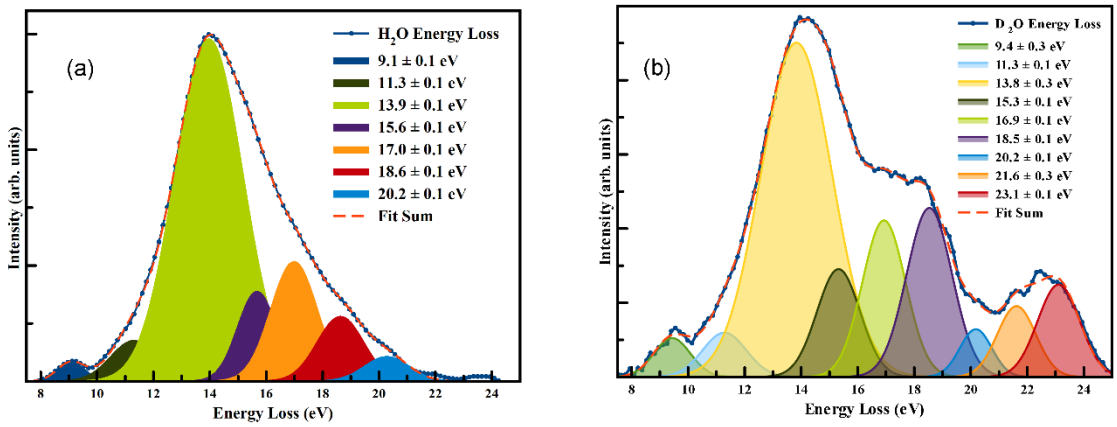

Figure 42 K^+ energy loss data upon collision with (a) H_2O and (b) D_2O in the forward scattering direction.

The next table is just a compilation of the most accessible electronic stest in electron transfer to H_2O and D_2O with the experimental electron affinities and their related dissociative electron attachment resonances from ref.[249].

Table 7 Fitted energy loss features of H_2O and D_2O.

K^+ energy loss feature (eV)	VEA (eV)	DEA resonances[249]
9.1 ± 0.1	− 4.8 ± 0.1	4.6; 4.8 (H^-, D^-)
11.3 ± 0.1	− 7.4 ± 0.1	7.0 (O^-, OH^-)
13.9 ± 0.1	− 9.6 ± 0.1	9.0 (O^-, H^-)
15.6 ± 0.1	−11.3 ± 0.1	11.5 (OH^-, H^-)
17.0 ± 0.1	− 12.7 ± 0.1	12.0 (O^-)
18.6 ± 0.1	− 14.3 ± 0.1	
20.2 ± 0.1	− 15.9 ± 0.1	
21.6 ± 0.1	− 17.3 ± 0.1	
23.1 ± 0.1	− 18.8 ± 0.1	

A comparative study of thermodynamic thresholds for various anionic formations from H_2O and D_2O can be found in the following. The enhancement in peak intensities above 18 eV in the case D_2O is clearly visible in the energy loss data. The role of doubly excited states in H_2O and D_2O can not be ignored, especially above ~18 eV energy loss [250], [251].

The reported bond dissociation energy for the $D(H-OH)$ is 5.16 eV , where as from H_2O energy loss feature of 11.3 ± 0.1 eV, we can attribute $D(H-OH) \cong 5.2 \pm 0.1$ eV experimentally, which is in excellent agrrement within the experimental error.

Similary, in the case of D_2O the bond dissociation energy for $D(D-OD)$ is not reported in the literature. If we follow the above−mentioned methodology, then from energy loss feature of D_2O at 11.3 ± 0.1 eV, we can attribute $D(D-OD) \cong 5.4 \pm 0.1$ eV . Considering the higher boiling point of D_2O with respect to H_2O, signifiers the difference of $\cong 0.2$ eV between $D(D-OD)$ and $D(H-OH)$.

Table 8 Comparison of thermodynamic thresholds and experimentally observed thresholds for various anions from H_2O and D_2O.

Source	Fragment Anion	Thermodynamic threshold (eV)	Experimental threshold (eV)	Comment
H_2O	H^-	8.74	10.52 ± 0.2	Assuming $E^{\#} \approx 1.78$ eV
H_2O	O^-	12.50	12.08 ± 0.2	
H_2O	OH^-	7.67	9.38 ± 0.2	Assuming $E^{\#} \approx 1.71$ eV
D_2O	D^-	8.85	10.98 ± 0.2	Assuming $E^{\#} \approx 1.0$ eV
D_2O	O^-	≤ 12.64	13.58 ± 0.2	Assuming $E^{\#} \approx 0.9$ eV
D_2O	OD^-	7.77	8.02 ± 0.2	

Where, $E^{\#}$ Is the expected kinetic energy release for anionic fragment in consideration upon dissociation.

Currently our theoretician co−workers are performing quantum chemical calculations on water to give details Information about the most accessible molecular orbitals in the electron transfer process. So, no further discussion will be given at this stage.

7.4 Summary

To summarize, it can be concluded that the mechanism of electron transfer in D_2O is similar to H_2O up to 15 eV energy loss, and OH^- and OD^- fragment anions are the most dominant in TOF−MS among all other fragment anions from H_2O and D_2O respectively. And differ by the threshold of formation of D^- , H^-, and O^-, as is evident from experimental results from negative ion formation TOF−MS and alkali energy loss spectroscopy.

8.

CONCLUSION AND FUTURE DIRECTIVES

In this chapter a summary of results and broad outcome of the experiments will be provided along with the future possibilities to further enhance our understanding in such collisions.

8.1 Introduction

In this thesis we started the discussion about molecules from three different perspectives. The first class included astrochemically relevent molecules. These molecules also provided a hands-on indepth experience of performing charge transfer experiments, such were the model compounds namely 4 different chlorinated benzenes. We have thorughly investigated the collision dynamics of these systems in atom-molecule collision experiments. Some of the results are first ever reported, especially in the case of C_6Cl_6, which led us to probe dichlorobenzene isomers for Cl_2^- formation.

The second class deals with nimorazole (NIMO), a radiosensitizer. Radiosensitizers have been the topic of investigation among the international scientific community due to their applications in cancer treatments. We have investigated the charge transfer mechanism in nimorazole upon potassium collision with the aid of state-of-the-art quantum calculations in the low energy collision region, i.e., from 10 eV up to 1 keV, and provided insight about the electronic state spectroscopy with the post collision alklai energy loss spectroscopy.

Finally, in biological environments, water is a key molecule, that still attracts the attention of the international scientific community, in a diverse of experimental setups and quantum chemical calculations as a phase of stage and aggregation.

In the upcoming sections, we will provide insight about the conclusions drawn from the experimental perspectives, and a possible extension of this work by proporsing a set of methodologies that can be implemented in the future.

8.2 Molecules of astrochemical relevance

We have reported a comprehensive investigation about the kinetic-energy release distributions of chlorobenzene $-h_5$ and $-d_5$, chlorocyclohexane and hexachlorobenzene at collision energies in the centre-of-mass frame of about 12, 40 and 118 eV. Such distributions have been obtained from the shape and width of the time-of-flight mass spectra of Cl^- ions. Collision induced dissociation results in an energy redistribution either through the different internal degrees of freedom (via vibrational excitation) or direct transformation of the excess energy via translational motion of the fragment anions involved. The statistical fittings of Cl^- distributions at low kinetic-energy release, ε_d, reveal at least three effective degrees of freedom, while the role of statistical and direct dissociation has been thoroughly discussed according to the nature of the different resonances obtained by dissociative electron attachment and/or electron transmission spectroscopy, where applicable. Additionally, we have made some considerations on the collision dynamics for the set of chosen molecules, and the conclusions drawn lend support to previous investigations of hexachlorobenzene negative ion formation in electron transfer experiments, while for the remaining molecular systems the present results will serve to help interpreting the underlying molecular mechanisms within electron transfer induced fragmentation.

In case of Cl^- formation from chlorinated benzenes, the influence of the vibration motion seems to reveal itself in the shape of the cross section at low energy collisions where t_{coll} is of the order of t_{vib}. The structures in the cross section seem to be reminiscent of vibrational motion with changing collision time, which significantly also affects the probability of population of different electronic states.

We have presented a novel comprehensive study on TOF mass spectrometry negative ion formation in neutral potassium atom collisions with neutral hexachlorobenzene molecules in the lab frame energy range from 10 up to 100 eV. The TOF mass spectra are dominated by the undissociated parent anion $C_6Cl_6^-$, and Cl^- and together with $C_6Cl_5^-$ these anions contribute to more than 80% of the ions recorded, where other fragments assigned to $C_6Cl_4^-$, $C_3Cl_2^-$, C_2Cl^- and Cl_2^-, amounting to less than 20% of the total anion yield. Theoretical calculations on the vertical excitation energies were performed at different levels of theory to help us in assigning the electronic transitions.

Potassium cation post-collision energy loss data has been obtained in the forward direction ($\theta \cong 0°$) at 162.2 eV in the centre−of−mass frame (205 eV lab frame), with a dominant feature assigned to an electronic transition with a vertical electron affinity of (–3.76 ± 0.20) eV. This has been assigned to a purely repulsive transition from C_6Cl_6 ground state to a σ^*_{C-Cl} state of the temporary negative ion yielding Cl^- formation. The energy loss data has revealed a weak

feature at (3.1 ± 0.3) eV, yielding a positive electron affinity of (1.24 ± 0.3) eV, where its lower limit value (0.94 eV) was assigned to C_6Cl_6 adiabatic electron affinity and is in very good agreement with the values reported in the literature. Moreover, the $C_6Cl_5^-$ and Cl_2^- thresholds of formation have been obtained from the experimental energy loss data, the former allowing to estimate a bond dissociation energy D $(C_6Cl_6 - Cl)$ = (3.26 ± 0.30) eV. We have also comprehensively investigated the reduction of hexachlorobenzene and dichlorobenzene isomers in electron transfer processes and obtained selective $C - Cl$ bond excisions to both molecular compounds in the gas-phase. This is achieved by the combined balance between bond dissociation energies and electron affinity of the chlorine molecule. The reactions are all endothermic and, corresponding to the different isomers, the presence of a barrier results in an energy balance that favors the *ortho* configuration. Although the efficiency in producing Cl_2^- is not particularly significant from the TOF negative ions branching ratios relative to other fragment anions, this is due to a relevant energy redistribution within the TNI upon electron capture that involves the different internal degrees of freedom through relevant vibronic coupling. The present findings may have implications in the role of a transition state in chemical reactions which are prevalent in different environments not only in the gas but in bulk systems. The sensitization of *ortho* positions in C_6Cl_6 and $C_6H_4Cl_2$ can be achieved upon molecular reduction, which in the present case is obtained through a potassium atom, making these geometrical effects in polyatomic molecules important in single electron transfer reactions. We can anticipate that within the scope of redox reactions, the effect of an electron donor (oxidized species) and an electron acceptor (reduced species), may offer in solution a particular selectivity as to the role of reactants and products.

8.3 Molecules of biological relevance

The current comprehensive study on collisions of neutral potassium atoms with neutral NIMO molecules, constitutes the most detailed and unique assignments on electron transfer experiments. Here we combine experimental TOF mass spectrometry and energy loss spectroscopy, together with state-of-the art theoretical calculations at different levels of accuracy. The information obtained has allowed to investigate the formation of the most representative anions in a wide collision energy range from 10 up to 400 eV in the laboratory frame. Special attention has been paid to the non-dissociated parent anion, $NIMO^{*-}$, NO_2^- and other fragment anions stemming from the 4-nitroimidazole and morpholine rings. Although we observe a rich fragmentation pattern related to both rings multiple bond breaking, their yields are not significant when compared to $NIMO^{*-}$ at 226 u and NO_2^- at 46 u. The role of K^+ in the collision complex $(K^+NIMO^{*-\#})$ seems to be a relevant stabilizing effect at low-energies (E_{CM} < 70 eV) opening

up different fragmentation channels, despite their lowest BRs, whereas at higher energies the collision dynamics is mostly dictated by the efficient energy redistribution within the different degrees of freedom of NIMO temporary negative ion, resulting mostly in a stable non-dissociated parent anion and a minor fragmentation yield (~15%).

Potassium cation energy loss spectrum in the forward scattering direction ($\theta \approx 0°$) at 157 eV in the centre-of-mass frame (205 eV in the lab frame), shows a dominant feature with a vertical electron affinity of (7.21 ± 0.03) eV, and assigned to a transition from NIMO neutral ground state to a repulsive σ^*_{CN} antibonding state of the TNI resulting in NO_2^- formation. This energy loss feature shows a threshold at ~ 5 eV which is in excellent agreement with the obtained value of 5.26 eV.

We also note some differences in the rich fragmentation pattern and the anion yields obtained from the present experiments, and those from electron attachment studies. Yet, NIMO is extremely efficient in capturing an extra electron either from a bound atomic compound via an electron transfer process or from a simple associate electron attachment mechanism. The present results also give relevant information as to the underlying molecular mechanisms governing the electron transfer process, showing the strong ability of this molecule to scavenge an electron supporting therefore the premise that NIMO is selectively cytotoxic to tumour cells via its reduction as a requirement for accumulation in the cell [243]. Thus, radical formation upon electron capture has been identified to be a pivotal mechanism for radiosensitisation of hypoxic cells by using nitroimidazoles' compounds as is the case of NIMO. The radiosensitisation effect is only operative if these chemical compounds are incorporated in cells prior to irradiation of the biological material [244]. Upon redox reactions in cells, formation of a non-dissociated parent anion (radical anion) is not responsible for cytotoxicity to DNA. The mechanism that seems to be operative in hypoxic cells, requires a proton transfer to the reduced chemical compound yielding a neutral radical species that will bind to DNA resulting in strand breaks [245]. Also, interesting to note is the relevance of OH° radicals from water radiolysis which attack DNA at specific sites where nitroimidazoles' agents bind to DNA, making these chemical compounds well−attuned to mimicking oxygen in hypoxic tumours. Finally, we believe that the present investigation is relevant to understand how NIMO accumulating in tumour cells can be used for further formulation of new radiopharmaceutical compounds.

8.4 Molecules relevant to biological environments

A comprehensive crossed beam experimental study on H_2O and D_2O has been performed. Using neutral potassium as a projectile, we have probed the dissociation dynamics in a wide energy range, from 10 eV up to 1keV. Alkali energy loss spectroscopy in post collision experiments in the forward direction gives valuable insight about the electronic states accessed in the formation of a temporary negative ion (TNI).
Negative ion formation in $K + H_2O$ collisions was investigated using TOF−MS from r−TOF. All previously reported anions (H^-, O^-, and OH^-) were observed. Thresholds of formation for each fragment anion were obtained, and these were found higher than the expected thermodynamically calculated energies. Such difference seems to be related to an excess of kinetic energy that is carried away by the fragment naion in the TNI unimolecular decomposition.

From the branching ratios obtained, we can infer that the OH^- anion is the most dominant and has the lowest threshold of formation in such electron transfer experiments. OH^- anion account for almost 80% of the total fragment anion ratio in the wide collision energy range probed.

The second mosty intense fragment anion is assigned to H^-, which accounts for approx. 10% of the total ratio.

The less intense naion is assigned to O^- and a close look at its branching ratio indicates that as soon as it is formed the intensity of the H^- anion is reduced.

In collision energies above 50 eV (in CM Frame) the braching ratios show a linear tendency. However below 40 eV collision energy, the braching ratio have slightly different pattern, careful analysis of such results may indicate contributions from different channels of anionic formation being activated.

In D_2O, negative ion formation, as expected OD^- is the most dominant fragment anion. However, as the collsion energy increases O^-, fragment anion appears before D^-, which is in contrast with H_2O where, O^- was observed after H^-. Another interesting fact is the different in threshold of formation for D^- from D_2O, in comparison to H^- from H_2O. Which is significantly huge. A detailed study of branching ratio of D_2O also indicate that O^- formation in D_2O has an increasing trend in higher energies which directly competes with OD^- formation. This indicates an interplay of different electron−transfer mechanism for ion-pair formation in D_2O than H_2O.

Finally, in analysis of alkali-energy loss spectroscopy of K^+ in forward direction upon collision with H_2O and D_2O. Assignemnt of the various vertical electron affinities was possible. A comparative study of H_2O and D_2O energy loss data tells us that upto 21 eV energy loss, both H_2O and D_2O have similar features. However, D_2O energy loss starts to differ from H_2O

energy loss above 16 eV. The energy loss spectra for D_2O between 16 and 20 eV are enhanced in comparison to H_2O. which tells us that in D_2O these channels are more dominant that H_2O.

Another interesting feature in energy loss of D_2O is spectra above 21 eV, which is absent in H_2O. this lends support to our branching ratio data, informing a diferent charge transfer mechanism.

It is possible that in alkali energy loss spectroscopy, our potassium approaches H_2O and D_2O with significantly high energy, and possibility of dipolar dissociation and or ionization can not be ignored.

To summarize, it can be concluded that mechanism of electron transfer in D_2O is similar up to 15 eV in energy loss, and OH^- and OD^- fragment anions are most dominant. and differes by the formation of D^-, H^-, and O^-, as is evident from experimental results from negative ion formation TOF-MS and alkali energy loss spectroscopy.

8.5 Future perspective: An experimental point of view

This thesis sheds some light on the fact that negative ion formation in electron transfer processes have significance in various biological and astrochemical environments. Negative ion chemistry of halogens can provide siginificant insight to cyano compounds due to their pseudo halogenic nature like CN^-, which are of great interest among the astrophysics and astrochemical community. Such charge transfer experiments mimic more realistic apporach to electron transfer mechanism in astrochemically environmets than DEA reactions. On the other hand, the dominance of electron transfer processes in biological environmets give these experiments an edge over free electron experiments. The mere possibility of probing vibration struture and their geometrical dependence from a weakly bound valence electron, as is the case in potassium, can provide detailed insight in terms of electron transfer reactions and possible fragmentation channels. Hence, these experiments can be extended to other stages of aggregation of the target beam, allowing to explore other molecular compounds that are found in prevalenet environments rather than gas-phase.

In order to achieve that, some experimental modifications can give deeper understanding of electron-transfer processes. Alkali energy loss spectroscopy is an excellent tool to probe vertical electron affinities (VEA) and may characterize vibrational as well as electronic state spectroscopy of various molecules. The present alkali-energy loss experimental setup, which is restricted by the beam current (in less than pA) resoultion and experimental configuration. Since the neutral beam produces a current in the order of pA, and depending on the reaction cross-section of charge transfer, upon collision with molecule it reduces further.

Some drastic changes to the experimental setup would require recharacterization of all other parameters, which would require at least two PhD projects working at the same time.

8.5.1 Future perspective: Modification of target source

Development of a cluster source to fully utilize and mimc the biological environmets would a great extension of this work. The alkali energy energy loss spectroscopy of such collisions would open up a completely new and unique field of research. With such improovment, it can play a significant role in understanding various mechanism at the forefront of physics, chemistry, and biology. A team of such experts would be a best combination to start with. These charge transfer processes have a great potential from calculation of electron affinities to measurement of cross-section, braching ratios, which can give insight about the role of fragment anions, and threshold of formations.

8.5.2 Future perspective: Modification of energy-loss analyzer

Due to immense potential of alkali-energy loss spectroscopy, a different dimension to it can be added by:

- Making the hemisherical energy loss analyzer rotatable, thus giving access to posibility of measurements of post collision cation formation at various scattering angles. This may allow the possibilty of measurements of ionic and covalent trajectories in electron transfer experiments.
- It would also give the possibility of differential cross-section measurements.
- By fixing the transmission energy into the energy loss analyzer and varying the beam energy would give insight about strength of a particular channel in such collision experiments.

REFERENCES

[1] J. C. Polanyi, "Some Concepts in Reaction Dynamics (Nobel Lecture)," *Nobel Lecture*, pp. 359–407, 1986, doi: 10.1002/anie.198709521.

[2] Y. T. Lee, "Molecular Beam Studies of Elementary Chemical Processes," *Nobel Lecture*, no. 1, pp. 320–354, 1986, doi: 10.1016/B978-0-08-042152-0.50007-7.

[3] D. R. Herschbach, "Molecular dynamics of Elementary Chemical Reactions," *Nobel Lecture*, pp. 265–314, 1986, doi: 10.1007/BF03156053.

[4] R. A. Marcus, "Electron Transfer Reactions in Chemistry : Theory and Experiment (Nobel Lecture)," *Angewandte Chemie International Edition in English*, vol. 32, no. 8, pp. 1111–1222, 1993.

[5] M. Patz and S. Fukuzumi, "Critical Review Electron Transfer in Organic Reactions," *J. Phys. Org. Chem*, vol. 10, pp. 129–137, 1997, [Online]. Available: https://s3.amazonaws.com/objects.readcube.com/articles/downloaded/wiley/500fb1dd1d29658a065a704367ed96920ba709bc625e0af28d78ba6cdaa3aeaa.pdf?X-Amz-Algorithm=AWS4-HMAC-SHA256&X-Amz-Credential=AKIAIS5LBPCM5JPOCDGQ%2F20180627%2Fus-east-1%2Fs3%2Faws4_request&

[6] C. Wan, T. Fiebig, S. O. Kelley, C. R. Treadway, J. K. Barton, and A. H. Zewail, "Femtosecond dynamics of DNA-mediated electron transfer," *Proc Natl Acad Sci U S A*, vol. 96, no. 11, pp. 6014–6019, 1999, doi: 10.1073/pnas.96.11.6014.

[7] D. Herschbach, "Chemical stereodynamics: Retrospect and prospect," *European Physical Journal D*, vol. 38, no. 1, pp. 3–13, 2006, doi: 10.1140/epjd/e2006-00027-1.

[8] "http://webbook.nist.gov/chemistry/," *NIST Chemistry WebBook*.

[9] J. A. Aten and J. Los, "Space charge related energy deficit in beams from charge exchange sources," *Journal of Physics E: Scientific Instruments*, vol. 8, no. 5, pp. 408–410, 1975, doi: 10.1088/0022-3735/8/5/022.

[10] T. M. da F. Cunha, "Negative ion formation in Potassium-Purine molecule collisions," PhD Thesis, 2018. doi: 10.1088/0953-4075/34/14/201.

[11] T. Cunha, M. Mendes, F. Ferreira Da Silva, S. Eden, G. García, and P. Limão-Vieira, "Communication: Site-selective bond excision of adenine upon electron transfer," *Journal of Chemical Physics*, vol. 148, no. 2, pp. 021101-1–5, 2018, doi: 10.1063/1.5018401.

[12] A. W. Kleyn, "Vibronic Excitation in Atom Molecule Collisions," PhD Thesis, 1980.

[13] D. Almeida *et al.*, "Electron transfer-induced fragmentation of thymine and uracil in atom-molecule collisions," *Physical Chemistry Chemical Physics*, vol. 13, no. 34, pp. 15657–15665, 2011, doi: 10.1039/c1cp21340g.

[14] F. F. da Silva *et al.*, "NCO-, a key fragment upon dissociative electron attachment and electron transfer to pyrimidine bases: Site selectivity for a slow decay process," *J Am Soc Mass Spectrom*, vol. 24, no. 11, pp. 1787–1797, 2013, doi: 10.1007/s13361-013-0715-9.

[15] D. Almeida, F. Ferreira Da Silva, S. Eden, G. García, and P. Limão-Vieira, "New fragmentation pathways in K-THF collisions as studied by electron-transfer experiments: Negative ion formation," *Journal of Physical Chemistry A*, vol. 118, no. 4, pp. 690–696, 2014, doi: 10.1021/jp407997w.

[16] D. Almeida, F. Ferreira Da Silva, G. García, and P. Limão-Vieira, "Selective bond cleavage in potassium collisions with pyrimidine bases of DNA," *Physical Review Letters*, vol. 110, no. 2, pp. 1–5, 2013, doi: 10.1103/PhysRevLett.110.023201.

[17] R. Antunes *et al.*, "Negative ion formation in potassium-nitromethane collisions," *Physical Chemistry Chemical Physics*, vol. 12, no. 39, pp. 12513–12519, 2010, doi: 10.1039/c004467a.

[18] D. Almeida, F. Ferreira Da Silva, J. Kopyra, G. García, and P. Limão-Vieira, "Anion formation in gas-phase potassium-uridine collisions," *International Journal of Mass Spectrometry*, vol. 365–366, pp. 243–247, 2014, doi: 10.1016/j.ijms.2014.01.023.

[19] O. de Paris, "Chemical composition and temperature structure of Titan's stratosphere," vol. 8, no. c, pp. 8–9, 2013.

[20] V. Vuitton *et al.*, "Negative ion chemistry in Titan's upper atmosphere," *Planetary and Space Science*, vol. 57, no. 13, pp. 1558–1572, 2009, doi: 10.1016/j.pss.2009.04.004.

[21] W. K. Gichuhi, "Astrochemical dynamics : Fundamental studies relevant to titan ' s atmosphere," 2011.

[22] A. J. Coates, F. J. Crary, G. R. Lewis, D. T. Young, J. H. Waite, and J. C. Sittler, "Discovery of heavy negative ions in Titan's ionosphere," *Geophysical Research Letters*, vol. 34, no. 22, pp. 6–11, 2007, doi: 10.1029/2007GL030978.

[23] M. L. Delitsky and C. P. McKay, "The photochemical products of benzene in Titan's upper atmosphere," *Icarus*, vol. 207, no. 1, pp. 477–484, 2010, doi: 10.1016/j.icarus.2009.11.002.

[24] M. Rahm, J. I. Lunine, D. A. Usher, and D. Shalloway, "Polymorphism and electronic structure of polyimine and its potential significance for prebiotic chemistry on Titan," *Proc Natl Acad Sci U S A*, vol. 113, no. 29, pp. 8121–8126, 2016, doi: 10.1073/pnas.1606634113.

[25] M. Khamesian *et al.*, "Formation of CN-, C3 N-, and C5 N- Molecules by Radiative Electron Attachment and their Destruction by Photodetachment," *Physical Review Letters*, vol. 117, no. 12, pp. 1–5, 2016, doi: 10.1103/PhysRevLett.117.123001.

[26] A. H. Becquerel, "On Radioactivity, a new property of matter," *Nobel Lecture*, pp. 52–70, 1903.

[27] L. Pecorino, *Molecular Biology of Cancer: Mechanisms, Targets, and Therapeutics*. 2012. [Online]. Available: http://books.google.com/books?id=tI_vcU85QU4C&pgis=1

[28] D. H. Roukos, "Genome-wide association studies : how predictable is a person´s cancer risk ?," *Expert Review of Anti-Infective Therapy*, vol. 9, no. 4, pp. 389–392, 2009, doi: 10.1586/era.09.12.

[29] "All cancers," 2020. https://gco.iarc.fr/today (accessed May 16, 2022).

[30] M. C. ; Joiner and K. A. J. van Der;, *Basic Clinical Radiobiology*. 2018. doi: 10.1201/9780429490606.

[31] G. P. Delaney and M. B. Barton, "Evidence-based Estimates of the Demand for Radiotherapy," *Clinical Oncology*, vol. 27, no. 2, pp. 70–76, 2014, doi: 10.1016/j.clon.2014.10.005.

[32] Y. Zheng, D. J. Hunting, P. Ayotte, and L. Sanche, "Role of secondary low-energy electrons in the concomitant chemoradiation therapy of cancer," *Physical Review Letters*, vol. 100, no. 19, pp. 1–4, 2008, doi: 10.1103/PhysRevLett.100.198101.

[33] P. J. Eifel, "Concurrent chemotherapy and radiation therapy as the standard of care for cervical cancer," *Nature Clinical Practice Oncology*, vol. 3, no. 5, pp. 248–255, 2006, doi: 10.1038/ncponc0486.

[34] H. A. Wagenknecht, "Electron transfer processes in DNA: Mechanisms, biological relevance and applications in DNA analytics," *Natural Product Reports*, vol. 23, no. 6, pp. 973–1006, 2006, doi: 10.1039/b504754b.

[35] J. R. ; Bolton, N. ; Mataga, and G. ; McLendon, "Introduction to Electron Transfer in Inorganic, Organic, and Biological Systems," *Advances in Chemistry ; American Chemical Society*, no. 11, pp. 1–18, 1991, doi: 10.4324/9780203702260-1.

[36] M. Lienemann, "Molecular mechanisms of electron transfer employed by native proteins and biological-inorganic hybrid systems," *Computational and Structural Biotechnology Journal*, vol. 19, pp. 206–213, 2021, doi: 10.1016/j.csbj.2020.12.004.

[37] L. Sanche, "Beyond radical thinking," *Nature*, vol. 461, no. 10, pp. 1100–1104, 2009, doi: 10.1038/ng.447.

[38] E. Alizadeh and L. Sanche, "Precursors of Solvated Electrons in Radiobiological Physics and Chemistry," *Chemical Reviews*, vol. 112, pp. 5578–562, 2012, doi: 10.1021/cr300063r.

[39] X. Luo, Y. Zheng, and L. Sanche, "DNA strand breaks and crosslinks induced by transient anions in the range 2-20 eV," *Journal of Chemical Physics*, vol. 140, no. 15, pp. 155101-1–11, 2014, doi: 10.1063/1.4870519.

[40] B. Boudaiffa, P. Cloutier, D. Hunting, M. A. Huels, and L. Sanche, "Resonant Formation of DNA Strand Breaks by Low-energy (3 to 20 eV) Electrons," *Science (1979)*, vol. 1533, no. March, pp. 215–221, 2000, doi: 10.1126/science.287.5458.1658.

[41] M. Baumann *et al.*, "Radiation oncology in the era of precision medicine," *Nature Reviews Cancer*, vol. 16, no. 4, pp. 234–249, 2016, doi: 10.1038/nrc.2016.18.

[42] R. Meißner *et al.*, "Low-energy electrons transform the nimorazole molecule into a radiosensitiser," *Nature Communications*, vol. 10, no. 1, pp. 1–7, Jun. 2019, doi: 10.1038/s41467-019-10340-8.

[43] R. Meißner, L. Feketeová, A. Bayer, P. Limão-Vieira, and S. Denifl, "Formation of negative and positive ions in the radiosensitizer nimorazole upon low-energy electron collisions," *Journal of Chemical Physics*, vol. 154, no. 7, p. 074306, 2021, doi: 10.1063/5.0040045.

[44] P. Wardman, "Some Reactions and Properties of Nitro Radical-Anions Important in Biology and Medicine," *Environmental Health Perspectives*, vol. 64, pp. 309–320, 1985.

[45] L. Feketeová *et al.*, "Formation of radical anions of radiosensitizers and related model compounds via electrospray ionization," *International Journal of Mass Spectrometry*, vol. 365–366, pp. 56–63, 2014, doi: 10.1016/j.ijms.2013.12.014.

[46] G. E. ; Adams, I. R. ; Flockhart, C. E. Smithen, I. J. ; Stratford, and M. E. ; Wardman, "Electron-Affinic Sensitization: VII. A Correlation between Structures, One-Electron Reduction Potentials, and Efficiencies of Nitroimidazoles as Hypoxic Cell Radiosensitizers," *Radiation Research*, vol. 67, no. 1, pp. 9–20, 1976.

[47] B. T. Oronsky, S. J. Knox, and J. Scicinski, "Six degrees of separation: The oxygen effect in the development of radiosensitizers," *Translational Oncology*, vol. 4, no. 4, pp. 189–198, 2011, doi: 10.1593/tlo.11166.

[48] A. Ribar, K. Fink, M. Probst, S. E. Huber, L. Feketeová, and S. Denifl, "Isomer Selectivity in Low-Energy Electron Attachment to Nitroimidazoles," *Chemistry - A European Journal*, vol. 23, no. 52, pp. 12892–12899, 2017, doi: 10.1002/chem.201702644.

[49] R. Meißner, L. Feketeová, A. Ribar, K. Fink, P. Limão-Vieira, and S. Denifl, "Electron Ionization of Imidazole and Its Derivative 2-Nitroimidazole," *J Am Soc Mass Spectrom*, vol. 30, no. 12, pp. 2678–2691, 2019, doi: 10.1007/s13361-019-02337-w.

[50] E. Itälä *et al.*, "Controlling NO Production Upon Valence Ionization of Nitroimidazoles," *Journal of Physical Chemistry A*, vol. 123, no. 14, pp. 3074–3079, 2019, doi: 10.1021/acs.jpca.8b11342.

[51] K. Tanzer, L. Feketeová, B. Puschnigg, P. Scheier, E. Illenberger, and S. Denifl, "Reactions in Nitroimidazole Triggered by Low-Energy (0 - 2 eV) Electrons: Methylation at N1-H Completely Blocks Reactivity," *Angewandte Chemie - International Edition*, vol. 53, no. 45, pp. 12240–12243, 2014, doi: 10.1002/anie.201407452.

[52] E. Itälä, K. Tanzer, S. Granroth, K. Kooser, S. Denifl, and E. Kukk, "Fragmentation patterns of 4(5)-nitroimidazole and 1-methyl-5-nitroimidazole — The effect of the methylation," *Journal of Mass Spectrometry*, vol. 52, no. 11, pp. 770–776, 2017, doi: 10.1002/jms.3979.

[53] S. Pandeti *et al.*, "Nitroimidazolic radiosensitizers investigated by electrospray ionization time-of-flight mass spectrometry and density functional theory," *RSC Advances*, vol. 7, no. 71, pp. 45211–45221, 2017, doi: 10.1039/c7ra08312b.

[54] J. M. Khreis, S. Pandeti, L. Feketeová, and S. Denifl, "High-energy collision-induced dissociation of radiosensitizer anions: Nimorazole and metronidazole," *International Journal of Mass Spectrometry*, vol. 431, pp. 1–7, 2018, doi: 10.1016/j.ijms.2018.05.015.

[55] S. Pandeti *et al.*, "Binding preference of nitroimidazolic radiosensitizers to nucleobases and nucleosides probed by electrospray ionization mass spectrometry and density functional theory," *Journal of Chemical Physics*, vol. 150, no. 1, 2019, doi: 10.1063/1.5062604.

[56] F. Ferreira Da Silva *et al.*, "Electron transfer processes in potassium collisions with 5-fluorouracil and 5-chlorouracil," *Physical Chemistry Chemical Physics*, vol. 13, no. 48, pp. 21621–21629, 2011, doi: 10.1039/c1cp22644d.

[57] M. Mendes, G. García, M. C. Bacchus-Montabonel, and P. Limão-Vieira, "Electron transfer induced decomposition in potassium–nitroimidazoles collisions: An experimental and theoretical work," *International Journal of Molecular Sciences*, vol. 20, no. 24, pp. 1–18, 2019, doi: 10.3390/ijms20246170.

[58] M. Mendes, M. Probst, T. Maihom, G. García, and P. Limão-Vieira, "Selective Bond Excision in Nitroimidazoles by Electron Transfer Experiments," *Journal of Physical Chemistry A*, vol. 123, no. 18, pp. 4068–4073, 2019, doi: 10.1021/acs.jpca.9b02064.

[59] P. Sonveaux, B. F. Jordan, B. Gallez, and O. Feron, "Nitric oxide delivery to cancer: Why and how?," *European Journal of Cancer*, vol. 45, no. 8, pp. 1352–1369, 2009, doi: 10.1016/j.ejca.2008.12.018.

[60] L. Kjellsson *et al.*, "Resonant Inelastic X-Ray Scattering Reveals Hidden Local Transitions of the Aqueous OH Radical," *Physical Review Letters*, vol. 124, no. 23, p. 236001, 2020, doi: 10.1103/PhysRevLett.124.236001.

[61] W. Q. Xu *et al.*, "Cross sections for valence-shell excitations of H2 O in the 9.85-12.15-eV energy-loss range studied by high-energy inelastic electron scattering," *Physical Review A*, vol. 105, no. 3, pp. 1–9, 2022, doi: 10.1103/PhysRevA.105.032801.

[62] F. Blanco, A. Muñoz, D. Almeida, F. F. da Silva, P. Limão-Vieira, and G. García, "Clustering and condensation effects in the electron scattering cross sections from water molecules," *International Journal of Mass Spectrometry*, vol. 365–366, pp. 287–294, 2014, doi: 10.1016/j.ijms.2014.02.001.

[63] D. Almeida *et al.*, "Mass spectrometry of anions and cations produced in 1-4 keV H -, O -, and OH - collisions with nitromethane, water, ethanol, and methanol," *International Journal of Mass Spectrometry*, vol. 311, pp. 7–16, 2012, doi: 10.1016/j.ijms.2011.11.009.

[64] B. C. Garrett *et al.*, "Role of water in electron-initiated processes and radical chemistry: Issues and scientific advances," *Chemical Reviews*, vol. 105, no. 1, pp. 355–389, 2005, doi: 10.1021/cr030453x.

[65] R. Mota *et al.*, "Water VUV electronic state spectroscopy by synchrotron radiation," *Chemical Physics Letters*, vol. 416, no. 1–3, pp. 152–159, 2005, doi: 10.1016/j.cplett.2005.09.073.

[66] C. R. Brundle and D. W. Turner, "High resolution molecular photoelectron spectroscopy II. Water and deuterium oxide," *Proceedings of the Royal Society of London. Series A. Mathematical and Physical Sciences*, vol. 307, no. 1488, pp. 27–36, 1968, doi: 10.1098/rspa.1968.0172.

[67] T. W. Marin, I. Janik, D. M. Bartels, and D. M. Chipman, "Vacuum ultraviolet spectroscopy of the lowest-lying electronic state in subcritical and supercritical water," *Nature Communications*, vol. 8, no. May, pp. 1–9, 2017, doi: 10.1038/ncomms15435.

[68] M. G. Curtis and I. C. Walker, "Dissociative electron attachment in water and methanol (5-14 eV)," *Journal of the Chemical Society, Faraday Transactions*, vol. 88, no. 19, pp. 2805–2810, 1992, doi: 10.1039/FT9928802805.

[69] W. Q. Xu *et al.*, "Cross sections for the electron-impact excitations A 1B1 and B 1A1 of H2 O determined by high-energy electron scattering," *Physical Review A*, vol. 103, no. 3, pp. 1–8, 2021, doi: 10.1103/PhysRevA.103.032808.

[70] N. B. Ram, V. S. Prabhudesai, and E. Krishnakumar, "Dynamics of the dissociative electron attachment in H2O and D2O: The A1 resonance and axial recoil approximationa," *Journal of Chemical Sciences*, vol. 124, no. 1, pp. 271–279, 2012, doi: 10.1007/s12039-012-0226-4.

[71] G. Mattioli *et al.*, "Water-biomolecule clusters studied by photoemission spectroscopy and multilevel atomistic simulations: hydration or solvation?," *Physical Chemistry Chemical Physics*, vol. 23, no. 28, pp. 15049–15058, 2021, doi: 10.1039/d1cp02031e.

[72] C. H. Greene and A. R. P. Rau, "Dipole threshold laws for single and double detachment from negative ions," *Physical Review A*, vol. 32, no. 3, pp. 1352–1356, 1985, doi: 10.1103/PhysRevA.32.1352.

[73] A. P. Gaiduk, T. A. Pham, M. Govoni, F. Paesani, and G. Galli, "Electron affinity of liquid water," *Nature Communications*, vol. 9, no. 1, pp. 4–9, 2018, doi: 10.1038/s41467-017-02673-z.

[74] D. R. (Editor) Lide, *Handbook of Chem. and Phys.* 1992.

[75] A. W. Kleyn and A. M. C. Moutinho, "Negative ion formation in alkali-atom-molecule collisions," *Journal of Physics B: Atomic, Molecular and Optical Physics*, vol. 34, no. 14, 2001, doi: 10.1088/0953-4075/34/14/201.

[76] E. A. Gislason and J. G. Sachs, "Multiple-crossing electron-jump model for reactions of metal atoms with diatomic halogen molecules," *The Journal of Chemical Physics*, vol. 62, no. 7, pp. 2678–2689, 1975, doi: 10.1063/1.430853.

[77] M. M. Hubers, A. W. Kleyn, and J. Los, "Ion pair formation in alkali-halogen collisions at high velocities," *Chemical Physics*, vol. 17, no. 3, pp. 303–325, 1976, doi: 10.1016/S0301-0104(76)80034-1.

[78] A. ; Danon and A. Amirav, "Surface-Molecule Electron Transfer: I2-Diamond Scattering at 1-12eV," *Physical Review Letters*, vol. 61, no. 26, pp. 2961–2964, 1988.

[79] G. B. Park, B. C. Krüger, D. Borodin, T. N. Kitsopoulos, and A. M. Wodtke, "Fundamental mechanisms for molecular energy conversion and chemical reactions at surfaces," *Reports on Progress in Physics*, vol. 82, no. 9, 2019, doi: 10.1088/1361-6633/ab320e.

[80] P. Haochang, T. C. M. Horn, and A. W. Kleyn, "Harpooning in Surface Scattering: 02-Formation in Collisions of 02+ from Ag(111)," *Phys. Rev. Lett.*, vol. 57, no. 24, pp. 3035–3038, 1986.

[81] A. M. Wodtke, "Electronically non-adiabatic influences in surface chemistry and dynamics," *Chemical Society Reviews*, vol. 45, no. 13, pp. 3641–3657, 2016, doi: 10.1039/c6cs00078a.

[82] P. J. Kuntz, M. H. Mok, and J. C. Polanyi, "Distribution of reaction products. V. Reactions forming an ionic bond, M+XC (3D)," *The Journal of Chemical Physics*, vol. 50, no. 11, pp. 4623–4652, 1969, doi: 10.1063/1.1670949.

[83] J. L. Magee, "The mechanism of reactions involving excited electronic states: The gaseous reactions of the alkali metals and halogens," *The Journal of Chemical Physics*, vol. 8, no. 9, pp. 687–698, 1940, doi: 10.1063/1.1750739.

[84] D. R. Herschbach, "Molecular Beam Studies of Internal Excitation of Reaction Products," *Applied Optics*, vol. 4, no. S1, p. 128, 1965, doi: 10.1364/ao.4.s1.000128.

[85] W. B. Miller, S. A. Safron, and D. R. Herschbach, "Exchange reactions of alkali atoms with alkali halides: A collision complex mechanism," *Discuss Faraday Soc*, vol. 44, no. 1, pp. 108–122, 1967, doi: 10.1039/DF9674400108.

[86] M. M. Hubers and J. Los, "Ion pair formation in alkali-SF6 collisions: Dependence on collisional and vibrational energy," *Chemical Physics*, vol. 10, no. 2–3, pp. 235–259, 1975, doi: 10.1016/0301-0104(75)87039-X.

[87] I. Mills, T. Cvita, K. Homann, N. Kallay, and K. Kozokuchitsu, *IUPAC gren book*. 1993.

[88] J. F. J. Todd, "Recommendations for nomenclature and symbolism for mass spectroscopy," *International Journal of Mass Spectrometry and Ion Processes*, vol. 142, no. 3, pp. 209–240, 1995, doi: 10.1016/0168-1176(95)93811-f.

[89] C. Wittig, "The Landau-Zener formula," *Journal of Physical Chemistry B*, vol. 109, no. 17, pp. 8428–8430, 2005, doi: 10.1021/jp040627u.

[90] N. A. Sinitsyn, J. Lin, and V. Y. Chernyak, "Constraints on scattering amplitudes in multistate Landau-Zener theory," *Physical Review A*, vol. 95, no. 1, pp. 1–16, 2017, doi: 10.1103/PhysRevA.95.012140.

[91] A. W. Kleyn, M. M. Hubers, and J. Los, "Ion-Pair formation in alkali atom-oxygen molecule collisions," *Chemical Physics*, vol. 34, pp. 55–63, 1978.

[92] A. Suits and Y. Lee, "Reactive Scattering," *Springer Handbooks*, no. 4, pp. 967–982, 2006, doi: 10.1007/978-0-387-26308-3_66.

[93] M. F. Geer, J. Mazzuca, M. D. Smith, and L. S. Shimizu, "Short, strong halogen bonding in co-crystals of pyridyl bis-urea macrocycles and iodoperfluorocarbons," *CrystEngComm*, vol. 15, no. 46, pp. 9923–9929, 2013, doi: 10.1039/c3ce41413b.

[94] T. R. Dinterman and J. B. Delos, "Generalization of the Rosen-Zener model of noncrossing interactions. II. Differential cross sections," *Physical Review A*, vol. 15, no. 2, pp. 475–478, 1977, doi: 10.1103/PhysRevA.15.475.

[95] U. C. Klomp and J. Los, "Orientational effects in Collisions of Cesium atoms with CO and N2," *Chemical Physics Letters*, vol. 84, no. 2, pp. 0–3, 1981.

[96] E. E. Nikitin and L. Zulicke, *Lecture Notes in Lecture Notes in Chemistry*, no. May. 1978.

[97] A. W. Kleyn, J. Los, and E. A. Gislason, "Vibronic coupling at intersections of covalent and ionic states," *Physics Reports*, vol. 90, no. 1, pp. 1–71, 1982, doi: 10.1016/0370-1573(82)90092-8.

[98] R. E. Olson, F. T. Smith, and E. Bauer, "Estimation of the Coupling Matrix Elements for One-Electron Transfer Systems," *Applied Optics*, vol. 10, no. 8, p. 1848, 1971, doi: 10.1364/ao.10.001848.

[99] A. W. Kleyn, "Orientation and harpooning in molecule-surface collisions," *Vacuum*, vol. 41, no. 1–3, pp. 248–251, 1990, doi: 10.1016/0042-207X(90)90325-S.

[100] M. Baer, "Born – Oppenheimer Approach : Diabatization," in *Beyond Born–Oppenheimer: Conical Intersections and Electronic Nonadiabatic Coupling Terms*, 2006, pp. 26–57.

[101] M. Born and R. Oppenheimer, "Zur Quantentheorie der Molekeln," *Ann Phys*, vol. 20, pp. 457–484, 1927.

[102] U. C. Klomp, M. R. Spalburg, and J. Los, "A Time-dependent quantal anlysis of vibronic excitation in alkali-diatom collisions," *Chemical Physics*, vol. 83, pp. 33–51, 1984.

[103] E. Bauer, E. R. Fisher, and F. R. Gilmore, "De-excitation of Electronically Excited Sodium by Nitrogen," *The Journal of Chemical Physics*, vol. 51, no. November, pp. 4173–4181, 1969.

[104] J. Franck, "Elementary Processes of Photochemical reactions," *Transactions of Faraday Society*, vol. 21, pp. 536–542, 1926, doi: 10.1201/ebk1420076370-c5.

[105] E. Condon, "A theory of intensity distribution in band systems," *Physical Review*, vol. 28, no. 6, pp. 1182–1201, 1926, doi: 10.1103/PhysRev.28.1182.

[106] L. J. Dube, "Multiple-scattering approaches to the electron transfer process : I . Some calculable approximations," *J. Phys. B: At. Mol. Opt. Phys.B.*, vol. 17, pp. 641–658, 1984.

[107] J. C. Tully and R. K. Preston, "Trajectory surface hopping approach to nonadiabatic molecular collisions: The reaction of H+ with D2," *The Journal of Chemical Physics*, vol. 55, no. 2, pp. 562–572, 1971, doi: 10.1063/1.1675788.

[108] J. C. Tully, "Mixed quantum–classical dynamics John," *Faraday Discussions*, no. 110, pp. 407–419, 1998.

[109] S. I. Sawada, A. Nitzan, and H. Metiu, "Mean-trajectory approximation for charge- and energy-transfer processes at surfaces," *Physical Review B*, vol. 32, no. 2, pp. 851–867, 1985, doi: 10.1103/PhysRevB.32.851.

[110] P. Ehrenfest, "Bemerkung über die angenäherte Gültigkeit der klassischen Mechanik innerhalb der Quantenmechanik," *Z. Physik*, vol. 45, pp. 455–457, 1927.

[111] S. Mai, F. Plasser, M. Pabst, F. Neese, A. Köhn, and L. González, "Surface hopping dynamics including intersystem crossing using the algebraic diagrammatic construction method," *Journal of Chemical Physics*, vol. 147, no. 18, pp. 0–12, 2017, doi: 10.1063/1.4999687.

[112] G. A. Jones, B. K. Carpenter, and M. N. Paddon-Row, "Application of trajectory surface hopping to the study of intramolecular electron transfer in polyatomic organic systems," *J Am Chem Soc*, vol. 120, no. 22, pp. 5499–5508, 1998, doi: 10.1021/ja9737533.

[113] T. R. Nelson *et al.*, "Non-adiabatic Excited-State Molecular Dynamics: Theory and Applications for Modeling Photophysics in Extended Molecular Materials," *Chemical Reviews*, vol. 120, no. 4, pp. 2215–2287, 2020, doi: 10.1021/acs.chemrev.9b00447.

[114] A. P. M. Baede, *Charge Transfer Between Neutrals at Hyperthermal Energies*. John Wiley & Sons, 1976. Accessed: Jun. 04, 2022. [Online]. Available: https://books.google.pt/books?hl=en&lr=&id=9gm-Q5NBhv8C&oi=fnd&pg=PA463&ots=P7sPccrg6d&sig=t5PT5J2NL_EzeMdRYPG1L_Ni2MY&redir_esc=y#v=onepage&q&f=false

[115] M. B. Faist and R. D. Levine, "Collisional ionization and elastic scattering in alkali-halogen atom collisions," *The Journal of Chemical Physics*, vol. 64, no. 7, pp. 2953–2970, 1976, doi: 10.1063/1.432555.

[116] R. Antunes, "The Role of Halouracils in Radiotherapy Studied by Electron Transfer in Atom-Molecule Collisions Experiments," PhD thesis, 2011.

[117] "HiPace® 2300 | Pfeiffer Vacuum." https://www.pfeiffer-vacuum.com/en/products/vacuum-generation/turbopumps/hybrid-bearing/hipace-2300/30846/hipace-2300-with-tc-1200-dn-250-cf-f (accessed May 30, 2022).

[118] "SD versions | Pfeiffer Vacuum." https://www.pfeiffer-vacuum.com/en/products/vacuum-generation/multi-stage-roots-pumps/light-duty-applications/air-cooled/sd-versions/12277/acp-28-standard-single-phase-permanent-gas-ballast (accessed May 30, 2022).

[119] "Model 6517A Electrometer/High Resistance Meter Getting Started Manual Rev. B | Tektronix." https://www.tek.com/en/manual/model-6517a-electrometer-high-resistance-meter-getting-started-manual-rev-b (accessed May 30, 2022).

[120] F. Stienkemeier, M. Wewer, F. Meier, and H. O. Lutz, "Langmuir-Taylor surface ionization of alkali (Li, Na, K) and alkaline earth (Ca, Sr, Ba) atoms attached to helium droplets," *Review of Scientific Instruments*, vol. 71, no. 9, pp. 3480–3484, 2000, doi: 10.1063/1.1287750.

[121] R. G. Wilson, "Surface Ionization Ion Sources," *IEEE Transactions on Nuclear Science*, no. JUNE, pp. 72–74, 1967.

[122] W. C. Wiley and I. H. McLaren, "Time-of-flight mass spectrometer with improved resolution," *Review of Scientific Instruments*, vol. 26, no. 12, pp. 1150–1157, 1955, doi: 10.1063/1.1715212.

[123] D. A. v Mamyrin and A. Shmikk, "The linear mass reflectron," *Zh. Eksp. Teor. Fiz.*, vol. 49, no. 5, pp. 762–764, 1979.

[124] B. A. Mamyrin, V. I. Karataev, D. v. Shmikk, and V. A. Zagulin, "The mass-reflectron, a new nonmagnetic time-of-flight mass spectrometer with high resolution," *Zh. Eksp.*

Teor. Fiz., vol. 37, no. 1, pp. 45–48, 1973, [Online]. Available: http://www.google.com/search?client=safari&rls=en-us&q=The+mass-reflectron,+a+new+nonmagnetic+time-of-flight+mass+spectrometer+with+high+resolution&ie=UTF-8&oe=UTF-8

[125] F. Hofer, F. P. Schmidt, W. Grogger, and G. Kothleitner, "Fundamentals of electron energy-loss spectroscopy," *IOP Conference Series: Materials Science and Engineering*, vol. 109, no. 1, 2016, doi: 10.1088/1757-899X/109/1/012007.

[126] D. Spence, R. H. Huebner, H. Tanaka, M. A. Dillon, and R. G. Wang, "Electronic structure of Cl2 from 5 to 15 eV by electron energy loss spectroscopy," *The Journal of Chemical Physics*, vol. 80, no. 7, pp. 2989–2996, 1984, doi: 10.1063/1.447133.

[127] S. Kumar, T. Kilich, M. Łabuda, G. García, and P. Limão-Vieira, "Anionic states of C6Cl6 probed in electron transfer experiments," *Physical Chemistry Chemical Physics*, vol. 24, no. 1, pp. 366–374, 2022, doi: 10.1039/d1cp04500h.

[128] M. Mendes *et al.*, "Ion-pair formation in neutral potassium-neutral pyrimidine collisions: Electron transfer experiments," *Frontiers in Chemistry*, vol. 7, no. APR. 2019. doi: 10.3389/fchem.2019.00264.

[129] K. Regeta *et al.*, "Combined Experimental and Theoretical Studies on Electron Transfer in Potassium Collisions with CCl4," *Journal of Physical Chemistry A*, vol. 124, no. 16, pp. 3220–3227, 2020, doi: 10.1021/acs.jpca.0c02076.

[130] J. C. Steelhammer and W. E. Wentworth, "Correlation of electron beam and thermal electron attachment studies for some chloro, bromo, iodo aromatic compounds," *J. Chem. Phys.*, vol. 51, pp. 1802–1814, 1969, doi: 10.1063/1.1672262.

[131] H. Shimamori, T. Sunagawa, Y. Ogawa, and Y. Tatsumi, "Low-energy electron attachment to C6H5X (X = Cl, Br and I)," *Chem. Phys. Lett.*, vol. 232, pp. 115–120, 1995, doi: 10.1016/0009-2614(94)01306-G.

[132] P. Nag, M. Tarana, and J. Fedor, "Effects of π∗-σ∗ Coupling on dissociative-electron-attachment angular distributions in vinyl, allyl, and benzyl chloride and in chlorobenzene," *Physical Review A*, vol. 103, no. 3, pp. 1–8, 2021, doi: 10.1103/PhysRevA.103.032830.

[133] J. Milhaud, "Dissociative Electron Attchment to Monohalogenated Benzenes," *Chem. Phys. Lett.*, vol. 118, pp. 167–173, 1985.

[134] R. v. Khatymov, M. v. Muftakhov, and V. A. Mazunov, "Phenol, chlorobenzene and chlorophenol isomers: Resonant states and dissociative electron attachment," *Rapid Communications in Mass Spectrometry*, vol. 17, no. 20, pp. 2327–2336, 2003, doi: 10.1002/rcm.1197.

[135] R. V. Khatymov, M. V. Muftakhov, P. V. Schukin, and V. A. Mazunov, "On the structure of negative ions formed by dissociative electron attachment by monochlorophenol molecules," *Russ. Chem. Bull.*, vol. 52, pp. 1974–1981, 2003, doi: 10.1023/B:RUCB.0000009641.29142.3c.

[136] L. G. Christophorou, R. N. Compton, G. S. Hurst, and P. W. Reinhardt, "Dissociative electron capture by benzene derivatives," *J. Chem. Phys.*, vol. 45, pp. 536–547, 1966, doi: 10.1063/1.1727601.

[137] N. L. Asfandiarov *et al.*, "Frozen shell approximation violation in negative ion formation from halogenated benzenes via dissociative attachment," *Rapid Commun. Mass Spectrom.*, vol. 14, pp. 274–279, 2000, doi: 10.1002/(SICI)1097-0231(20000229)14:4<274::AID-RCM878>3.0.CO;2-M.

[138] P. D. Burrow, A. Modelli, and K. D. Jordan, "Temporary anion states of the chlorobenzenes," *Chemical Physics Letters*, vol. 132, no. 4–5, pp. 441–447, 1986, doi: 10.1016/0009-2614(86)80642-X.

[139] D. Mathur and J. B. Hasted, "Resonant scattering of slow electrons from benzene and substituted benzene molecules," *Journal of Physics B: Atomic and Molecular Physics*, vol. 9, no. 3, 1976, doi: 10.1088/0022-3700/9/3/003.

[140] J. K. Olthoff, J. A. Tossell, and J. H. Moore, "Electron attachment by haloalkenes and halobenzenes," *The Journal of Chemical Physics*, vol. 83, no. 11, pp. 5627–5634, 1985, doi: 10.1063/1.449687.

[141] K. L. Stricklett, S. C. Chu, and P. D. Burrow, "Dissociative attachment in vinyl and allyl chloride, chlorobenzene and benzyl chloride," *Chemical Physics Letters*, vol. 131, no. 3, pp. 279–284, 1986, doi: 10.1016/0009-2614(86)80561-9.

[142] X. Li, L. Sanche, and M. D. Sevilla, "Dehalogenation of 5-halouracils after low energy electron attachment: A density functional theory investigation," *J. Phys. Chem. A*, vol. 106, pp. 11248–11253, 2002, doi: 10.1021/jp021669q.

[143] A. Modelli, P. Bolognesi, and L. Avaldi, "Temporary anion states of pyrimidine and halopyrimidines," *J. Phys. Chem. A*, vol. 115, pp. 10775–10782, 2011, doi: 10.1021/jp206559d.

[144] T. Skalický, C. Chollet, N. Pasquier, and M. Allan, "Properties of the π* and σ* states of the chlorobenzene anion determined by electron impact spectroscopy," *Physical Chemistry Chemical Physics*, vol. 4, no. 15, pp. 3583–3590, 2002, doi: 10.1039/b202494b.

[145] C. Makochekanwa, O. Sueoka, and M. Kimura, "A comparative study of electron and positron scattering from chlorobenzene (C6H5Cl) and chloropentafluorobenzene (C6F5Cl) molecules," *Journal of Chemical Physics*, vol. 119, no. 23, pp. 12257–12263, 2003, doi: 10.1063/1.1626115.

[146] S. L. Lunt, D. Field, S. v Hoffmann, R. J. Gulley, and J.-P. Ziesel, "Very low energy electron scattering in C6H5F, C6H5Cl, C6H5Br and C6H5," *J. Phys. B: At. Mol. Opt. Phys.*, vol. 32, pp. 2707–2717, 1999, doi: 10.1002/cber.19250580530.

[147] I. V. Beregovaya and L. N. Shchegoleva, "Potential energy surface and dissociative cleavage of chlorobenzene radical anion," *Chem. Phys. Lett.*, vol. 348, pp. 501–506, 2001, doi: 10.1016/S0009-2614(01)01171-X.

[148] A. S. Barbosa *et al.*, "Theoretical and experimental study on electron interactions with chlorobenzene: Shape resonances and differential cross sections," *Journal of Chemical Physics*, vol. 145, no. 8, 2016, doi: 10.1063/1.4961649.

[149] J. Kocisek and J. Fedor, "Experiments probing symmetry lowering in DEA to chlorobenzene," p. Private communication.

[150] W. B. Knighton, J. A. Bognar, and E. P. Grimsrud, "Reactions of Selected Molecular Anions with Oxygen," *Journal of Mass Spectrometry*, vol. 30, no. September, pp. 557–562, 1995.

[151] J. R. Wiley, E. C. M. Chen, E. S. D. Chen, P. Richardson, W. R. Reed, and W. E. Wentworth, "The determination of absolute electron affinities of chlorobenzenes, chloronaphthalenes and chlorinated biphenyls from reduction potentials," *Journal of Electroanalytical Chemistry*, vol. 307, no. 1–2, pp. 169–182, 1991, doi: 10.1016/0022-0728(91)85546-2.

[152] D. Almeida, F. Ferreira da Silva, G. García, and P. Limão-Vieira, "Selective bond cleavage in potassium collisions with pyrimidine bases of DNA," *Phys. Rev. Lett.*, vol. 110, p. 023201, 2013.

[153] R. Antunes *et al.*, "Negative ion formation in potassium–nitromethane collisions," *Phys. Chem. Chem. Phys.*, vol. 12, pp. 12513–12519, 2010.

[154] P. Limão-Vieira, A. M. C. Moutinho, and J. Los, "Dissociative ion-pair formation in collisions of fast potassium atoms with benzene and fluorobenzene," *J. Chem. Phys.*, vol. 124, p. 054306, 2006, doi: 10.1063/1.2161217.

[155] A. Rebelo, T. Cunha, M. Mendes, F. F. da Silva, G. García, and P. Limão-Vieira, "Kinetic-energy release distributions of fragment anions from collisions of potassium atoms with D-Ribose and tetrahydrofuran," *Eur. Phys. J. D*, vol. 70, p. 130, 2016, doi: 10.1140/epjd/e2016-70159-8.

[156] P. Limão-Vieira, A. M. C. Moutinho, and J. Los, "Dissociative ion-pair formation in collisions of fast potassium atoms with benzene and fluorobenzene," *J. Chem. Phys.*, vol. 124, p. 054306, 2006, doi: 10.1063/1.2161217.

[157] J. Milhaud, "Dissociative Electron Attchment to Monohalogenated Benzenes," *Chem. Phys. Lett.*, vol. 118, pp. 167–173, 1985.

[158] H. Shimamori, T. Sunagawa, Y. Ogawa, and Y. Tatsumi, "Low-energy electron attachment to C6H5X (X = Cl, Br and I)," *Chem. Phys. Lett.*, vol. 232, pp. 115–120, 1995, doi: 10.1016/0009-2614(94)01306-G.

[159] A. Modelli, "Electron attachment and intramolecular electron transfer in unsaturated chloroderivatives," *Physical Chemistry Chemical Physics*, vol. 5, no. 14, pp. 2923–2930, 2003, doi: 10.1039/b304083f.

[160] L. G. Christophorou, R. N. Compton, G. S. Hurst, and P. W. Reinhardt, "Dissociative electron capture by benzene derivatives," *J. Chem. Phys.*, vol. 45, pp. 536–547, 1966, doi: 10.1063/1.1727601.

[161] M. H. Palmer *et al.*, "A combined theoretical and experimental study of the valence and Rydberg states of iodopentafluorobenzene," *J. Chem. Phys.*, vol. 146, p. 124302, 2016, doi: 10.1063/1.4981919.

[162] M. H. Palmer *et al.*, "A combined theoretical and experimental study of the valence and Rydberg states of iodopentafluorobenzene," *J. Chem. Phys.*, vol. 146, p. 124302, 2016, doi: 10.1063/1.4981919.

[163] T. Ari, H. Güven, and N. Ecevit, "Electron energy-loss spectroscopy in monosubstituted benzenes," *J. Electron Spectrosc. Relat. Phenom.*, vol. 73, pp. 13–23, 1995, doi: 10.1016/0368-2048(94)02267-4.

[164] S. Köring, "PhD thesis in Energy Distribution in Dissociation of Polyatomic Molecules," University of Amsterdam, 1989.

[165] V. K. Voora, "Molecular Electron Affinities Using the Generalized Kohn-Sham Semicanonical Projected Random Phase Approximation," *Journal of Physical Chemistry Letters*, vol. 12, no. 1, pp. 433–439, 2021, doi: 10.1021/acs.jpclett.0c03362.

[166] S. Kumar, F. Izadi, M. Oncak, P. Limao-Vieira, and S. Denifl, "Hexachlorobenzene negative ions formation in electron attachment experiments," *Phys. Chem. Chem. Phys.*, vol. 24, pp. 13335–13342, 2022, doi: 10.1039/d2cp01360f.

[167] A. A. Zembekov, "On the mechanism of the reaction K + Br2 → K+ + Br2- near the threshold," *Chemical Physics Letters*, vol. 11, no. 4, pp. 415–416, 1971.

[168] G. M. Kendall and R. Grice, "Vibrational coordinates in the electron jump model," *Molecular Physics*, vol. 24, no. 6, pp. 1373–1382, 1972, doi: 10.1080/00268977200102441.

[169] A. M. C. Moutinho, A. W. Kleyn, and J. Los, "Ion-pair formation in some potassium-molecule collisions, Dependence on the vibrational energy," *Chemical Physics Letters*, vol. 61, no. 2, pp. 249–253, 1979.

[170] J. A. Aten, G. E. H. Lanting, and J. Los, "Influence of the iodine internal energy on differential cross sections for ion-pair formation in Na, K, Cs + I2 Collisions," *Chemical Physics*, vol. 22, pp. 333–339, 1977.

[171] W. W. Brubaker and R. A. Hites, "Experimental Section," *Environ. Sci. Technol.*, vol. 32, pp. 766–769, 1998, doi: 10.1111/j.1748-1716.1962.tb02520.x.

[172] M. P. Ormad, N. Miguel, A. Claver, J. M. Matesanz, and J. L. Ovelleiro, "Pesticides removal in the process of drinking water production," *Chemosphere*, vol. 71, no. 1, pp. 97–106, 2008, doi: 10.1016/j.chemosphere.2007.10.006.

[173] "Toxicologic profile of hexachlorobenzene, U.S. Department of Health and Human Services, Public Health Service, Agency for Toxic Substances and Disease Registry, Division of Toxicology and Human Health Sciences, Environmental Toxicology Branch," Atlanta, Georgia, 2015.

[174] S. L. Simonich and R. A. Hites, "Global distribution of persistent organochlorine compounds," *Science (1979)*, vol. 269, no. 5232, pp. 1851–1854, 1995, doi: 10.1126/science.7569923.

[175] G. W. Patton, M. D. Walla, T. F. Bidleman, and L. A. Barrie, "Polycyclic aromatic and organochlorine compounds in the atmosphere of northern Ellesmere Island, Canada," *Journal of Geophysical Research*, vol. 96, no. D6. 1991. doi: 10.1029/91jd00010.

[176] M. Oehme, "Further evidence for long-range air transport of polychlorinated aromates and pesticides: North America and Eurasia to the Arctic," *Ambio*, vol. 20, no. 7, pp. 293–297, 1991, doi: 10.2307/4313848.

[177] P. Roche and M. Prados, "Removal of Pesticides by Use of Ozone or Hydrogen Peroxide/Ozone," *Ozone Sci. Eng.*, vol. 17, pp. 657–672, 1995, doi: 10.1080/01919512.1995.10555777.

[178] H. Scharping, C. Zetzsch, and H. A. Dessouki, "The UV absorption spectra of the trichlorobenzenes and the higher chlorinated benzenes in the gas phase and in n-hexane solution," *Journal of Molecular Spectroscopy*, vol. 123, no. 2, pp. 382–391, 1987, doi: 10.1016/0022-2852(87)90286-4.

[179] M. B. Robin, *Higher Excited States of Polyatomic Molecules, Volume II*. Academic Press, 1975.

[180] S. Saëki, "The Assignment of the Molecular Vibrations of Hexachlorobenzene," *Bull Chem Soc Jpn*, vol. 35, no. 2, pp. 322–326, 1962, doi: 10.1246/bcsj.35.322.

[181] J. R. Scherer and J. C. Evans, "Vibrational spectra and assignments for sixteen chlorobenzenes," *Spectrochimica Acta*, vol. 19, no. 11, pp. 1739–1775, 1963, doi: 10.1016/0371-1951(63)80193-9.

[182] B. Ruščić, L. Klasinc, A. Wolf, and J. V. Knop, "Photoelectron spectra of and ab initio calculations on chlorobenzenes. 3. Hexachlorobenzene," *Journal of Physical Chemistry*, vol. 85, no. 11, pp. 1495–1497, 1981, doi: 10.1021/j150611a008.

[183] P. P. Romańczyk, G. Rotko, and S. S. Kurek, "Dissociative electron transfer in polychlorinated aromatics. Reduction potentials from convolution analysis and quantum chemical calculations," *Physical Chemistry Chemical Physics*, vol. 18, no. 32, pp. 22573–22582, 2016, doi: 10.1039/c6cp02222g.

[184] T. Kato and T. Yamabe, "Vibronic interactions and charge transfer in negatively charged chloroacenes," *Chemical Physics*, vol. 321, no. 1–2, pp. 149–158, 2006, doi: 10.1016/j.chemphys.2005.07.041.

[185] J. R. Wiley, E. C. M. Chen, E. S. D. Chen, P. Richardson, W. R. Reed, and W. E. Wentworth, *The determination of absolute electron affinities of chlorobenzenes, chloronaphthalenes and chlorinated biphenyls from reduction potentials*, vol. 307, no. 1–2. 1991. doi: 10.1016/0022-0728(91)85546-2.

[186] W. Xu and A. Gao, "DFT study on the electron affinities of the chlorinated benzenes," *J. Mol. Struct.-Theochem*, vol. 732, pp. 63–70, 2005, doi: 10.1016/j.theochem.2005.07.007.

[187] S. Yamada, Y. Naito, M. Takada, S. Nakai, and M. Hosomi, "Photodegradation of hexachlorobenzene and theoretical prediction of its degradation pathways using quantum chemical calculation," *Chemosphere*, vol. 70, pp. 731–736, 2008, doi: 10.1016/j.chemosphere.2007.06.039.

[188] R. Antunes *et al.*, "Negative ion formation in potassium–nitromethane collisions," *Phys. Chem. Chem. Phys.*, vol. 12, pp. 12513–12519, 2010.

[189] K. Regeta *et al.*, "Combined Experimental and Theoretical Studies on Electron Transfer in Potassium Collisions with CCl4," *Journal of Physical Chemistry A*, vol. 124, no. 16, pp. 3220–3227, 2020, doi: 10.1021/acs.jpca.0c02076.

[190] E. Bene, Á. Vibók, G. J. Halász, and M. C. Bacchus-Montabonel, "Ab initio molecular treatment of charge transfer processes induced by collision of C2+ ions with the OH radical: A linear approach," *Chem. Phys. Lett.*, vol. 455, pp. 159–163, 2008.

[191] M. C. Bacchus-Montabonel and Y. S. Tergiman, "Radiation damage on biomolecular systems : Dynamics of ion induced collision processes," *Comput. Theor. Chem*, vol. 990, pp. 177–184, 2012, doi: 10.1016/j.comptc.2011.11.004.

[192] M. C. Bacchus-Montabonel and Y. S. Tergiman, "Charge transfer dynamics of carbon ions with uracil and halouracil targets at low collision energies," *Chem. Phys. Lett.*, vol. 503, pp. 45–48, 2011.

[193] M. C. Bacchus-Montabonel, M. Łabuda, Y. S. Tergiman, and J. E. Sienkiewicz, "Theoretical treatment of charge-transfer processes induced by collision of Cq+ ions with uracil," *Phys. Rev. A*, vol. 72, p. 052706, 2005, doi: 10.1103/PhysRevA.72.052706.

[194] E. Erdmann, M.-C. Bacchus-Montabonel, and M. Łabuda, "Modelling charge transfer processes in C2+-tetrahydrofuran collision for ion-induced radiation damage in DNA

building blocks," *Phys. Chem. Chem. Phys.*, vol. 19, pp. 19722–19732, 2017, doi: 10.1039/c7cp02100c.

[195] D. Almeida, M.-C. Bacchus-Montabonel, F. Ferreira da Silva, G. García, and P. Limão-Vieira, "Potassium-uracil/thymine ring cleavage enhancement as studied in electron transfer experiments and theoretical calculations," *J. Phys. Chem. A*, vol. 118, pp. 6547–6552, 2014.

[196] L. Salem, *Electrons in Chemical Reactions: First Principles*. Wiley Interscience: New York, 1982.

[197] M. C. Bacchus-Montabonel and Y. S. Tergiman, "An ab initio study of ion induced charge transfer dynamics in collision of carbon ions with thymine," *Phys. Chem. Chem. Phys.*, vol. 13, pp. 9761–9767, 2011.

[198] M. C. Bacchus-Montabonel, "Ab Initio Treatment of Ion-Induced Charge Transfer Dynamics of Isolated 2 - Deoxy - D - ribose," *J. Phys. Chem. A*, vol. 118, pp. 6326–6332, 2014.

[199] M. C. Bacchus-Montabonel and F. Calvo, "Nanohydration of uracil: Emergence of three-dimensional structures and proton-induced charge transfer," *Phys. Chem. Chem. Phys.*, vol. 17, pp. 9629–9633, 2015.

[200] A. Schäfer, C. Huber, and R. Ahlrichs, "Fully optimized contracted Gaussian basis sets of triple zeta valence quality for atoms Li to Kr," *J. Chem. Phys.*, vol. 100, pp. 5829–5835, 1994, doi: 10.1063/1.467146.

[201] F. Neese, "The ORCA program system," *Wiley Interdiscip. Rev. Comput. Mol. Sci.*, vol. 2, pp. 73–78, 2012, doi: 10.1002/wcms.81.

[202] H.-J. Werner, P. J. Knowles, G. Knizia, F. R. Manby, and M. Schütz, "Molpro: A general-purpose quantum chemistry program package," *Wiley Interdiscip. Rev. Comput. Mol. Sci.*, vol. 2, pp. 242–253, 2012.

[203] A. Nicklass, M. Dolg, H. Stoll, and H. Preuss, "Ab initio energy-adjusted pseudopotentials for the noble gases Ne through Xe: Calculation of atomic dipole and quadrupole polarizabilities," *J. Chem. Phys.*, vol. 102, pp. 8942–8952, 1995.

[204] B. O. Roos, *Ab initio methods in Quantum Chemistry II*. Chichester: Wiley-VCH, 1987.

[205] H. J. Werner and P. J. Knowles, "A second order multiconfiguration SCF procedure with optimum convergence," *J. Chem. Phys.*, vol. 82, pp. 5053–5063, 1985, doi: 10.1063/1.448627.

[206] P. J. Knowles and H. J. Werner, "An efficient second-order MC SCF method for long configuration expansions," *Chem. Phys. Lett.*, vol. 115, pp. 259–267, 1985, doi: 10.1016/0009-2614(85)80025-7.

[207] S. Grimme, J. Antony, S. Ehrlich, and H. Krieg, "A consistent and accurate ab initio parametrization of density functional dispersion correction (DFT-D) for the 94 elements H-Pu," *J. Chem. Phys.*, vol. 132, p. 154104, 2010, doi: 10.1063/1.3382344.

[208] A. W. Kleyn and A. M. C. Moutinho, "Negative ion formation in alkali-atom – molecule," *J. Phys. B: At. Mol. Opt. Phys.*, vol. 4075, pp. R1–R44, 2001.

[209] P. Limão-Vieira, A. M. C. Moutinho, and J. Los, "Dissociative ion-pair formation in collisions of fast potassium atoms with benzene and fluorobenzene," *J. Chem. Phys.*, vol. 124, p. 054306, 2006, doi: 10.1063/1.2161217.

[210] E. Illenberger, "Energetics of Negative Ion Formation in Dissociative Electron Attachment to CCl4, CFCl3, CF2Cl2, and CF3Cl," *Ber. Bunsenges. Phys. Chem.*, vol. 86, pp. 252–261, 1982.

[211] H.-U. Scheunemann, E. Illenberger, and H. Baumgartel, "Dissociative Electron Attachment to CCl4, CHCl3, CH2C12 and CH3Cl," *Ber. Bunsenges. Phys. Chem.*, vol. 84, pp. 580–585, 1980.

[212] P. G. Wenthold, R. R. Squires, and W. C. Lineberger, "Ultraviolet photoelectron spectroscopy of the o-, m-, and p-benzyne negative ions. Electron affinities and singlet-triplet splittings for o-, m- , and p-benzyne," *J Am Chem Soc*, vol. 120, no. 21, pp. 5279–5290, 1998, doi: 10.1021/ja9803355.

[213] J. D. D. Martin and J. W. Hepburn, "Determination of bond dissociation energies by threshold ion-pair production spectroscopy: An improved D0(HCl)," *Journal of Chemical Physics*, vol. 109, no. 19, pp. 8139–8142, 1998, doi: 10.1063/1.477476.

[214] J. C. Polanyi and A. H. Zewail, "Direct observation of the transition state," *Accounts of Chemical Research*, vol. 28, pp. 119–132, 1995.

[215] R. Meißner *et al.*, "Low-energy electrons transform the nimorazole molecule into a radiosensitiser," *Nature Communications*, vol. 10, no. 1, pp. 1–7, 2019, doi: 10.1038/s41467-019-10340-8.

[216] Y. Zhao and D. G. Truhlar, "The M06 suite of density functionals for main group thermochemistry, thermochemical kinetics, noncovalent interactions, excited states, and transition elements: Two new functionals and systematic testing of four M06-class functionals and 12 other function," *Theor. Chem. Account*, vol. 120, pp. 215–241, 2008, doi: 10.1007/s00214-007-0310-x.

[217] M. J. Frisch *et al.*, "Gaussian 16 Rev. C.01, Wallingford, CT." Wallingford, CT, 2016.

[218] J. P. Blaudeau, M. P. McGrath, L. A. Curtiss, and L. Radom, "Extension of Gaussian-2 (G2) theory to molecules containing third-row atoms K and Ca," *J. Chem. Phys.*, vol. 107, pp. 5016–5021, 1997, doi: 10.1063/1.474865.

[219] A. D. McLean and G. S. Chandler, "Contracted Gaussian basis sets for molecular calculations. I. Second row atoms, Z=11-18," *J. Chem. Phys.*, vol. 72, pp. 5639–5648, 1980, doi: 10.1063/1.438980.

[220] M. Petersilka, U. J. Gossmann, and E. K. U. Gross, "Excitation Energies from Time-Dependent Density-Functional Theory," *Physical Review Letters*, vol. 76, no. 8, pp. 1212–1215, Feb. 1996, doi: 10.1103/PhysRevLett.76.1212.

[221] "NIST Chemistry webbook," *NIST Chemistry WebBook*, 2022. http://webbook.nist.gov/chemistry (accessed on 6 May 2022)

[222] D. Almeida, F. Ferreira da Silva, S. Eden, G. García, and P. Limão-Vieira, "New fragmentation pathways in K-THF collisions as studied by electron-transfer experiments: Negative ion formation," *J. Phys. Chem. A*, vol. 118, no. 4, pp. 690–696, 2014, doi: 10.1021/jp407997w.

[223] D. Almeida, F. Ferreira Da Silva, J. Kopyra, G. García, and P. Limão-Vieira, "Anion formation in gas-phase potassium-uridine collisions," *International Journal of Mass Spectrometry*, vol. 365–366, pp. 243–247, 2014, doi: 10.1016/j.ijms.2014.01.023.

[224] A. I. Lozano, S. Kumar, B. Kerkeni, G. García, and P. Limão-Vieira, "Methanol Negative Ion Fragmentation Probed in Electron Transfer Experiments," *Journal of Physical Chemistry A*, vol. 126, no. 7, pp. 1076–1084, 2022, doi: 10.1021/acs.jpca.1c07588.

[225] D. Almeida *et al.*, "N-site de-methylation in pyrimidine bases as studied by low energy electrons and ab initio calculations," *Phys. Chem. Chem. Phys.*, vol. 15, no. 27, p. 11431, 2013, doi: 10.1039/c3cp50548k.

[226] F. Ferreira da Silva, G. Meneses, O. Ingólfsson, and P. Limão-Vieira, "Side chain effects in reactions of the potassium-tyrosine charge transfer complex," *Chem. Phys. Lett.*, vol. 662, pp. 19–24, 2016, doi: 10.1016/j.cplett.2016.08.004.

[227] M. Mendes *et al.*, "Ion-pair formation in neutral potassium-neutral pyrimidine collisions: Electron transfer experiments," *Front. Chem.*, vol. 7, pp. 1–10, 2019.

[228] F. F. da Silva *et al.*, "Electron-Transfer-Induced Side-Chain Cleavage in Tryptophan Facilitated through Potassium-Induced Transition-State Stabilization in the Gas Phase," *Journal of Physical Chemistry A*, vol. 125, no. 11, pp. 2324–2333, 2021, doi: 10.1021/acs.jpca.1c00690.

[229] F. F. da Silva, M. Lança, D. Almeida, G. García, and P. Limão-Vieira, "Anionic fragmentation of glycine upon potassium-molecule collisions," *European Physical Journal D*, vol. 66, no. 3, 2012, doi: 10.1140/epjd/e2012-20751-y.

[230] F. F. Silva, M. Mendes, G. García, and P. Limão-Vieira, "Radiation in Bioanalysis, Spectroscopic Techniques and Theoretical Methods," 1st ed., A. S. Pereira, P. Tavares, and P. Limão-Vieira, Eds. Cham, Switzerland: Springer, 2019, pp. 329–348.

[231] A. Kleyn, J. Los, and E. A. Gislason, "Vibronic Coupling At Intersections of Covalent and Ionic States," *Phys. Rep.*, vol. 90, pp. 1–71, 1982, doi: 10.1016/0370-1573(82)90092-8.

[232] A. W. Kleyn and A. M. C. Moutinho, "Negative ion formation in alkali-atom – molecule," *J. Phys. B: At. Mol. Opt. Phys.*, vol. 4075, pp. R1–R44, 2001.

[233] G. Meneses *et al.*, "Unravelling the dissociation pathways of acetic acid upon electron transfer in potassium collisions: Experimental and theoretical studies," *Physical Chemistry Chemical Physics*, vol. 19, no. 2, 2017, doi: 10.1039/c6cp06375f.

[234] X. Su, X. Cheng, C. Meng, and X. Yuan, "Quantum chemical study on nitroimidazole, polynitroimidazole and their methyl derivatives," *J. Hazard. Mater.*, vol. 161, pp. 551–558, 2009, doi: 10.1016/j.jhazmat.2008.03.135.

[235] "NIST Chemistry webbook," *NIST Chemistry WebBook*, 2022.

[236] M. Mendes, G. García, M. C. Bacchus-Montabonel, and P. Limão-Vieira, "Electron transfer induced decomposition in potassium–nitroimidazoles collisions: An experimental and theoretical work," *Int. J. Mol. Sci.*, vol. 20, p. 6170, 2019, doi: 10.3390/ijms20246170.

[237] M. Mendes, M. Probst, T. Maihom, ‖ G García, and P. Limã O-Vieira, "Selective Bond Excision in Nitroimidazoles by Electron Transfer Experiments," 2019, doi: 10.1021/acs.jpca.9b02064.

[238] T. Cunha *et al.*, "Electron transfer driven decomposition of adenine and selected analogs as probed by experimental and theoretical methods," *J. Chem. Phys.*, vol. 148, p. 134301, 2018, doi: 10.1063/1.5021888.

[239] J. Cadet, T. Douki, and J. L. Ravanat, "Oxidatively generated base damage to cellular DNA," *Free Radic. Biol. Med.*, vol. 49, pp. 9–21, 2010, doi: 10.1016/j.freeradbiomed.2010.03.025.

[240] J. Cadet, T. Douki, and J. L. Ravanat, "Measurement of oxidatively generated base damage in cellular DNA," *Mutat. Res.*, vol. 711, pp. 3–12, 2011, doi: 10.1016/j.mrfmmm.2011.02.004.

[241] E. Dumont and A. Monari, "Understanding DNA under oxidative stress and sensitization: The role of molecular modeling," *Front. Chem.*, vol. 3, p. 43, 2015, doi: 10.3389/fchem.2015.00043.

[242] J.-L. Ravanat, J. Cadet, and T. Douki, "Oxidatively Generated DNA Lesions as Potential Biomarkers of In Vivo Oxidative Stress," *Curr. Mol. Med.*, vol. 12, pp. 655–671, 2012, doi: 10.2174/156652412800792651.

[243] P. Wardman, "Chemical Radiosensitizers for Use in Radiotherapy," *Clin. Oncol.*, vol. 19, pp. 397–417, 2007, doi: 10.1016/j.clon.2007.03.010.

[244] P. Wardman, "Chemical Radiosensitizers for Use in Radiotherapy," *Clin. Oncol.*, vol. 19, pp. 397–417, 2007, doi: 10.1016/j.clon.2007.03.010.

[245] P. Wardman, "The mechanism of radiosensitization by electron-affinic compounds," *Radiat. Phys. Chem.*, vol. 30, pp. 423–432, 1987, doi: 10.1016/1359-0197(87)90111-1.

[246] M.-Y. Song *et al.*, " Cross Sections for Electron Collisions with H 2 O ," *Journal of Physical and Chemical Reference Data*, vol. 50, no. 2, p. 023103, 2021, doi: 10.1063/5.0035315.

[247] J. R. Smith, J. B. Kim, and W. C. Lineberger, "High-resolution threshold photodetachment spectroscopy of OH-," *Physical Review A - Atomic, Molecular, and Optical Physics*, vol. 55, no. 3, pp. 2036–2043, 1997, doi: 10.1103/PhysRevA.55.2036.

[248] A. I. Lozano, S. Kumar, B. Kerkeni, G. García, and P. Limão-Vieira, "Methanol Negative Ion Fragmentation Probed in Electron Transfer Experiments," *Journal of Physical Chemistry A*, vol. 126, no. 7, pp. 1076–1084, 2022, doi: 10.1021/acs.jpca.1c07588.

[249] J. Fedor *et al.*, "Fragmentation of transient water anions following low-energy electron capture by H2O/D2O," *Journal of Physics B: Atomic, Molecular and Optical Physics*, vol. 39, no. 18, pp. 3935–3944, 2006, doi: 10.1088/0953-4075/39/18/022.

[250] T. Tsuchida *et al.*, "Doubly excited states of water as studied by electron energy loss spectroscopy in coincidence with detecting Lyman-α photons," *Journal of Physics B: Atomic, Molecular and Optical Physics*, vol. 44, no. 17, 2011, doi: 10.1088/0953-4075/44/17/175207.

[251] M. Kato, T. Odagiri, K. Kodama, M. Murata, K. Kameta, and N. Kouchi, "Doubly excited states of water in the inner valence range," *Journal of Physics B: Atomic, Molecular and Optical Physics*, vol. 37, no. 15, pp. 3127–3148, 2004, doi: 10.1088/0953-4075/37/15/009.

A

SUPPORTING MATERIAL FOR HEXACHLOROBENZENE

This appendix serves as a supplementary information for the chapter 5. A detailed theoretical methodology implemented using various basis sets and complementary experimental results are provided.

A.1 Theoretical Methodology

Hexachlorobenzene molecule was considered in the D_{2h} symmetry for benchmarking the calculations and choice of the molecular framework. Then, the geometry of the ground S_0 $^1A'$ singlet state of C_6Cl_6 was considered to be of C_{2v} symmetry and has been optimized by means of Møller-Plesset perturbation theory (MP2) calculations with the balanced polarized triple-zeta def2-TZVP basis set[200] which has been shown to be computationally efficient and provides accurate structures and transition energies. All calculations have been performed using the ORCA and MOLPRO packages of *ab initio* programmes.[201], [202] The energy of the optimized molecule is E_{MP2} = -2986.35880 a.u. The HOMO is located at $20b_1$ with an energy E_{HOMO} = -9.68 eV and the LUMO at $22a_1$ with an energy E_{LUMO} = 1.83 eV. The LUMO-HOMO energy difference is 11.51 eV.

A.2 C_6Cl_6 Molecular orbitals

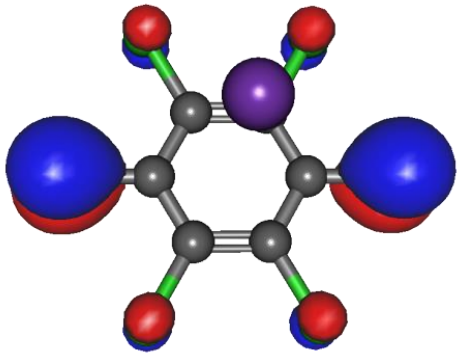	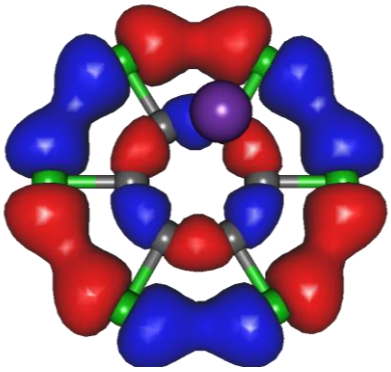
HOMO-7, n_{Cl} (out-of-plane)	HOMO-6
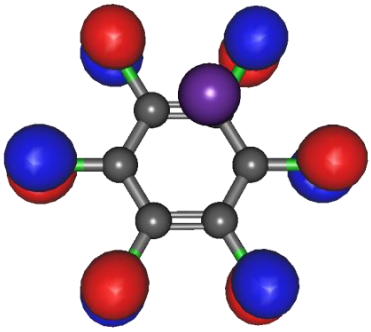	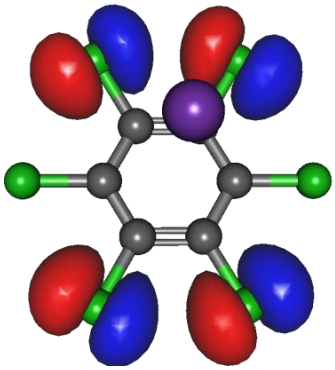
HOMO-5, n_{Cl} (out-of-plane)	HOMO-4, $\bar{n}_{Cl}$ (in-plane)
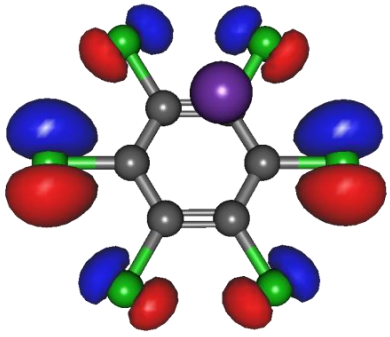	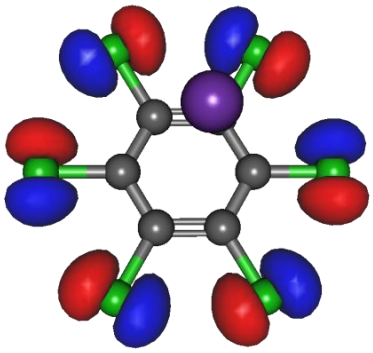
HOMO-3, $\bar{n}_{Cl}$ (in-plane)	HOMO-2, $\bar{n}_{Cl}$ (in-plane)

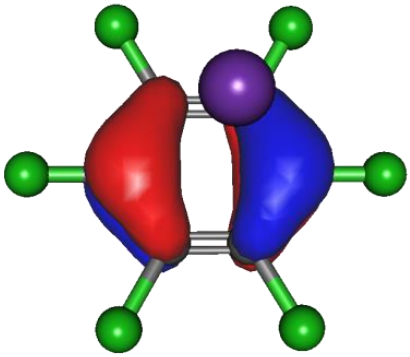	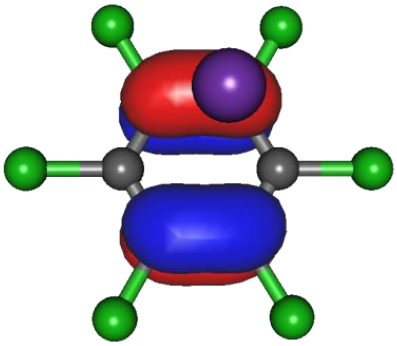
HOMO-1, π_{CCl}	HOMO, π_{CC}
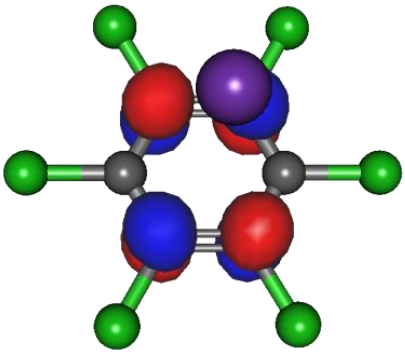	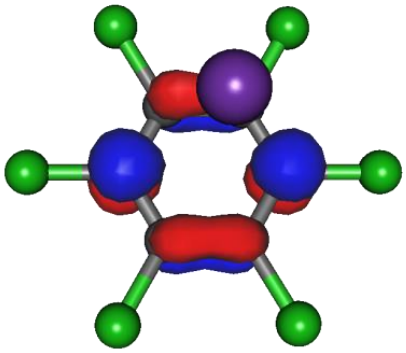
LUMO, π_{CC}^*	LUMO+1, $\pi_{CC}^*/\sigma_{CC}^* + \sigma_{CCl}^*$
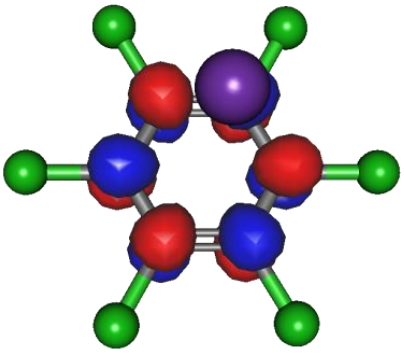	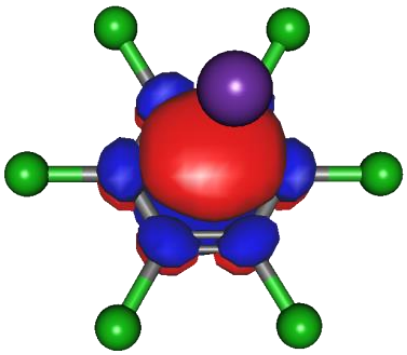
LUMO+2, π_{CC}^*	LUMO+3, σ_{CC}^*
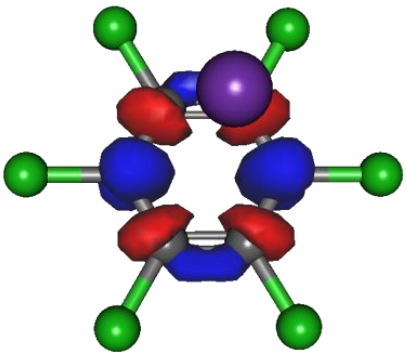	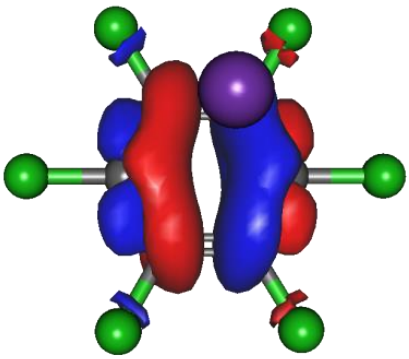
LUMO+4, σ_{CC}^*	LUMO+5, $\sigma_{CC}^* + \sigma_{CCl}^*$

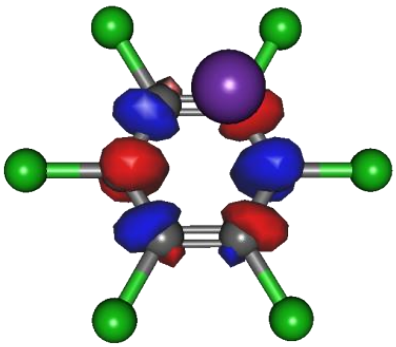	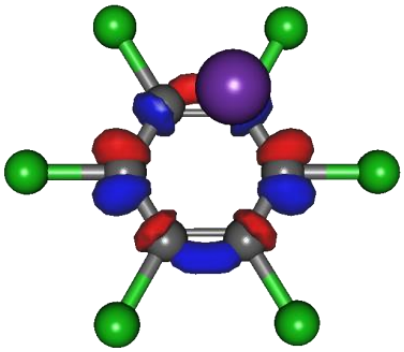
LUMO+6, σ_{CC}*	LUMO+7, σ_{CC}*
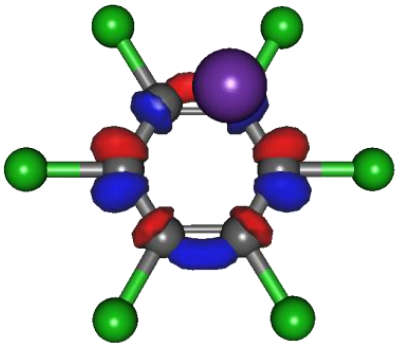	
LUMO+8, σ_{CC}*	

Fig. A1 Selection of the molecular orbitals for $K + C_6Cl_6$ (K = Magenta, C= Grey, Cl= Green) at CAS (13,16).

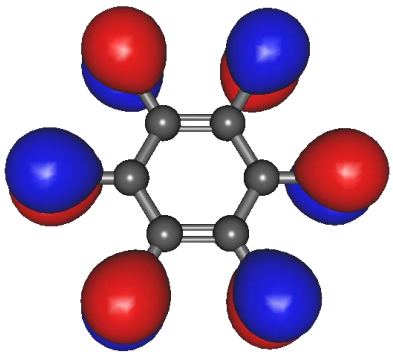	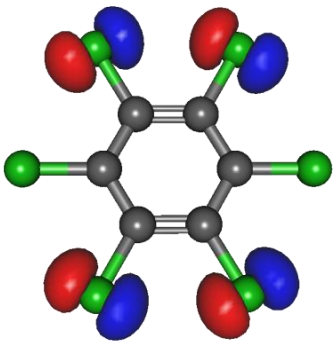
HOMO-5, n_{Cl} (out-of-plane)	HOMO-4, $\bar{n}_{Cl}$ (in-plane)

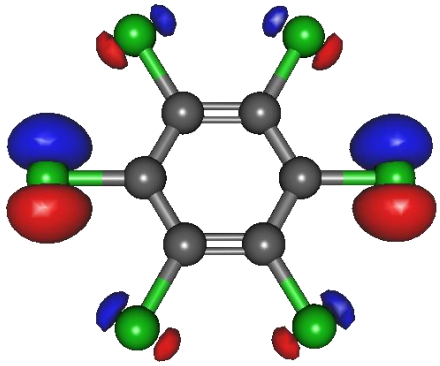	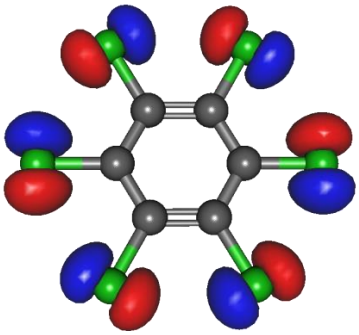
HOMO-3, $\bar{n}_{Cl}$ (in-plane)	HOMO-2, $\bar{n}_{Cl}$ (in-plane)
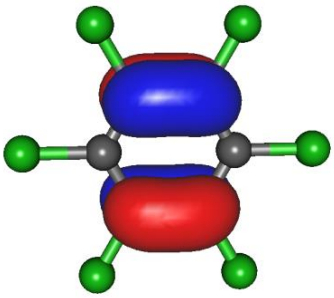	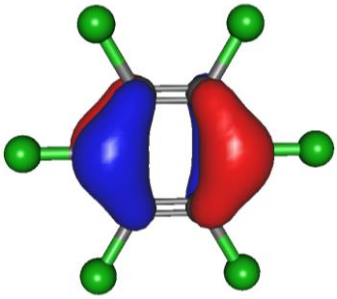
HOMO-1, π_{CC}	HOMO, π_{CCl}
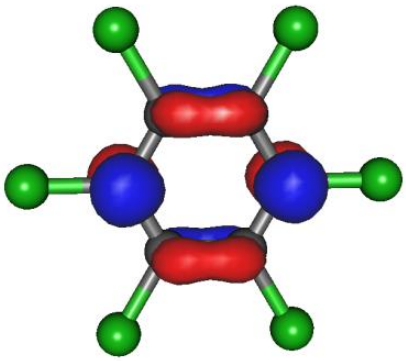	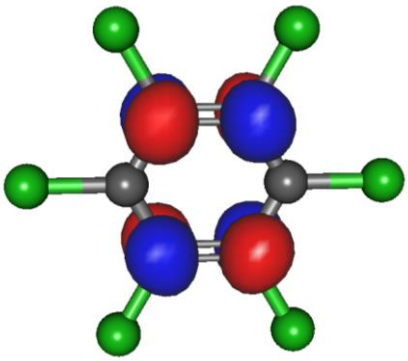
LUMO, $\pi_{CC}^*/\sigma_{CC}^* + \sigma_{CCl}^*$	LUMO+1, π_{CC}^*
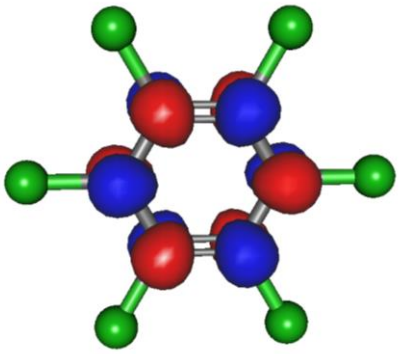	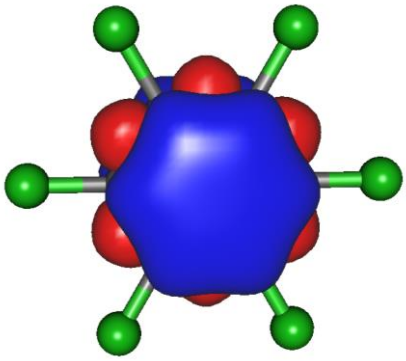
LUMO+2, π_{CC}^*	LUMO+3, σ_{CC}^*

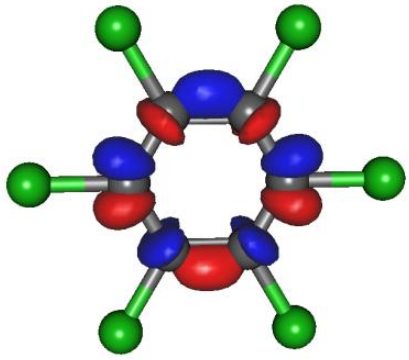	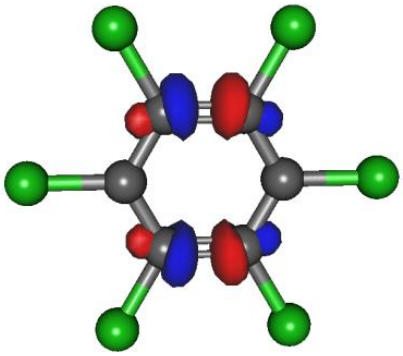
LUMO+4, σ_{CC}*	LUMO+5, π_{CC}* + σ_{CC}*

Fig. A2 Selection of molecular orbitals for C_6Cl_6 (C= Grey, Cl= Green) at CAS (12,12).

A.3 Parent anion ($C_6Cl_6^-$) molecular orbitals

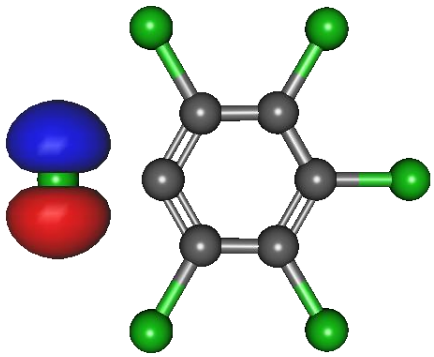	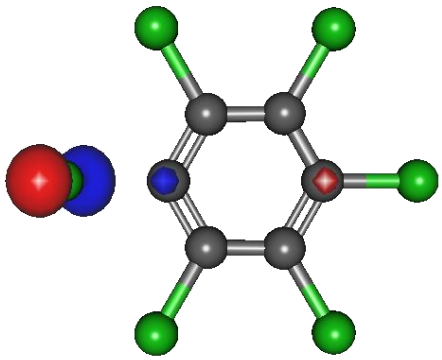
68, π (-3.366 eV)	69, π (-3.148 eV)
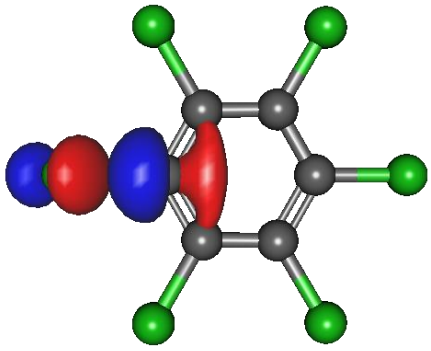	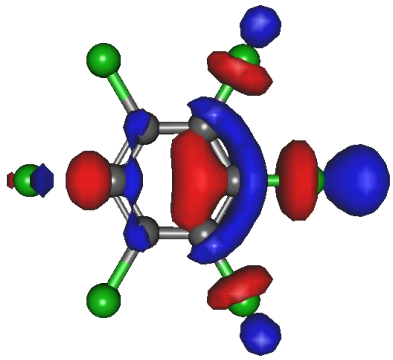
70, SOMO, π_{CCl} (-1.096 eV)	71, σ_{CCl}* (1.918 eV)

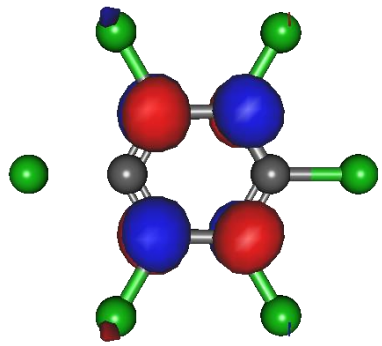	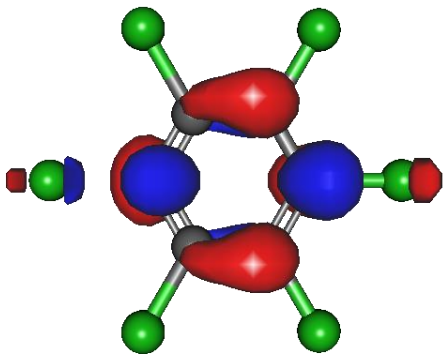
72, π* (2.174 eV)	73, σ_{CCl}* (2.435 eV)

Fig. A3 $C_6Cl_6^-$ molecular orbitals (C=Grey, Cl= Green)

In case of parent anion, 68 and 69 represent highest doubly occupied molecular orbitals. Where 70 is the singly occupied molecular orbital. 71, 72 and 73 are the lowest unoccupied molecular orbitals, performed at (RKS, B3LYP+D3) level.

A.4 Cl_2^- formation

Potassium cations formed post-collision experiments were energy loss analyzed in the forward scattering direction, where such experiments were not performed in coincidence with TOF mass spectrometry. The analyzer was operated in constant transmission mode, hence keeping the resolution constant throughout the entire scan. The estimated energy resolution during the experiments was ~1.2 ± 0.2 eV. The energy loss scale was calibrated using the K^+ beam profile from the potassium ion source serving as the elastic peak. Hexachlorobenzene (C_6Cl_6) and 1,2−, 1,3− and 1,4−dichlorobenzene ($C_6H_4Cl_2$) were supplied by Aldrich with a stated purity ≥ 98%, 99%, ≥ 99% and ≥ 99%. The liquid samples (1,2− and 1,3 − $C_6H_4Cl_2$) were degassed through repeated freeze−pump−thaw cycles. The solid samples (C_6Cl_6 and 1,4 − $C_6H_4Cl_2$) were used as obtained and gently heated up to 340 K and 363 K through a temperature PID (proportional-integral-derivate controller) unit. In order to test for any thermal decomposition products within the different molecular beams, mass spectra were recorded at different temperatures and no differences in the relative peak intensities as a function of temperature were observed.

Energy thresholds for the dissociation of Cl, Cl_2 and their anions from C_6Cl_6 and $C_6H_4Cl_2$ were calculated by means of quantum chemistry. The B3LYP-GD3 density functional with the aug-cc-pVTZ basis-sets and the quantum thermochemical extrapolation methods G4MP2 and CBS-QB3 served as model chemistries. The results from these independent methods are as close as can reasonably be expected, thus lending credibility to our data. All possible configurations and isomers were considered. The vibrational modes of C_6Cl_6 (neutral and anion

species) and $C_6H_4Cl_2$ (ortho, para and meta isomers) were also calculated (B3LYP-GD3/aug-cc-pVTZ), together with various orbital energies and charge distributions. All calculations were performed using the software package Gaussian 16 at the LEO HPC facilities of the University of Innsbruck.

We explored asymmetric internal Cl migration pathways as precursor to Cl_2^- detachment. The lowest-energy reaction pathways were obtained from calculations with the density functional M062X and the 6-31G (d, p) basis set.

Finally, the symmetric direct abstraction of Cl_2^- was studied. The $Cl-Cl$ distance in the leaving Cl_2 was decreased to its equilibrium value, while also setting the $C-C$ bond length of the carbon atoms from which Cl_2 dissociates to its equilibrium value in C_6Cl_4.

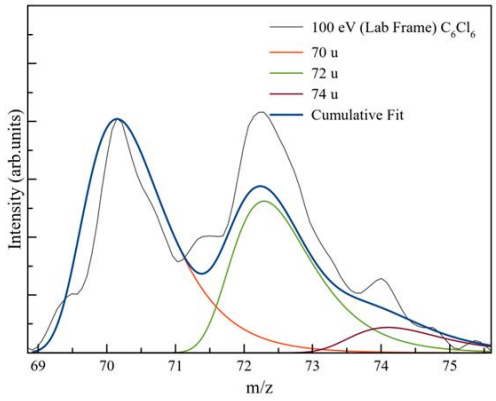

Fig. A4 TOF mass spectrum of Cl_2^- anion at 100 eV collision energy and fitted with Gaussian functions to reproduce its isotope contributions at 70 u (100%), 72 u (~65%) and 74 u (~15%).

A.4.1 Cl_2^- (Cl_2) detachment reaction via asymmetric internal Cl migration

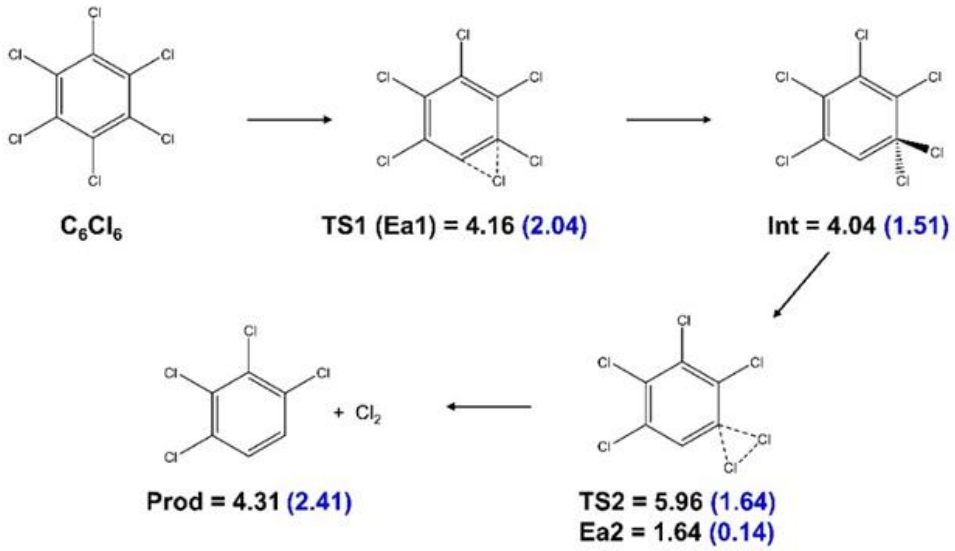

Fig. A5 Detachment of Cl_2 and Cl_2^- from sites at ortho position in C_6Cl_6. Energies in eV; values in parenthesis are for the anionic system.

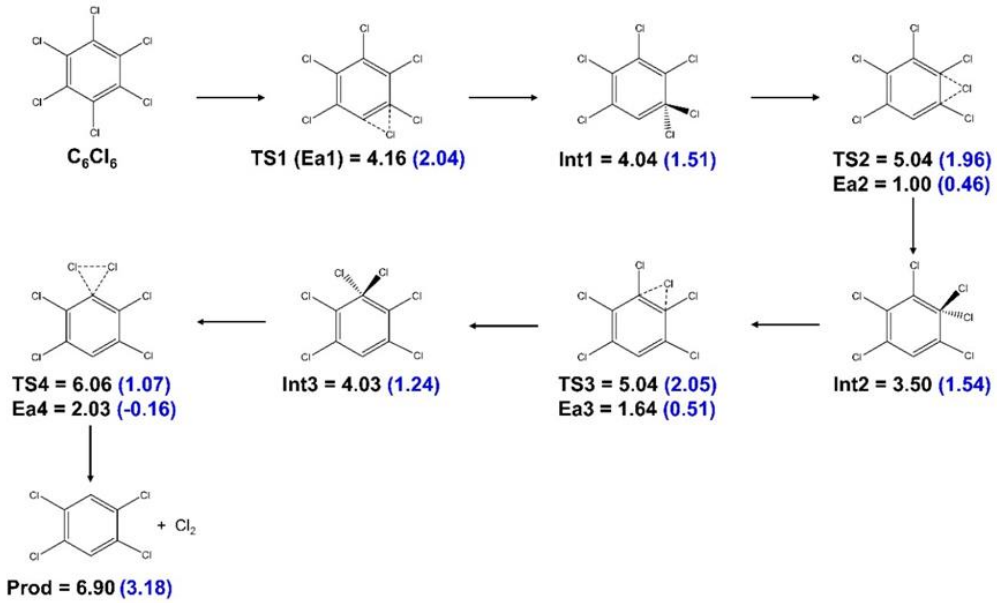

Fig. A6 Detachment of Cl_2 and Cl_2^- from sites at para position in C_6Cl_6. Energies in eV; values in parenthesis are for the anionic system.

A.4.2 TOF-MS of negative ions from C_6Cl_6 and $C_6H_4Cl_2$ Isomers

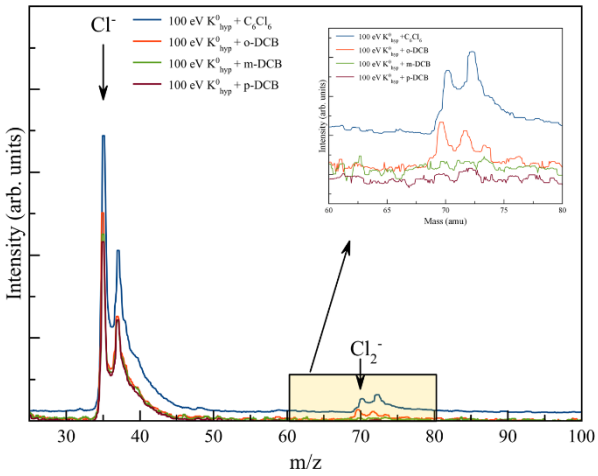

Fig. A7 Time-of-flight mass spectra of negative ions formed in electron transfer experiments from potassium atoms to hexachlorobenzene (C_6Cl_6)and dichlorobenzene (DCB) isomers at 100 eV collision energy in the lab frame.

A.5 Character and energy of calculated molecular orbitals

Table A1 Character and energy of calculated molecular orbitals for $K + C_6Cl_6$ with an active space CAS (13,16) at the MP2/def2-TZVP level of theory in C_{2v} symmetry.

Character	Energy (a.u.)	Energy (eV)
HOMO-2	-0.4420	-12.027
HOMO-1	-0.3903	-10.621
HOMO	-0.3884	-10.569
SOMO	-0.0604	-1.644
LUMO	0.1061	2.887
LUMO+1	0.1138	3.097
LUMO+2	0.3617	9.842
LUMO+3	0.5812	15.815
LUMO+4	0.5946	16.180
LUMO+5	0.6113	16.634
LUMO+6	0.6537	17.788
LUMO+7	0.6746	18.357
LUMO+8	0.9701	26.398

Table A2 Character and energy of calculated molecular orbitals for C_6Cl_6 with an active space CAS (12,12) at the MP2/def2-TZVP level of theory in C_{2v} symmetry.

Character	Energy (a.u)	Energy (eV)
HOMO-4	-0.4734	-12.882
HOMO-3	-0.4734	-12.882
HOMO-2	-0.4404	-11.984
HOMO-1	-0.3860	-10.504
HOMO	-0.3848	-10.471
LUMO	0.1059	2.882
LUMO+1	0.1090	2.966
LUMO+2	0.3571	9.717
LUMO+3	0.6252	17.013
LUMO+4	0.6310	17.170
LUMO+5	0.6428	17.491

Table A3 Adiabatic and vertical ionisation energies, adiabatic and vertical electron affinities, and vertical detachment energy (VDE) at RKS/B3LYP+D3/aug-cc-pVTZ

system\method	**B3LYP+D3**	**B3LYP**	**RMP2**	**RHF-SCF**
IE (adiab) – eV	8.84	8.84	9.19	8.67
IE (vetrical) – eV	9.01	9.01	9.47	8.95
EA (adiab) – eV	1.05	0.94	0.49	-0.06
EA (vertical) – eV	0.39	0.39	-0.20	-1.13
VDE – eV	2.73	2.73	2.58	2.23

Table A4 Energies (in a.u.) of the neutral, anion and cation of C_6Cl_6 at RKS/B3LYP+D3/aug-cc-pVTZ in geometry optimized for each molecular system.

system\method	**B3LYP+D3**	**B3LYP**	**RMP2**	**RHF-SCF**
C_6Cl_6 in anion geometry	-2989.601659	-2989.597136	-2986.482425	-2984.343918
C_6Cl_6 in neutral geometry	-2989.577687	-2989.576910	-2986.457291	-2984.304869

system\method	B3LYP+D3	B3LYP	RMP2	RHF-SCF
C_6Cl_6 in cation geometry	-2989.238383	-2989.237596	-2986.126717	-2984.027626

B

BOUND ELECTRON ENHANCED RADIOSENSITISATION OF NIMORAZOLE UPON CHARGE TRANSFER

B.1 Calculated Geometry and Molecular orbitals

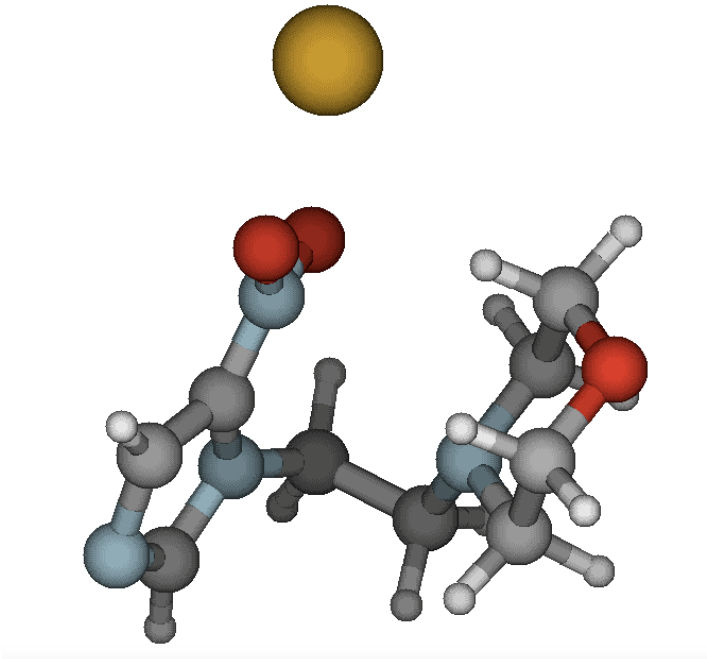

Fig. B1 Fully optimised geometry of nimorazole at the M06-2X/6-311++g (d, p) level of theory. Fully optimized molecular structure of the K + nimorazole collisional system K−O ≈ 5.1 Å. K: yellow, O: red, C: grey, N: light blue, and H: white. Cartesian coordinates (in Å.)

Cartesian coordinates (in Å).

C	-1.420369	0.935288	-0.002623
C	-2.173875	1.301569	1.093023
C	-2.763699	-0.681986	0.585502
N	-1.812232	-0.343711	-0.339432
H	-2.145992	2.245774	1.609137
H	-3.241564	-1.651108	0.562053
N	-0.481321	1.677568	-0.687116
O	-0.095453	2.803273	-0.171942
O	-0.108712	1.352728	-1.894973
C	-1.127140	-1.314816	-1.183171
H	-1.863916	-2.060121	-1.492879
H	-0.752059	-0.795845	-2.061864
C	0.008225	-1.982200	-0.400485
H	0.468590	-2.770692	-1.019343
H	-0.419992	-2.467095	0.481591
N	0.970923	-0.991773	0.034944
O	3.361762	0.290946	0.792860
C	2.007597	-0.717105	-0.945513
H	1.537980	-0.493391	-1.905521
H	2.686518	-1.582196	-1.061822
C	2.803816	0.495525	-0.490399
H	2.127998	1.362282	-0.463349
H	3.640056	0.686577	-1.166570
C	2.340919	0.030164	1.742421
H	2.837580	-0.109915	2.702912
H	1.660440	0.890794	1.799458
C	1.541132	-1.205151	1.354725
H	2.199143	-2.092655	1.383743
H	0.729244	-1.347031	2.073211
N	-3.010278	0.275255	1.441875
K	0.993434	3.583190	-2.269275

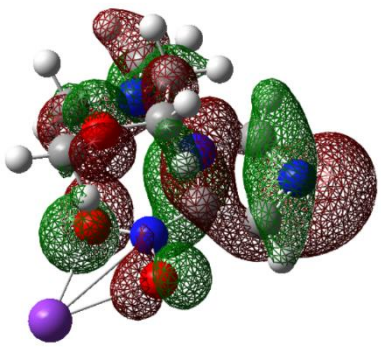	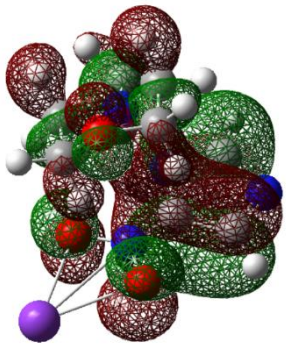
HOMO-3 (-8.57)	HOMO-2 (-7.86)

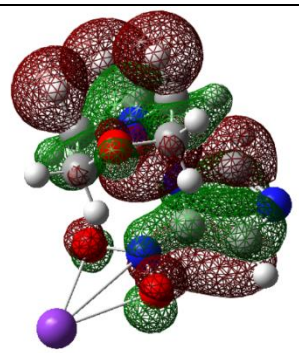	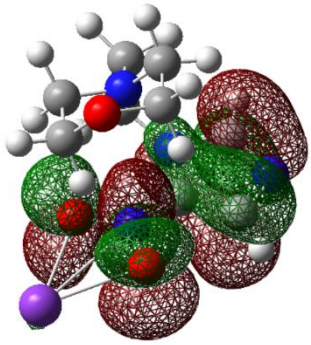
HOMO-1 (-7.22)	HOMO (-5.02)
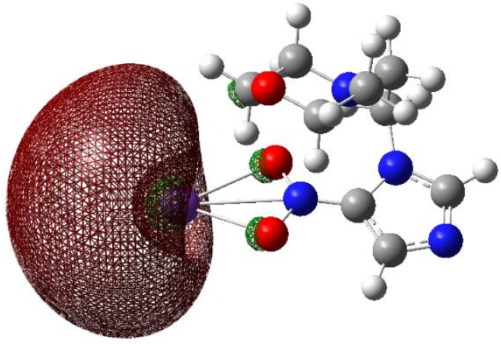	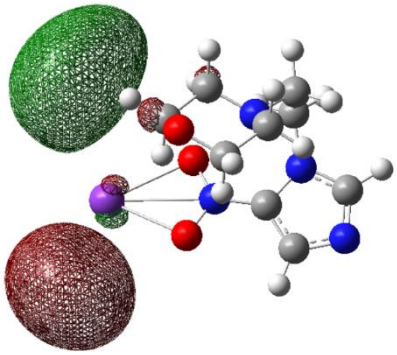
LUMO (-1.25)	LUMO+1 (-0.33)
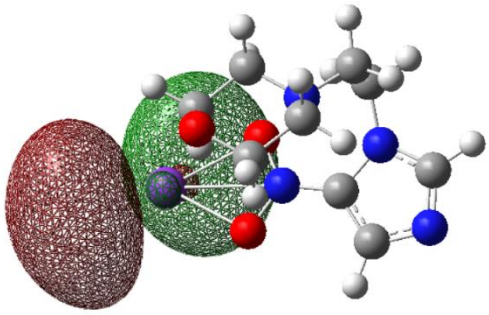	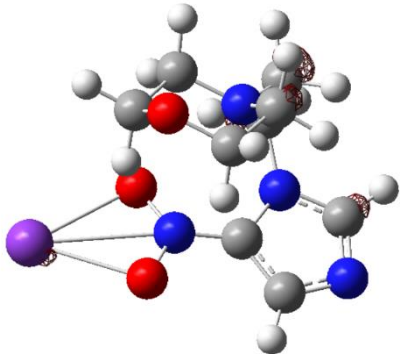
LUMO+2 (-0.27)	LUMO+3 (-0.07)
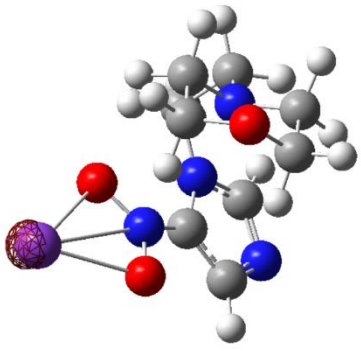	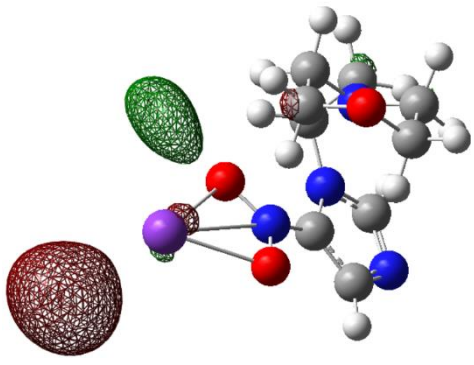
LUMO+4 (0.01)	LUMO+5 (0.23)

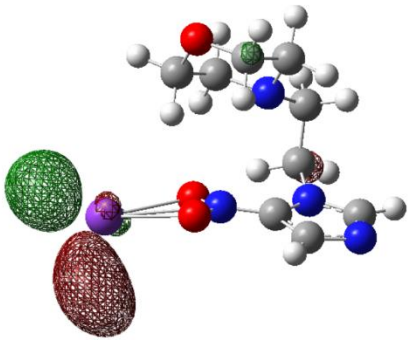	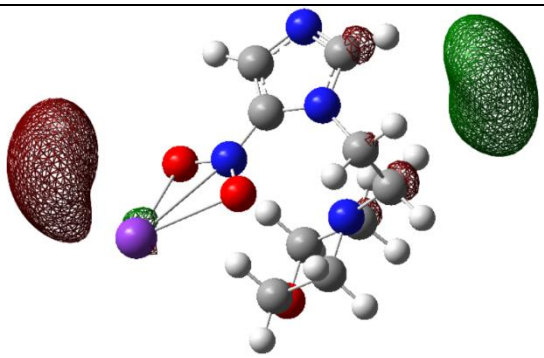
LUMO+6 (0.26)	LUMO+7 (0.38)
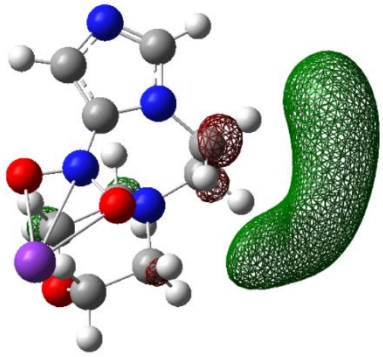	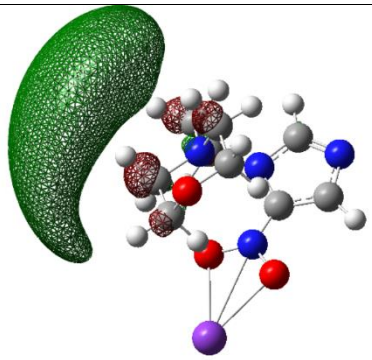
LUMO+8 (0.54)	LUMO+9 (0.60)
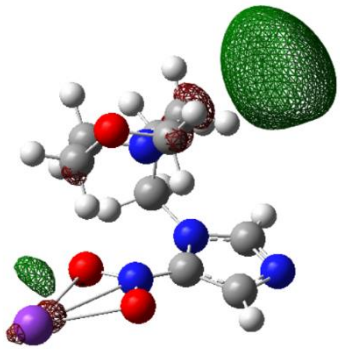	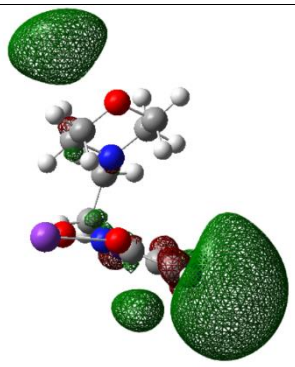
LUMO+10 (0.76)	LUMO+15 (1.32)
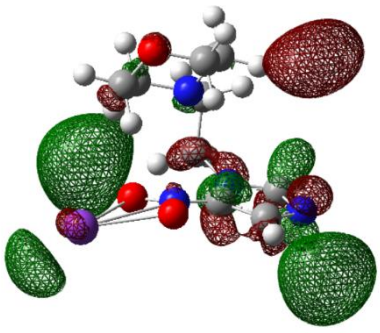	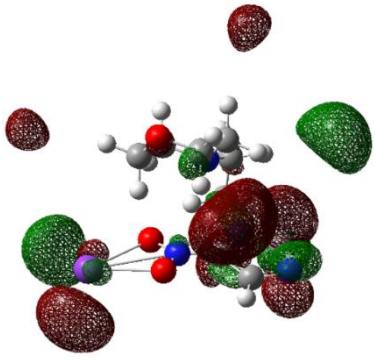
LUMO+20 (1.84)	LUMO+25 (2.39)

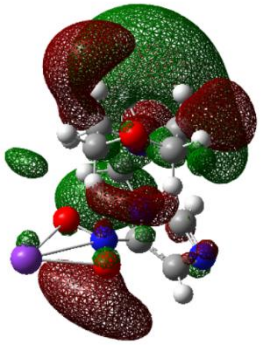	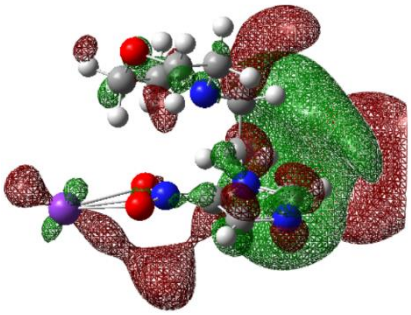
LUMO+30 (2.93)	LUMO+35 (3.51)
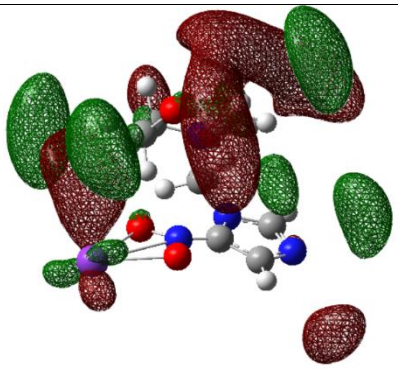	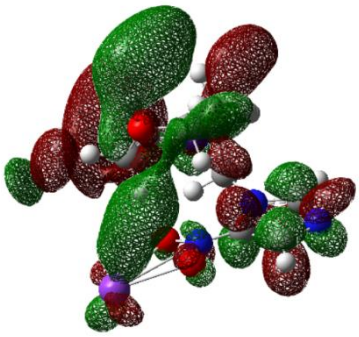
LUMO+40 (3.94)	LUMO+45 (4.38)
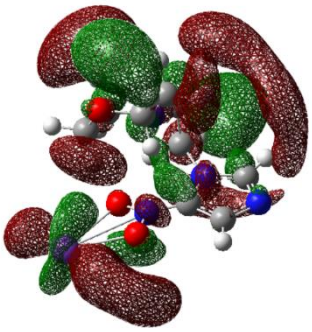	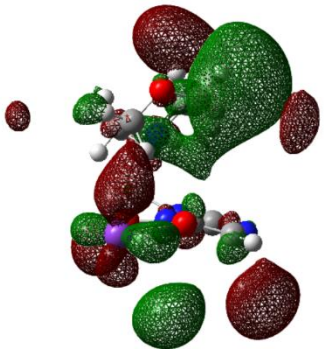
LUMO+50 (4.81)	LUMO+55 (5.11)
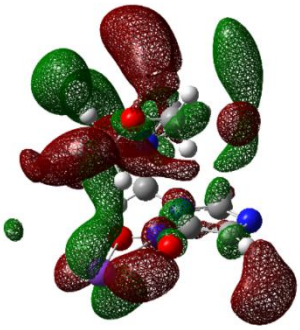	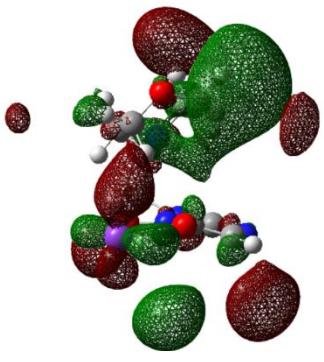
LUMO+56 (5.20)	LUMO+60 (5.69)

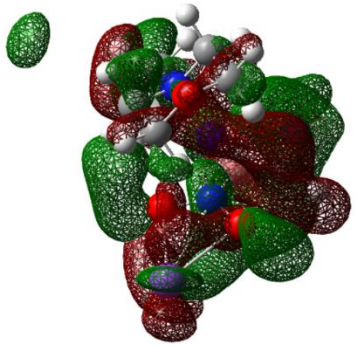	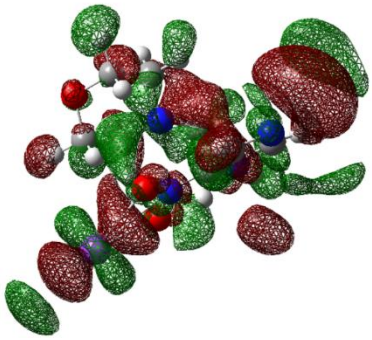
LUMO+70 (7.01)	LUMO+80 (8.28)
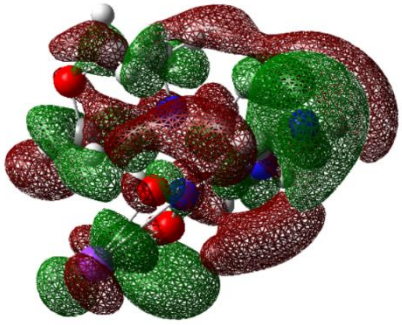	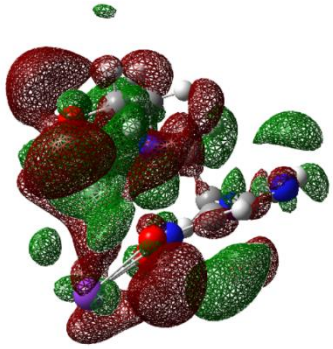
LUMO+90 (9.17)	LUMO+100 (10.01)

Fig. B2 Energy (in eV) and shape of a selection of the molecular orbitals (VTZ/6-311G) for K + NIMO (K: purple, C: grey, N: blue, O: red, and H: white). The straight lines between the K atom and the $-NO_2$ end in the nitroimidazole ring are just to indicate the spatial mutual position.

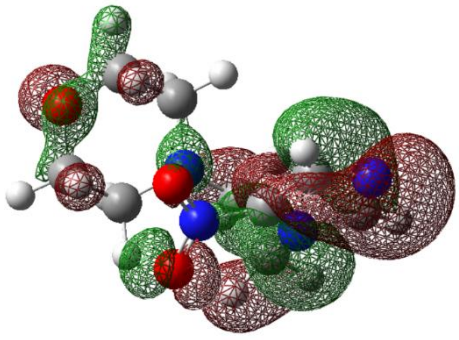	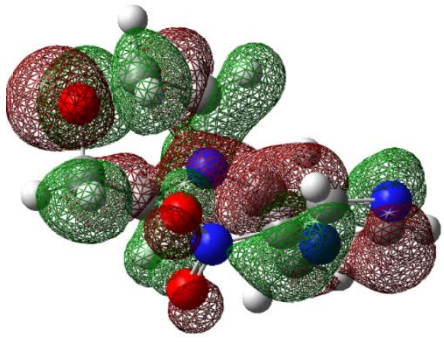
HOMO-3 (-9.91)	HOMO-2 (-9.14)

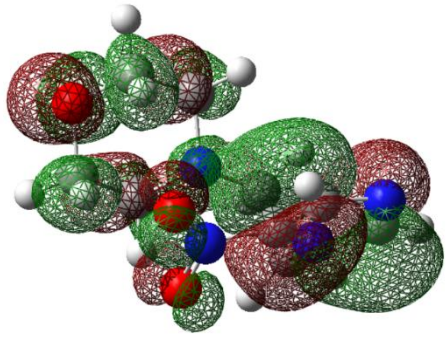	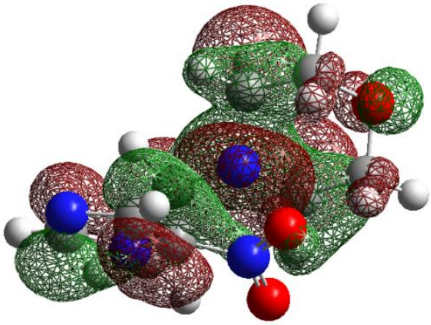
HOMO-1 (-8.76)	HOMO (-8.12)
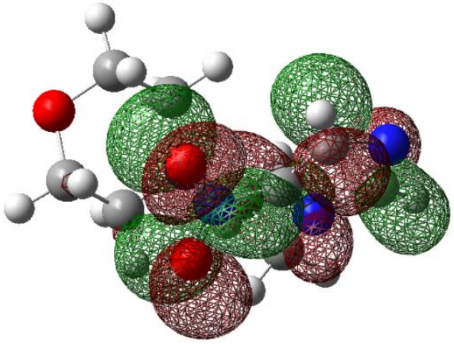	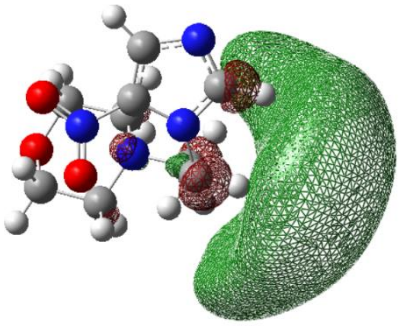
LUMO (-1.48)	LUMO+1 (-0.38)
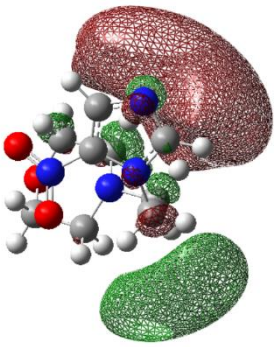	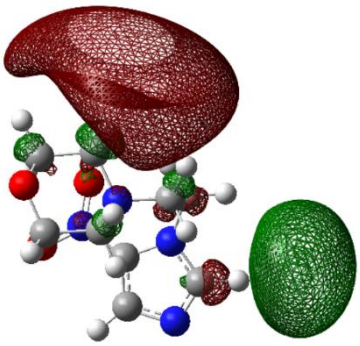
LUMO+2 (0.02)	LUMO+3 (0.10)
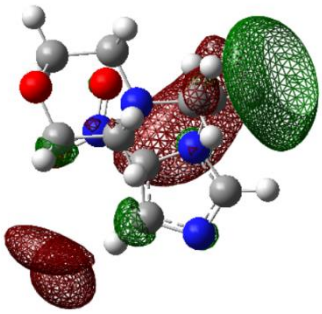	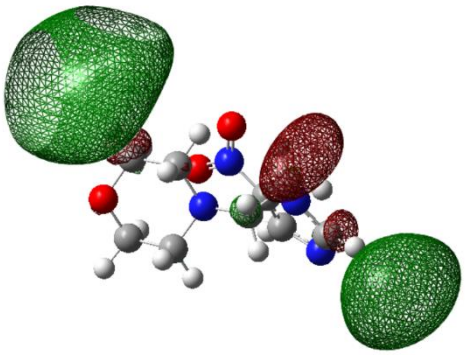
LUMO+4 (0.22)	LUMO+5 (0.56)

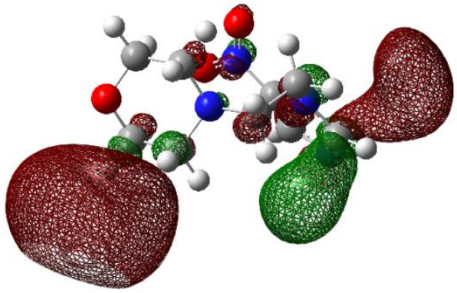	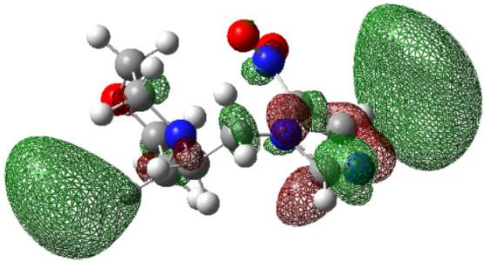
LUMO+6 (0.61)	LUMO+7 (0.63)
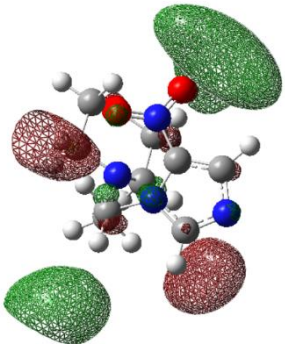	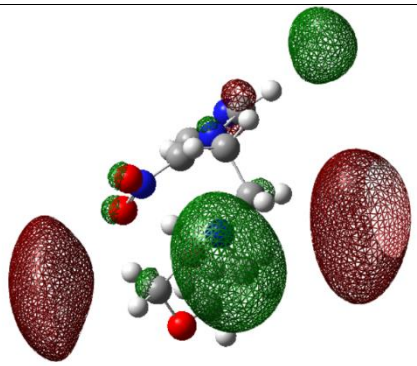
LUMO+8 (0.75)	LUMO+9 (1.00)
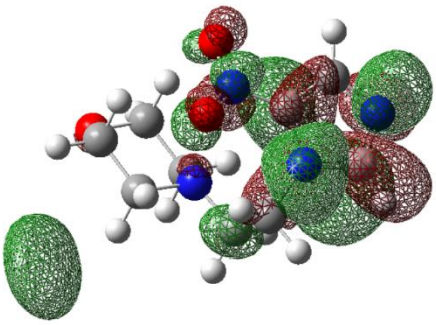	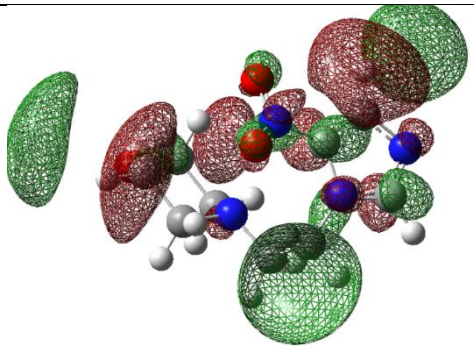
LUMO+10 (1.16)	LUMO+15 (1.66)
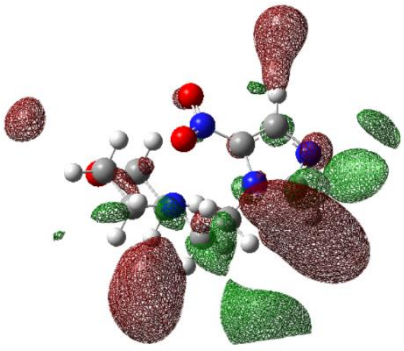	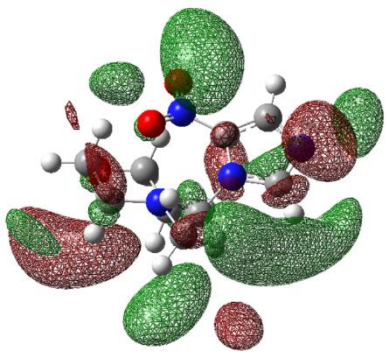
LUMO+20 (2.40)	LUMO+25 (3.05)

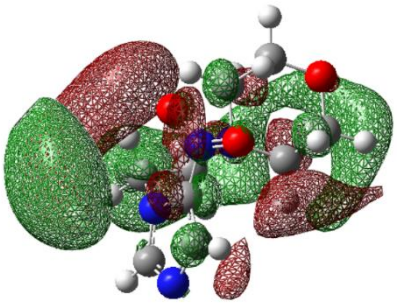	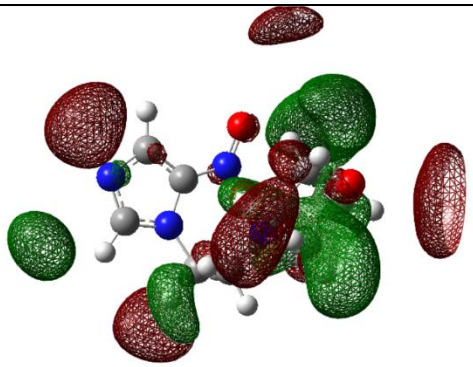
LUMO+30 (3.54)	LUMO+40 (4.28)
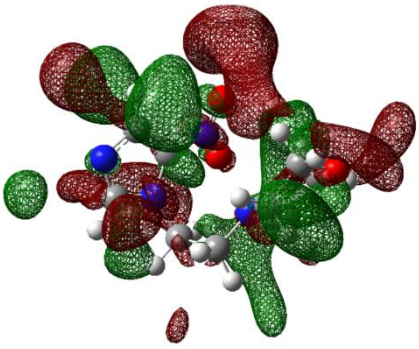	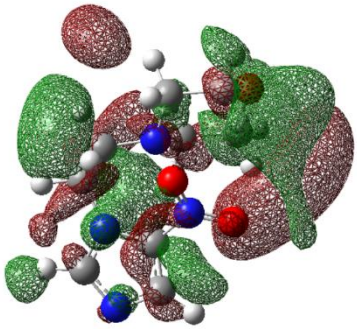
LUMO+50 (5.28)	LUMO+56 (5.41)
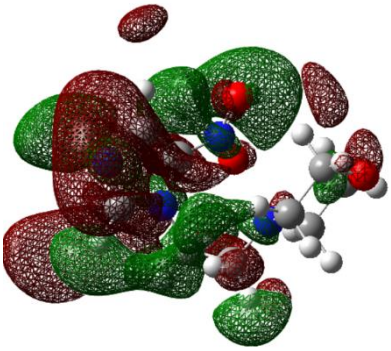	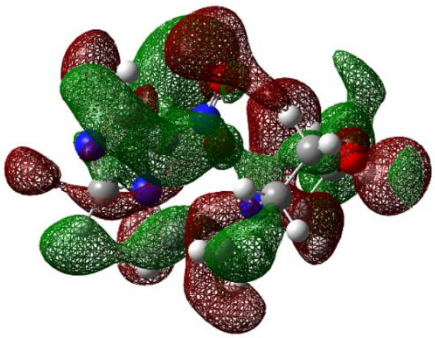
LUMO+60 (6.68)	LUMO+70 (7.80)
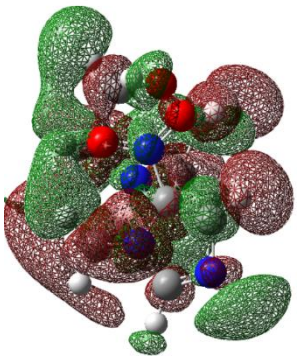	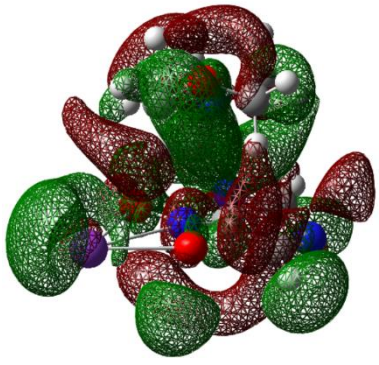
LUMO+80 (8.86)	LUMO+90 (10.03)

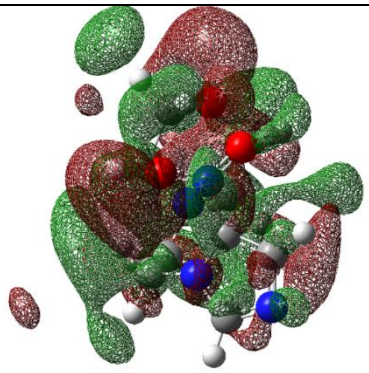	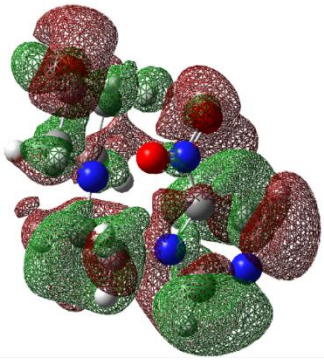
LUMO+100 (11.53)	LUMO+120 (17.30)
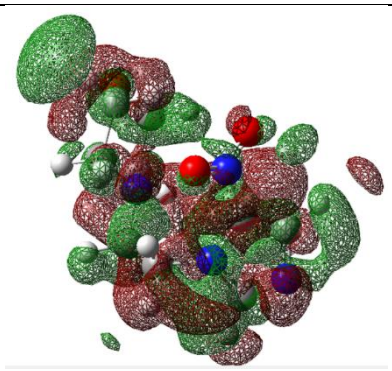	
LUMO+140 (21.5)	

Fig. B3 Energy (in eV) and shape of a selection of the molecular orbitals (M06-2X/6-311++g(d,p)) for NIMO (C: grey, N: blue, O: red, and H: white).

C

LIST OF PUBLICATIONS

This appendix contains detailed list of publications.

C.1 Papers published in peer review journals

Papers published in international peer review journals up to the present date:

1. A combined experimental and theoretical study of the lowest-lying valence, Rydberg and ionic electronic states of 2,4,6-trichloroanisole
S Kumar, D Duflot, S V Hoffmann, N C Jones, P Bolognesi, L Carlini, R Richter, L Avaldi, M J Brunger, and P Limão-Vieira, *J. Quant. Spectrosc. Rad. Transfer* 271 (2021) 107751**. (IF: 2.468)**

2. Cl^- kinetic-energy release distributions from chlorobenzene and related molecules in electron transfer experiments
Sarvesh Kumar, Pedro J. S. Pereira, Gustavo García & Paulo Limão-Vieira *Eur. Phys. J. D* ***75,*** *294 (2021)* **(IF: 1.425).**

3. *Anionic states of C_6Cl_6 probed in electron transfer experiments
S Kumar, T Kilich, M Łabuda, G García, and P Limão-Vieira ***Phys. Chem. Chem. Phys.,*** 2022, (24), 366-374. **(IF: 3.676)**

   *This article was in the monthly newletter (December 2021) of MD Gas Cost -action CA18212

4. *Unexpected oxidation of benzene in collisions with superoxide anions
C Guerra, **S Kumar**, F Aguilar-Galindo, S Díaz-Tendero, A I Lozano, M Mendes, P Limão-Vieira, and G García *Sci Rep 11****,*** *23125 (2021).* **(IF: 4.379)**

   *This article was in the monthly newsletter (December 2021) of MD Gas Cost -action CA18212.

5. Combined experimental and theoretical studies on electron-transfer in potassium collisions with CCl_4
K Regeta, **S Kumar**, T Cunha, M Mendes, A I Lozano, P J S Pereira, G García, A M C Moutinho, M-C Bacchus-Montabonel, and P Limão-Vieira, *J. Phys. Chem. A* **124** (2020) 3220. **(IF: 2.781)**

6. Ion-pair formation in neutral potassium-neutral pyrimidine collisions: electron transfer experiments
M Mendes, B Pamplona, **S. Kumar**, F Ferreira da Silva, A Aguilar, G García, M-C Bacchus-Montabonel and P Limão-Vieira, *Front. Chem*. **7** (2019) 264. **(IF: 5.221)**

7. Absolute photoabsorption cross-sections of methanol for terrestrial and astrophysical relevance

E Lange, A I Lozano, N C Jones, S V Hoffmann, **S Kumar**, M A Śmiałek, D Duflot, M J Brunger, P Limão-Vieira, *J. Phys. Chem. A* **124** (2020) 8496. **(IF: 2.781)**

8. The electronic excited states of dichloromethane in the 5.8-10.8 eV energy range investigated by experimental and theoretical methods
E Lange, N C Jones, S V Hoffmann, A I Lozano, **S Kumar**, M G P Homem, M A Smiałek, D Duflot, M J Brunger, P Limão-Vieira, *J. Quant. Spectrosc. Rad. Transfer* **253** (2020) 107172. **(IF: 2.468)**

9. Total electron detachment and induced cationic fragmentation cross sections for superoxide anion (O_2^-) collisions with benzene (C_6H_6) molecules
Carlos Guerra, **Sarvesh Kumar**, Fernando Aguilar-Galindo, Sergio Díaz-Tendero, Ana I. Lozano, Mónica Mendes, Juan C. Oller, Paulo Limão-Vieira, and Gustavo García. *Int. J. Mol. Sci. **2022**, 23(3), 1266.* **(IF: 5.924).**

10. Absolute total electron detachment and relative ionisation cross sections for O2- collisions with O2 in the energy range (10-1500 eV)
Carlos Guerra, Ana I. Lozano, Mónica F. Mendes, **Sarvesh Kumar**, Juan C. Oller, Paulo Limão-Vieira and Gustavo García, *PSST (2022) **31,** 035011*. **(IF: 3.584)**

11. Methanol negative ions fragmentation probed in electron transfer experiments
A.I. Lozano, **S. Kumar**, B. Kerkeni, G. García and P. Limão-Vieira, *J.Phys.Chem. A 2022, 126, 7, 1076–1084 (***IF: 2.781)**

12. Understanding the mechanisms of L-shell X-ray emission from Os atoms bombarded by 4-6 MeV/u fluorine ions
Soumya Chatterjee, Sunil Kumar, **Sarvesh Kumar**, M Oswal, Biraja Mohanty, D. Mehta, D. Mitra, A.M.P. Mendez, D.M. Mitnik, C. C. Montanari, L. Sarkadi, and T. Nandi, *Physica Scripta 97 (2022)045405* **(IF: 2.487)**

13. Hexachlorobenzene negative ions formation in electron attachment experiments
S. Kumar, F. Izadi, M. Ončák, P. Limão-Vieira and S. Denifl.
Phys. Chem. Chem. Phys 2022, **24**, 13335-13342. **(IF: 3.676).**

14. Sensing the *ortho* Positions in C_6Cl_6 and $C_6H_4Cl_2$ from Cl_2^- Formation upon Molecular Reduction
S. Kumar, J Romero, M Probst, T Maihom, G. García, and P. Limão-Vieira *Molecules* **2022**, *27*(15), 4820. **(IF: 4.927).**

15. Bound electron enhanced radiosensitisation of nimorazole upon charge transfer

S Kumar, Islem Ben Chouikha, B Kerkeni, G García and P Limão-Vieira *Molecules* **2022**, *27*(13), 4134. **(IF: 4.927).**

C.2 Papers under review/submitted/under preparation in peer review journals

16. The Lowest-Lying Potential Energy Curves of Carbon tetrachloride Anion
S. Kumar, P J S Pereira, G García, and P Limão-Vieira (under preparation).

C.3 Oral presentation in international meetings

P1. Electron Transfer Processes in Molecules of Biological Relevance
Seminar at J. Heyrovsky Institute of Physical Chemistry **on 30th March 2022**.

P2. Electronic state spectroscopy of polyatomic molecules using different methods
RaBBiT International Meeting 9-11th May 2022.

P3. Bound electron enhanced radiosensitisation of nimorazole upon charge transfer
11th International Meeting on Atomic and Molecular Physics and Chemistry (**IMAMPC) Vila Lanna Prague June 13th -17 th 2022**.

C.4 International conference abstracts

International conference abstracts up to the present date:

C1. Cl_2^- formation mediated by Steric hindrance upon electron transfer processes in hexachlorobenzene and dichlorobenzene molecules
S Kumar, G García and P Limão-Vieira, Virtual POSMOL 2021, Notre Dame, USA, July 2021.

C2. Methanol fragmentation probed in electron transfer experiments
A I Lozano, B Kerkeni, **S Kumar**, G García, P Limão-Vieira, *Virtual ICPEAC, July 2021(B20).*

C3. Probing the lowest-lying anionic states of CCl_4 by energy loss measurements in electron transfer experiments
S Kumar, P J S Pereira, G García, P Limão-Vieira, *combined virtual WG1 & WG2 meeting of the MD-GAS Action, Bulgaria (2021) 57.*

C4. Total Relative Cross Sections from Chlorobenzene in Electron Transfer Experiments
S Kumar, M Mendes, A I Lozano, F Ferreira da Silva, J Fedor, G García and P Limão-Vieira, *NOVA Biophysica, Lisbon, Portugal (2019) 34*.

C5. Total Cross Sections from Chlorobenzene in Electron Transfer Experiments
S Kumar, M Mendes, A I Lozano, F Ferreira da Silva, J Fedor, G García and P Limão-Vieira, *POSMOL 2019, Belgrade, Serbia (2019) 140*.

C6. Ion-Pair Formation in Neutral Potassium-Neutral Pyrimidine Collisions: Electron Transfer Experiments
A I Lozano, M Mendes, B Pamplona, **S Kumar**, F Ferreira da Silva, A Aguilar, G García, M-C Bacchus-Montabonel, P Limão-Vieira, *POSMOL 2019, Belgrade, Serbia (2019) 103.*

C7. Characterization of Thin Aluminized Polypropylene Backed Atomic Targets Using 2 MeV He^+ Ions
Sarvesh Kumar, Sunil Kumar, Deepak Kumar Swami, D.P. Goyal and T. Nandi, *ISAMP TC-7 Tirupati (2018).*

C8. *L* X-ray Production Cross Sections in ultra-thin 76 Os using 4-6 MeV/u Fluorine ions
Sunil Kumar, **Sarvesh Kumar,** Deepak Kumar Swami, D.P. Goyal and T. Nandi, *ISAMP TC-7 Tirupati (2018).*

C9. Molecular Orbital interpretation to the couplings in collisions of 2.5 and 3 MeV Xe 10+,12+ - Au and Zr systems

Punita Verma, Kajol Chakraborty, Ruchika Gupta, **Sarvesh Kumar**, Gaurav Sharma, Deepak Swami, Samit K. Mandal, C.P. Safvan, *ICPEAC (2017) Journal of Physics: Conf. Series 875 (2017) 092029.*

C10. Transfer reaction measurements for 28Si + 92;96Zr systems Khushboo, S. Mandal, S. Nath, N. Madhavan, J. Gehlot, A. Banerjee, N. Kumar, T Banerjee, G. Kaur, K. Rojeeta, Unnati, A. Jhingan, T. Varughese, Indu Bala, S. Muralithar, R. P. Singh, Visakh A. C., Ch. Vikar, H. Arora, **Sarvesh,** S. Kumar, S. Verma, and P. Verma DAE-*BRNS Symposium (2016) India.*

C11. An experimental set-up for ion atom collision studies at Low Energy Ion Beam facility of IUAC, New Delhi. **Sarvesh Kumar**, Punita Verma, C.P. Safvan, Q-Pace 2016, Dhanbad, India.

C12. Preparation of Gold Target through Electron Vapor Deposition and " Paras " the Rutherford Back Scattering Experimental setup @ IUAC. **Sarvesh Kumar**, Tulika Sharmay, Pranav Bhardwaj, Avnee Chauhan, Shruti Kapoor, and Punita Verma *NCIL (2015), New Delhi.*

C13. Impact Parameter Dependent X Ray Investigations in Heavy Ion Heavy Atom Collisions **Sarvesh Kumar**, Kajol Chakraborty, Lakshmi Dagar, and Punita Verma *NCIL (2015), New Delhi.*

Caparica, May 30th, 2022.

_____

Sarvesh Kumar

Electron Transfer Processes in Biologically Relevant Molecules

⟨2022⟩